PREDICTING FIRST-ORDER PMD OUTAGE RATES ON LONG-HAUL OPTICAL FIBER LINKS USING MEASURED AND MODELED TEMPORAL AND SPECTRAL DGD DATA

By

Pradeep Kumar Kondamuri

M.S. (Electrical Engineering)
University of Kansas, 2002

Submitted to the Department of Electrical Engineering and Computer Science and the
Faculty of the Graduate School of the University of Kansas
In partial fulfillment of the requirements for the degree of
Doctor of Philosophy

_____
Chairperson

_____

_____

_____

_____

Date defended: _____

The Dissertation Committee for Pradeep Kumar Kondamuri certifies that this is the approved version of the following dissertation:

PREDICTING FIRST-ORDER PMD OUTAGE RATES ON LONG-HAUL OPTICAL FIBER LINKS USING MEASURED AND MODELED TEMPORAL AND SPECTRAL DGD DATA

Committee:

_____
Chairperson

_____

_____

_____

_____

Date approved: _____

To
My Parents and Sisters

ACKNOWLEDGEMENTS

ABSTRACT

Polarization-mode dispersion (PMD) is a major impairment for high bit rate systems resulting in pulse broadening and distortion and thus leading to system performance degradation. Given the stochastic nature of PMD, it is extremely important to characterize PMD and perform system outage analysis to gain a better understanding of its impact on network reliability. The objective of this research work is to develop a numerical model that would accurately model the temporal and spectral PMD characteristics on buried long-haul optical fiber links and use the model to predict first-order PMD outage rates and also study how the outage rates vary with link length.

To achieve the above objective, a three-fold approach was followed. First, the first-order outage rate expression given by Caponi et al. [1] was simplified to a closed-form expression that depends only on two parameters. Second, the existing numerical model for PMD was enhanced by adding the temporal component to it and the model was validated by replicating the PMD characteristics observed through measurements on several buried fiber links. Third, the enhanced model was used to simulate the PMD characteristics on long-haul optical fiber links of different lengths and using the simulated data and the simplified first-order outage rate expression outage rates were predicted on long-haul links and the variation of outage rates with link length was studied.

From the analysis of measured differential-group delay (DGD), it was determined empirically that DGD time derivative ($\Delta\tau'$) has a Laplacian PDF and this led to the simplified first-order outage rate expression which showed that the outage rates are inversely proportional to the Laplacian parameter (α). The enhanced numerical model was able to replicate all of the major PMD characteristics observed from measurements. A simulation study of the long-haul links showed that the Laplacian parameter is inversely related to the link length and that the outage rates increase monotonically with the link length provided the receiver DGD threshold is

greater than the link mean DGD. This important finding will have a great impact on the network design of all the major carriers that are pushing for high-speed, all-optical, ultra long-haul optical fiber links. The above finding implies that realizing such links requires sophisticated PMD mitigation strategies to ensure network reliability.

TABLE OF CONTENTS

LIST OF FIGURES

LIST OF TABLES

1. INTRODUCTION

In spite of the recent telecom bubble, statistics show that the net traffic growth (combined Internet, data and voice traffic) remains at the same level as it was four years ago and network capacity is being exhausted at the same rate as it was during the pre-bubble time [2]. Applications such as videoconference, telephony, movies on demand, distance learning, telemedicine and technologies like fiber-to-the-home (FTTH) and fiber-to-the-premise (FTTP) are expected to fuel the future bandwidth demand and soon the existing infrastructure will run out of capacity and new capacity will have to be added to accommodate the ever-growing need for bandwidth [2]. One way to add capacity is to increase the transmission speeds. However, certain technical challenges need to be addressed to enable long-haul high-speed transmission. Two such challenges are polarization-mode dispersion (PMD) and chromatic dispersion variability, and of these two, PMD is the more difficult one because of its stochastic nature. While there are PMD challenges facing carriers at 10 Gb/s, these challenges are not as severe as originally feared. A marked improvement in the PMD tolerance of 10 Gb/s long-reach receivers will likely satisfy most length demands, obviating the need for PMD mitigation in many systems. However, transmission speeds of 40 Gb/s and beyond will most likely require some form of PMD mitigation in long-haul applications [3].

PMD is caused by optical birefringence and is a fundamental property of single-mode optical fiber and fiber-optic components in which signal energy at a wavelength is resolved into two orthogonal polarization modes of slightly different propagation velocities. PMD results in pulse broadening and distortion thereby leading to system performance degradation [4]. Unlike the chromatic dispersion, PMD varies stochastically in time making it particularly difficult to assess, counter or cope with [5]. Active research is being conducted by different groups on different issues of PMD for more than a decade. The key issues of PMD research can be broadly classified into three categories [2]: (i) fundamental understanding of the phenomenon and its impact, (ii) measurement, and (iii) mitigation strategies. The

objective of the PMD research is to understand the stochastic nature of PMD thoroughly through analytical analysis, simulations and/or analysis of measured data and determine an efficient means for mitigating PMD effects on long-haul fiber networks.

To ensure signal quality on their fiber at higher rates, network engineers must anticipate the impact of PMD on various fiber routes. Design of a reliable network requires a good model of the PMD characteristics on each link. An understanding of the temporal and spectral variability of both the differential group delay (DGD) and principal states of polarization (PSPs) is required to specify appropriate transmission parameters and also the required speed of PMD compensators. Factors such as the mean DGD, PMD correlation time and bandwidth, as well as second-order effects together with performance prediction models can provide this understanding [3],[6]. Also, a solid understanding of PMD-induced system outages will help engineers and researchers to develop new and cost-efficient mitigation alternatives to PMD compensators.

The first part of chapter 2 of this report reviews the PMD work published by others in the PMD research community on the specific issues of temporal and spectral behavior of PMD, system outage analysis and numerical modeling of PMD. The second part of chapter 2 describes the work that I have done as part of my Master's degree that is directly related to the current work. The third part of chapter 2 explains the objective and the significance of the current work. The simplified first-order PMD outage rate expression is discussed in chapter 3. Chapter 4 details the enhancements made to the simple numerical model to accurately model the temporal and spectral PMD characteristics of buried single-mode fibers. The results from simulations using the enhanced numerical model and a comparison with the measurements are shown in chapter 5. A simulation study of variation of first-order PMD outage rates with link length is presented in chapter 6. Chapter 6 is followed by conclusions and various ideas for future work.

2. LITERATURE REVIEW AND PREVIOUS WORK

2.1. Literature review

This section of the chapter reviews the published research work by others in specific areas of PMD which are related to the work presented in this report. The specific PMD areas that are reviewed are temporal behavior, spectral behavior, system outage analysis and numerical modeling.

2.1.1. Temporal behavior of PMD

2.1.1.1. Reported rates of change of PMD

The PMD characteristics of buried/aerial fibers are much different from the spooled fiber in the laboratory and hence it is important to characterize buried/aerial fibers rather than spooled fibers. A number of research groups have made long-term PMD measurements on buried/aerial fibers and reported different time rates of change of PMD ranging from a few minutes to few days. The general consensus is that temperature changes in buried fibers are slow in general and cause slow PMD variations whereas in aerial fibers temperature changes and hence the PMD variations are much faster. This section surveys the time rates of change of PMD reported by different groups.

Karlsson et al. [7] conducted a detailed long term study with simultaneous measurements on two 127-km dispersion-shifted fibers in the same embedded cable. PMD was measured roughly once every 2 hours alternately on the two fibers from 1505 to 1565 nm in steps of 0.1 nm using Jones matrix method for about 36 days. Mean DGD (averaged over wavelength and time) values of 2.75 and 2.89 ps and correlation times of 3 and 5.7 days were reported on the two fibers. A strong correlation between the changes in DGD and PSPs was reported and the study also indicated that the rate of temporal change of the PMD increased with the cable length and mean DGD. Contour plots of measured DGD versus wavelength and time on one of the fibers studied by Karlsson et al. [7] is shown in figure 2.1.
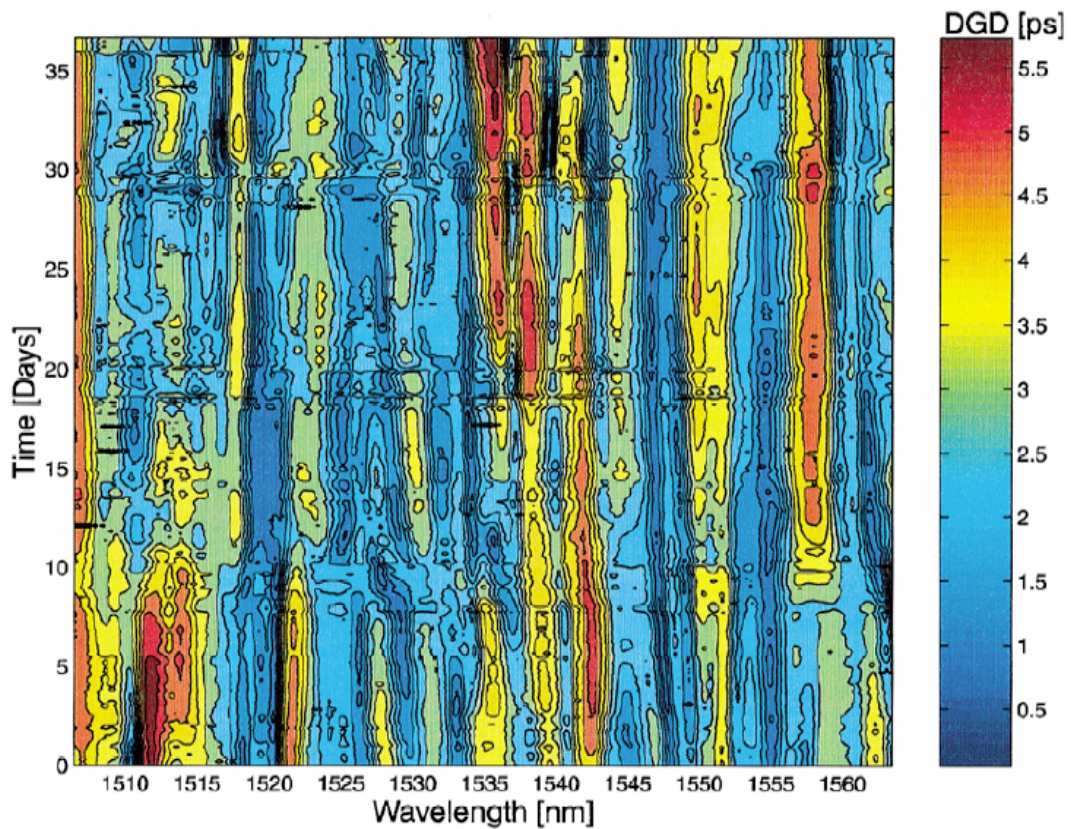
Figure 2.1. DGD vs. wavelength and time on one of the
fibers studied by Karlsson et al. [7].

In another study, Nagel et al. [8] measured DGD and PSPs on a 41-ps mean
DGD embedded single-mode fiber (114-km long) once every 5-10 minutes over a 70-
day period using a custom algorithm. Average correlation times of 19 hours for DGD
and 5 hours for PSPs were reported indicating that the PSPs change more rapidly than
DGD. Cameron et al. [9] measured wavelength-averaged DGD using interferometric
method on a 48.8-km buried standard single-mode fiber once every 58 seconds for
about 15 hours. It was reported that the time scale of mean DGD change over the 15-
hour measurement period varied between 1 and 2 hours. It was also reported that
small values of PMD had large fluctuations in PMD measurements and that the
magnitude of the fluctuations decreased as the PMD increased. De Angelis et al. [10]
reported a correlation time of at least 20 minutes from the data measured over 17-km
of buried fiber (fiber type not specified) for about 27 hours. In addition it was

reported that the correlation between the temperature fluctuations and evolution of DGD and PSP is much stronger in links which includes connectors that are exposed to temperature variations. Bulow et al. [11] reported the fastest PMD fluctuations in a time scale of 6 to 13 ms on a 52-km, 7.3-ps mean DGD buried cable. Such fast changes were attributed to moving of the fiber pigtails in the central office.

For submarine cables, Takahashi et al. [12] reported a DGD correlation time of about 1 hour on 119-km fiber (fiber type not specified) and Kawazawa et al. [13] observed PMD changes with a period of about two months on a 62-km dispersion shifted fiber. Takahashi et al. also reported that the time scale of DGD and PSP evolution also depends on the product of fiber length and time which implies shorter correlation time for longer fibers.

Cameron et al. [9] reported that DGD variations on a 96-km aerial cable (SMF) exhibited time scales ranging from 5 to 90 minutes depending on the air temperature rate of change.

Some groups have also reported DGD correlation times for spools of fiber in a laboratory environment. These are included here for completeness of the survey. Bahsoun et al. [14] reported a correlation time of about 3 hours on a 10-km spool of dispersion shifted fiber. A correlation time of about 30 minutes was reported by Poole et al. [15] on 31.6-km spool of dispersion shifted fiber.

2.1.1.2. Temporal autocorrelation functions

From a mathematical point of view, the temporal behavior of PMD can be understood by studying the autocorrelation functions. Karlsson et al. [7] derived the analytical expressions for autocorrelation functions of SOP s(ω, t) and PMD vector Ω(ω, t). The temporal autocorrelation function for two polarization states at the same frequency was shown to be

$$E[s(t_1) \cdot s(t_2)] = \exp\left(\frac{-|\Delta t|}{t_d}\right) \qquad (2.1)$$

and the temporal autocorrelation function for the PMD vector at the same frequency was shown to be

$$E[\Omega(t_1) \cdot \Omega(t_2)] = E[\Delta\tau^2] \frac{1 - \exp\left(\dfrac{-|\Delta t|}{t_d}\right)}{\dfrac{|\Delta t|}{t_d}} \qquad (2.2)$$

where $\Delta t = t_1 - t_2$, $\Delta\tau$ is the instantaneous DGD, E[.] is expectation and t_d is the average drift time for both absolute polarization states and PMD vector of an installed fiber.

The parameter t_d indicates the time scale over which the absolute polarization states and the PMD vector changes and it depends on installation-specific data such as the amount of environmental perturbations and disturbances. It cannot be predicted or estimated from known fiber parameters, it must be measured for each fiber. However, it has been shown that t_d depends on 'b', the PMD coefficient (ps/√km), as [7]

$$t_d = \frac{2t_0}{\left(3\omega^2 E[\Delta\tau^2]\right)} = \frac{2t_0}{\left(3\omega^2 b^2 L\right)} \qquad (2.3)$$

where ω is the carrier frequency, L is the total length of the fiber, and t_0 is a measure of the drift time of the index difference in the birefringent element used to model the fiber. (2.3) implies that the drift is more rapid for long fibers and high PMD [7].

2.1.2. Spectral behavior of PMD

2.1.2.1. Frequency autocorrelation functions

Karlsson et al. [16], Shtaif et al. [17], and Mecozzi et al. [18] derived the frequency autocorrelation function of the PMD vector Ω which is given by

$$E[\Omega(\omega_1) \cdot \Omega(\omega_2)] = 3 \frac{1 - \exp\left(\dfrac{-E[\Delta\tau^2]\Delta\omega^2}{3}\right)}{\Delta\omega^2} \qquad (2.4)$$

where $\Delta\omega = \omega_1 - \omega_2$, $\Delta\tau$ is the instantaneous DGD and E[.] is the expectation. Karlsson et al. [16] also noted that the main contribution to the autocorrelation function of (2.4) comes from the de-alignment of the principal states rather than from

a change of the DGD. Shtaif et al. [17] reported that the frequency autocorrelation of DGD takes the form

$$E[\Delta\tau(\omega_1)\cdot\Delta\tau(\omega_2)] \cong \frac{3\pi-8}{\pi}\left\{\frac{2}{\Delta\omega^2} - \frac{6}{\Delta\omega^4 E[\Delta\tau^2]}\left[1 - \exp\left(\frac{-\Delta\omega^2 E[\Delta\tau^2]}{3}\right)\right]\right\} + \frac{8}{3\pi}E[\Delta\tau^2]$$

where $\Delta\omega = \omega_1-\omega_2$, $\Delta\tau$ is the instantaneous DGD and E[.] is the expectation.   (2.5)

2.1.2.2. Correlation bandwidths

Karlsson et al. [16] showed the correlation bandwidth of the PMD vector to be $4\sqrt{2}/E[\Delta\tau]$ which is close to the one reported by Shtaif et al. [17]. Shtaif et al. [17] also showed that the correlation bandwidths of the length of the PMD vector (DGD) and the angle of the PMD vector are comparable to each other and are given by $4/E[\Delta\tau]$ and $5.2/E[\Delta\tau]$. This means that the rate at which the length of the PMD vector changes with optical frequency is comparable with the rate at which its orientation changes in Stokes space. From the expressions for the correlation bandwidths it is clear that fiber with a high mean DGD have narrower correlation bandwidth than fibers with a low mean DGD.

2.1.3. System outage analysis

2.1.3.1. Definitions of a PMD outage

Different definitions for a PMD outage can be found in literature. The most common definition is to define a PMD outage as an event where the penalty due to PMD exceeds a given value. The penalty could be power penalty [19], [20], eye-opening penalty [20], [21], OSNR penalty [20] or Q penalty [22]. Another definition for PMD outage (used by Bulow [23], and Damask et al. [24]), is an event where the BER value exceeds a given value (typically 10^{-12}). A different definition is given by Caponi et al. [1] where the outage is defined as an event where the DGD exceeds a given threshold value. The advantage of Caponi et al.'s definition is that the outage probabilities can be calculated directly from the Maxwellian distribution of DGD by integrating the distribution over the limits.

2.1.3.2. Outage probabilities, rates and durations

Using the definition of PMD outage given by Caponi et al. [1], the outage probability P_{out} due to first-order PMD can be calculated from the Maxwellian PDF, $f_{\Delta\tau}(\cdot)$ as

$$P_{out} = P(\Delta\tau \geq \Delta\tau_{th}) = 1 - \int_0^{\Delta\tau_{th}} f_{\Delta\tau}(\Delta\tau)d\Delta\tau \qquad (2.6)$$

where $\Delta\tau_{th}$ is the DGD threshold value. P_{out} is often expressed in minutes/year. P_{out} is fiber independent and will be the same for all installations. If the probability of an outage is quite small, P_{out} represents the annualized outage probability based on long time records. Accurate estimation of the impact of PMD on network availability requires statistical analysis of DGD variability. Caponi et al. [1] showed how the mean time between PMD-related outages could be estimated from the temporal characteristics of DGD variations and the Maxwellian PDF. The calculation of mean outage rate, R_{out}, which is defined as the mean number of outage events per unit time (with units of 1/year), is a simple application of the 'Level Crossing' problem and has been derived by Caponi et al. [1] as

$$R_{out} = \frac{1}{2} f_{\Delta\tau}(\Delta\tau_{th}) \int_{-\infty}^{\infty} f_{\Delta\tau'}(\Delta\tau')|\Delta\tau'|d\Delta\tau' \qquad (2.7)$$

where $\Delta\tau'$ is the time derivative of the DGD, and $f_{\Delta\tau'}(\cdot)$ is the PDF of $\Delta\tau'$. Caponi et al. observed $\Delta\tau$ and $\Delta\tau'$ to be statistically independent and also found that R_{out} is cable and installation dependent. Caponi et al. numerically evaluated the PDF of $\Delta\tau'$, $f_{\Delta\tau'}(\cdot)$, from measured DGD data. The mean time between the outages (MTBO) is the inverse of R_{out}. The mean duration of DGD-induced outages can be determined using statistical analysis as well. Caponi et al. [1] showed that the mean outage duration, T_{out}, is

$$T_{out} = P_{out}/R_{out} \qquad (2.8)$$

which has units of minutes. Since T_{out} is found using R_{out}, which is cable and installation dependent, T_{out} will also be cable and installation dependent.

Using the above analysis, Caponi et al. [1] predicted that for the 37-km buried link they studied, the DGD will exceed three times the mean DGD once every 2.5 years with a mean outage duration of 56 minutes. A similar study was conducted by Nagel et al. [8] on a 114-km buried link and it was reported that on that link the DGD will exceed three times its mean value once every 3.5 years with a mean outage duration of between 10 and 20 minutes.

2.1.3.3. Other methods

Many of the research groups working on the PMD outage analysis [20], [21], [22], [23], [24], [25] used either the penalty definition or the BER definition of PMD outage mentioned in section 2.3.1 and derived analytical expressions for PMD outage probabilities based on the assumptions made (such as considering just first-order PMD, first- and second- order PMD, DGD and PSP variation etc.). Results from simulations and emulations were also reported to show the validity of the analytical expressions derived. Over the last 2 to 3 years a couple of research groups studied and reported [26], [27], [28] and [29] ways to apply the concept of importance sampling and its variations for computing outage probabilities due to first- and second-order PMD. The importance sampling method for PMD is still evolving and it could be a while before PMD emulators using importance-sampled algorithms are developed.

2.1.4. PMD in fiber-optic components

An optical fiber communication link has many components apart from the fiber such as the modulators, WDM multiplexer/demultiplexer, optical amplifiers, optical add/drop multiplexers, chromatic-dispersion compensating devices, etc. that exhibit PMD. However, PMD in these components, except for the dispersion compensating fiber (DCF), is deterministic in nature and is time-invariant. Also, with the increased awareness of the effects of PMD on system performance, component manufacturers are using advanced and sophisticated manufacturing processes that would minimize the PMD in their components.

2.1.4.1. PMD in erbium-doped fiber amplifiers (EDFAs)

Geiser et al. [30], [31] studied the behavior of PMD in EDFAs and other fiber amplifiers. They used Jones Matrix Eigenanalysis (JME) method with some special input conditions to measure PMD in EDFAs over long time periods and at different temperatures. Through their analysis Geiser et al. reported that the PMD of the EDFAs is deterministic in nature and it is not affected by random coupling changing with time or with external conditions like temperature [30]. They also observed DGD values to be < 0.12 ps for newer EDFAs and up to 0.7 ps for older EDFAs [31].

2.1.4.2. PMD in dispersion compensating fibers (DCFs)

Studies [32] [33] have shown that PMD in dispersion compensating fiber is quite significant and it shows strong temperature dependence. Hence when modeling PMD on optical fiber link that has DCF, the PMD characteristics of the DCF should be taken into account along with the PMD characteristics of the single-mode fiber. However, effects of PMD are significant only at higher data rates of 40 Gbps or above and at those rates DCFs are generally not used to compensate or manage the chromatic dispersion, instead sophisticated fixed or tunable chromatic dispersion management devices are used and these devices exhibit very low deterministic PMD.

2.1.5. Numerical modeling of PMD

Prediction of PMD-induced outages on realistic link lengths (> 500 km) would require long-term access to such a link and is not economically feasible at this time. Another approach to obtain PMD-induced outage statistics is to develop numerical models that realistically reflect the PMD-characteristics of buried fiber. While PMD numerical models exist, they do not include the necessary temporal variations needed for PMD-induced outage analysis.

Dal Forno et al. [34] described a model for numerical simulation using coarse-step method. It considers a SMF as a concatenation of unequal length segments with a given mean birefringence and random coupling angles. The Jones matrix T (ω) that

describes a concatenation of unequal sections of birefringent fiber can be expressed as [34]

$$T(\omega) = \prod_{n=1}^{N} B_n(\omega) R(\alpha_n)$$

(2.9)

$$T(\omega) = \prod_{n=1}^{N} \begin{bmatrix} e^{j\left(\sqrt{\frac{3\pi}{8}}b\omega\sqrt{h_n}/2+\phi_n\right)} & 0 \\ 0 & e^{-j\left(\sqrt{\frac{3\pi}{8}}b\omega\sqrt{h_n}/2+\phi_n\right)} \end{bmatrix} \begin{bmatrix} \cos\alpha_n & \sin\alpha_n \\ -\sin\alpha_n & \cos\alpha_n \end{bmatrix}$$

(2.10)

where N is number of segments, $B_n(\omega)$ represents the birefringence matrix of nth segment with h_n length (in km), $R(\alpha_n)$ is the matrix of a rotator that represent the random coupling angle between the segment axes, b is the PMD coefficient of the fiber in ps /√km and ω is the optical frequency in radians.

For a given value of total PMD and fiber length L, the length of the each segment is randomly generated from a Gaussian distribution around the mean length L/N with standard deviation around 20% of the mean length. The phase ϕ_n in (2.10) accounts for the small temperature fluctuations along the fiber and it is a stochastic variable with a uniform distribution between 0 and 2π. α_n is the random coupling angle between the segment axes and is a random variable with uniform distribution between 0 and 2π.

The DGD, $\Delta\tau$, for a single wavelength can be found by calculating the eigenvalues of the matrix $T_\omega(\omega)*T^{-1}(\omega)$, where $T_\omega(\omega)$ is the frequency derivative of the transmission matrix. T_ω can be approximated as $[T(\omega+\Delta\omega)-T(\omega)]/\Delta\omega$ for a small frequency step, $\Delta\omega$. The DGD is determined using the expression [1]

$$\Delta\tau = \left| \frac{\tan^{-1}\left(\frac{\rho_1}{\rho_2}\right)}{\Delta\omega} \right|$$

(2.11)

where ρ_1 and ρ_2 are the eigenvalues described above.

11

The above model, if used as described by Dal Forno et al. [34], would give insight into the Maxwellian nature of DGD and the non-periodic DGD spectral dependence. However, to match the temporal and spectral characteristics measured on a particular fiber, the free variables in the model (namely b, ϕ_n, and α_n) should be varied in accordance with the temperature and other environmental variations over the measurement period.

2.2. Previous work [Master's level research]

This section of the chapter summarizes my previous PMD research work, which is closely related to the current work. The work mainly involved making long-term measurements of DGD versus wavelength and time on three buried standard single-mode fiber spans each of ~ 95 km and analyzing the data. In this section, first the measurement setup used is described followed by the results from the data analysis.

2.2.1. Automated PMD measurement setup

The measurement setup used to make automated DGD measurements across a given wavelength band and over time using the Agilent lightwave polarization analyzer (PA) is shown in figure 2.2. Jones Matrix Eigenanalysis (JME) method is used for making DGD measurements. The measurement setup is controlled by the visual basic (VB) software running on the system controller PC. This setup can be used to measure DGD as well as polarization-dependent loss (PDL). For measuring DGD it makes use of the JME application in the polarization analyzer.

One measurement at a specific wavelength and at a specific time takes about 4 seconds. The measurement time for an across-the-band measurement is a function of the range of wavelength band and the wavelength step size used. Typically, one measurement across the 35-nm EDFA band with a step size of 0.1-nm takes about 23 minutes while one measurement across 1510 nm – 1625 nm band with a 0.1 nm step size takes about 90 minutes. The maximum measurable DGD using the JME method

varies with the wavelength step and the band of operation. As per the PA user manual [35], in the 1550-nm band the maximum measurable DGD is about 40 ps with a 0.1-nm step size and it is 4 ps with a 1-nm step size. The uncertainty in measuring DGD using JME method is also a function of step size. The uncertainty is about ± 310 fs for a 0.1-nm step size and ± 90 fs for a 1-nm step size [35].
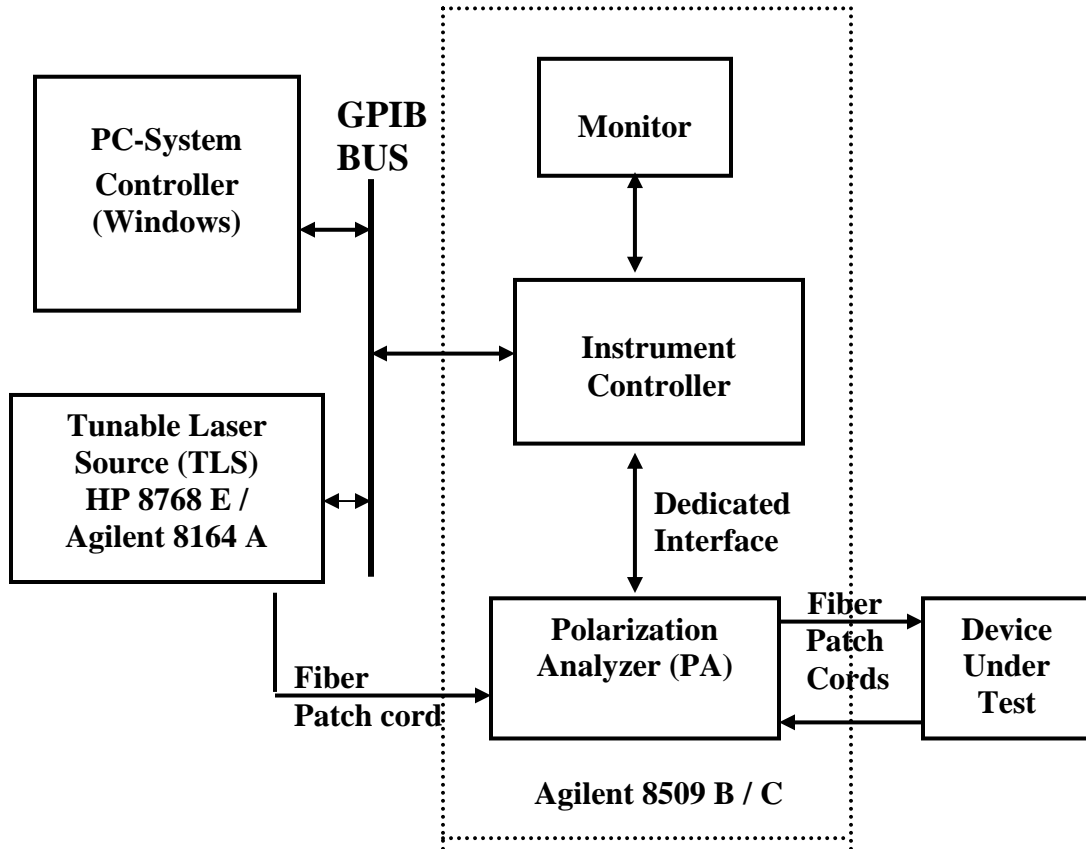
Figure 2.2. Automated PMD measurement setup.

The measured data are automatically stored into text files. The size of these files depends on the number of measurement points and they are about 8 KB to 30 KB.

The measurement system shown in figure 2.2 is usually very reliable and the measurements are stable. However, occasionally (once in a month or so) any of the instruments might become frozen and the measurements are stopped. The best thing to do to avoid loss of data due to such errors is to check the measurements often

(several times a day) and then restart the measurement system when such errors occur. To avoid losing data due to unintended power failures, uninterruptible power supplies (UPS) were used.

2.2.2. Long-term measurements of buried single-span links

2.2.2.1. Measurement setup

Single-span link 1 / Single-span link 2 /
Single-span link 3

~ 95 km

Automated PMD
measurement setup
shown in figure 2.2
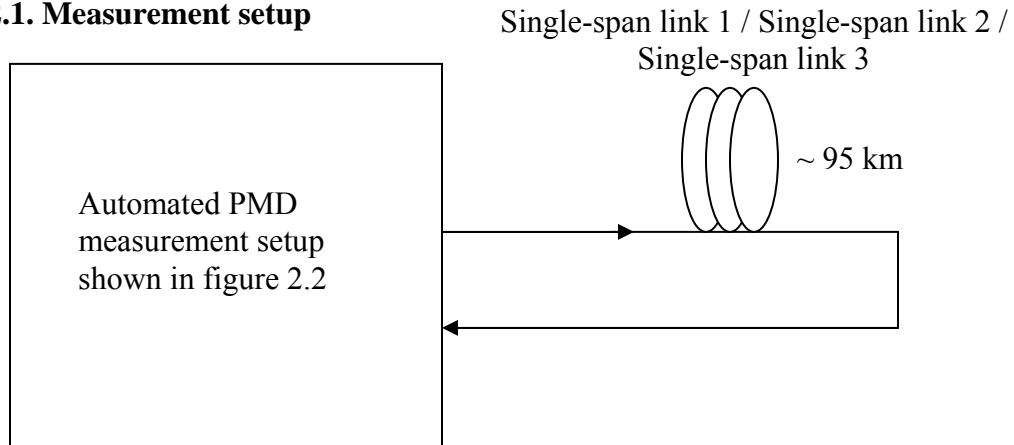
Figure 2.3. Measurement setup for characterizing buried single-span links.

2.2.2.2. Plots of DGD vs. wavelength and time

Given the dynamic nature of PMD and the low probability of excursions to intolerable levels, measurements of $\Delta\tau(\lambda, t)$ on the three buried single-span links were made over long periods to enable prediction of the potential impact of PMD on network availability. Of particular interest are the frequency and duration of these rare events. On link 1, the DGD was measured roughly every 3 hours for 86 days (692 measurements from November 9, 2001 through February 2, 2002) at wavelengths from 1510 nm to 1625 nm with a spectral resolution of 0.1 nm (about 12.5 GHz). The DGD on link 2 was measured about every 1½ hrs for 14 days (236 measurements from May 4, 2002 through May 18, 2002) over the same spectral band and with the same resolution as link 1. The DGD measurements on link 3 were repeated roughly every 1½ hrs and they were carried out for about 64 days (1072 measurements from May 29, 2002 through Aug. 1, 2002) over the same spectral band with the same resolution. The plots in figure 2.4 show the normalized DGD measured on these three single-span links in a color-coded format.

It is clear from figure 2.4 that for buried fibers, DGD changes with time. This variation is random and differs from fiber to fiber, but is very slow. This is evident by comparing figure 2.4 (b) with figures 2.4 (a) and (c). Figure 2.4 (b) corresponds to 14 days of DGD data on link 2 and no appreciable change in DGD can be observed over time in that figure, whereas in figures 2.4 (a) and (c), which show DGD data over longer periods on links 1 and 3, a significant change in DGD over time can be observed. Also, it is evident that DGD varies significantly with wavelength and relatively high-DGD events are spectrally localized.
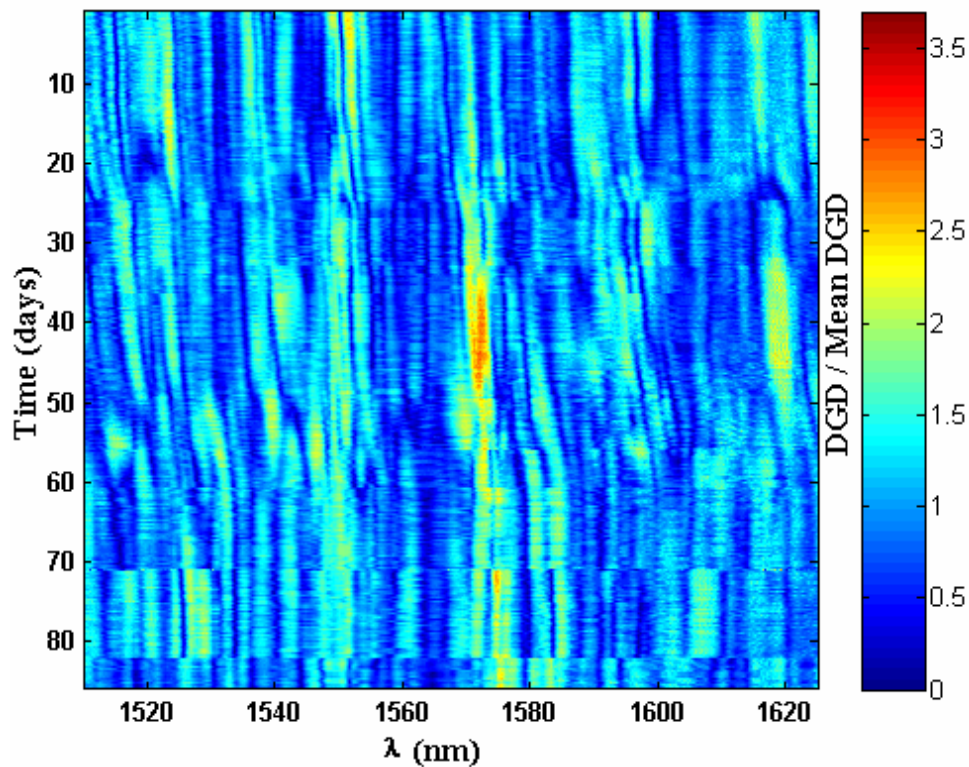
Figure 2.4. (a) Measured, normalized DGD vs. wavelength
and time on link 1 for 86 days.

15
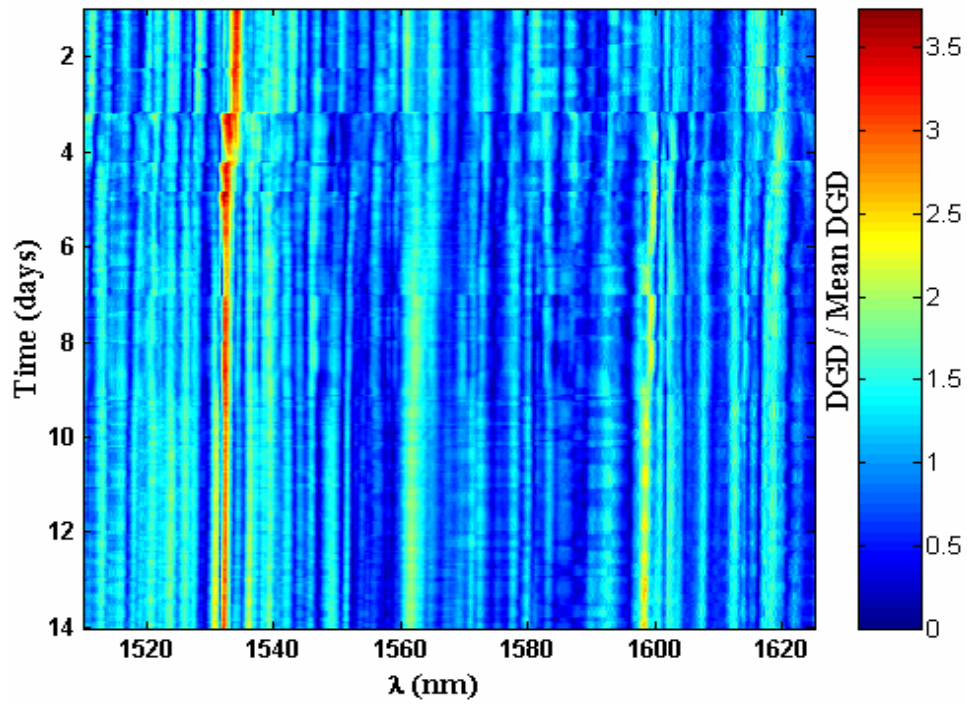
Figure 2.4. (b) Measured, normalized DGD vs. wavelength
and time on link 2 for 14 days.
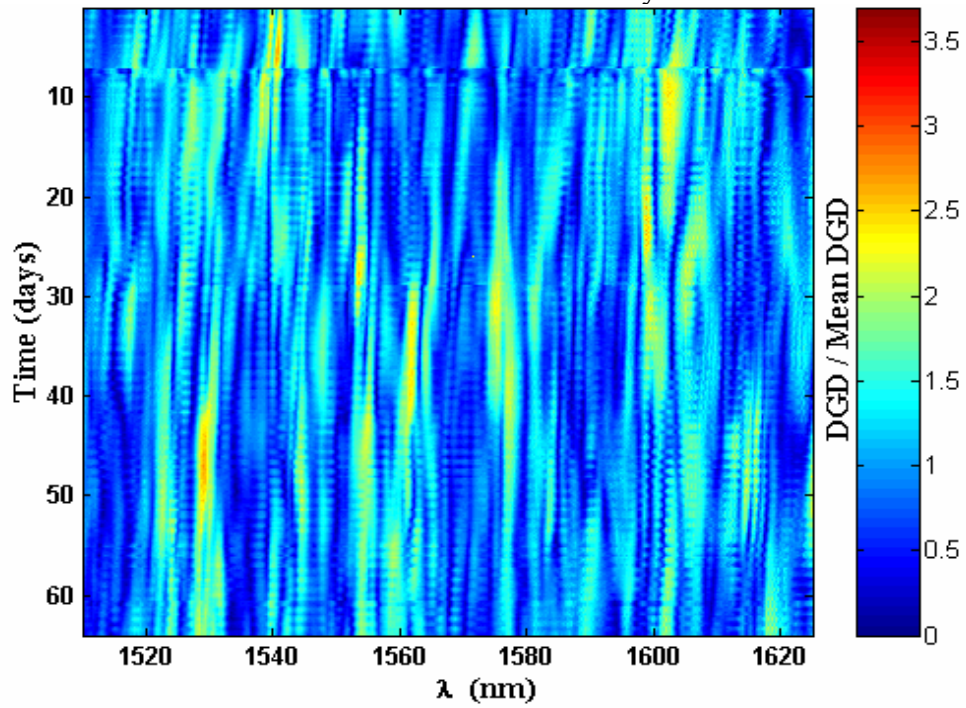
Figure 2.4. (c) Measured, normalized DGD vs. wavelength
and time on link 3 for 64 days.

2.2.2.3. Histograms of measured DGD data

Histograms of the normalized DGD data on all the three single-span links in linear and log scales are shown in figures 2.5 and 2.6. It can be observed that these histograms have shapes consistent with a Maxwellian distribution, as expected. Curves representing a Maxwellian distribution for 1-ps mean DGD are also plotted for comparison. These curves fit very well to the measured data, particularly for links 1 and 3, as there is large amount of data from these links. Results from the modified chi-square goodness-of-fit test (details of which are described in Appendix A) performed on these histograms are given in table 2.1.

Table 2.1. Results from the modified chi-square test for measured
DGD histograms on single-span links.

Fiber Configuration	Degrees of Freedom	Critical Value At Significance Level $\alpha = 0.9$	chi-square Test Statistic From Data	Hypothesis Accept or Reject?
Link 1	96	78.73	7.56	Accept
Link 2	93	76.01	482.76	Reject
Link 3	97	79.63	4.90	Accept

2.2.2.4. Mean DGD variation with time

To observe the time-dependent nature of DGD more closely, 1150 measurements of DGD over all wavelengths were averaged together to obtain frequency-averaged DGD data, denoted as $<DGD>_\lambda$ normalized by the overall mean DGD, denoted as $<<DGD>_\lambda>_t$. Since temperature is a known driver of DGD variation [7], hourly air temperature data for the region were obtained from National Climatic Data Center website [36]. The variation of normalized frequency-averaged DGD and temperature with time on the three single-span links is shown in figure 2.7. From those plots it can be observed that the variation in frequency-averaged DGD is less than 10 % over the measurement period. It is apparent (see top plot figure 2.7) that longer-term temperature variations do correlate with variations in the frequency-averaged mean DGD.
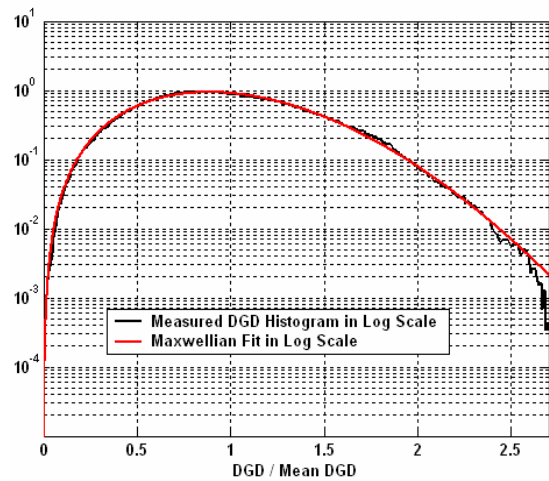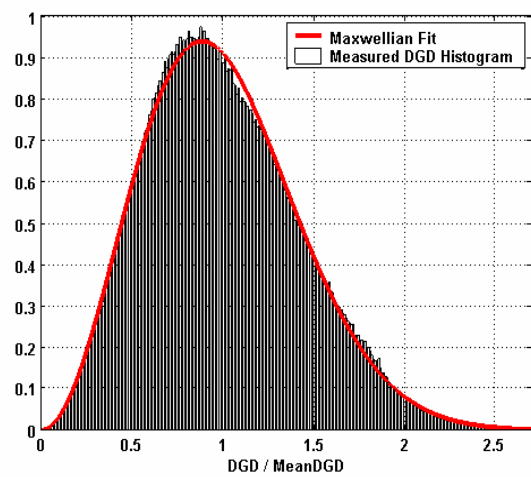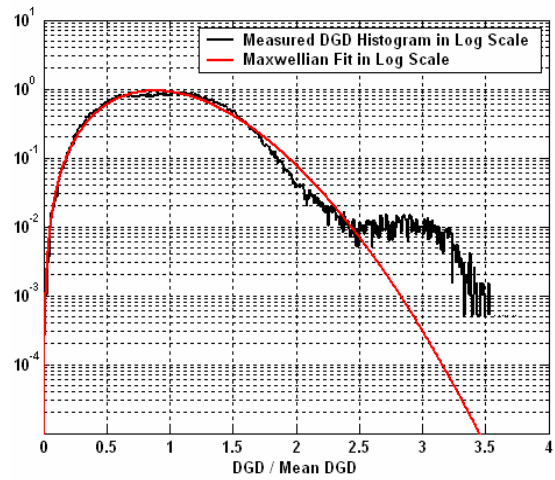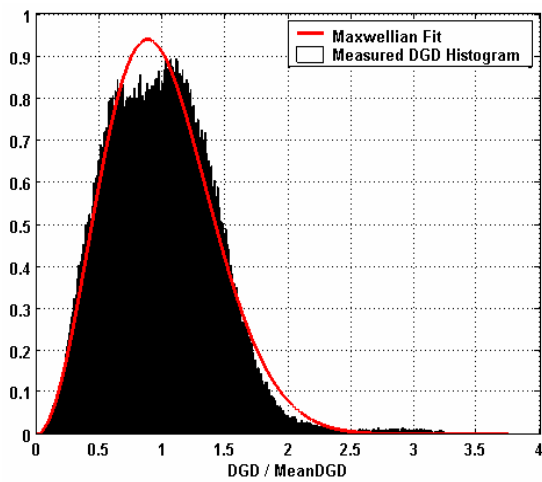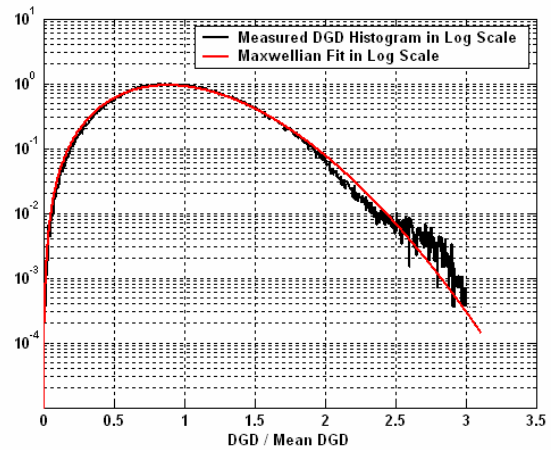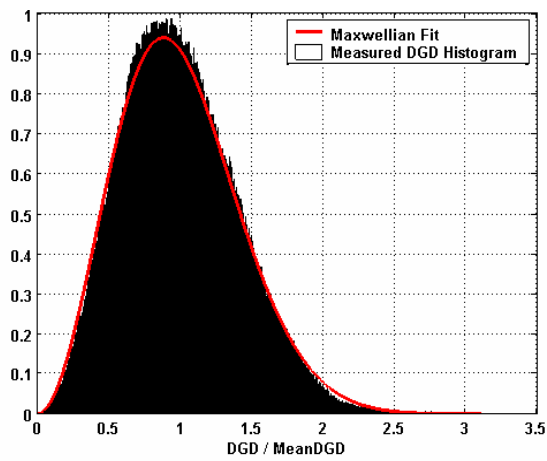
Figure 2.5. Histogram of measured, normalized DGD data in linear scale on link 1 (top), link 2 (middle) and link 3 (bottom).

Figure 2.6. Histogram of measured, normalized DGD data in log scale on link 1 (top), link 2 (middle) and link 3 (bottom).
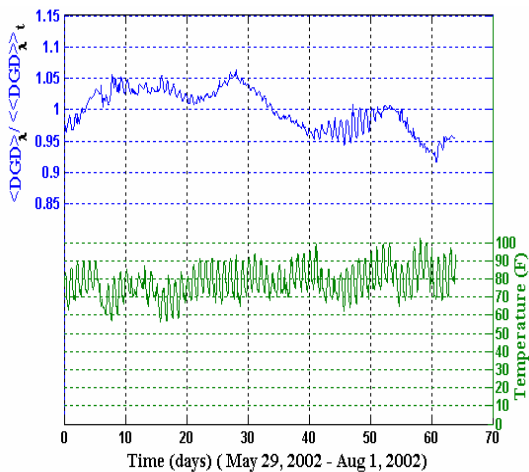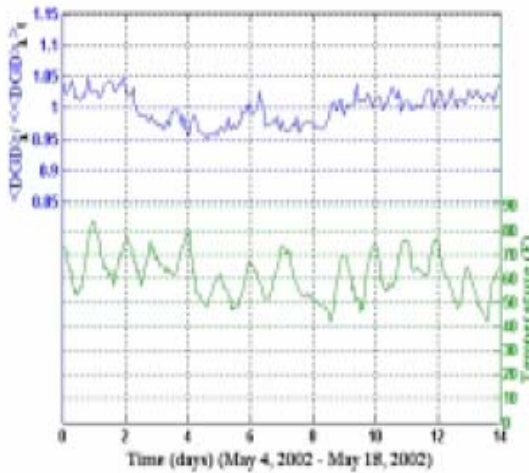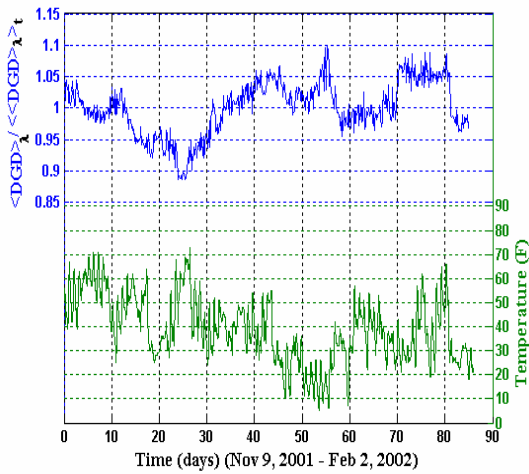
Figure 2.7. Frequency-averaged DGD and air temperature vs. time for link 1 (top), link 2 (middle) and link 3 (bottom).
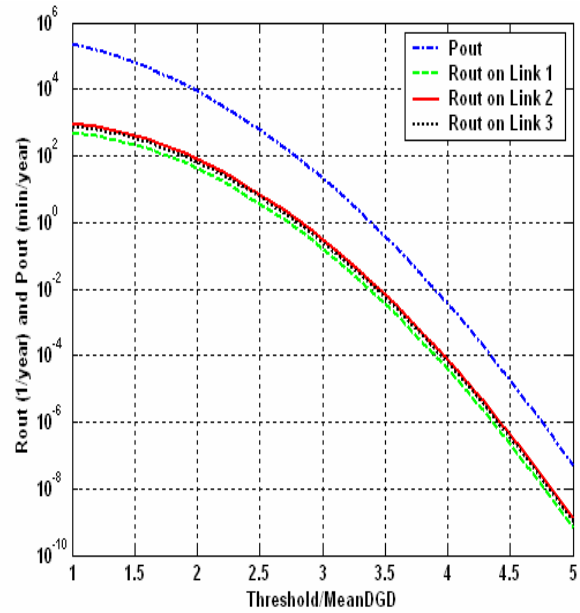
Figure 2.8. Calculated outage probability, P_{out}, and relative mean outage rate R_{out}, versus threshold/mean DGD for the three single-span links.
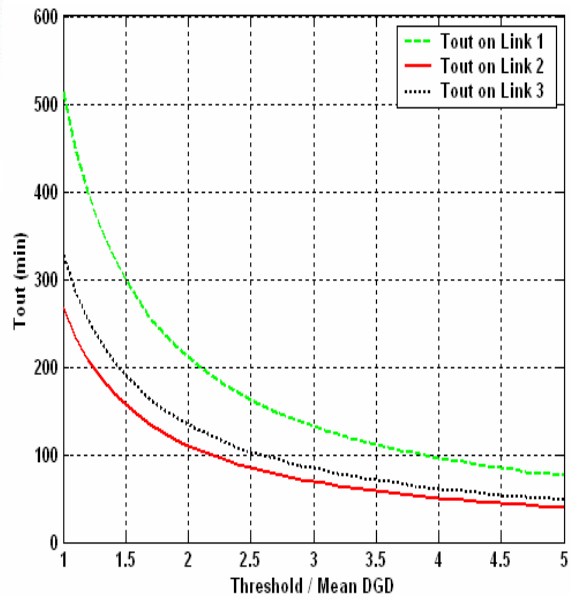
Figure 2.9. Calculated relative mean outage duration, T_{out}, as a function of threshold/mean DGD for the three single span links.

19

2.2.2.5. System outage analysis

A detailed discussion of theoretical concepts of system outage analysis was presented in section 2.1.3. Following that discussion, the outage probability P_{out}, is determined using the Maxwellian distribution, the mean outage rate R_{out} and the mean outage duration T_{out} are determined from the measured DGD data on the three fibers.

Figure 2.8 shows the calculated outage probability, P_{out}, and the relative mean outage rate, R_{out}, (actual mean outage rate multiplied by the mean DGD (in ps) of the link) for a given system threshold relative to the mean DGD on the three links. Figure 2.9 shows the calculated relative mean outage duration, T_{out}, (actual mean outage duration divided by the mean DGD (in ps) of the link) as a function of system threshold relative to the mean DGD on the three links.

From the above analysis, we can estimate the relative mean time between outages (MTBO) and relative mean outage durations for various DGD tolerances for these links. Table 2.2 lists these values for system thresholds of 3 and 3.7 times the mean DGD. To determine the actual values, the relative values in table 2.2 should be multiplied by the mean DGD (in ps) of the link. For example, if the mean DGD were 2 ps (not the actual value), MTBO for a threshold of 3 times mean DGD would be 12.78 years and the mean outage duration would be 272 minutes.

Table 2.2. Predicted relative mean time between outages (MTBO) and relative mean outage durations for different DGD tolerances.

	3*\<DGD\>	**3.7*\<DGD\>**
Link 1 MTBO Outage duration	6.39 years 136 min	1648 years 108 min
Link 2 MTBO Outage duration	3.25 years 69 min	833 years 55 min
Link 3 MTBO Outage duration	3.96 years 84 min	1021 years 67 min

2.2.3. Long-term measurements of two-span links

To study the behavior of PMD on links of greater length, experiments were conducted to measure the instantaneous DGD on two fiber spans concatenated with an EDFA in between, with an effective length of about 190 km. Three different combinations of the three single-span fibers were used in the experiments. Single-span links 1 and 2 were concatenated to form the two-span link 1-2, single-span links 2 and 3 were concatenated to form the two-span link 2-3 and likewise links 1 and 3 were concatenated to form the two-span link 1-3. The measurement setup for these experiments is shown in figure 2.10.

Measurements of two-span links were made at wavelengths from 1535 nm to 1565 nm and were repeated once every 23 minutes. Since EDFAs were used in the loop, the λ-band had been reduced to the EDFA band. Measurements were carried on for 18 days on link 1-2 (Aug. 22, 2002-Sept. 9, 2002), for 21 days on link 2-3 (Aug. 1, 2002-Aug. 22, 2002) and for 16 days on link1-3 (Sept. 27, 2002-Oct. 13, 2002).

2.2.3.1 Measurement setup
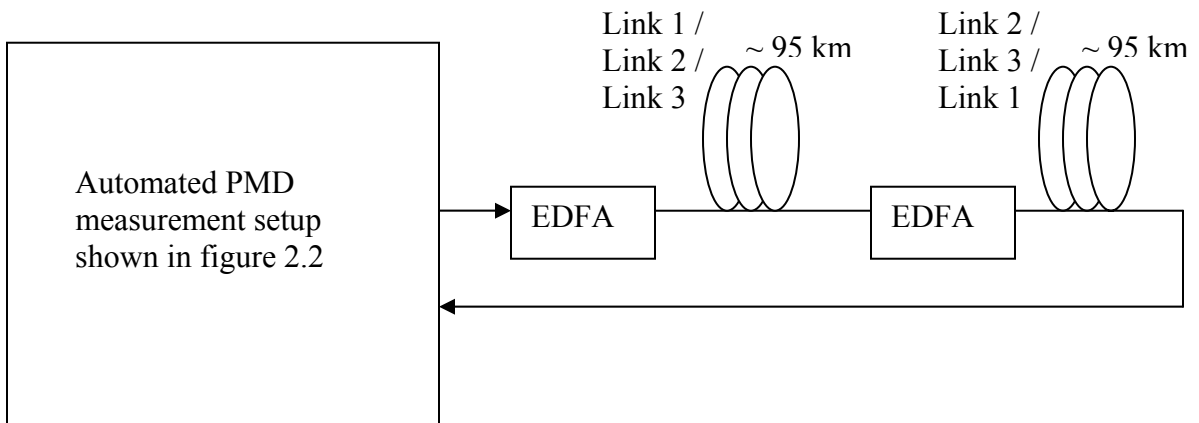
Figure 2.10. Measurement setup for characterizing the concatenated fiber spans.

2.2.3.2. Plots of DGD vs. wavelength and time

The plots in figure 2.11 show the normalized DGD measured on the three two-span links respectively in color-coded format.
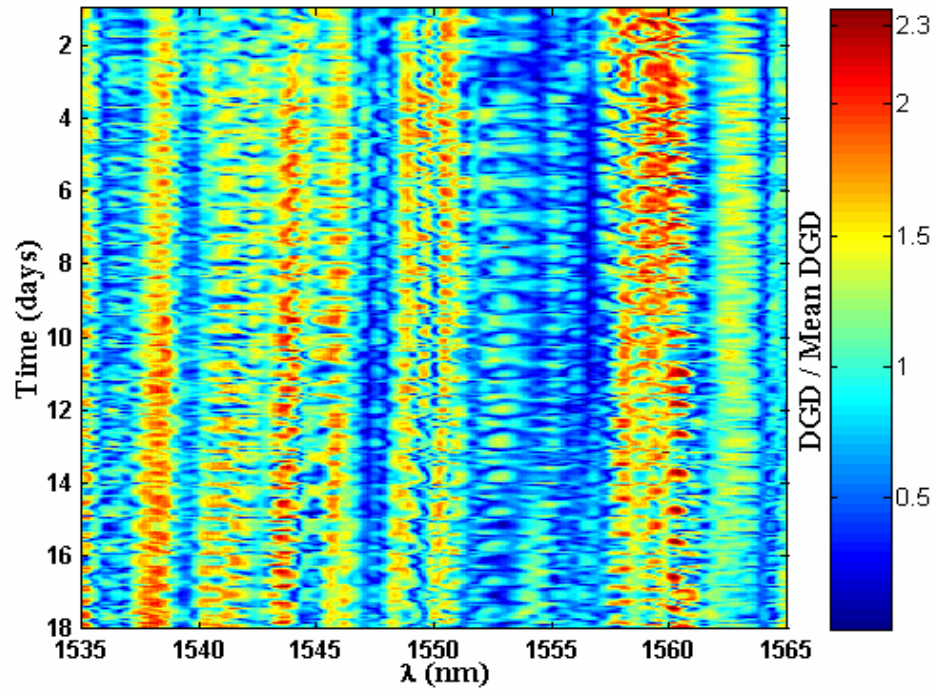
Figure 2.11. (a) Measured, normalized DGD vs. wavelength
and time on two-span link 1-2 for 18 days.
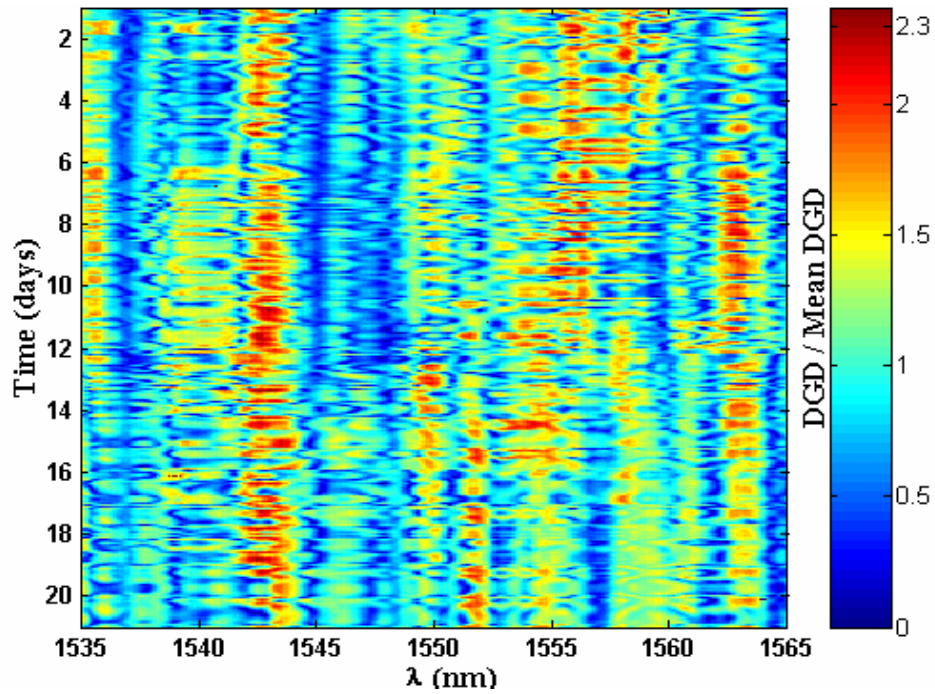
Figure 2.11. (b) Measured, normalized DGD vs. wavelength
and time on two-span link 2-3 for 21 days.
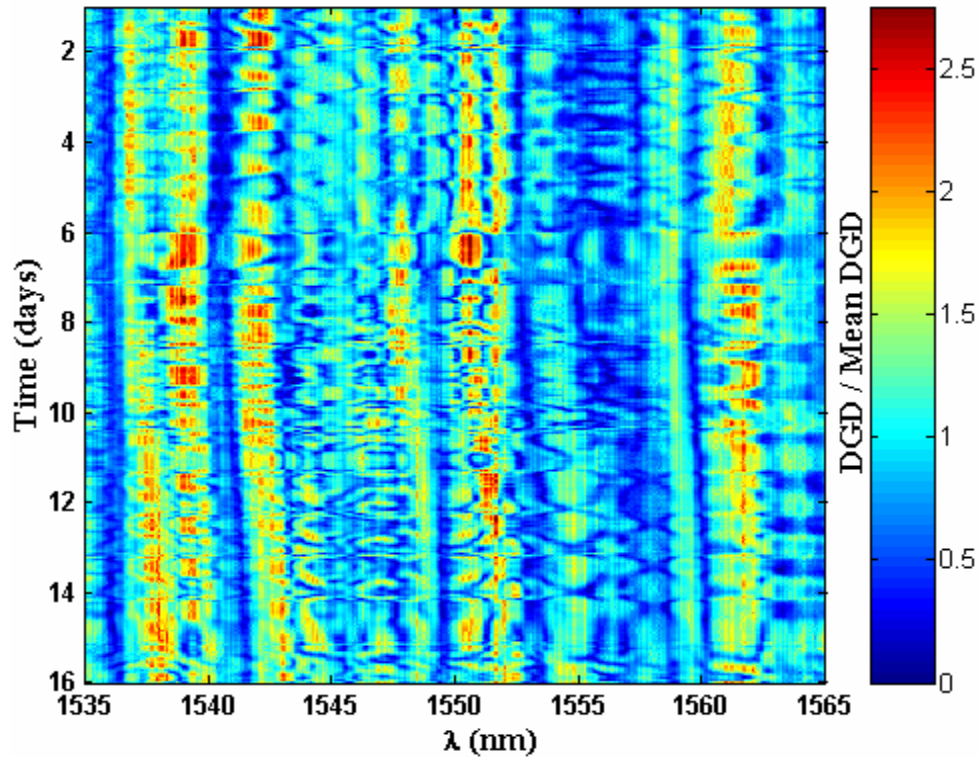
Figure 2.11. (c) Measured, normalized DGD vs. wavelength
and time on two-span link 1-3 for 16 days.

It can be observed from the color maps in figure 2.11 that the DGD on the two-span links changes with time and wavelength. However, unlike the single-span links, the variation of DGD with time on two-span links is more rapid. This might be due to the fact that on two-span links, light is transmitted through the first buried fiber span, amplified at the end of first span in the laboratory and then retransmitted through the second buried span. The temperature of the laboratory was not maintained at a constant value and so it varied during the day. To observe any periodic variations in the DGD a discrete Fourier transform (DFT) of the DGD data is obtained and examined. Figure 2.12 shows normalized DGD variations with time at 1560 nm wavelength on link 1-2. Figure 2.13 shows the DFT of the DGD data (with mean value subtracted). It can be observed from figure 2.13 that there are many periodic components, however, the 1-day component is the most dominant followed by the ½ day component. Even though the mean value is subtracted from the data, the

DC component in figure 2.13 is still relatively strong. This might be because of the variation of mean DGD over time. Similar observations were made at other wavelengths as well which showed similar results.
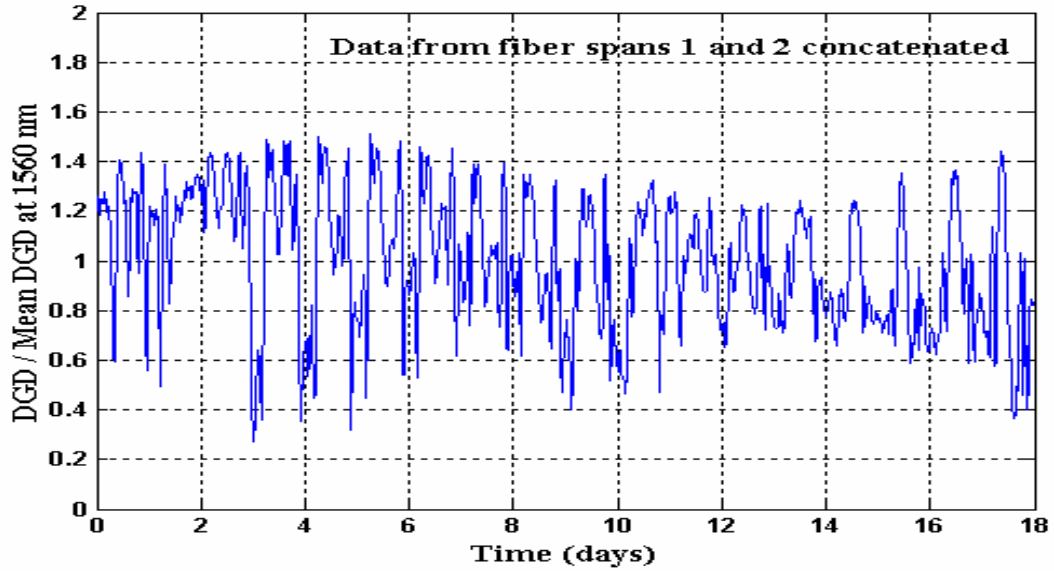
Figure 2.12. DGD/Mean DGD vs. Time at 1560 nm on link 1-2.
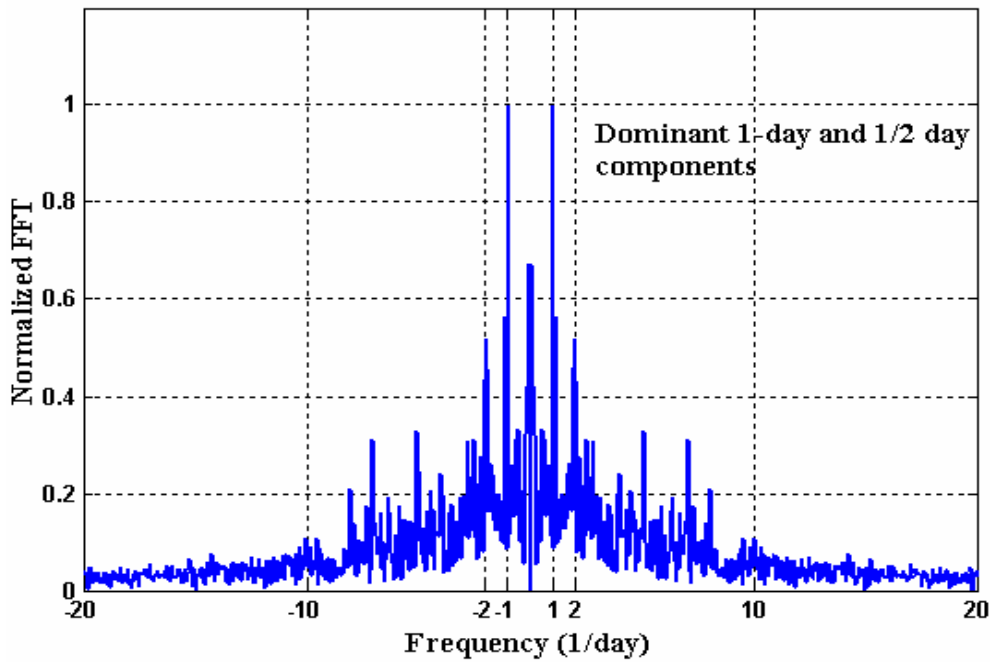
Figure 2.13. DFT of DGD at 1560 nm with mean value subtracted from DGD data.

2.2.3.3. Histograms of measured DGD data

To verify the Maxwellian nature of the measured DGD, histograms of the normalized DGD data measured on the three two-span links are obtained in linear and log scales and are shown in figures 2.14 and 2.15. Curves representing a Maxwellian distribution for 1-ps mean DGD are also plotted for comparison. It can be observed from the figures that the histograms show a good agreement with the theoretical Maxwellian curve-fits. Results from the modified chi-square goodness-of-fit test (details of which are described in Appendix A) performed on these histograms are given in table 2.3.

Table 2.3. Results from the modified chi-square test for measured
DGD histograms on two-span links.

Fiber Configuration	Degrees of Freedom	Critical Value At Significance Level $\alpha = 0.9$	chi-square Test Statistic From Data	Hypothesis Accept or Reject?
Link 1-2	100	82.36	211.88	Reject
Link 2-3	100	82.36	65.7	Accept
Link 1-3	90	73.29	53.04	Accept

2.2.3.4. Mean DGD variation with time

The variation of frequency-averaged DGD data, denoted as $<DGD>_\lambda$ normalized by the overall mean DGD, denoted as $<<DGD>_\lambda>_t$ and temperature with time on the three concatenated fiber spans is shown in figure 2.16. The temperature shown in these plots is the hourly air temperature data for the region and not the laboratory temperature. It can be observed from the plots in figure 2.16 that the variation in frequency-averaged DGD on the link 1-2 and link 1-3 is less than 10 % over the measurement period and is less than 20 % on link 2-3.
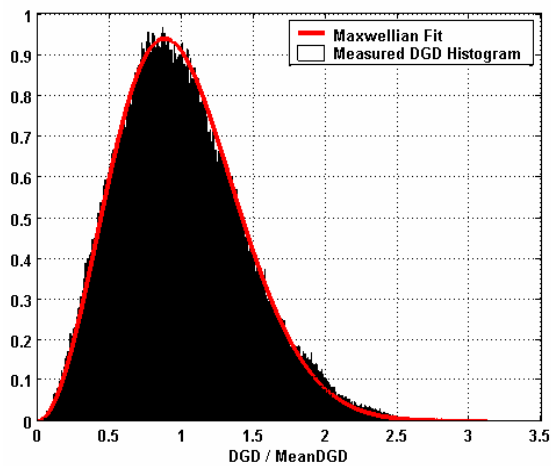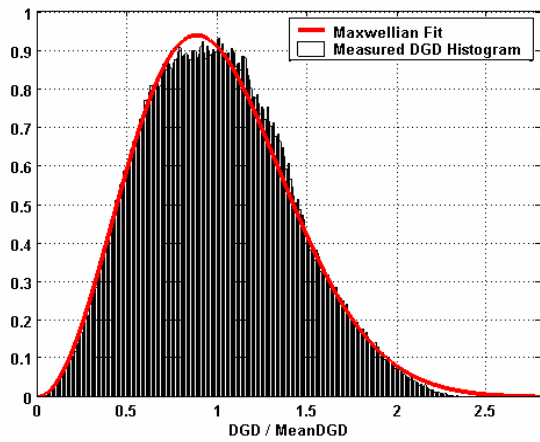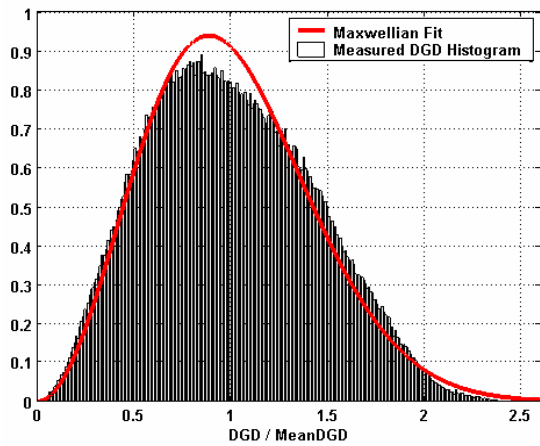
Figure 2.14. Histogram of measured, normalized DGD data on two-span links in linear scale; link 1-2 (top), link 2-3 (middle), and link 1-3 (bottom).
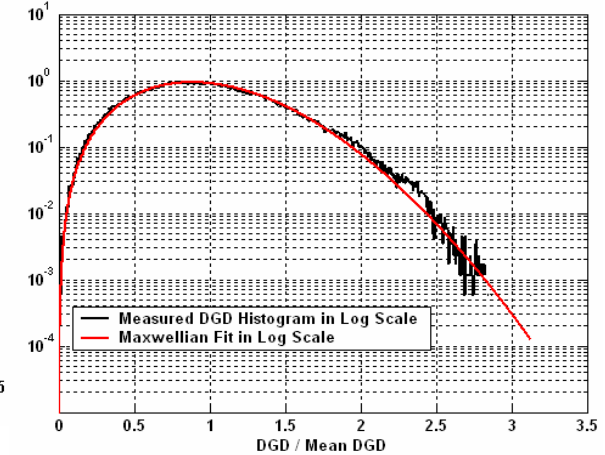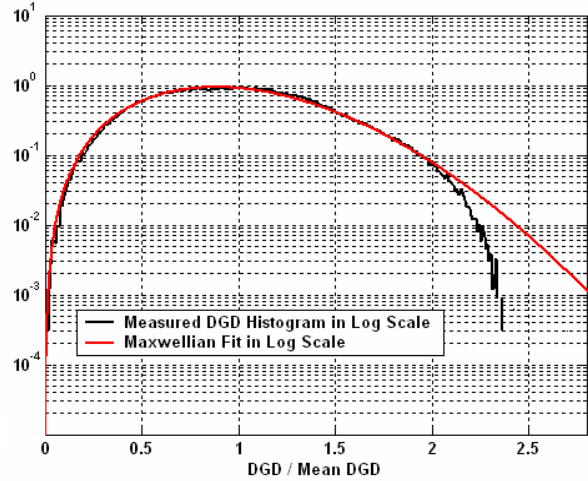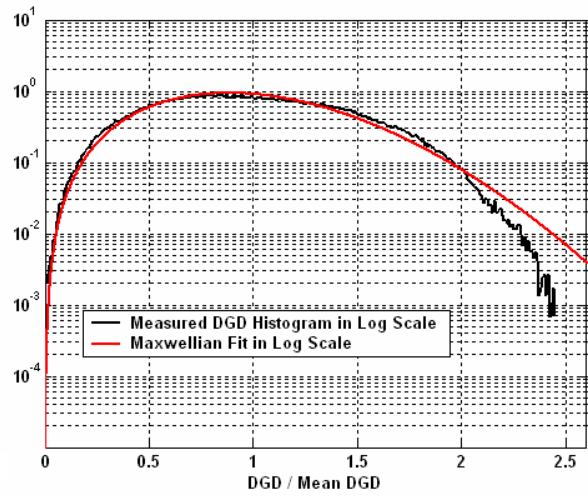
Figure 2.15. Histogram of measured, normalized DGD data on two-span links in log scale; link 1-2 (top), link 2-3 (middle), and link 1-3 (bottom).

Figure 2.17. Calculated outage probability, P_{out}, and relative mean outage rate R_{out}, versus threshold/mean DGD for the two-span links.
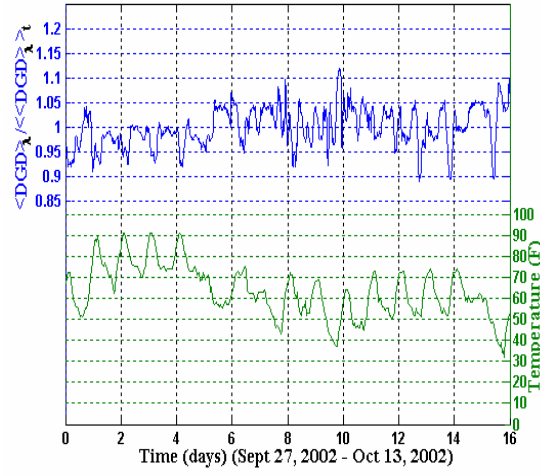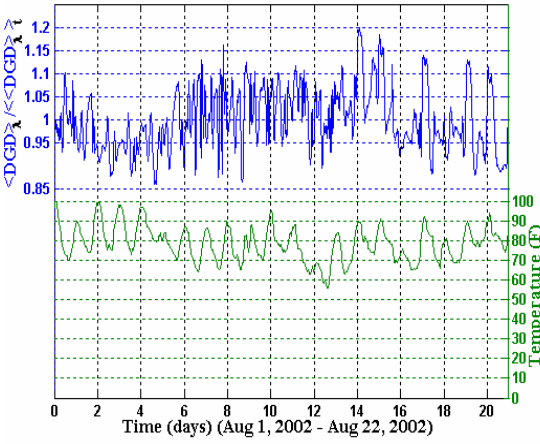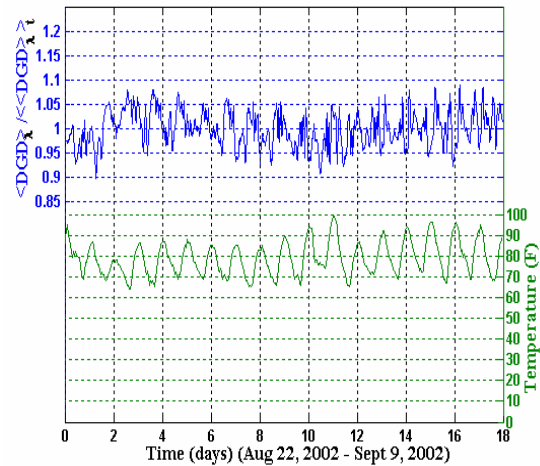
Figure 2.16. Frequency-averaged DGD and air temperature vs. time for two-span links; link 1-2 (top), link 2-3 (middle) and link 1-3 (bottom).
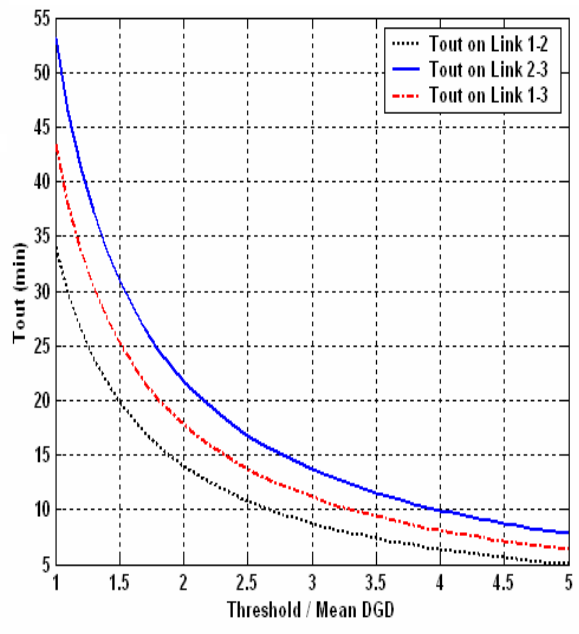
Figure 2.18. Calculated relative mean outage duration, T_{out}, as a function of threshold/mean DGD for the two-span links.

2.2.3.5. System outage analysis

The outage probability, P_{out}, for different threshold values is calculated from the Maxwellian distribution using (2.6). The mean outage rate, R_{out}, and the mean outage duration, T_{out}, for different threshold values are calculated from the DGD data measured on the two-span links using (2.7) and (2.8) respectively. The calculated P_{out}, relative R_{out} and relative T_{out} values as a function of normalized threshold are shown in figures 2.17 and 2.18. Table 2.4 lists the values of relative mean time between outages (MTBO) and relative mean outage durations for system thresholds of 3 and 3.7 times the mean DGD.

A comparison of values from table 2.4 with those of table 2.2 by taking into account the actual mean DGD values (not mentioned in this report) showed that the outage rates are higher for two-span links than for single-span links and the corresponding outage durations are lower for the two-span links. In section 2.2.3.2, from the color maps of the DGD we observed that the DGD varied at a much faster rate with time on two-span links compared to the single-span links. As a result the chances of an outage occurrence also increase. On single-span links, for example link 1, DGD drifted at a very slow rate and so it takes years to observe a high-DGD outage event (like 3.7 times the mean). On the other hand, since DGD drifted at a much higher rate on the two-span links the rate occurrence of a high-DGD outage event is higher but the outage event lasts for a much shorter duration.

Table 2.4. Predicted relative mean time between outages (MTBO) and mean outage durations for different DGD tolerances.

	3*<DGD>	3.7*<DGD>
Link 1-2 MTBO Outage duration	0.413 years 9 min	106 years 7 min
Link 2-3 MTBO Outage duration	0.644 years 14 min	167 years 11 min
Link 1-3 MTBO Outage duration	0.525 years 11 min	135 years 9 min

2.2.4. Long-term measurements of the three-span link

To study the behavior of PMD on links of greater length, experiments were conducted to measure the instantaneous DGD on the three single-span links concatenated with an effective length of about 285 km. These measurements were possible only after placing EDFAs along two of the three links. Measurements of the three-span link 1-2-3 were made at wavelengths from 1535 nm to 1565 nm with a wavelength step of 0.1 nm and were repeated once every 23 minutes. Measurements were carried on for 34 days from April 13, 2004 - May 17, 2004.

2.2.4.1. Measurement setup
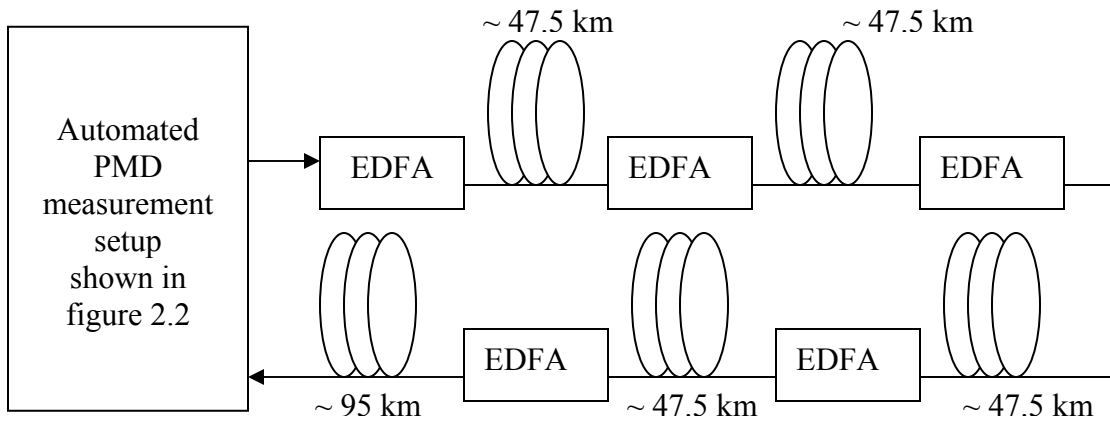
Figure 2.19. Measurement setup for characterizing the three-span link 1-2-3.

2.2.4.2. Plot of DGD vs. wavelength and time

The plot in figure 2.20 shows the normalized DGD measured on the three-span link 1-2-3 using the set up shown in figure 2.19 in color-coded format. The mean DGD of the link (the actual value not mentioned) was observed to satisfy the concatenation rule which says that the effective DGD on concatenated fiber spans is the square root of the sum of the squares of the mean DGD on individual fiber spans. It can be observed from the color map in figure 2.20 that the DGD on three-span link 1-2-3 changes with time and wavelength. Moreover, the change in DGD with time is rapid just like the two-span links. This might be again due to the fact that one end of each of the fiber span is in the laboratory where the temperature was not maintained constant.
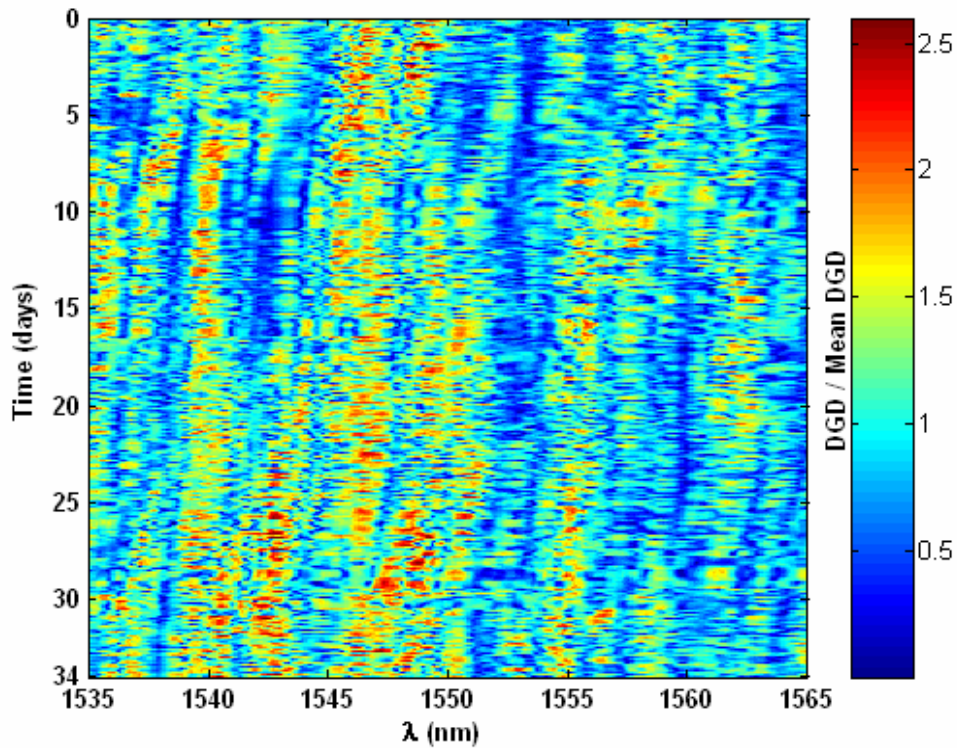
Figure 2.20. Measured, normalized DGD vs. wavelength
and time for the three-span link 1-2-3.

2.2.4.3. Histogram of measured DGD data

The histogram of the normalized DGD obtained from measured data in linear and log scales is shown in figure 2.21. A curve representing Maxwellian distribution for 1-ps mean DGD is also plotted for comparison. It can be observed from the figure that the histogram is in good agreement with the theoretical Maxwellian curve-fit. Results from the modified chi-square goodness-of-fit test (details of which are described in Appendix A) performed on these histograms are given in table 2.5.

Table 2.5. Results from the modified chi-square test for measured
DGD histograms on the three-span link 1-2-3.

Fiber Configuration	Degrees of Freedom	Critical Value At Significance Level $\alpha = 0.9$	chi-square Test Statistic From Data	Hypothesis Accept or Reject?
Link 1-2-3	100	82.36	20.74	Accept
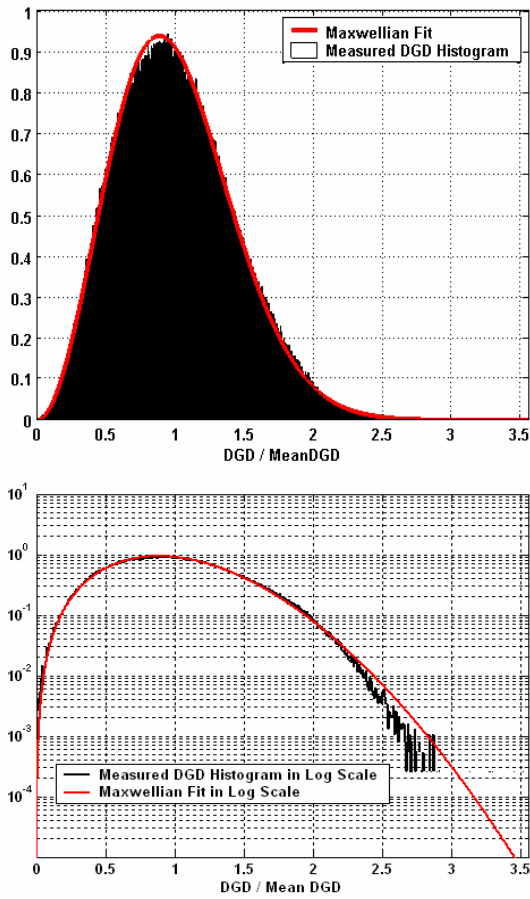
Figure 2.21. Histogram of measured, normalized DGD data on the three-span link 1-2-3 in (a)linear (top) and (b) log (bottom) scales.
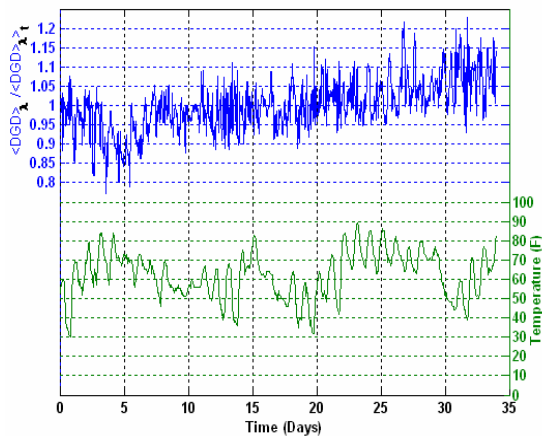
Figure 2.22. Frequency-averaged DGD and air temperature vs. time for the three-span link 1-2-3.
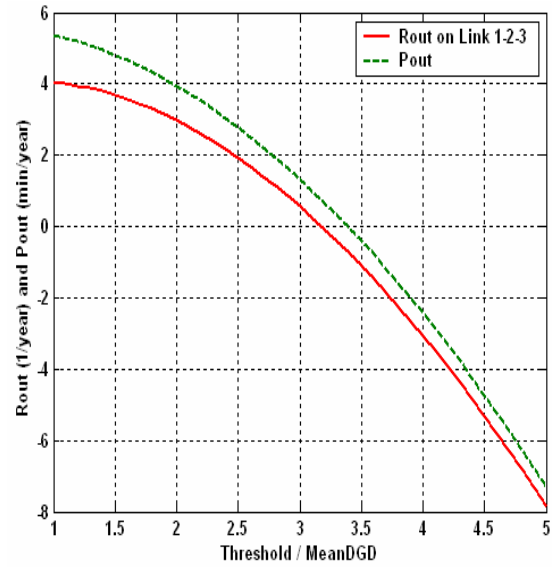

Figure 2.23. Calculated outage probability, P_{out}, and relative mean outage rate R_{out}, versus threshold/mean DGD for the three-span link 1-2-3.
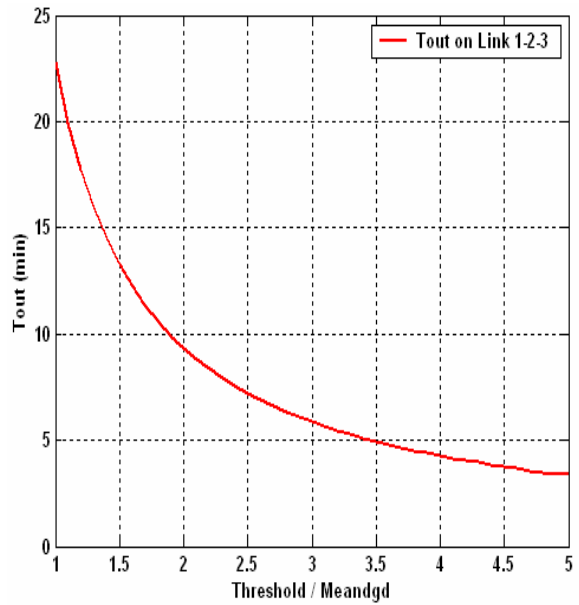

Figure 2.24. Calculated relative mean outage duration, T_{out}, as a function of threshold/mean DGD for the three-span link 1-2-3.

31

2.2.4.4. Mean DGD variation with time

The variation of frequency-averaged DGD data, denoted as $<DGD>_\lambda$ normalized by the overall mean DGD, denoted as $<<DGD>_\lambda>_t$ and temperature with time on the three-span link is shown in figure 2.22. The temperature shown in these plots is the hourly air temperature data for the region and not the laboratory temperature. It can be observed from figure 2.22 that the variation in frequency-averaged DGD on the link 1-2-3 is less than 20 % over the measurement period.

2.2.4.5. System outage analysis

The outage probability, P_{out}, for different threshold values is calculated from the Maxwellian distribution using (2.6). The mean outage rate, R_{out}, and the mean outage duration, T_{out}, for different threshold values are calculated from the DGD data measured on the three-span link using (2.7) and (2.8) respectively. The calculated P_{out}, relative R_{out} and relative T_{out} values as a function of normalized threshold are shown in figures 2.23 and 2.24. Table 2.6 lists the relative values of the mean time between outages (MTBO) and the mean outage durations for system thresholds of 3 and 3.7 times the mean DGD.

Table 2.6. Predicted relative mean time between outages (MTBO) and mean outage durations for different DGD tolerances.

	3*<DGD>	**3.7*<DGD>**
Link 1-2-3 MTBO Outage duration	0.2762 years 6 min	71 years 4.6 min

A comparison of the values from table 2.6 with those of table 2.4 and table 2.2 by taking into the account the actual mean DGD values showed that the outage rates are much higher for the three-span link than for the two- and single-span links and the outage durations are correspondingly lower for the three-span link. However, the increase in the outage rates from two-span links to the three-span link is not as high as it is from single-span links to the two-span links.

2.3. Objective of the current work

The objective of the current work is to expand on the common understanding of the temporal behavior of PMD and predict PMD-induced outage rates on long-haul optical fiber links. This can be achieved through a three-fold process:

1. Simplify the expression for predicting first-order PMD outage rates given by Caponi et al. [1] into a simple closed-form expression that depends only on two parameters

2. Enhance the existing numerical model for PMD to include the temporal component and then, using the enhanced model, simulate the PMD characteristics observed from the measurements on the seven different fiber configurations discussed in chapter 2 to validate the model.

3. Using the enhanced PMD model, simulate the PMD characteristics on long-haul optical fiber links of different lengths and use this information along with the simplified first-order PMD outage rate expression to predict the outage rates on long-haul links and study the variation of the PMD outage rates with link length.

Step 1 can be achieved first by determining the histograms of measured DGD time derivative ($\Delta\tau'$) numerically and fitting a standard probability density function (PDF) curve to them and then simplifying the integral in (2.7) using the expression for the standard PDF fit. In step 2, the enhancements to the PMD model include incorporating the knowledge of temporal and spectral nature of PMD gained through detailed analyses of measured DGD data on different buried fiber links discussed in chapter 2. The basic idea of steps 2 and 3 is to use the enhanced model first to simulate the temporal and spectral nature of PMD observed from the measurements on relatively short length fiber links and then predict the temporal and spectral characteristics of PMD on long-haul optical links. Using this information and the simplified PMD outage rate expression, first-order PMD outage rates and durations are predicted on long-haul optical fiber links.

2.3.1. Significance of the current work

The above-mentioned work is very significant in the sense that it enables the network engineers to predict quantitatively the impact of PMD, in terms of the outage rates, while planning ultra long-haul all optical fiber links. This work also gives insight into the variation of the outage rates with link length, the knowledge of which is very useful in designing long-haul links. Using the enhanced model it is possible to simulate the PMD characteristics of a long-haul optical link of arbitrary length and with arbitrary number of spans.

In this report the PMD outage analysis is limited to only first-order. This does not mean that second- and other higher-order PMD effects are insignificant. It was reported [37] that the frequency dependence of PMD becomes significant only in systems with relatively high mean DGD values. However, first-order PMD is still an issue on fibers with relatively low mean DGD and it needs to be dealt with properly to ensure network reliability. A solid understanding of the first-order PMD outage analysis itself is lacking within the PMD community and as of now there is not a single model available that would help study the first-order outage analysis (some statistical models are available) and to my knowledge no group is working on such a thing. Hence this work will be a good step forward in understanding the effects of PMD on network availability.

Moreover, the enhanced PMD model is not limited to just first-order. Second- and other higher-order PMD information, including PSP information, can be extracted from the model, which would facilitate the higher-order PMD outage analysis.

3. SIMPLIFIED FIRST-ORDER PMD OUTAGE RATE EXPRESSION

3.1. The PDF of DGD time derivative (Δτ')

In chapter 2 the PMD-induced outage rates (R_{out}) on the single-span, two-span and the three-span links were calculated using (2.7). However, while calculating those outage rates the integral in (2.7) was evaluated numerically using measured DGD data. In order to simplify (2.7) into a closed-form expression, the next logical step is to study the PDF of the DGD time derivative (Δτ') and determine, if possible, a mathematical expression for it. Then, the expression for PDF of Δτ' could be used to simplify the integral in (2.7) thereby expressing (2.7) in a closed-form.

To determine the PDF of Δτ', first Δτ' values were calculated by numerically differentiating the measured DGD data on the seven links, discussed in section 2.3, and then the histograms of Δτ' were obtained from the calculated data in linear and log scales, which are shown in figures 3.1 to 3.7. Through curve fitting it was determined emperically that these histograms closely resemble a Laplacian PDF (a two-sided, first-order exponential) of the form

$$f_{\tau'}(\Delta\tau') = \frac{\alpha}{2}e^{-\alpha|\Delta\tau'|} \tag{3.1}$$

where $\alpha = \dfrac{\sqrt{2}}{\sigma}$ and is the Laplacian parameter with units of hours/picosecond and σ is the standard deviation of Δτ'. For comparison, Laplacian fits with corresponding α values are also shown in figures 3.1 to 3.7. This finding was reported in [38].To determine how good the agreement is between the measured Δτ' histograms and their corresponding Laplacian fits, modified chi-square goodness-of-fit test (described in Appendix A) is applied in each case and the results from these tests are listed in table 3.1. From the table a good agreement is evident.
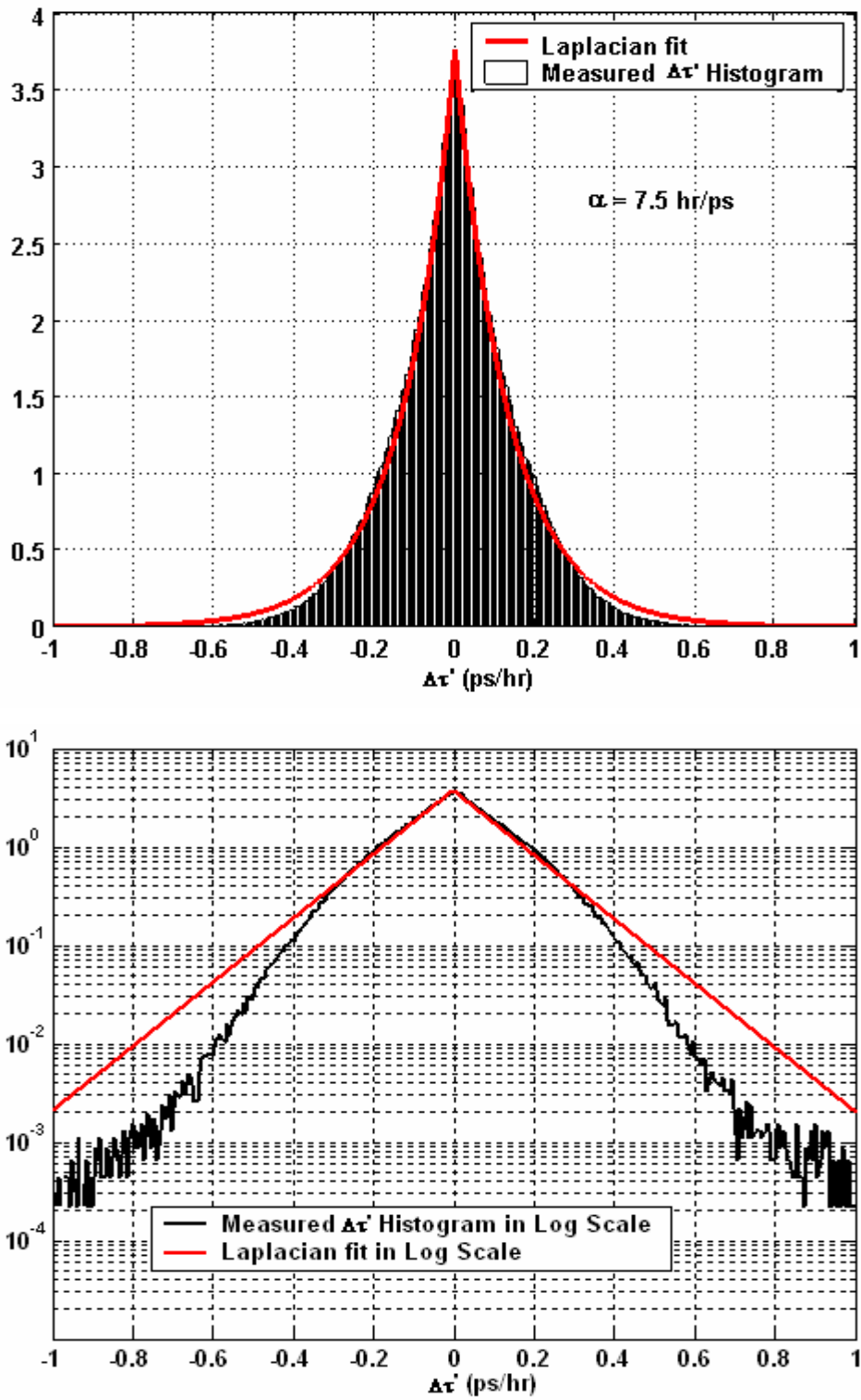
Figure 3.1. Histogram of measured $\Delta\tau'$ data from Link 1 and its Laplacian fit in (a) linear scale (top) and (b) log scale (bottom).
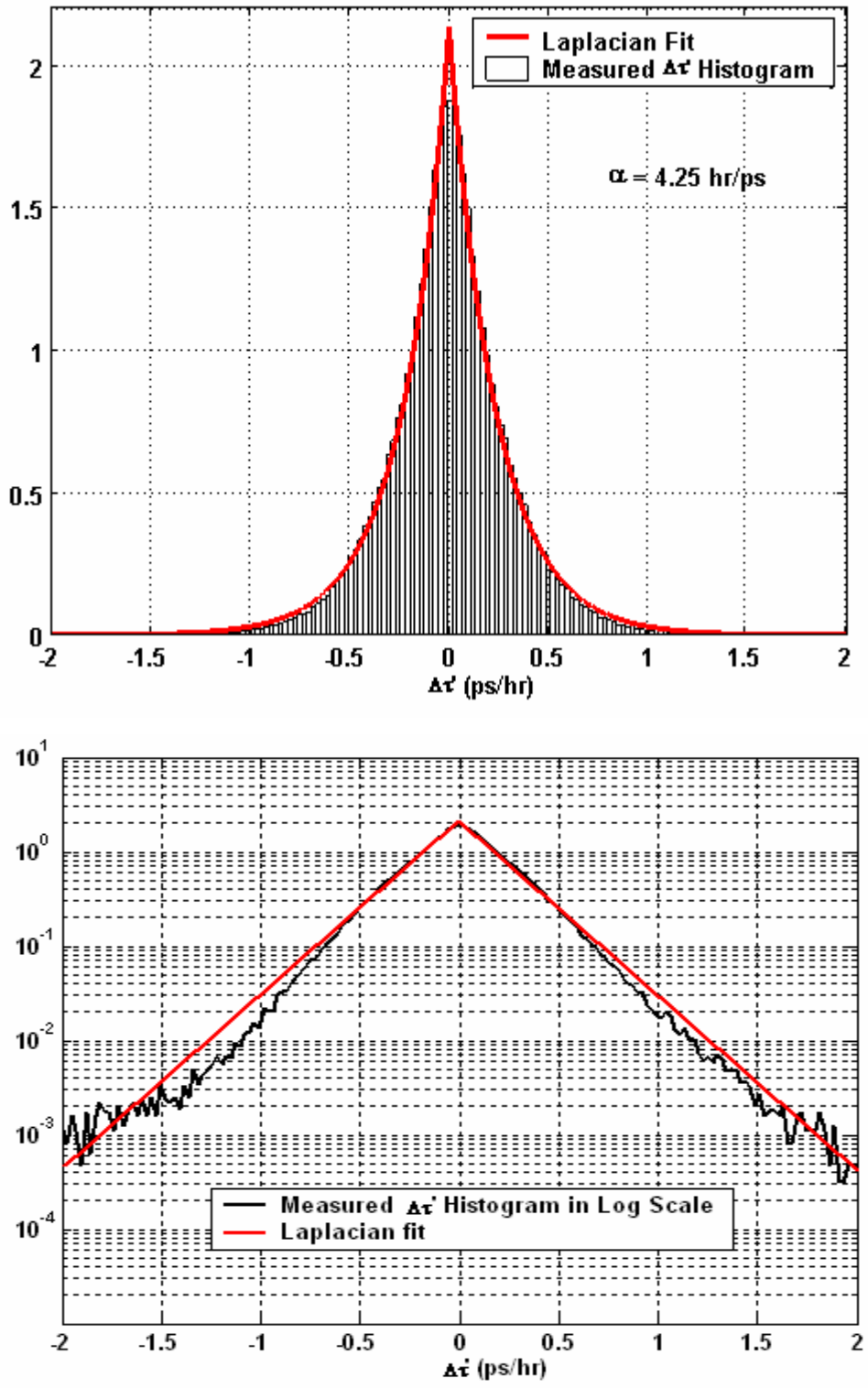
Figure 3.2. Histogram of measured $\Delta\tau'$ data from Link 2 and its Laplacian fit in (a) linear scale (top) and (b) log scale (bottom).
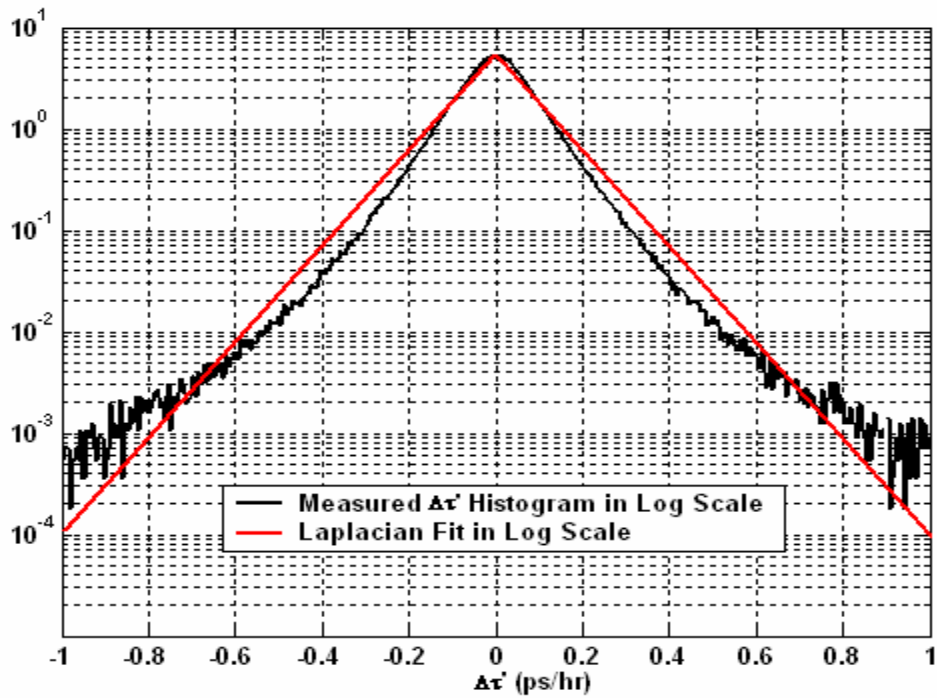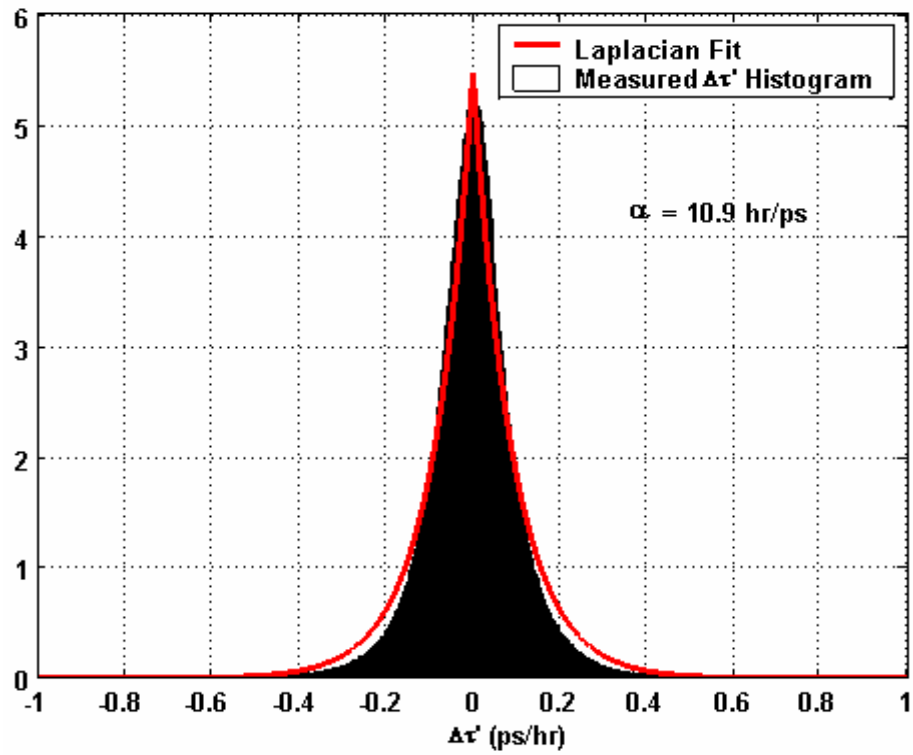
Figure 3.3. Histogram of measured Δτ' data from Link 3 and its Laplacian fit in (a) linear scale (top) and (b) log scale (bottom).
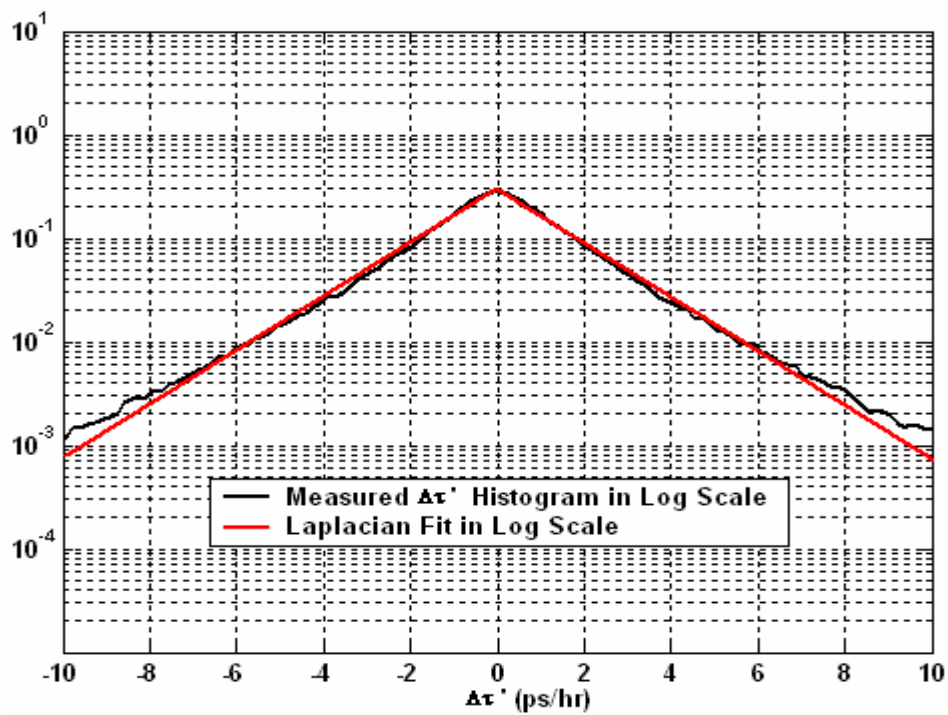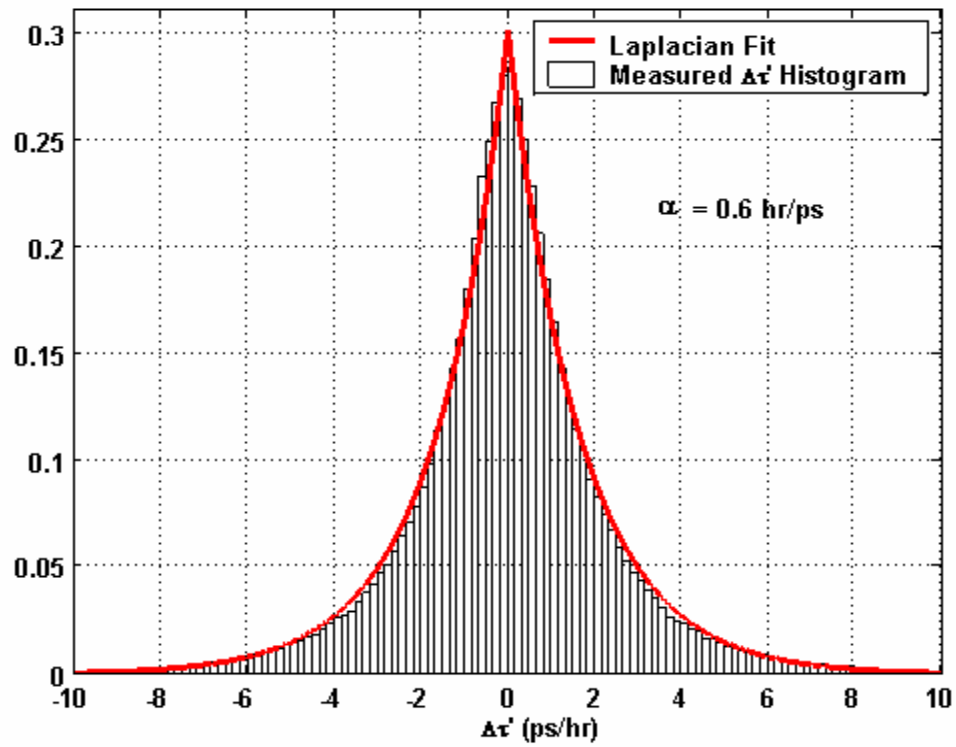
Figure 3.4. Histogram of measured $\Delta\tau'$ data from Link 1-2 and its Laplacian fit in (a) linear scale (top) and (b) log scale (bottom).
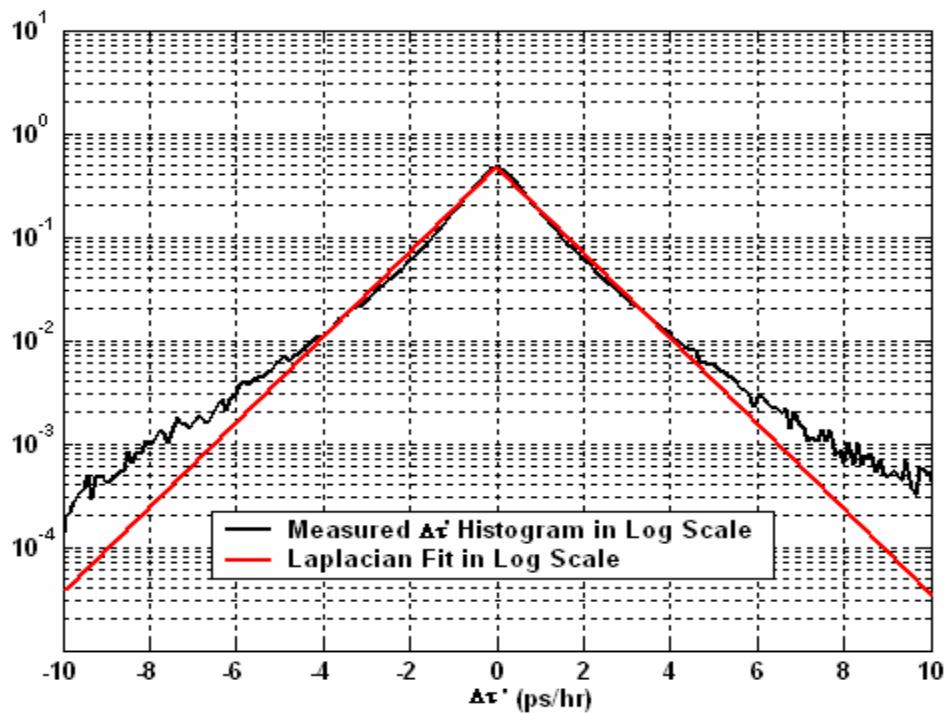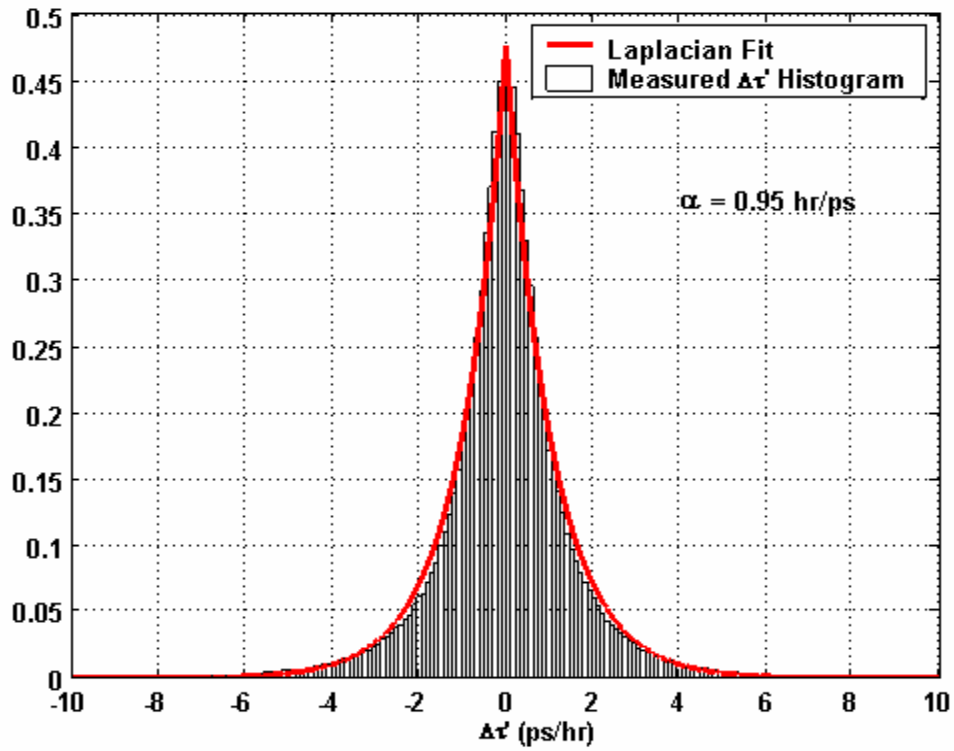
Figure 3.5. Histogram of measured Δτ' data from Link 2-3 and its Laplacian fit in (a) linear scale (top) and (b) log scale (bottom).
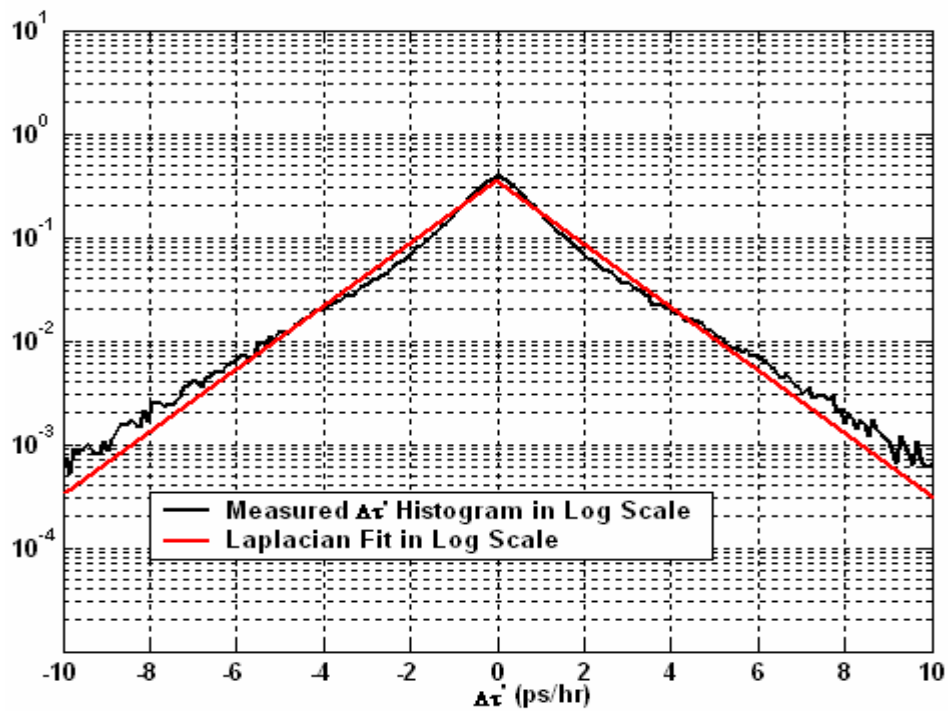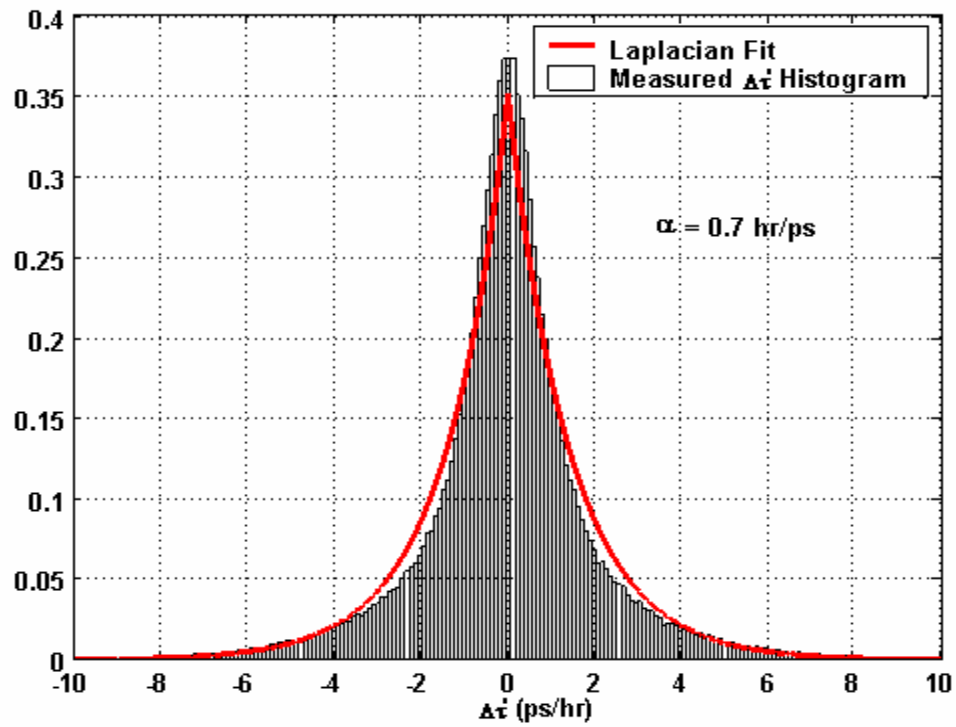
Figure 3.6. Histogram of measured Δτ' data from Link 1-3 and its Laplacian fit in (a) linear scale (top) and (b) log scale (bottom).
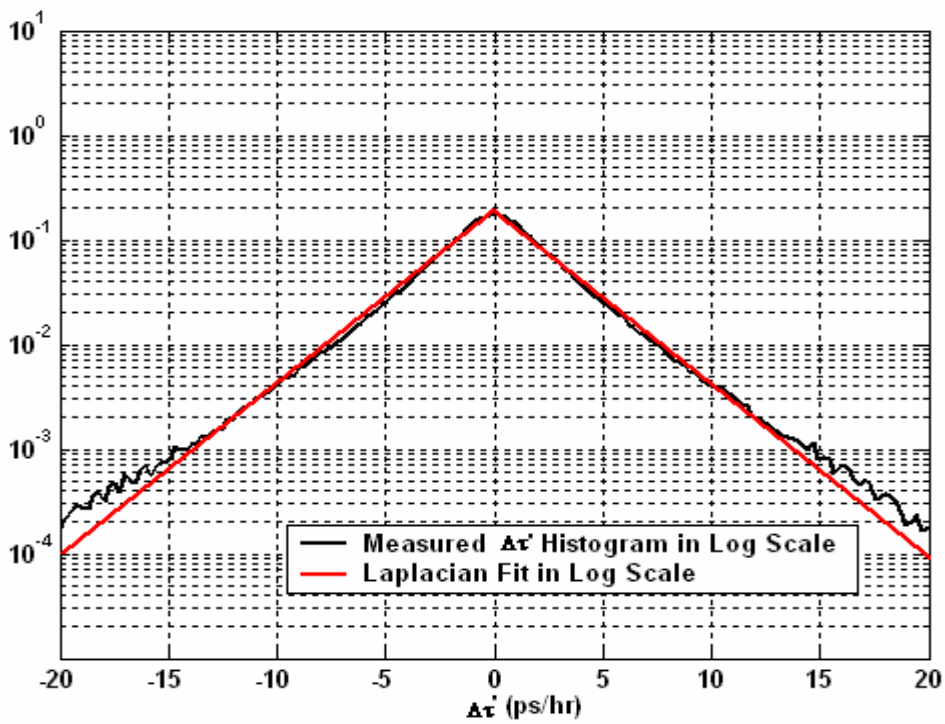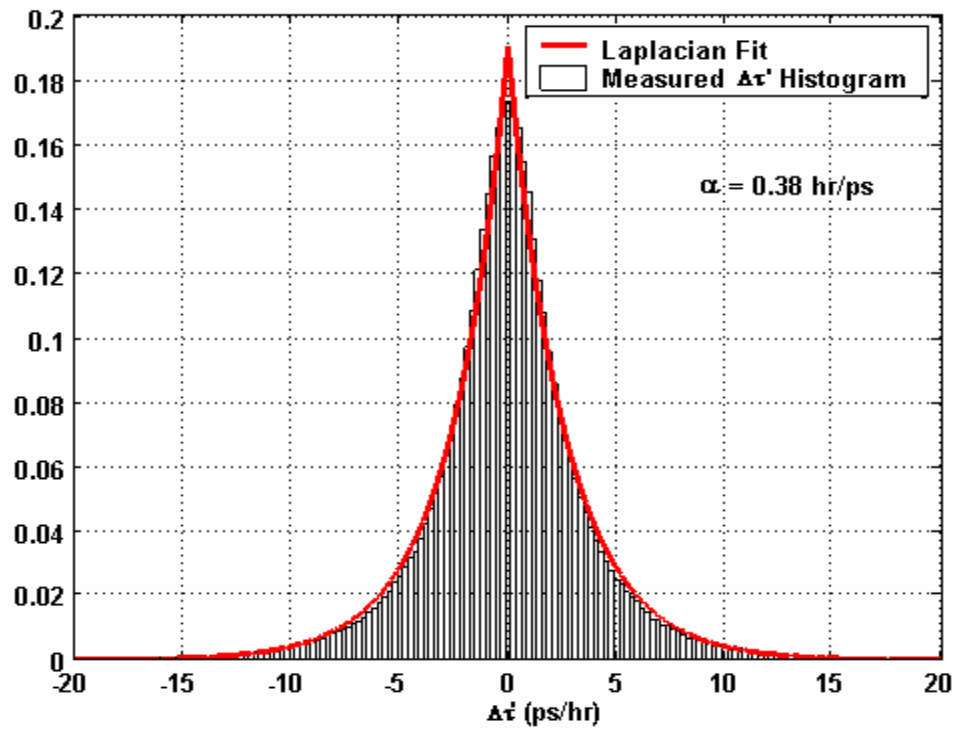
Figure 3.7. Histogram of measured Δτ' data from Link 1-2-3 and its Laplacian fit in (a) linear scale (top) and (b) log scale (bottom).

Table 3.1. Results from the modified chi-square test for measured $\Delta\tau'$ histograms on single-, two- and three- span links.

Fiber Configuration	Degrees of Freedom	Critical Value At Significance Level $\alpha = 0.9$	chi-square Test Statistic From Data	Hypothesis Accept or Reject?
Link 1	81	65.18	29.98	Accept
Link 2	86	69.68	15.93	Accept
Link 3	83	66.98	51.61	Accept
Link 1-2	100	82.36	79.1	Accept
Link 2-3	95	77.82	76.65	Accept
Link 1-3	100	82.36	266.22	Reject
Link 1-2-3	84	67.88	59.82	Accept

3.2. Closed-form expression for R_{out}

Using the Laplacian distribution as the $\Delta\tau'$ PDF, a closed form solution for the integral in (2.7), and hence R_{out}, can be obtained. Substituting (3.1) for the PDF of $\Delta\tau'$, the integral in (2.7) evaluates to $1/\alpha$. Then the expression for R_{out} in (2.7) reduces to

$$R_{out} = \frac{1}{2\alpha} f_{\Delta\tau}\left(\Delta\tau_{th}\right) \qquad (3.2)$$

The significance of (3.2) is that the mean outage rate due to PMD on any fiber route can be readily estimated given its mean DGD and Laplacian parameter α, greatly simplifying the route's PMD-induced outage analysis. Whereas the fiber's mean DGD may be known from its PMD coefficient (ps/$\sqrt{km}$), the Laplacian parameter α must be estimated from a time series of DGD measurements made on each fiber. The simplified closed-form expression in (3.2) for R_{out} was also published in our journal paper [38]. Figures 3.8 to 3.14 show an excellent agreement between the relative R_{out} values calculated using numerical integration in (2.7) and the values calculated using the closed-form expression in (3.2).
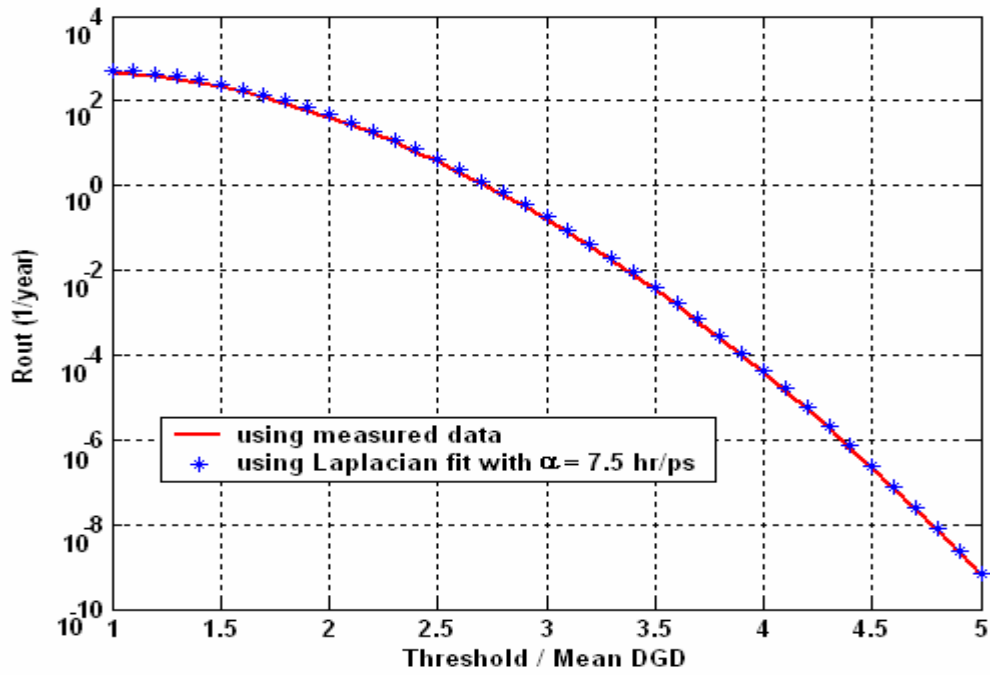
Figure 3.8. Comparison of relative R_{out} values on Link 1
calculated using (2.7) and (3.2).
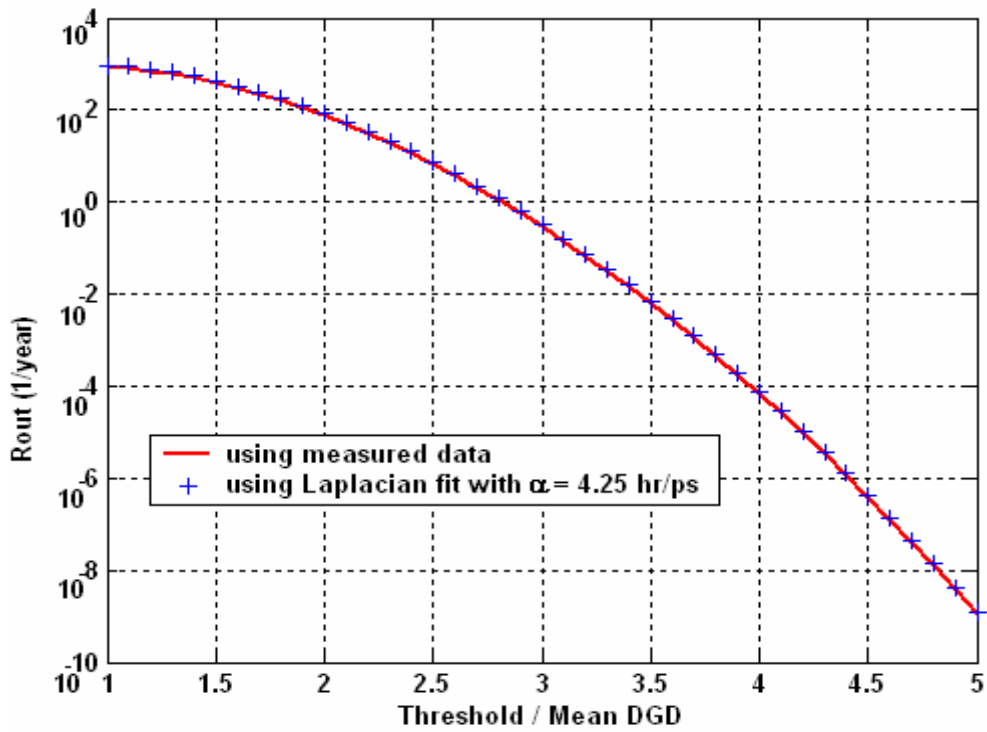
Figure 3.9. Comparison of relative R_{out} values on Link 2
calculated using (2.7) and (3.2).
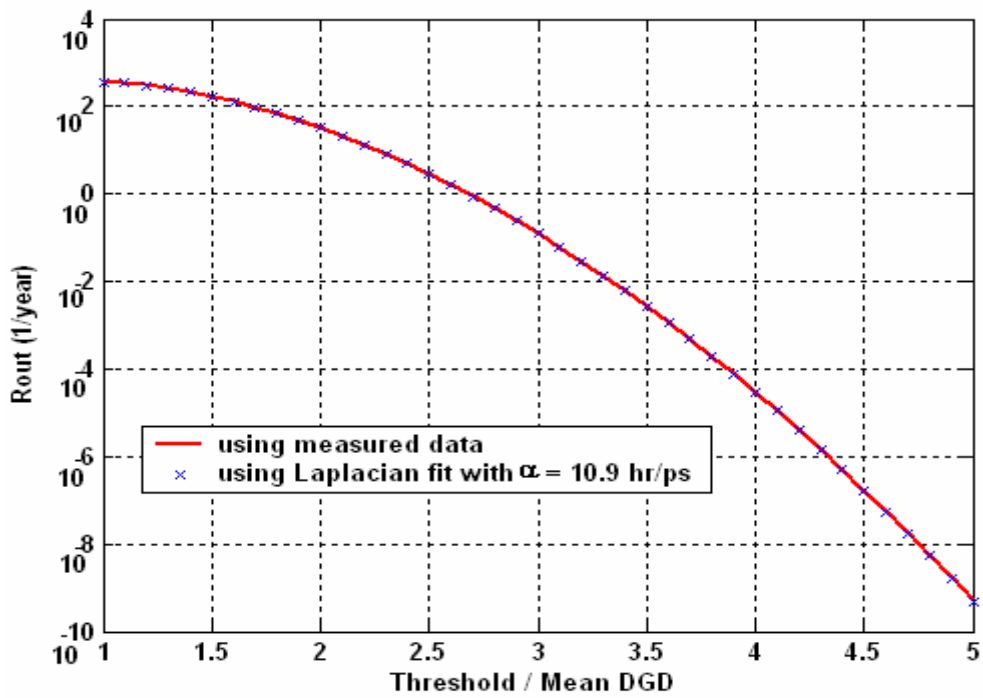
Figure 3.10. Comparison of relative R_{out} values on Link 3
calculated using (2.7) and (3.2).
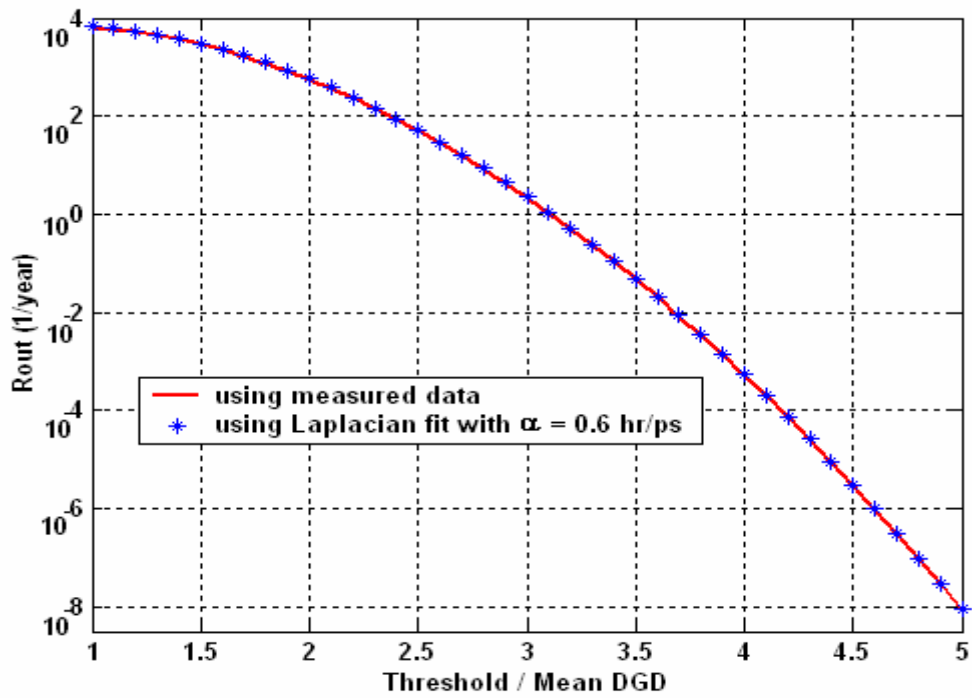
Figure 3.11. Comparison of relative R_{out} values on Link 1-2
calculated using (2.7) and (3.2).
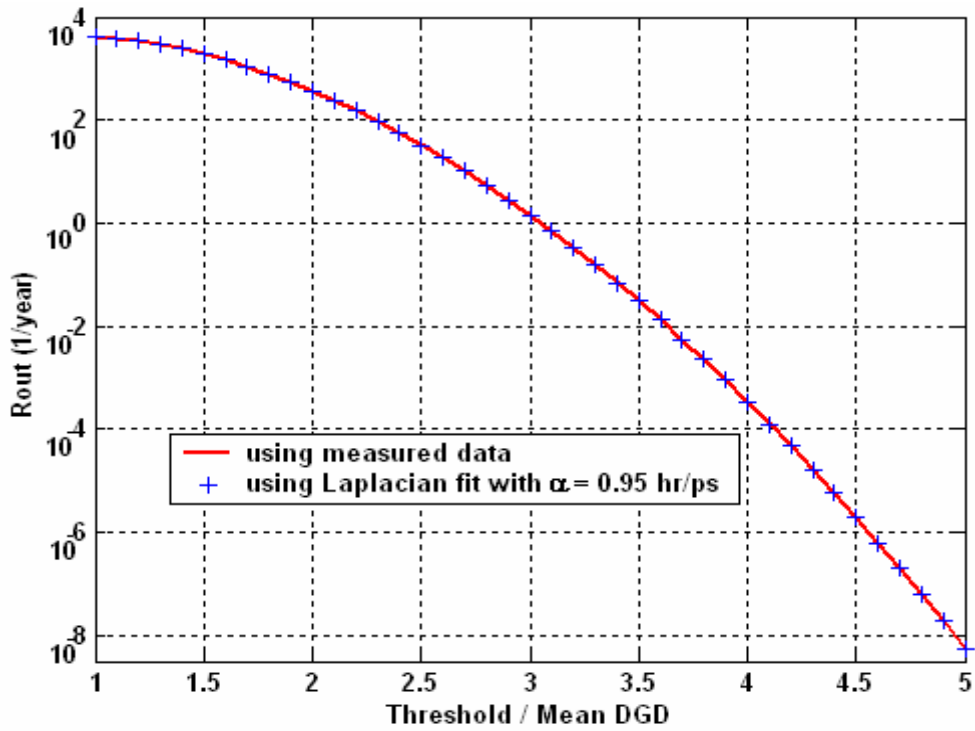
Figure 3.12. Comparison of relative R_{out} values on Link 2-3
calculated using (2.7) and (3.2).
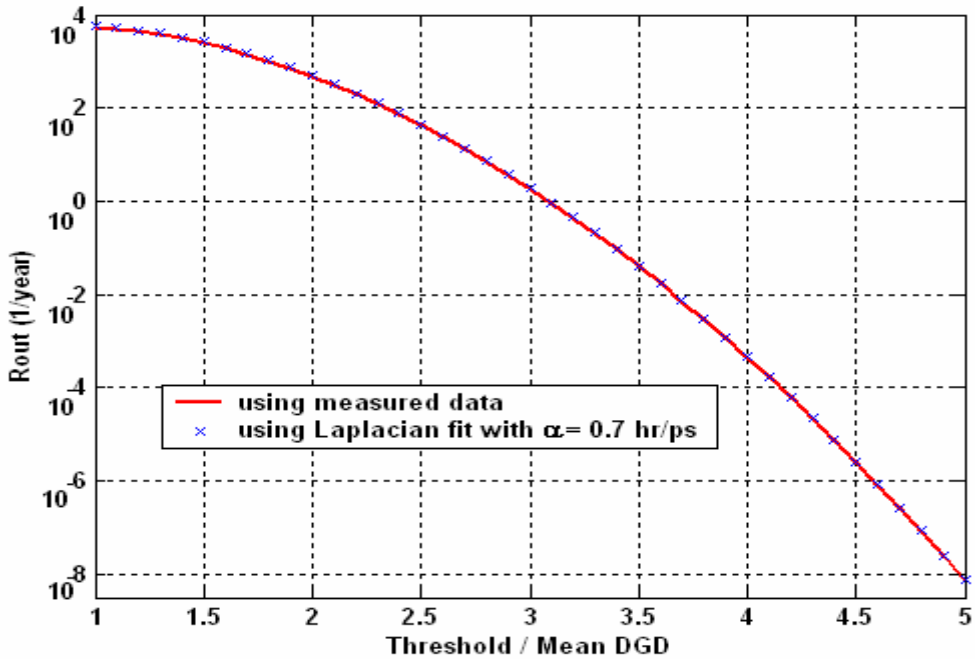
Figure 3.13. Comparison of relative Rout values on Link 1-3
calculated using (2.7) and (3.2).
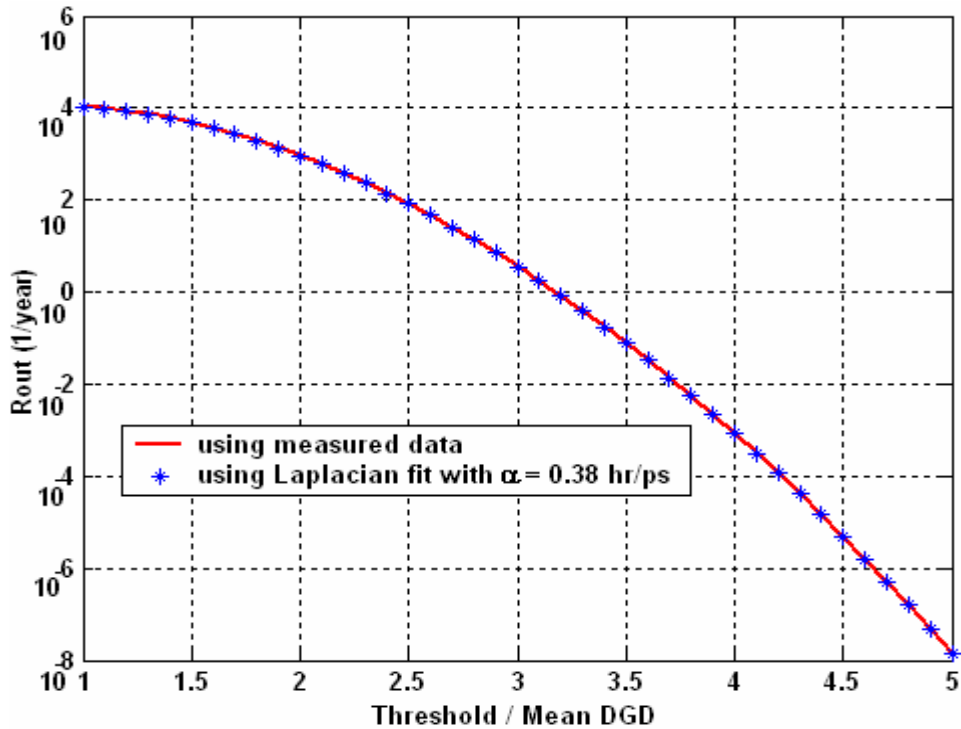
Figure 3.14. Comparison of relative R_{out} values on Link 1-2-3

calculated using (2.7) and (3.2).

3.3. Required measurement period to obtain a good estimate of α

The closed-form expression of (3.2) enables us to calculate first-order PMD outage rates using the mean DGD and the Laplacian parameter α of the fiber link under study. The next step would be to determine how long the measurements should be made to get a good estimate of α. To study this, $\Delta\tau'$ data sets from the concatenated links were divided into smaller sets of different sizes each corresponding to a different observation period. Using these smaller sets of $\Delta\tau'$ data the normalized values of α (the actual value being 1) were determined. Figure 3.15 shows the normalized α values as a function of observation period. From the figure it can be said that measurements need to be made for 10 to 14 days to estimate the value of α to within 10% of its actual value.
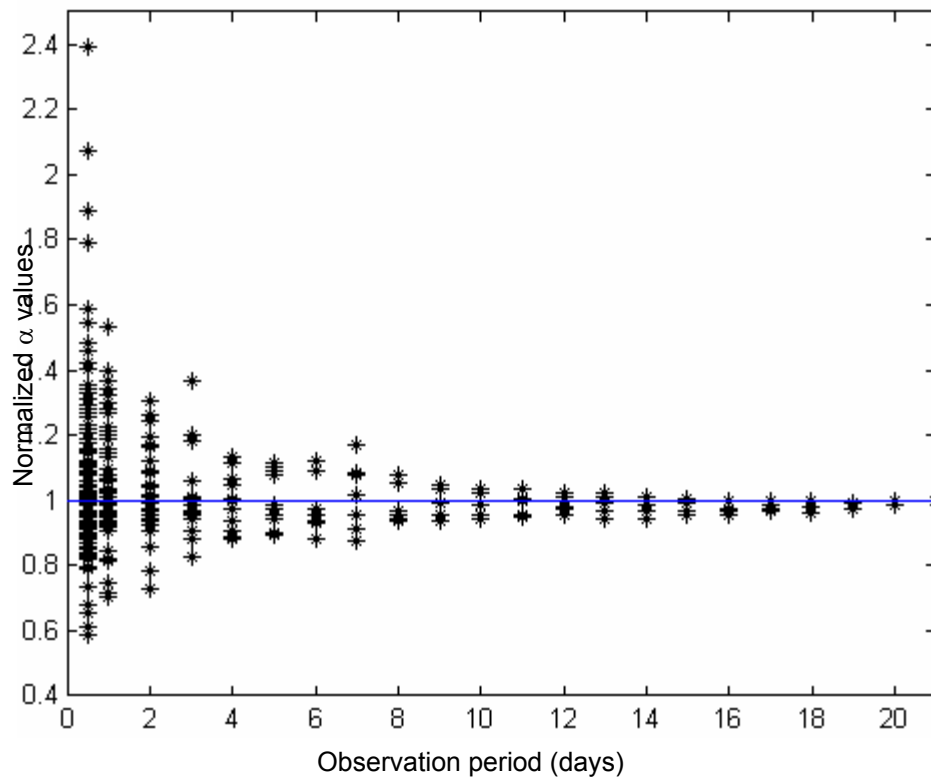
Figure 3.15. Normalized α values as a function of observation period.

4. NUMERICAL MODELING OF PMD

4.1. Purpose

In the previous chapter it was shown that the DGD time derivative has a Laplacian PDF and the first-order PMD mean outage rate is inversely proportional to the Laplacian parameter (α). To understand how the mean outage rate varies with link length, it is necessary to determine how the Laplacian parameter varies with link length. Predicting PMD-induced outages on realistic link lengths (> 500 km) through PMD measurements would require long-term access to such a link and is not economically feasible at this time. Hence, the approach taken here is to enhance the numerical model of section 2.1.5 by including a temporal component that would simulate the PMD behavior observed from the buried dark fiber PMD measurements and to use this model to determine the variation of the Laplacian parameter, and hence the mean outage rate, with link length.

4.2. Base model

The numerical model given by Dal Forno et al. discussed in section 2.1.5 is used as the base model for simulating the DGD temporal and spectral characteristics on buried standard single-mode fibers. This model, if used as described by Dal Forno et al. [34], would give insight into the Maxwellian nature of DGD and the non-periodic DGD spectral dependence. However, to match the temporal and spectral characteristics measured on a particular fiber, the free variables in the model (namely b, ϕ_n, and α_n) should be varied in accordance with the temperature and other environmental variations over the measurement period.

4.3. Significance of the model parameters

4.3.1. Segment length h_n

The parameter h_n is the length of the nth fiber segment. It should be set to a value that is greater than the fiber coupling length (following the mode-coupling

concept), which is typically in the range of a few tens of meters to a kilometer. Using a fixed value for h_n of each segment will result in an artificial periodicity in the spectral domain. This is illustrated in figures 4.1 and 4.2. Figures 4.1 and 4.2 were obtained from simulations using the base model mentioned in the previous section and by varying the angle ϕ_n of only a few segments (this concept is explained in detail in a later section) as a function of two different temperature profiles (not shown here), one with slower rate of change and other with faster rate of change respectively. A total of 100 fiber segments, of which 4 of them having temperature dependent ϕ_n, and a PMD coefficient (b) of 0.7 ps/√km were used in the simulation. Periodicity in spectral domain is evident in figures 4.1 and 4.2.
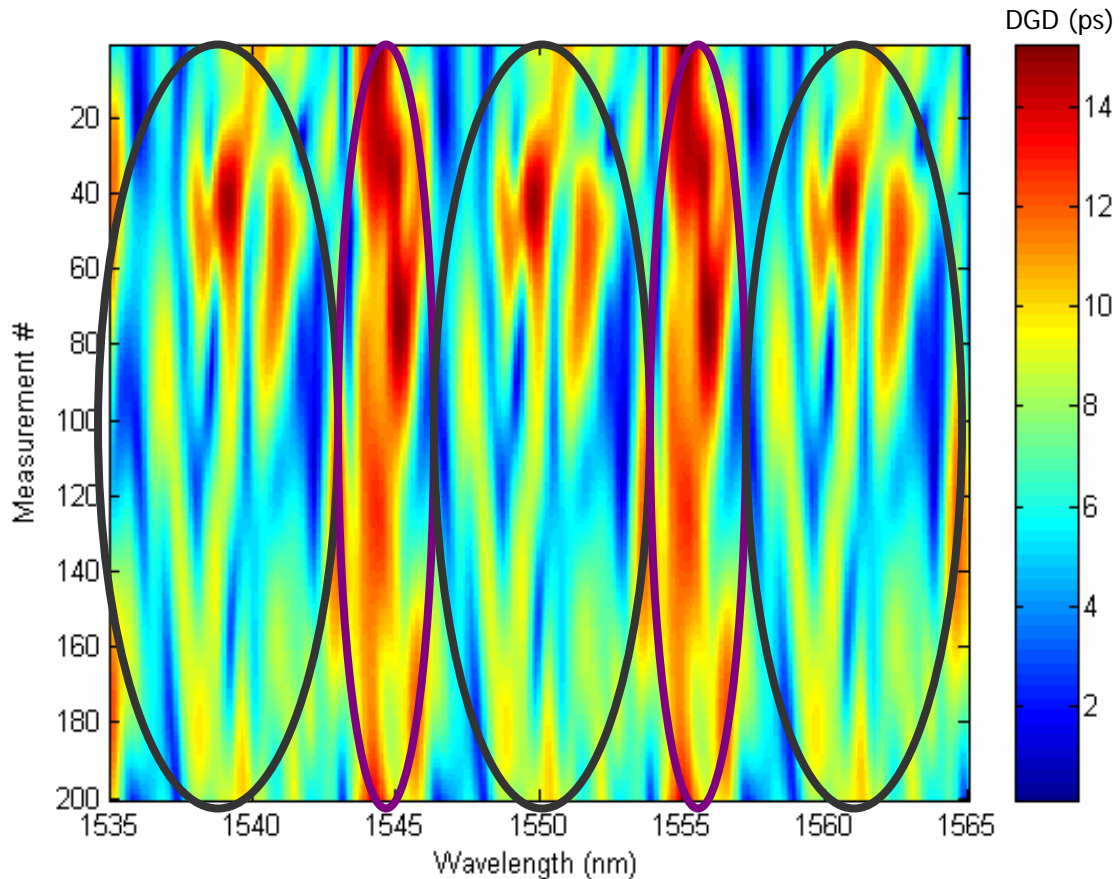
Figure 4.1. DGD colormap obtained from simulations using fixed segment lengths and a temperature profile with slower variations, showing periodicity in spectral domain.
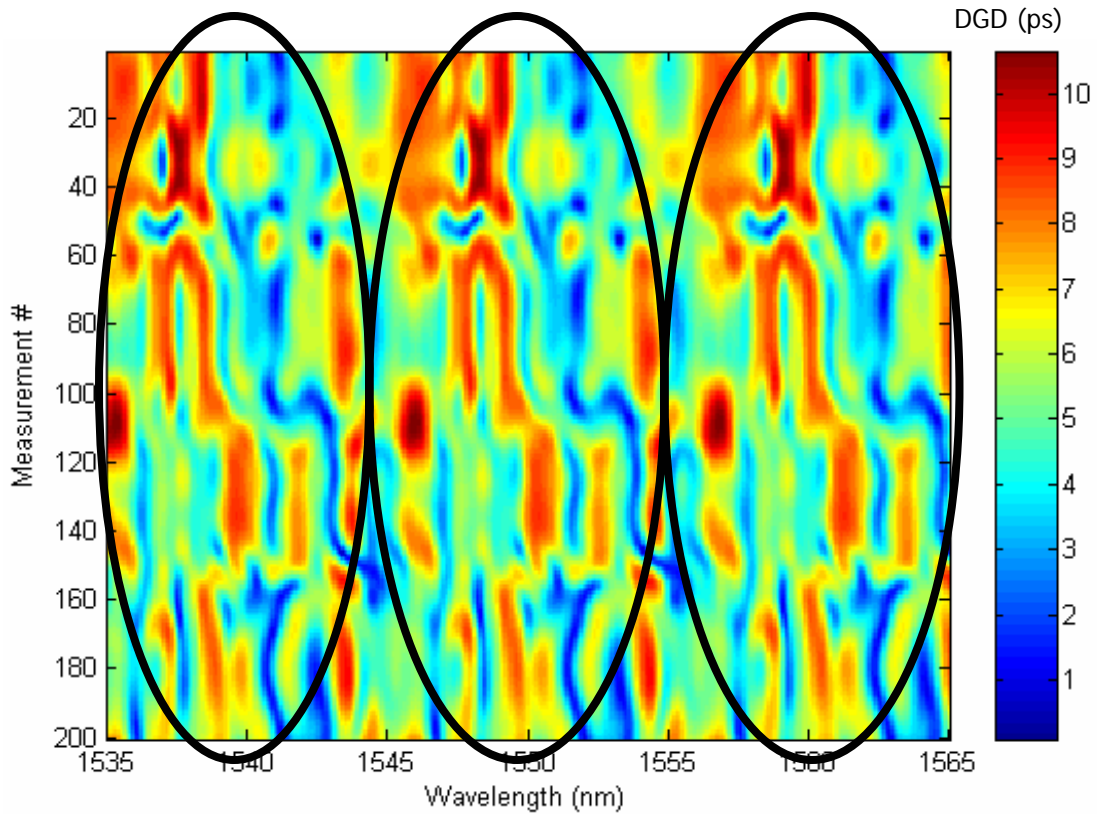
Figure 4.2. DGD colormap obtained from simulations using fixed
segment lengths and a temperature profile with faster variations,
showing the periodicity is spectral domain.

Making the segment length a random variable will remove this artificial periodicity in the spectral domain. Dal Forno et al. [34] showed that using a Gaussian variable for the segment length, with a mean value of total link length/number of segments and variance of 20% of mean value would remove the above discussed periodicity. Figures 4.3 and 4.4 illustrate this concept. The simulation parameters used were the same as with figures 4.1 and 4.2 except that the segment lengths were made Gaussian. Clearly figures 4.3 and 4.4 do not show any periodicity in spectral domain as was seen in figures 4.1 and 4.2.
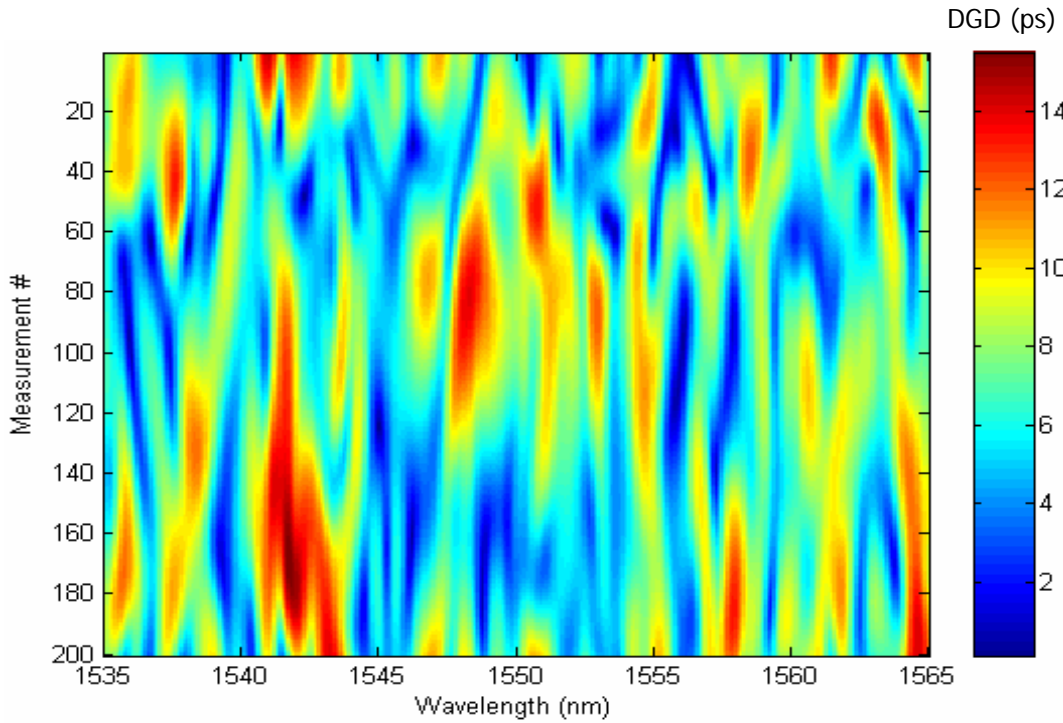
Figure 4.3. DGD colormap obtained from simulations using Gaussian segment lengths and a temperature profile with slower variations; periodicity in spectral domain is absent.
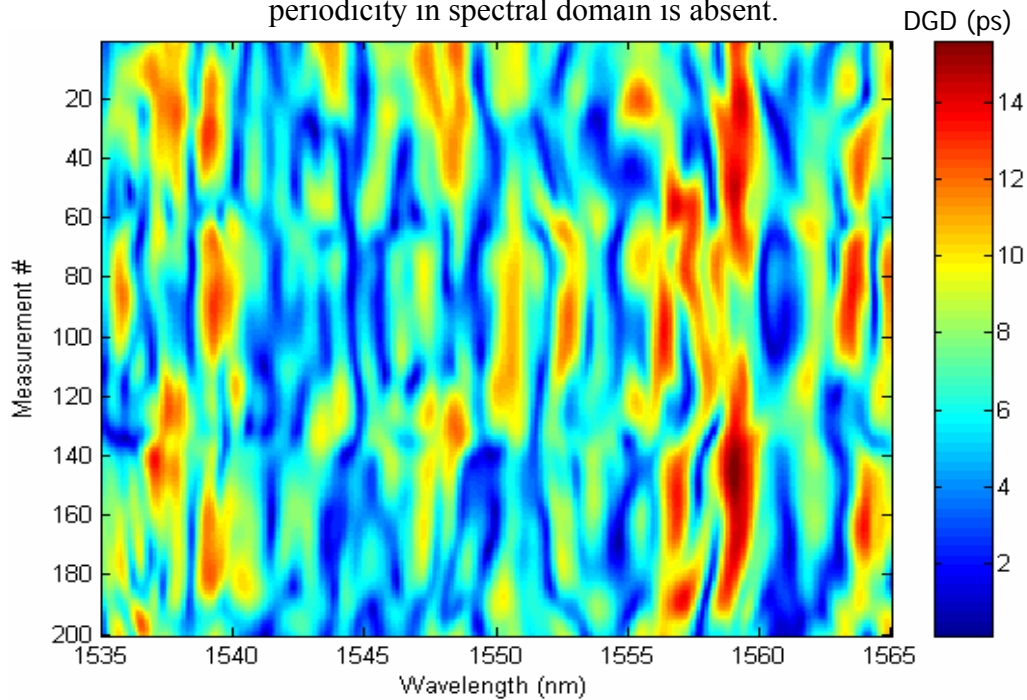
Figure 4.4. DGD colormap obtained from simulations using Gaussian segment lengths and a temperature profile with faster variations; periodicity in spectral domain is absent.

4.3.2. Number of fiber segments N

The parameter N in the model denotes the total number of fiber segments. The model described in section 2.1.5 represents a SMF as a concatenation of smaller length fiber segments. The number of fiber segments (N) is the link length (L) divided by the mean segment length (h) (N=L/h). For a given link length, using a very large value for mean segment length (much larger than the coupling length) leads to a small value for N and this would affect the repeatability of the simulations. Hence, the mean segment length should be chosen judiciously such that it is larger than the coupling length but not too large to force a smaller value for N.

4.3.3. PMD coefficient 'b'

The parameter 'b' in the model is the PMD coefficient of the fiber. For multi-span link simulations, if the PMD coefficients of all the spans are different then the corresponding values of 'b' for different spans should be used in the simulation. Varying the parameter 'b' as a function of temperature will result in a drift in the spectral domain. This concept is illustrated below. Figure 4.5 shows hourly temperature for a location obtained from [39]. Studies [40], [41] have reported values for the relative temperature sensitivity of DGD in the range of $5 \times 10^{-4}\,^{\circ}C^{-1}$ to $7 \times 10^{-4}\,^{\circ}C^{-1}$. Using a value of $6 \times 10^{-4}\,^{\circ}C^{-1}$ for the relative temperature sensitivity of DGD and an initial value of $0.7\ ps/\sqrt{km}$ for 'b', the corresponding variation in 'b' in response to the temperature profile in figure 4.5 is shown is figure 4.6. Figure 4.7 shows the plot of DGD vs. wavelength and time obtained using the PMD model with the following parameters: 95 km link length; 100 fiber segments, the size of the each segment randomly generated from a Gaussian distribution around the mean length of 0.95 km (coupling length); 35 nm wavelength band (1535-1565 nm); two different sets of uniform random values for α_n and ϕ_n and the PMD coefficient profile shown in figure 4.6. It is clear from figure 4.7 that DGD drifts either to the left or right along the wavelength axis corresponding to a change in the PMD coefficient induced by the temperature variation.
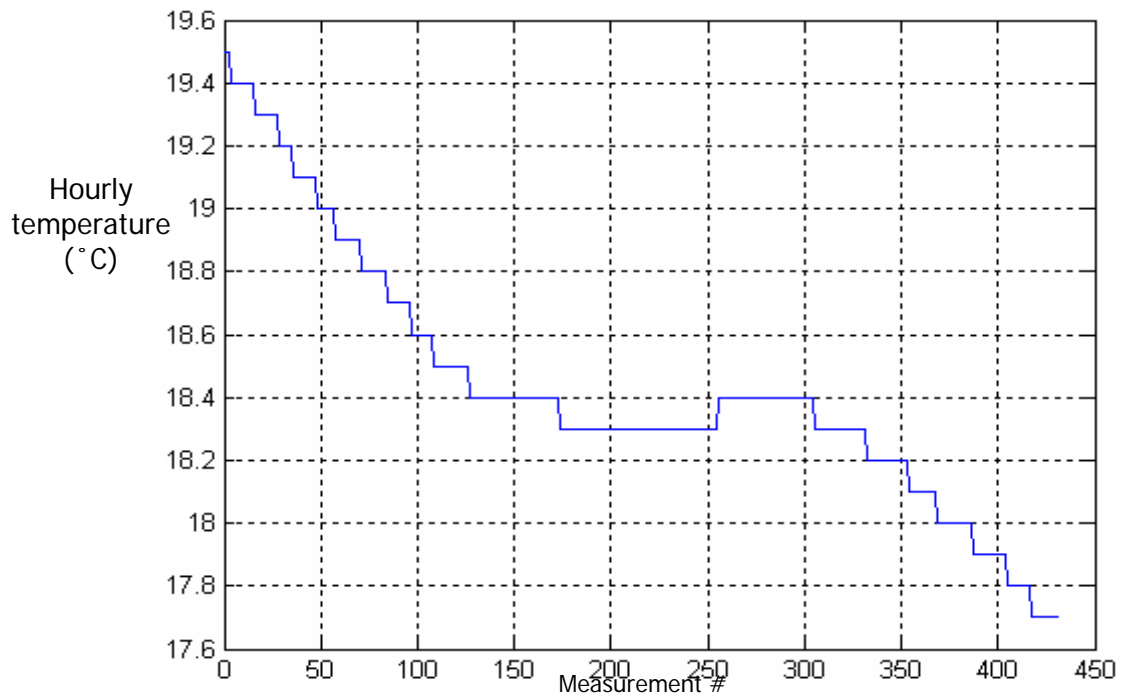
Figure 4.5. Measured hourly temperature at one location [39].
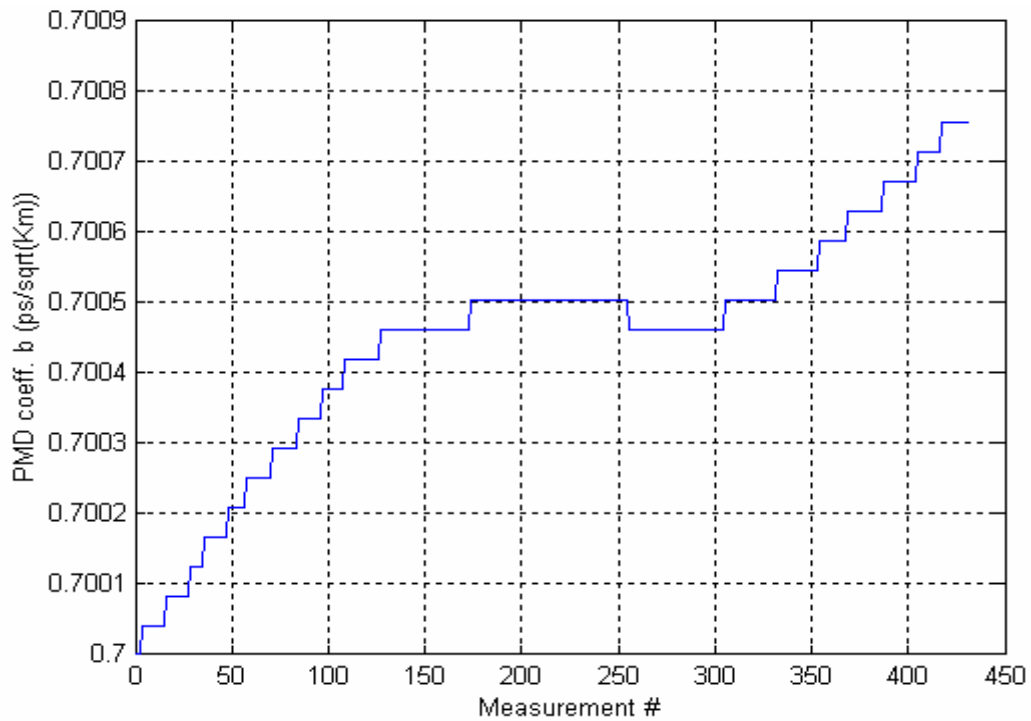
Figure 4.6. PMD coefficient variation modeled based on the
temperature profile in figure 4.5.
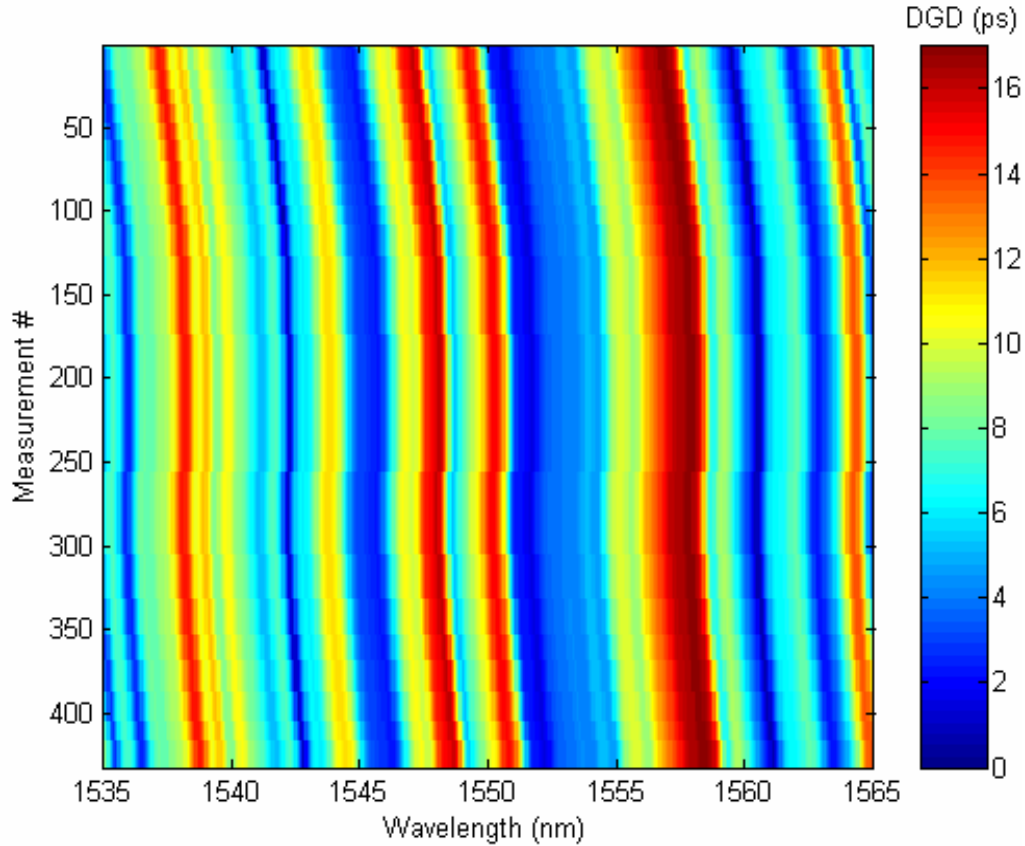
Figure 4.7. DGD colormap obtained using the modeled PMD coefficient in figure 4.6.

The DGD drift in the spectral domain discussed above was also observed in the measured DGD colormaps shown in chapter 2. Figure 4.8 shows the measured DGD colormap on single-span fiber link 1 and the variation of air temperature over the measurement period. Looking at the plots in figure 4.8 closely, particularly between 50 to 60 day period (figure 4.9), a dip in the temperature over that period and a drift in the DGD towards right on the wavelength axis can be observed.
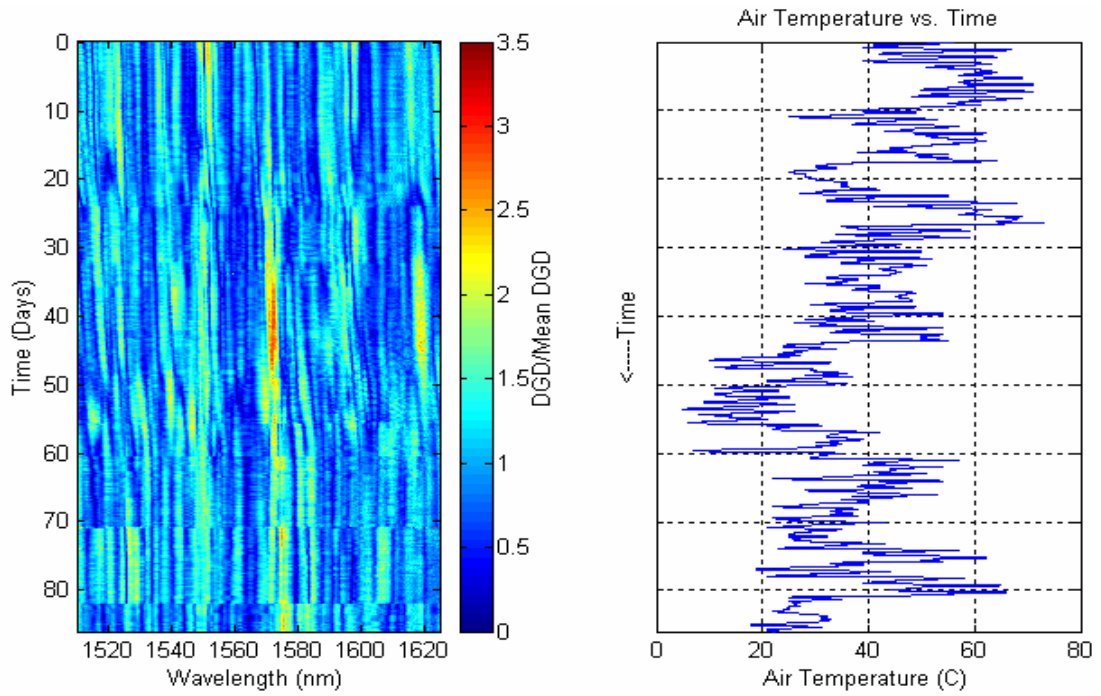
Figure 4.8. DGD colormap measured over a 95-km buried fiber link and hourly air temperature vs. time over the same 86-day measurement period.
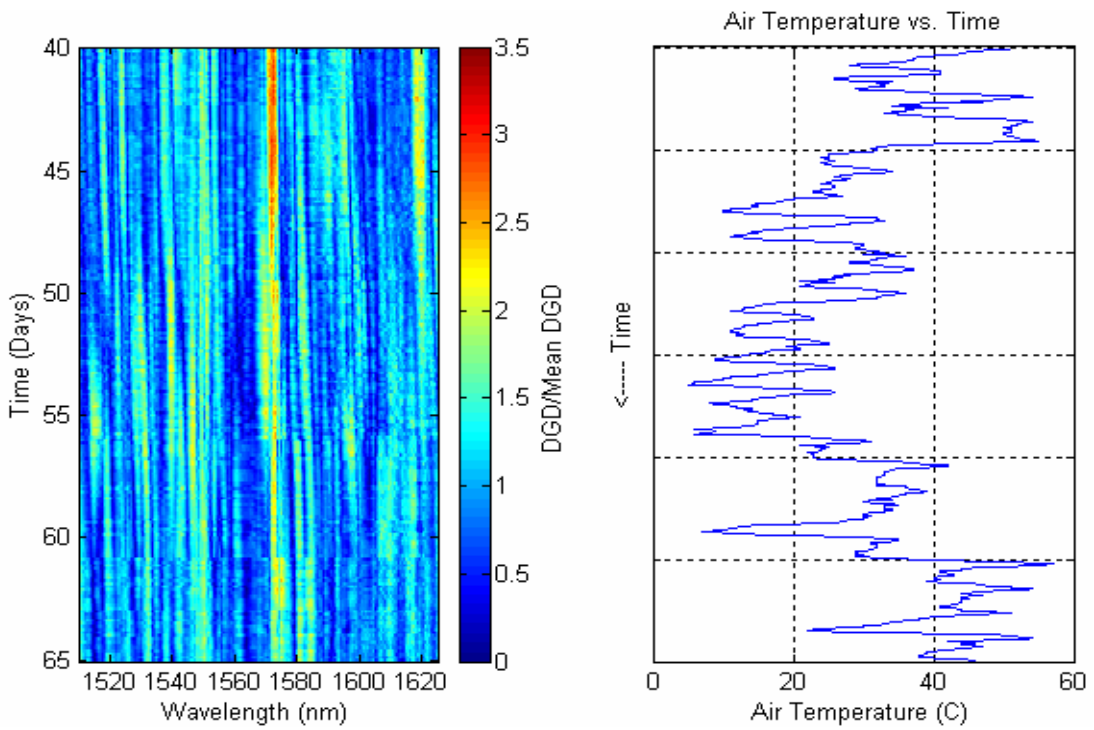
Figure 4.9. Figure 4.8 zoomed in to show the period including days 40 to 65.

4.3.4. Coupling angle α_n

The parameter α_n in the model is the coupling angle between the segment axes. For a given buried fiber, the coupling angles are determined by the fiber manufacturing and cabling processes and also the installation procedure. However, once the fiber is buried the coupling angles remain the same and do not vary significantly over time. As mentioned earlier in section 2.5.1, the parameter α_n can be modeled as a uniform random variable between 0 and 2π and the same set of values can be used to repeat the simulations in time. However, if it is required to model different fibers, different sets of uniform random variables could be used for the coupling angles of different fibers.

4.3.5. Angle ϕ_n

The parameter ϕ_n in the model accounts for the environmental fluctuations along the fiber and is the crucial parameter that determines the temporal characteristics of PMD. For fiber links that experience time-invariant environmental fluctuations, ϕ_n can be modeled just as a uniform random variable between 0 and 2π. But for fiber links that experience time variant environmental fluctuations (the common scenario) other terms that are functions of different environmental factors should be included to obtain the temporal characteristics of PMD.

Studies [42] [43] have shown a strong correlation between DGD and air temperature variations without any time lag and such correlation was attributed to a small number of segments of buried fiber (like the man holes, bridge attachments, EDFA huts, etc.) exposed to the air temperature variations. The number of segments exposed to the air temperature variations could be anywhere from 4 to 10 per span depending on the fiber route. This implies that temporal variations of PMD could be modeled by varying the parameter ϕ_n of only a few segments of fiber.

Although temperature is the most dominant environmental factor that determines the temporal nature of PMD, there are other stress-inducing factors like atmospheric pressure, rain events, surface vibrations, etc. that also affect the temporal nature of PMD, but only in a small way. The effects of temperature could be modeled

by making ϕ_n a linear function of temperature and the effects of all other environmental factors can be modeled by adding a Gaussian variable to it, invoking the central limit theorem. Hence the parameter ϕ_n for a few segments of each span can be modeled as

$$\phi_n = U[0 \; 2\pi] + k * \text{Air Temperature}(°F) + N[0, \text{G\_var}] \tag{4.1}$$

where $U[0 \; 2\pi]$ is a uniformly distributed random variable from 0 to 2π, $N[0, \text{G\_var}]$ is a Gaussian random variable with a mean of 0 and variance of G_var (units: radian^2), and k is the proportionality constant with units of radians/$°F$.

The proportionality constant k is link-dependent and would vary from link to link. The Gaussian variance G_var depends on how fast the environmental factors other than temperature are changing and could vary from time to time. As mentioned before, the linear temperature term in (4.1) accounts for the temporal variations due to few segments being exposed to the air temperature, but, in reality the fiber segments are not directly exposed to the open air and the intervening enclosures (conduit, hut, man hole, etc.) buffer the temperature variation to some extent. Hence, raw air temperature data could be filtered using a low pass filter to remove any high frequency terms before using the data in the model. However, as can be seen in the later sections the use of this filter is not critical for accurate modeling of longer, multi-span fiber links.

If the parameters α_n and ϕ_n are modeled using different, independent uniform random value sets in time, then the DGD values obtained from the simulation will be totally uncorrelated and noise-like as shown in figure 4.10. The DGD colormap in figure 4.10 is obtained from a simulation with the following parameters: L = 100 km, h_n = 1 km (fixed), N = 100, b = 2.7 ps/$\sqrt{\text{km}}$, spectral band is 1480 nm to 1580 nm with 0.1 nm step and different, independent sets of uniform random values for α_n and ϕ_n for each of 100 simulation runs. But using the base model described in section 2.5.1 along with the profiles for b, α_n, and ϕ_n discussed in this chapter, it is possible to model the temporal characteristics of PMD accurately and obtain a Laplacian PDF for the DGD time derivative ($\Delta\tau'$). The free parameters here are the proportionality

constant k, Gaussian variance G_var, the filter bandwidth and the number of time varying segments.
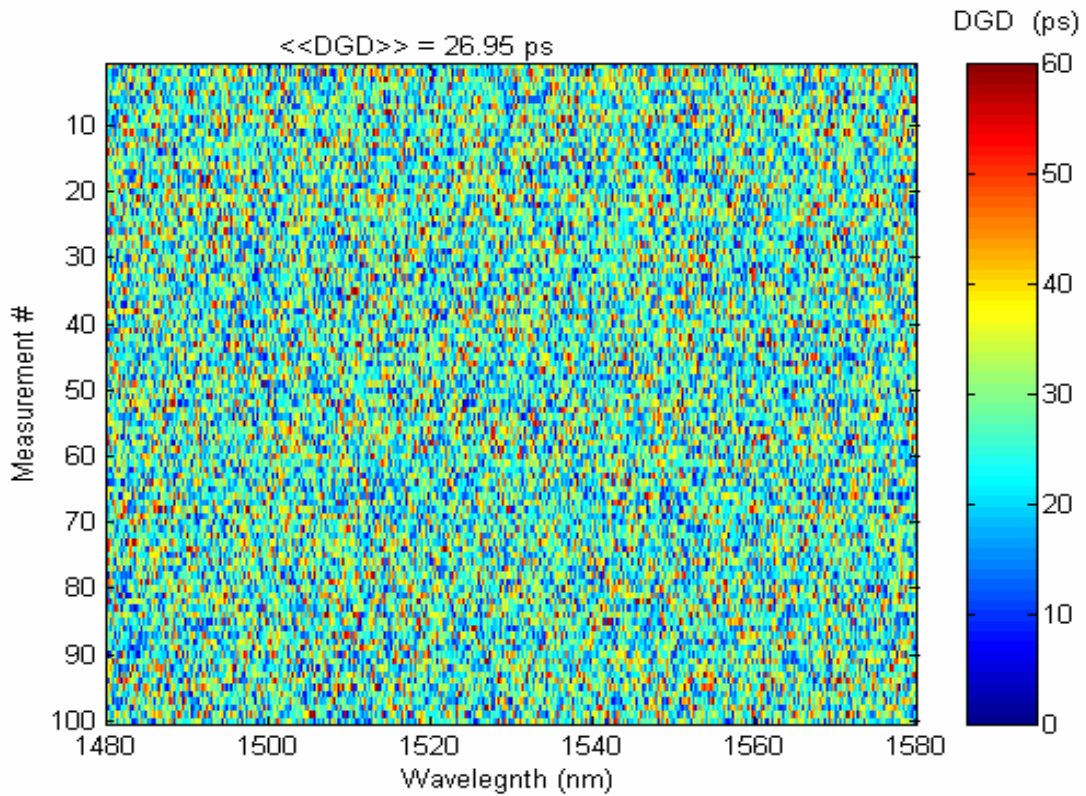
Figure 4.10. DGD colormap from a simulation using different, independent uniform random value sets for α_n, and ϕ_n for each simulation run.

Using a very small number of time varying segments (less than 4) could result in a non-Laplacian PDF for DGD time derivative with a strong central peak around the mean $\Delta\tau'$ value of zero. Also, DGD under-sampling - DGD measurements/samples taken at intervals greater than the correlation time - would result in non-Laplacian PDF like the Gaussian distribution for $\Delta\tau'$. Examples of these cases are shown in later chapters.

In the next two chapters the results from simulations of different fiber links using the enhanced numerical model and the temporal profiles of the model parameters discussed in this chapter are presented.

5. ENHANCED-MODEL VALIDATION

This is the first of the two chapters on the results obtained from simulations using the enhanced numerical model discussed in chapter 4. In this chapter the coefficients for the model parameters will be determined for the 7 fiber configurations used for measurements discussed in chapter 2 that yield simulated DGD data that are comparable to the measured DGD data. Through this process the ability of the simulation to predict the overall behavior of a fiber link can be established. In chapter 7, this validated simulation model will be used to simulate DGD data for link lengths greater than 3 spans in order to evaluate PMD-induced outage rates on longer fiber-optic links.

5.1. Model accuracy metrics

The following metrics will be used to gauge the accuracy of the simulation results:

- Mean DGD (time and wavelength averaged DGD) value – how do the simulation results compare with measured data

- Goodness of Maxwellian PDF fit to the simulated DGD data

- Goodness of Laplacian PDF fit to the simulated DGD time derivative data

- Laplacian parameter value – how does the value from simulated data match with the corresponding value from measured data

- Decorrelation time and bandwidth – how do these values from simulations compare with those from measurements

- Overall appearance of the DGD colormap – how do the colormaps from simulations compare with those of measurements

For each fiber configuration, plots showing the temperature profile used, the normalized DGD colormap, the normalized DGD histogram and Maxwellian fit in linear and log scales, the DGD time derivative histogram and Laplacian fit in linear and log scales are shown. A comparison is drawn between the simulation results and the measurements in chapter 2 to show the accuracy of the numerical model.

5.2. Model parameters

For all the fiber configurations discussed in this chapter as well as the next chapter the following profiles are used for the parameters of the numerical model: the segment length h_n is modeled as a Gaussian variable with mean value determined by the PMD coefficient and the link length and with a variance of 20 % of mean value; the PMD coefficient 'b' is modeled as a time-invariant parameter specific to each link; each span is modeled as a concatenation of 500 fiber segments (N); the coupling angle α_n is modeled as a time-invariant uniform random variable between 0 and 2π; the static part of the parameter ϕ_n is modeled as a time-invariant uniform random variable between 0 and 2π.

The free parameters, namely, the proportionality constant k, the Gaussian variance G_var, the filter bandwidth and the number of time varying segments, are link and temperature profile dependent. A fixed number (four) of equally-spaced, time varying segments are used per span, hence a single-span link would have 4 time varying segments, and a two-span link would have 8 time varying segments and so on. The other free parameters are varied following the general understanding of the parameters to obtain desired results, in this case results closely matching the measured results. The exact values of these parameters for each fiber configuration are determined by trial and error.

5.3. Individual (single-span) Links

In this section the simulation results for the three single-span links are discussed. Each of these links is 95 km long. A 110-nm wavelength band (1510 nm to 1625 nm) is used in all of the simulations.

5.3.1. Single-span link 1

Table 5.1 shows the values of the free parameters used in the simulation of link 1. A Butterworth low-pass filter is used to filter the raw temperature data. A filter bandwidth parameter of 1 corresponds to half of the sampling frequency and the filter

bandwidth parameter in table 5.1 shows the bandwidth relative to half the sampling frequency. A value of 0.001 indicates that it is a very narrow low pass filter.

Table 5.1. Values of free parameters for link 1.

Proportionality constant k (radians/°F)	Number of time-varying sections	Relative filter bandwidth parameter	Gaussian std. deviation (radians)
0.2	4	0.001	$\pi/22$

Figure 5.1 shows the measured hourly air temperature (top plot) at one location over the 86-day measurement period for link 1 obtained from National Climatic Data Center website [36] and the corresponding filtered temperature (bottom plot) used in the simulation.
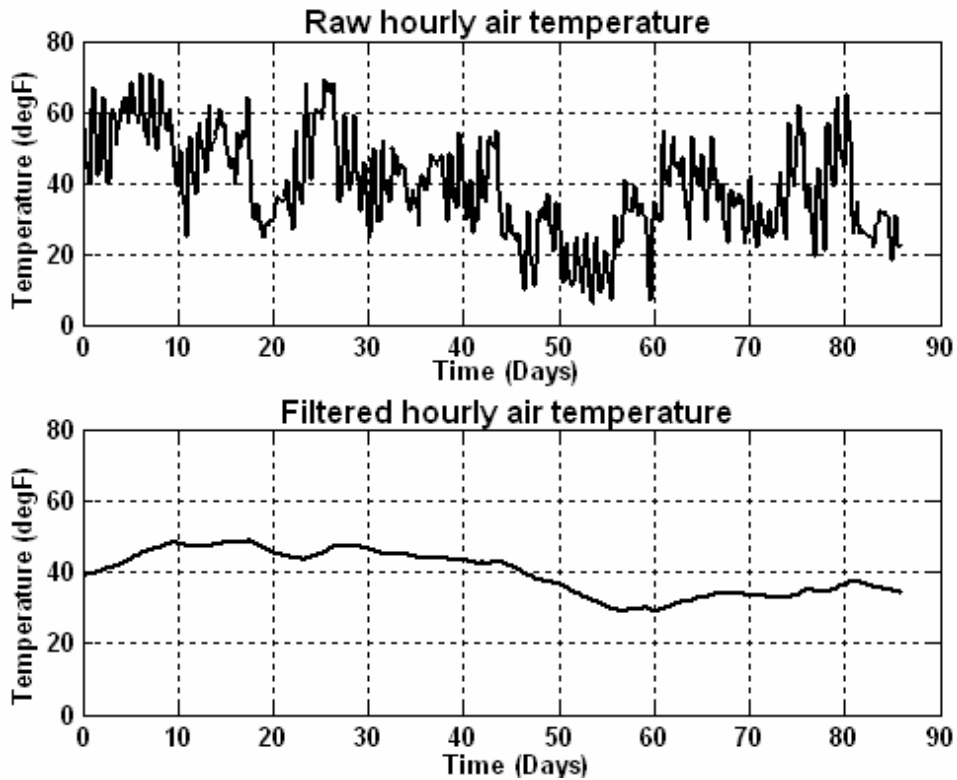
Figure 5.1. (a). Hourly air temperature; (b) Corresponding filtered temperature.
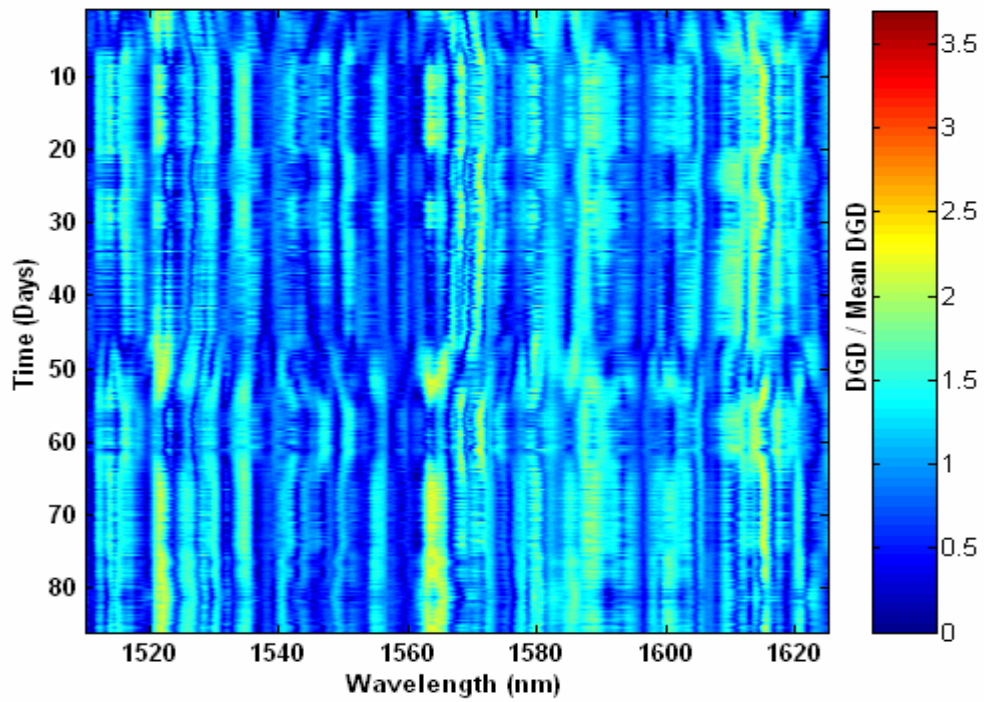
Figure 5.2. (a). Normalized DGD colormap obtained from link 1 simulation
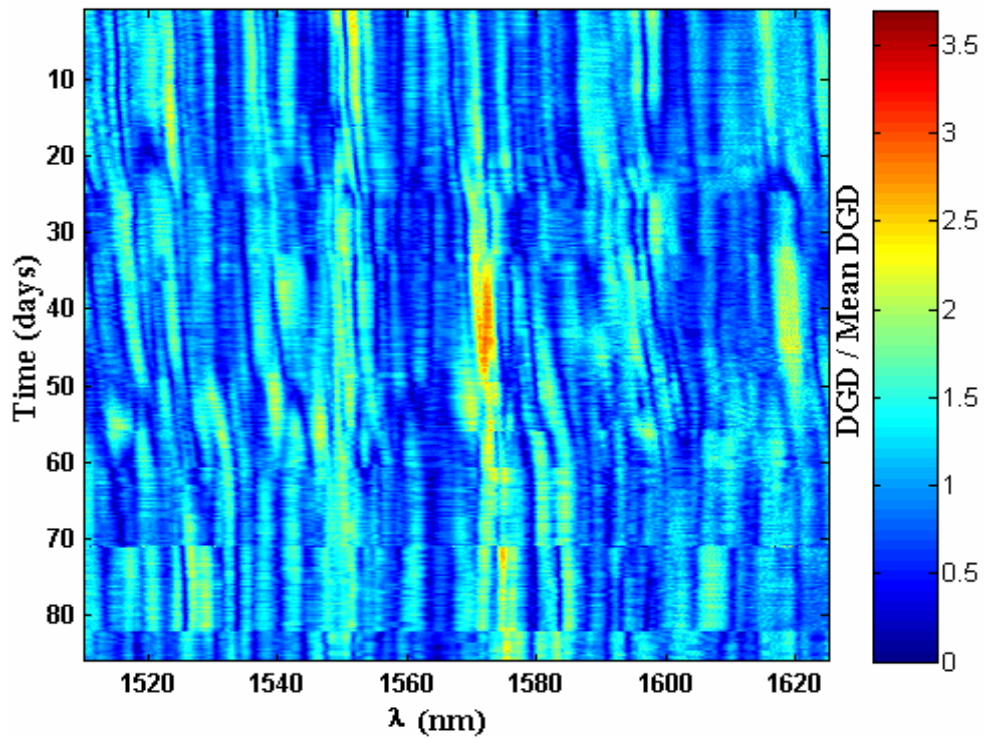
Figure 5.2. (b) Normalized DGD colormap obtained from link 1 measurements shown in chapter 2, reproduced here for comparison.

Figure 5.2 (a) shows the normalized DGD (DGD normalized by the mean DGD) colormap obtained from link 1 simulation using the filtered temperature profile shown in figure 5.1 (b) and the parameter values shown in table 5.1. The colormap obtained from measurements on link 1, shown in chapter 2, is repeated here as figure 5.2 (b) for comparison. Simulations in time were repeated at 1 hour intervals but DGD was calculated every 3 hours to be consistent with the measurements on link 1 which were repeated every 2 hours and 55 minutes. Comparing the colormaps in figure 5.2 it is clear that both the colormaps look very similar although not exactly the same. Both the colormaps have the same features like DGD varying rapidly with wavelength but rather slowly with time and the high DGD events being spectrally localized. The actual mean DGD obtained from simulation, although not mentioned here, was very close (< 1 % difference) to the value from the measurements.

Figures 5.3 (a) and 5.3 (b) show the histogram of simulated normalized DGD and its Maxwellian fit for link 1 in linear and log scales respectively. It can be observed that the histogram has a shape consistent with the Maxwellian distribution except at the very end of the tail where not enough independent samples are present. Results from the modified chi-square test on the simulated DGD data are included in table 5.9.
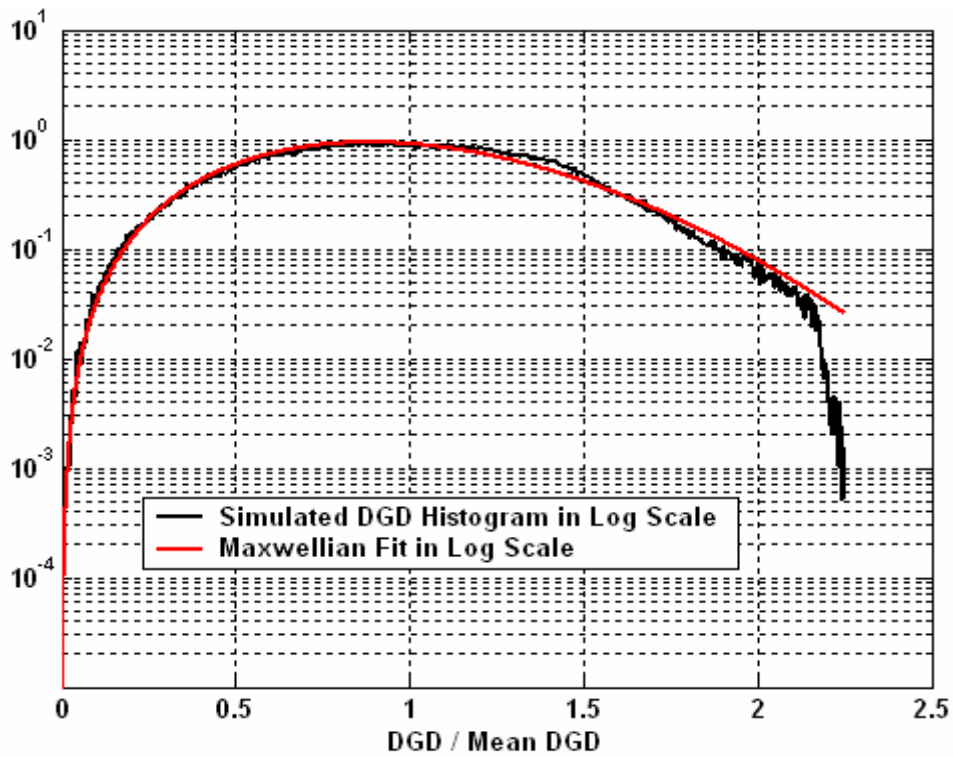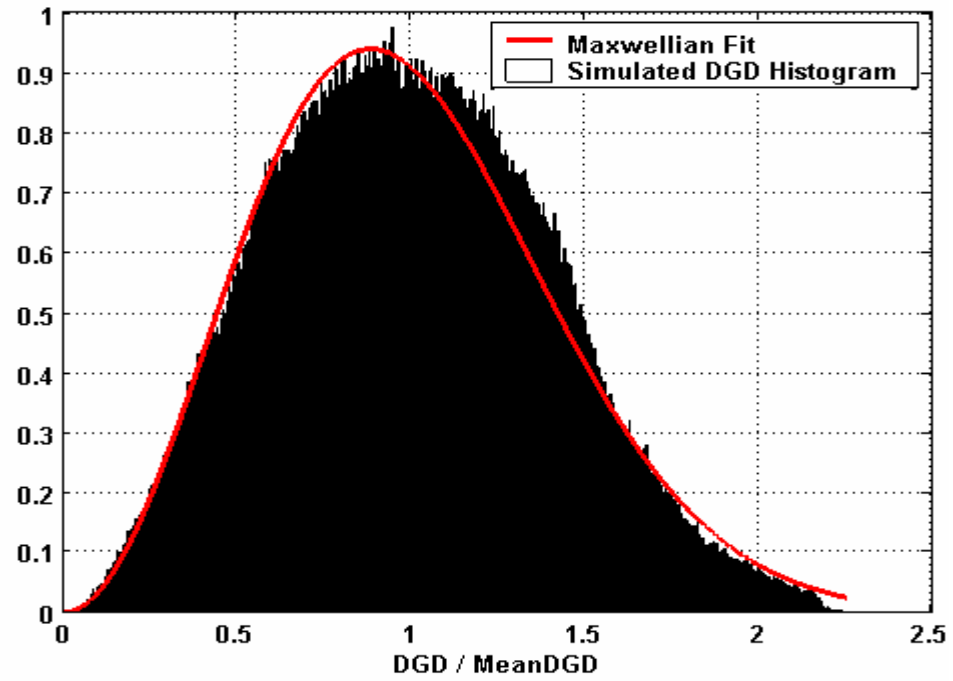
Figure 5.3. Histogram of simulated normalized DGD and its Maxwellian fit for link 1 in (a) linear scale (top) and (b) log scale (bottom).
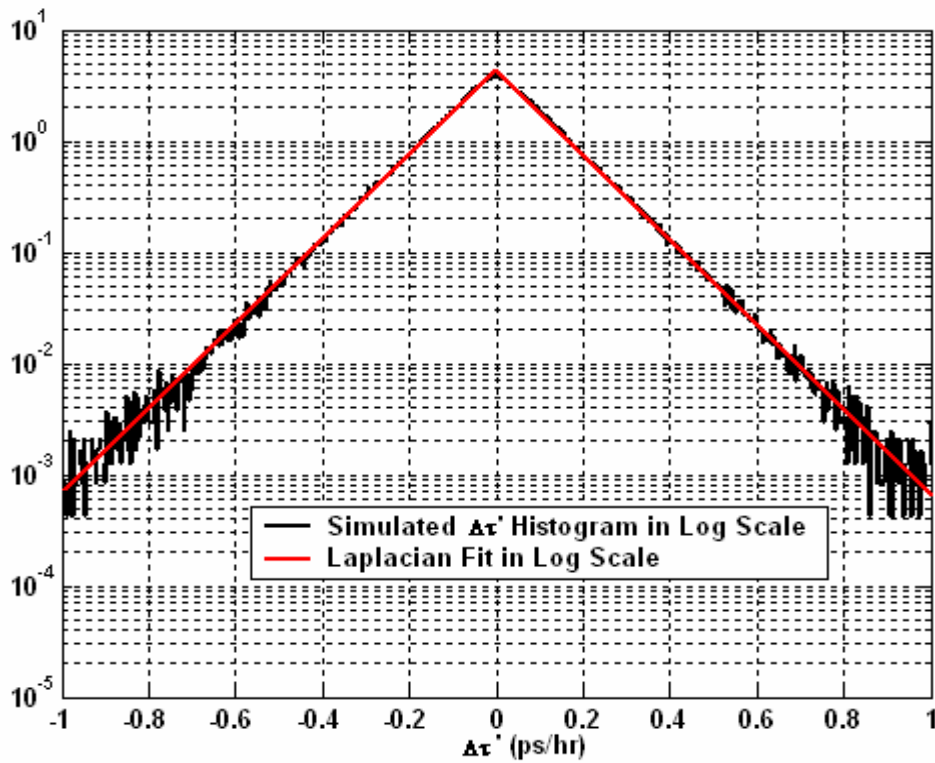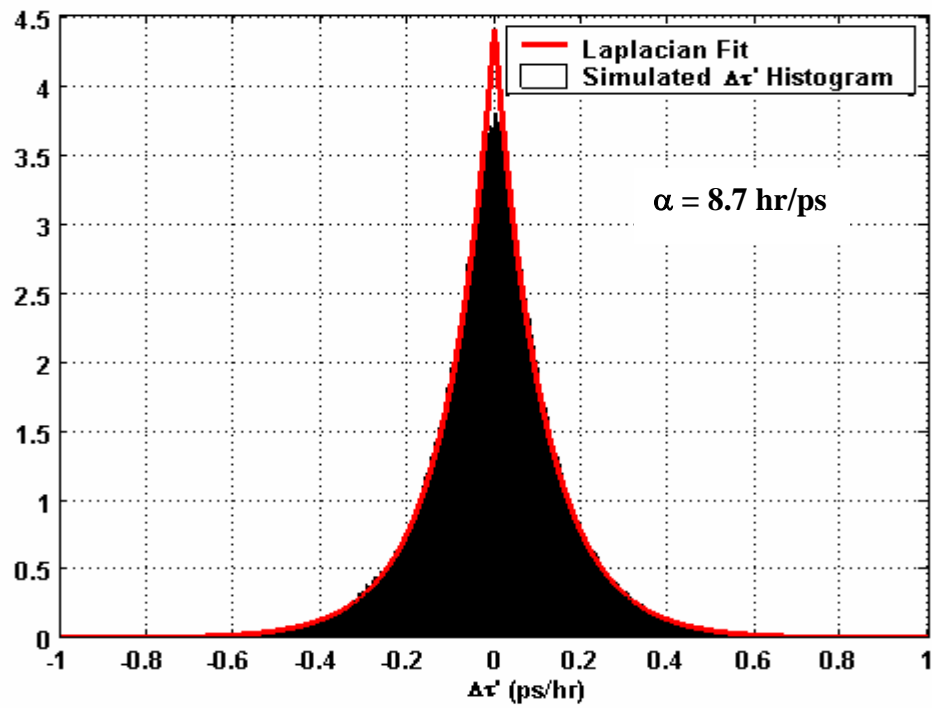
Figure 5.4. Histogram of simulated $\Delta\tau'$ and it Laplacian fit for link 1 in
(a) linear scale (top) and (b) log scale (bottom).

Figures 5.4 (a) and 5.4 (b) show the histogram of simulated $\Delta\tau'$ and its Laplacian fit for link 1 in linear and log scales respectively. It can be observed that there is a good agreement between the $\Delta\tau'$ histogram and the Laplacian distribution, and this agreement between the two is much better than from measured data presented in chapter 2. Results from the modified chi-square test on the simulated $\Delta\tau'$ data are included in table 5.10. The Maxwellian and Laplacian fits shown in this report are not optimized fits (like the least-squares fit) and the parameter values governing these distributions are calculated either from measured or simulated data.

The Laplacian parameter (α) value corresponding to the Laplacian fit shown in figure 5.4, calculated from simulated data is 8.7 hr/ps which is close to the value of 7.5 hr/ps obtained from measured data. A comparison of the relative first-order mean outage rates using these α values and the simplified outage rate expression (3.2) is shown in figure 5.5. From the figure it is clear that the values show good agreement.
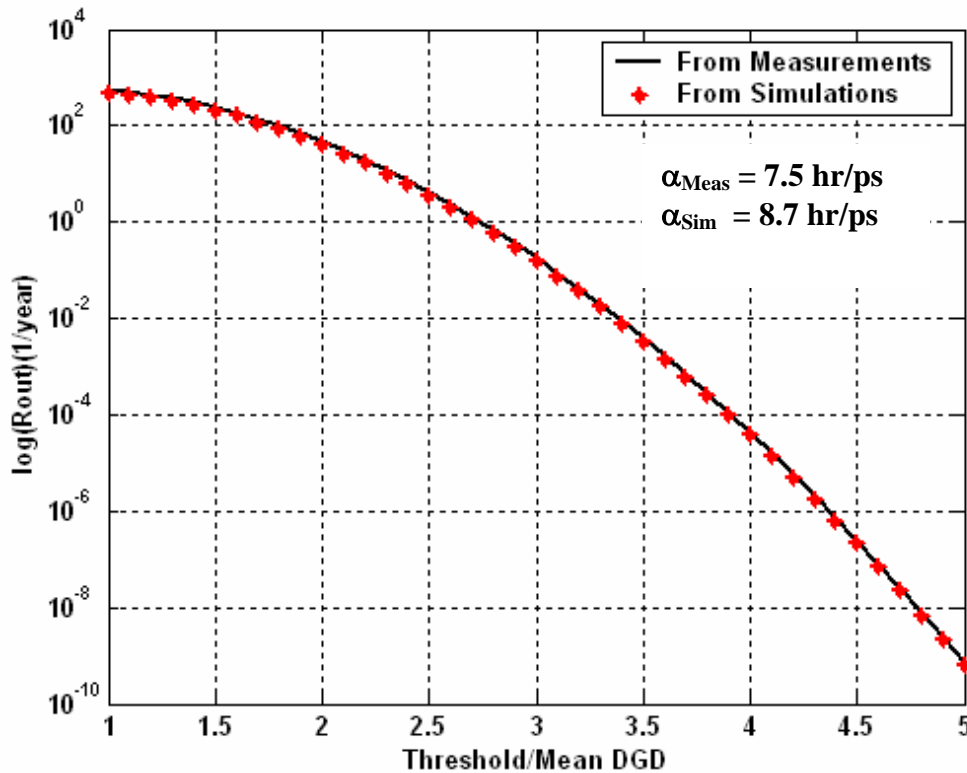
Figure 5.5. Comparison of relative R_{out} values from measured data and simulation data on link 1 calculated using the simplified outage rate expression.

The decorrelation time and decorrelation bandwidth are determined from simulated and measured data for link 1 and these are the full width half maximum (FWHM) values of the time autocorrelation and frequency autocorrelation functions of measured/simulated DGD data respectively. The decorrelation time from the simulated data was around 4 days which is slightly different from the value from the measured data of 4.6 days. The decorrelation bandwidth from the simulated data differed from the value from measured data by about 30 %, although a better agreement between the two is desired.

5.3.2. Single-span link 2

Table 5.2 shows the values of the free parameters used in the simulation of link 2. The same narrowband filter as in the case of link 1 is used to filter the raw temperature data.

Table 5.2. Values of free parameters for link 2.

Proportionality constant k (radians/°F)	Number of time-varying sections	Relative filter bandwidth parameter	Gaussian std. deviation (radians)
0.2	4	0.001	$\pi/48$
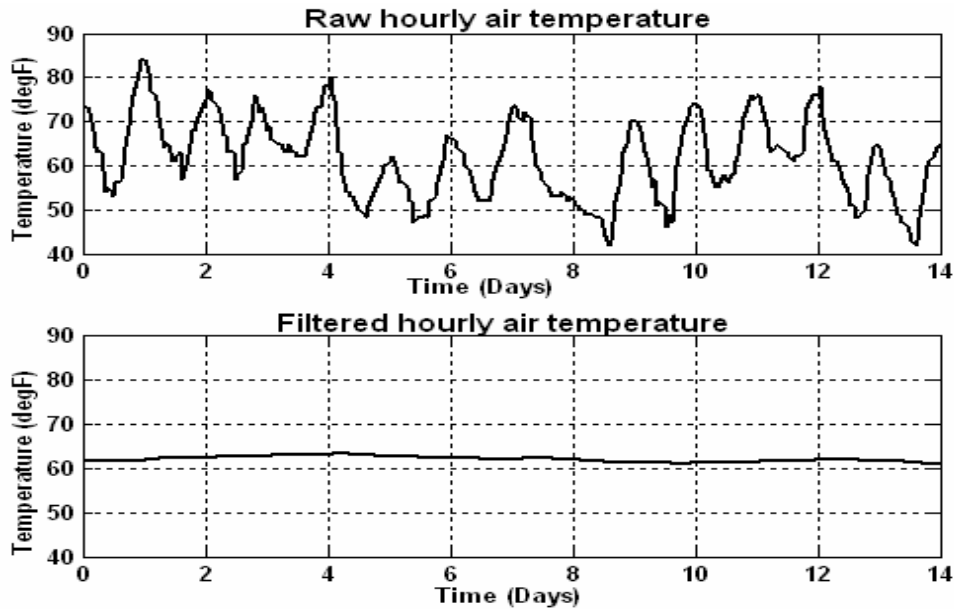
Figure 5.6. (a). Hourly air temperature; (b) Corresponding filtered temperature.

68
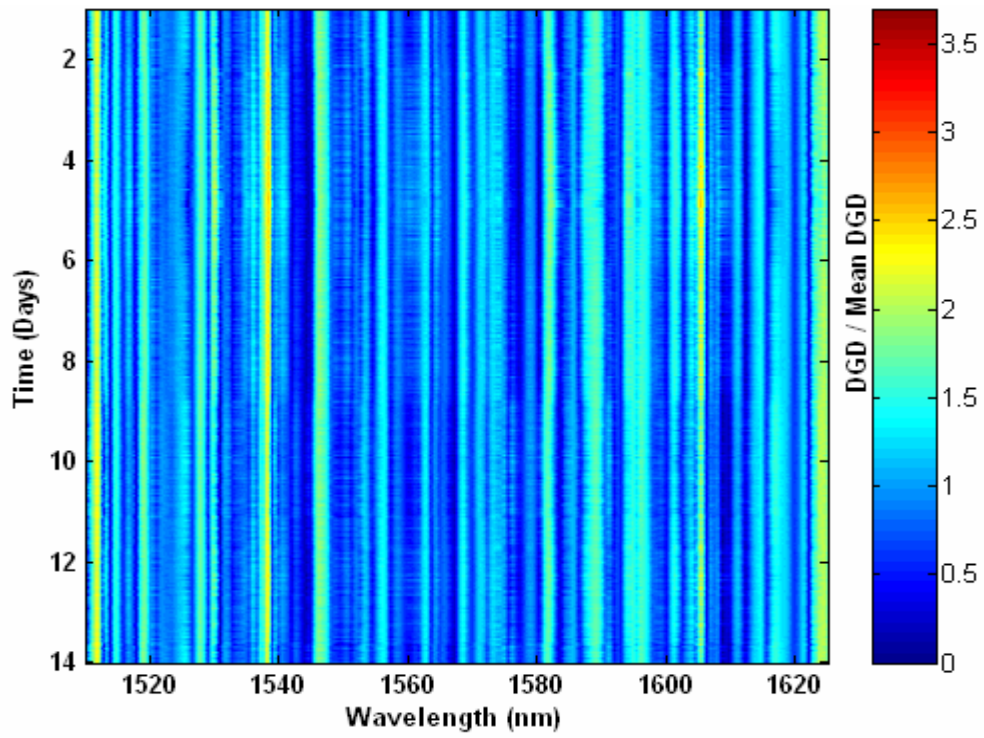
Figure 5.7. (a) Normalized DGD colormap obtained from link 2 simulation.
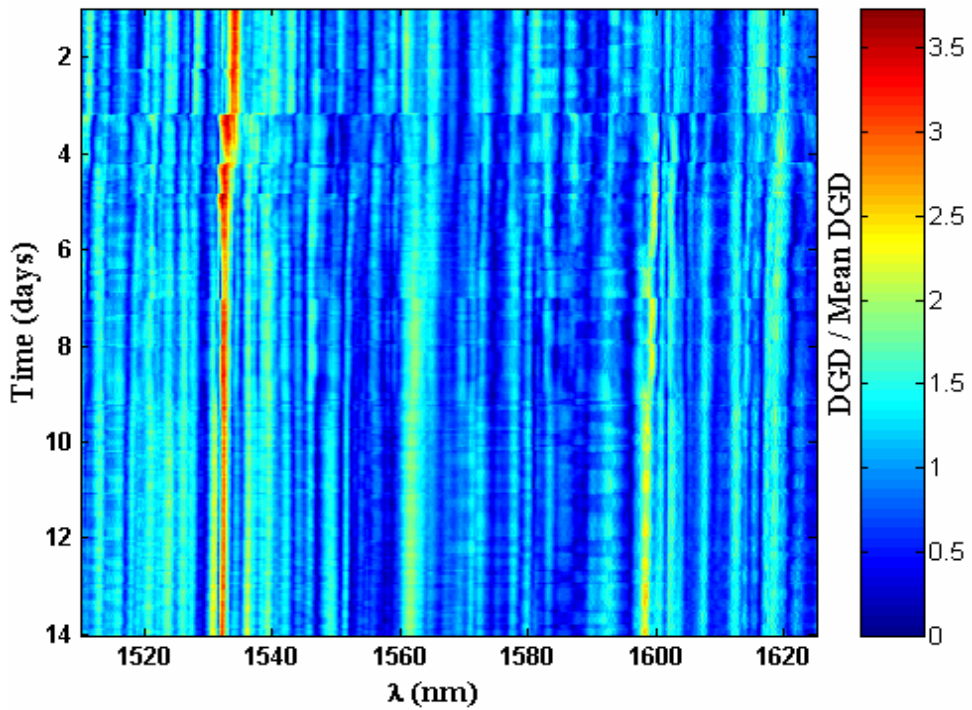
Figure 5.7. (b) Normalized DGD colormap obtained from link 2 measurements shown in chapter 2, reproduced here for comparison.

Figure 5.6 shows the measured hourly air temperature (top plot) at one location over the 14-day measurement period for link 2 discussed in chapter 2 and the corresponding filtered temperature (bottom plot) used in the simulation.

Figure 5.7 (a) shows the normalized DGD colormap obtained from link 2 simulation using the filtered temperature profile shown in figure 5.6 (b) and the parameter values shown in table 5.2. The colormap obtained from measurements on link 2, shown in chapter 2, is repeated here as figure 5.7 (b) for comparison. Simulations in time were repeated at 1 hour intervals and DGD was calculated every hour. This is different from the measurements on link 2 which were repeated every 1 hour and 25 minutes. Comparing the colormaps in figure 5.7 it is clear that both the colormaps look very similar in the sense that there is no significant temporal change in DGD over the 14-day period. A slight drift across the wavelengths observed in the measured DGD colormap is absent in the simulated DGD colormap and this could be attributed to using a fixed value of 'b' in the simulations. The actual mean DGD obtained from simulation, although not mentioned here, was close (< 5 % difference) to the value from the measurements.

Figures 5.8 (a) and 5.8 (b) show the histogram of simulated normalized DGD and its Maxwellian fit for link 2 in linear and log scales respectively. It can be observed that the agreement between the histogram and the Maxwellian distribution is not very good and this could be because there are not enough independent DGD samples over the 14-day observation period. Results from the modified chi-square test on the simulated DGD data are included in table 5.9.
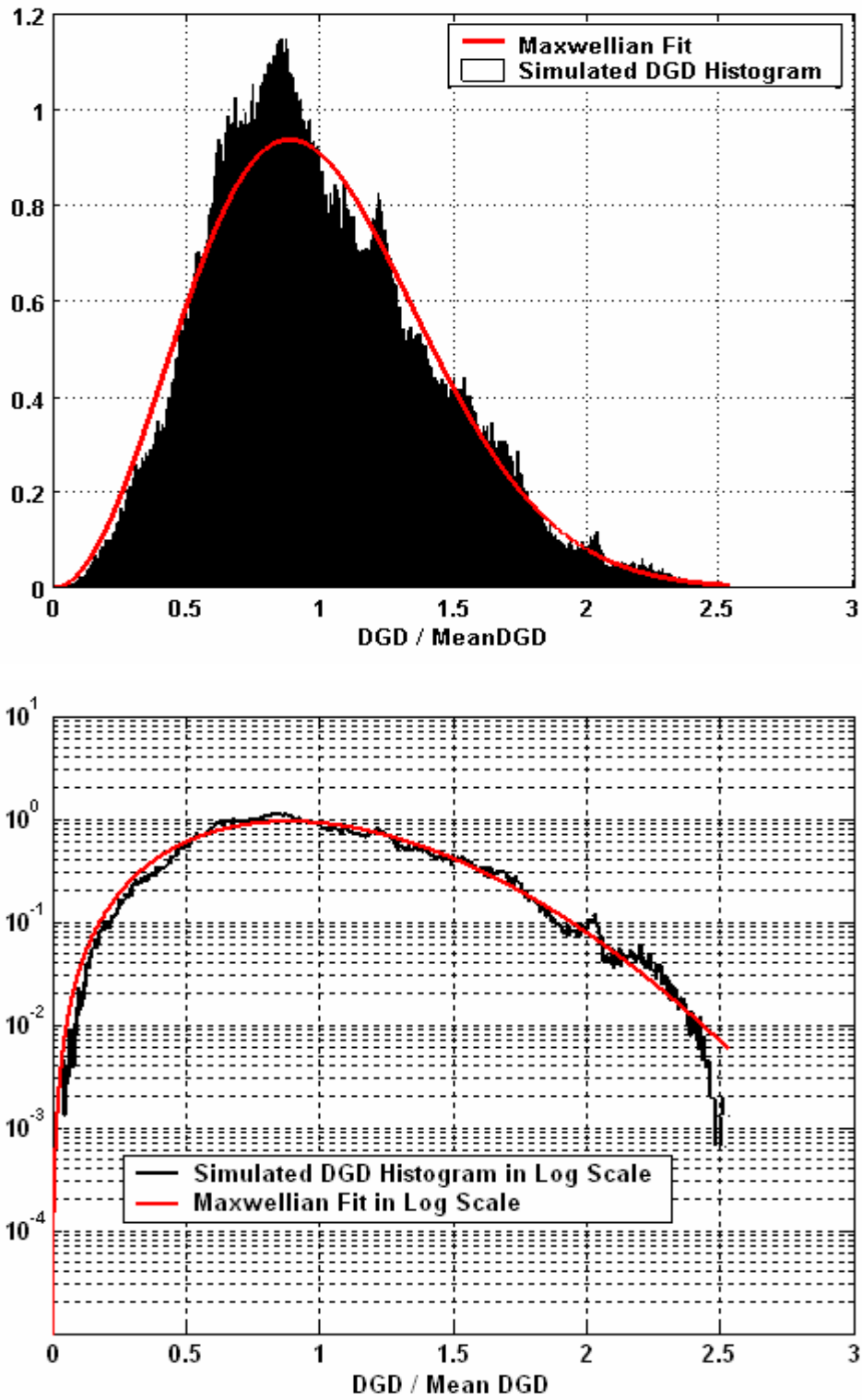
Figure 5.8. Histogram of simulated normalized DGD and its Maxwellian fit for link 2 in (a) linear scale (top) and (b) log scale.
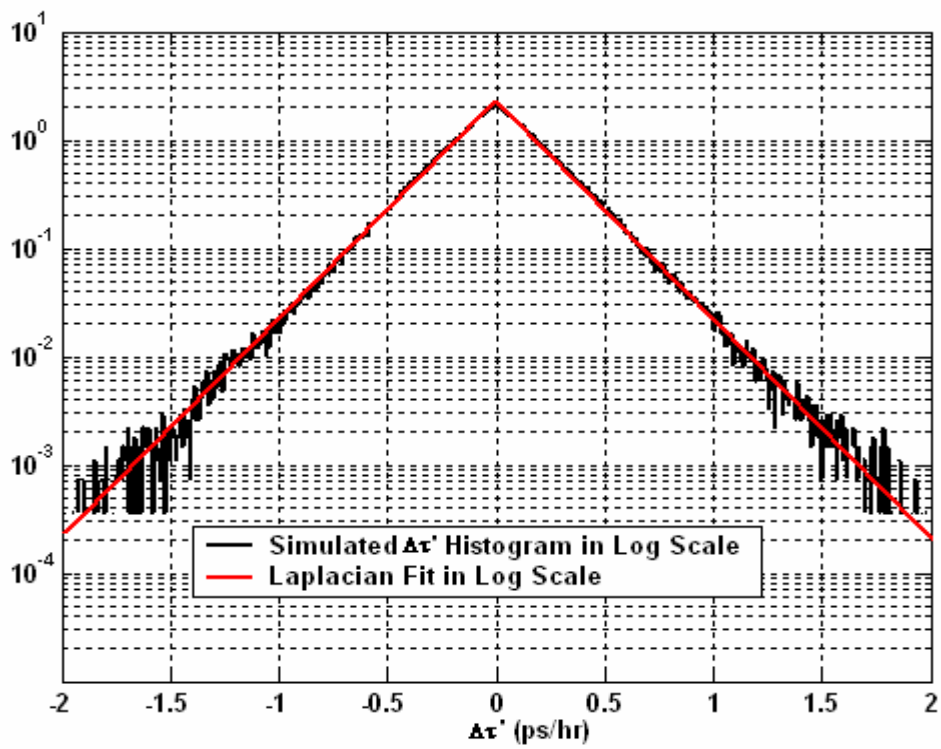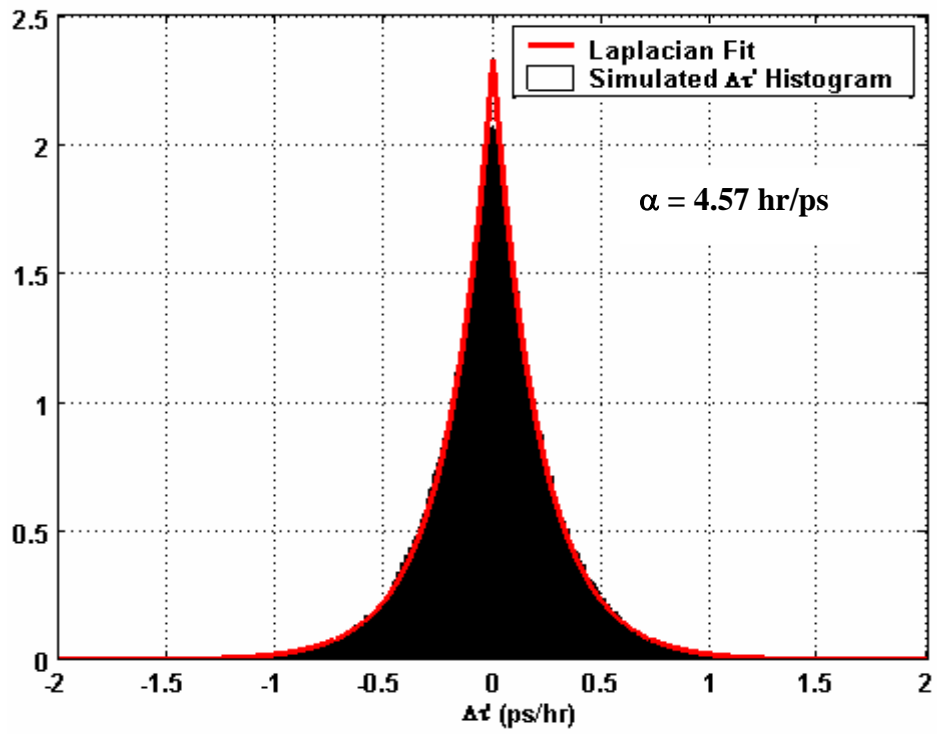
Figure 5.9. Histogram of simulated Δτ' and it Laplacian fit for link 2 in (a) linear scale (top) and (b) log scale (bottom).

Figures 5.9 (a) and 5.9 (b) show the histogram of simulated $\Delta\tau'$ and its Laplacian fit for link 2 in linear and log scales respectively. It is evident from the figures that there is a good agreement between the $\Delta\tau'$ histogram and the Laplacian distribution, and this agreement between the two is much better than from measured data presented in chapter 2. Results from the modified chi-square test on the simulated $\Delta\tau'$ data are included in table 5.10.

The Laplacian parameter (α) value corresponding to the Laplacian fit shown in figure 5.9, calculated from simulated data is 4.57 hr/ps which is close to the value of 4.25 hr/ps obtained from measured data. Figure 5.10 shows a comparison of the relative first-order mean outage rates using these α values and the simplified outage rate expression (3.2). A good agreement between the values calculated from simulated and measured data is evident from the figure.
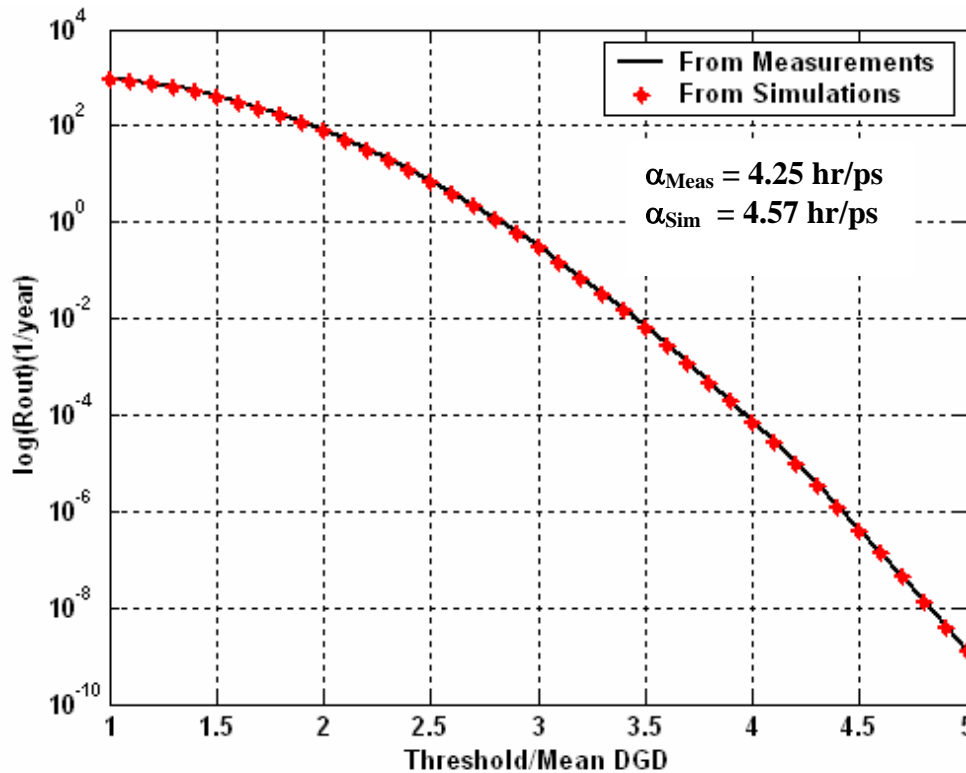
Figure 5.10. Comparison of relative R_{out} values from measured data and simulation data on link 2 calculated using the simplified outage rate expression.

The decorrelation time from the simulated data was around 0.87 days which is very close to the value from the measured data of 0.83 days. The decorrelation bandwidth from the simulated data differed from the value from measured data by about 10 %.

5.3.3. Single-span link 3

Table 5.3 shows the values of the free parameters used in the simulation of link 3. A filter parameter of 0.002 is used in this case which implies a slightly wider low pass filter than in the cases of links 1 and 2.

Table 5.3. Values of free parameters for link 3.

| Proportionality constant k (radians/°F)	Number of time-varying sections	Relative filter bandwidth parameter	Gaussian std. deviation (radians)
0.2	4	0.002	$\pi/120$
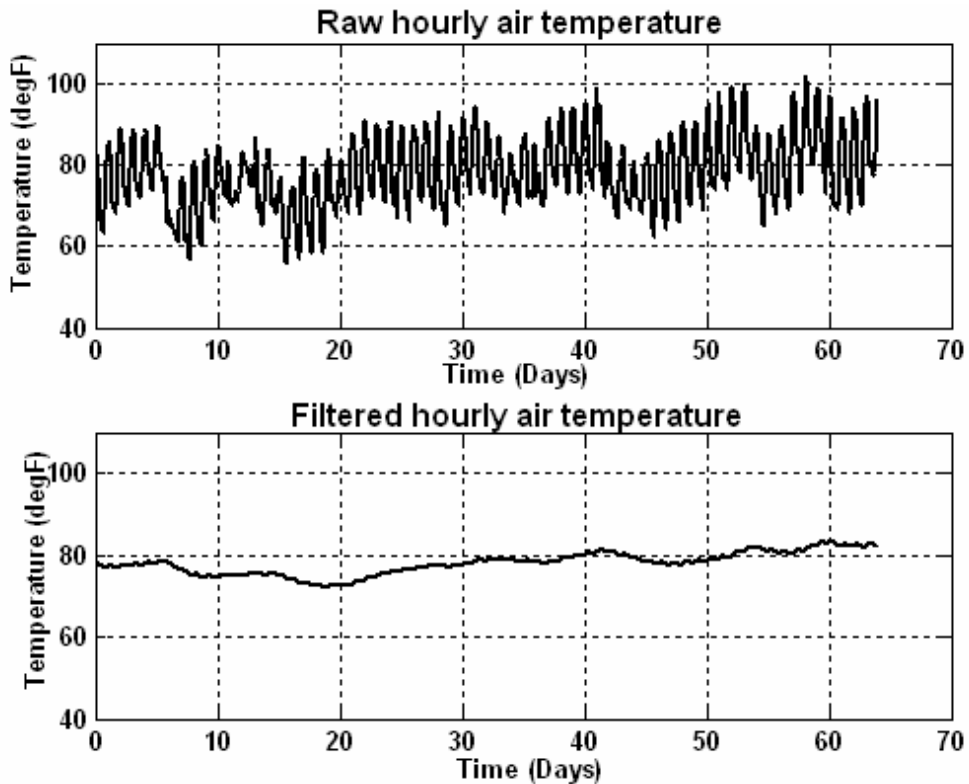
Figure 5.11. (a). Hourly air temperature; (b) Corresponding filtered temperature.
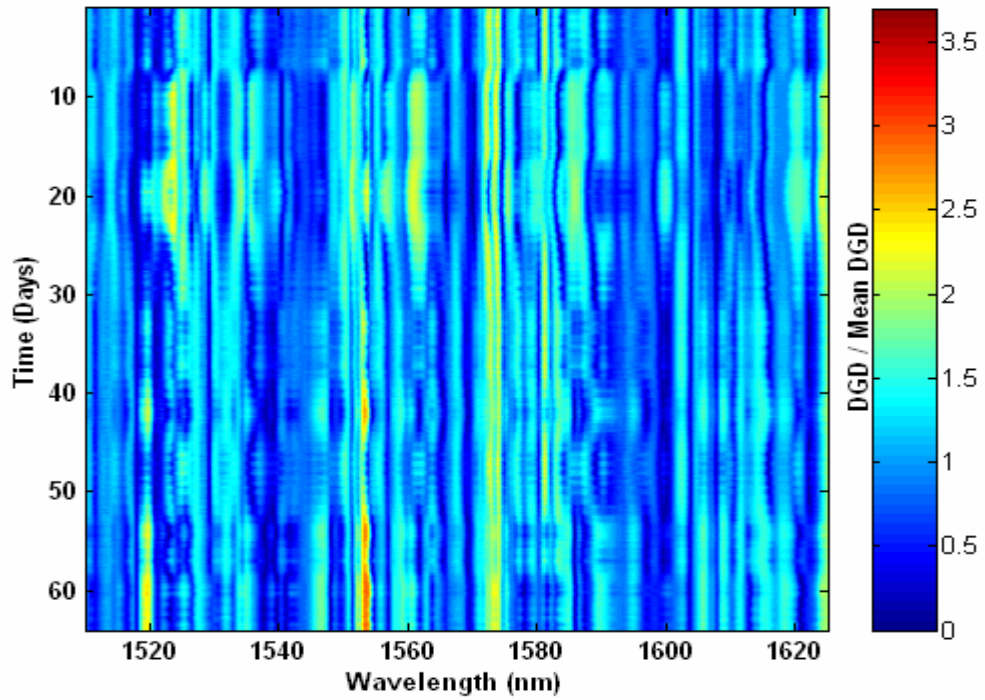
Figure 5.12. (a) Normalized DGD colormap obtained from link 3 simulation.
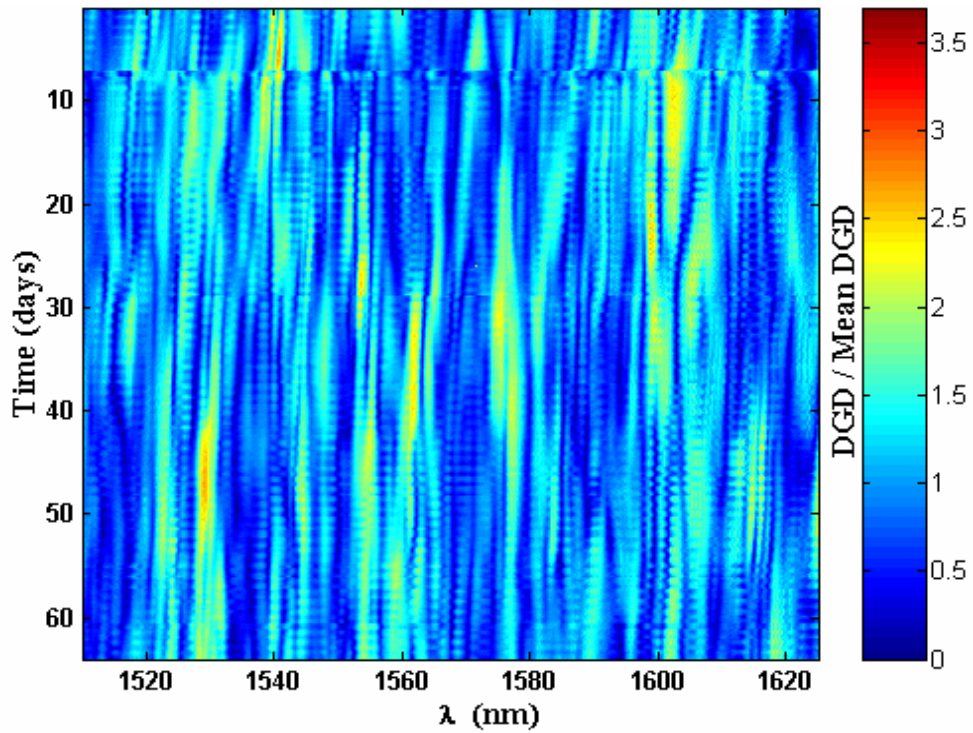
Figure 5.12. (b) Normalized DGD colormap obtained from link 3 measurements shown in chapter 2, reproduced here for comparison.

Figure 5.11 shows the measured hourly air temperature (top plot) at one location over the 64-day measurement period for link 3 discussed in chapter 2 and the corresponding filtered temperature (bottom plot) used in the simulation.

Figure 5.12 (a) shows the normalized DGD colormap obtained from link 3 simulation using the filtered temperature profile shown in figure 5.11 (b) and the parameter values shown in table 5.3. The colormap obtained from measurements of link 3, shown in chapter 2, is repeated here as figure 5.12 (b) for comparison. As in the case of link 2, simulations in time were repeated at 1 hour intervals and DGD was calculated every hour. This is different from the measurements on link 3 which were repeated every 1 hour and 25 minutes. Comparing the colormaps in figure 5.12 it is clear that both the colormaps look very similar except for the slight drift across the wavelengths observed only in the measured DGD colormap. The absence of this drift in the simulated DGD colormap could again be attributed to using a fixed value of 'b' in the simulations. The simulated DGD colormap shows an interesting feature around day 9 that also appears in the measured DGD colormap. The actual mean DGD obtained from simulation, although not mentioned here, was close (< 5 % difference) to the value from the measurements.

Figures 5.13 (a) and 5.13 (b) show the histogram of simulated normalized DGD and its Maxwellian fit for link 3 in linear and log scales respectively. It can be observed that the agreement between the histogram and the Maxwellian distribution is not very good and a better agreement between the two is desired. Results from the modified chi-square test on the simulated DGD data are included in table 5.9.
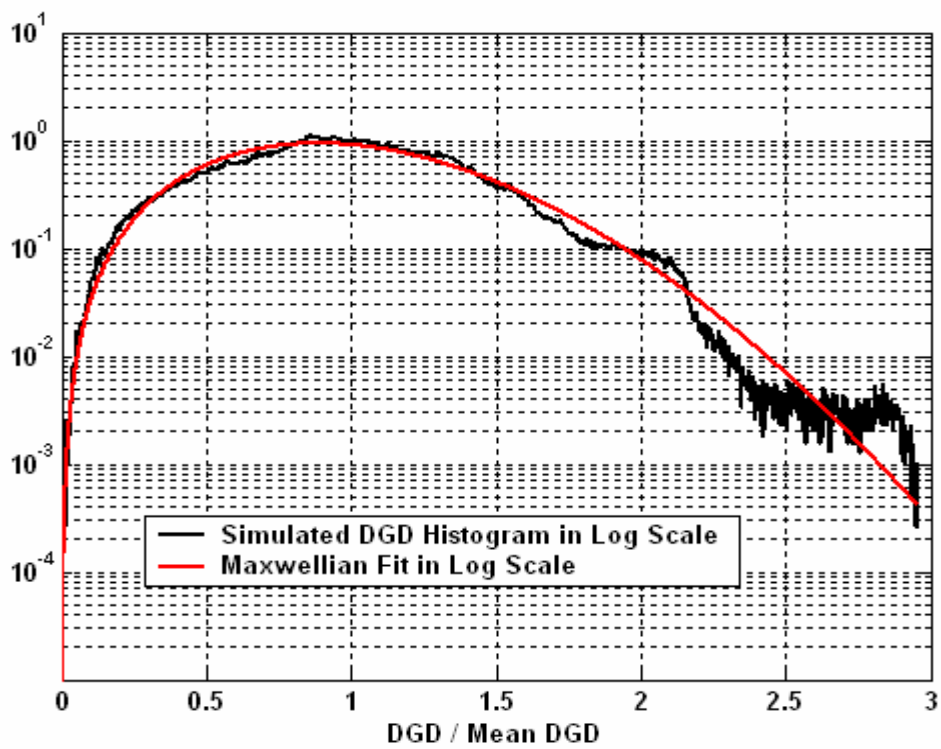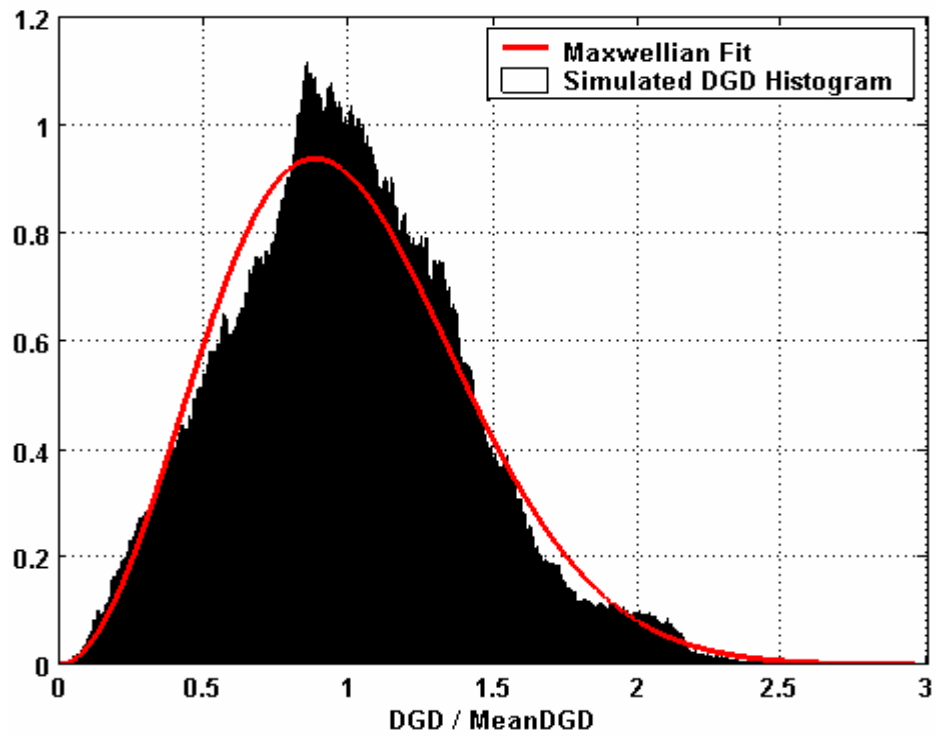
Figure 5.13. Histogram of simulated normalized DGD and its Maxwellian fit
for link 3 in (a) linear scale (top) and (b) log scale (bottom).
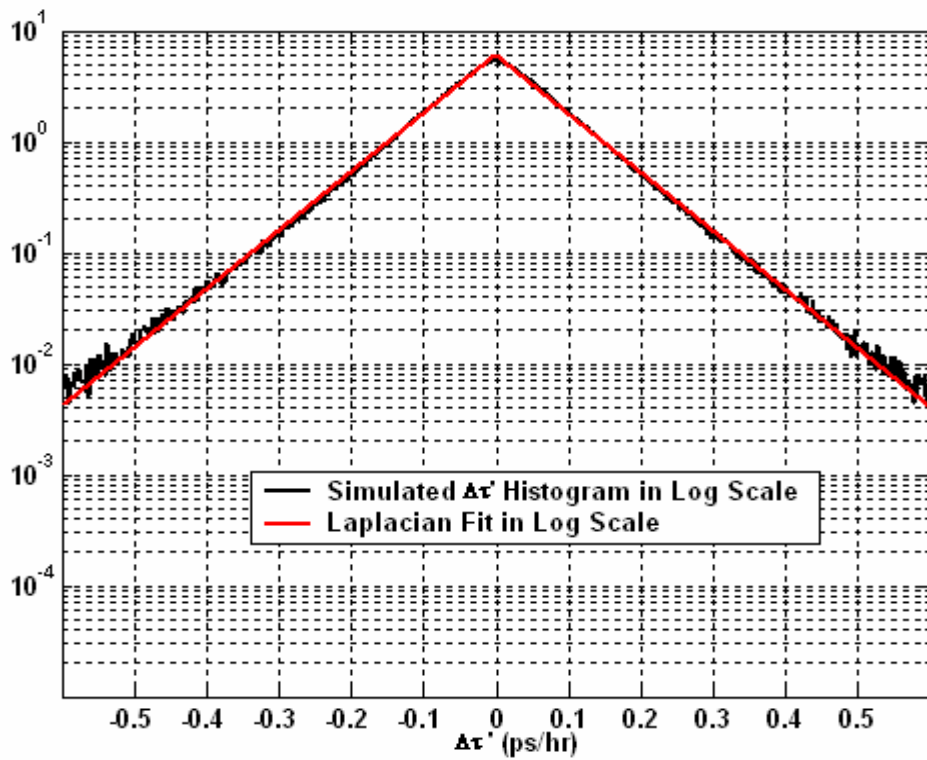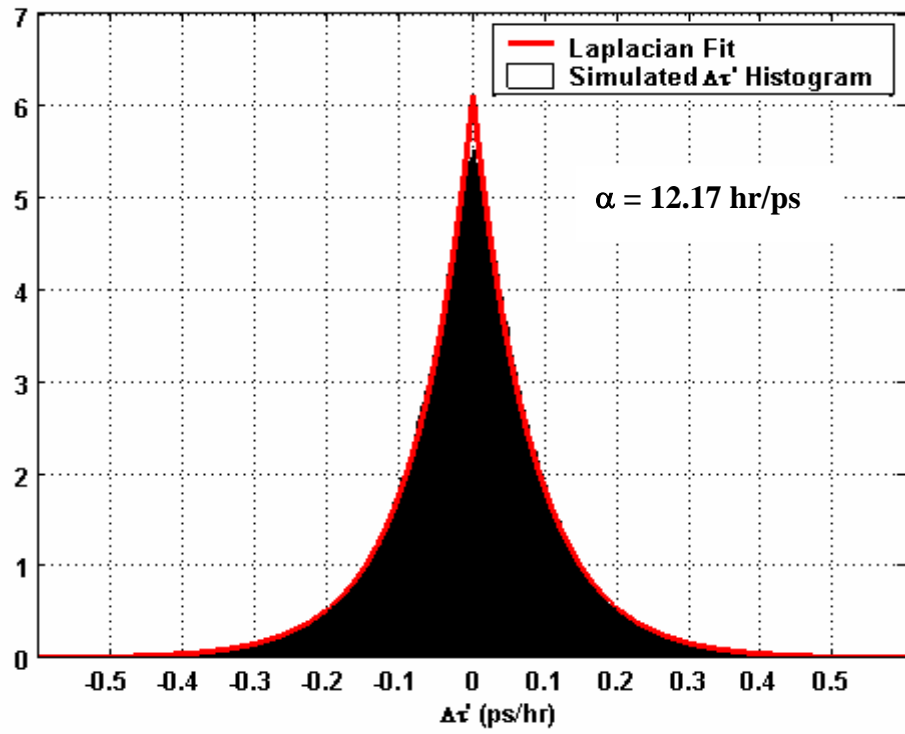
Figure 5.14. Histogram of simulated $\Delta\tau'$ and it Laplacian fit for link 3 in (a) linear scale (top) and (b) log scale (bottom).

Figures 5.14 (a) and 5.14 (b) show the histogram of simulated $\Delta\tau'$ and its Laplacian fit for link 3 in linear and log scales respectively. It can be observed that there is a good agreement between the $\Delta\tau'$ histogram and the Laplacian distribution, and this agreement between the two is much better than from measured data presented in chapter 2. Results from the modified chi-square test on the simulated $\Delta\tau'$ data are included in table 5.10.

The Laplacian parameter (α) value corresponding to the Laplacian fit shown in figure 5.14, calculated from simulated data is 12.17 hr/ps which is close to the value of 10.9 hr/ps obtained from measured data. A comparison of the relative first-order mean outage rates using these α values and the simplified outage rate expression (3.2) is shown in figure 5.15. From the figure it is clear that the values show good agreement.
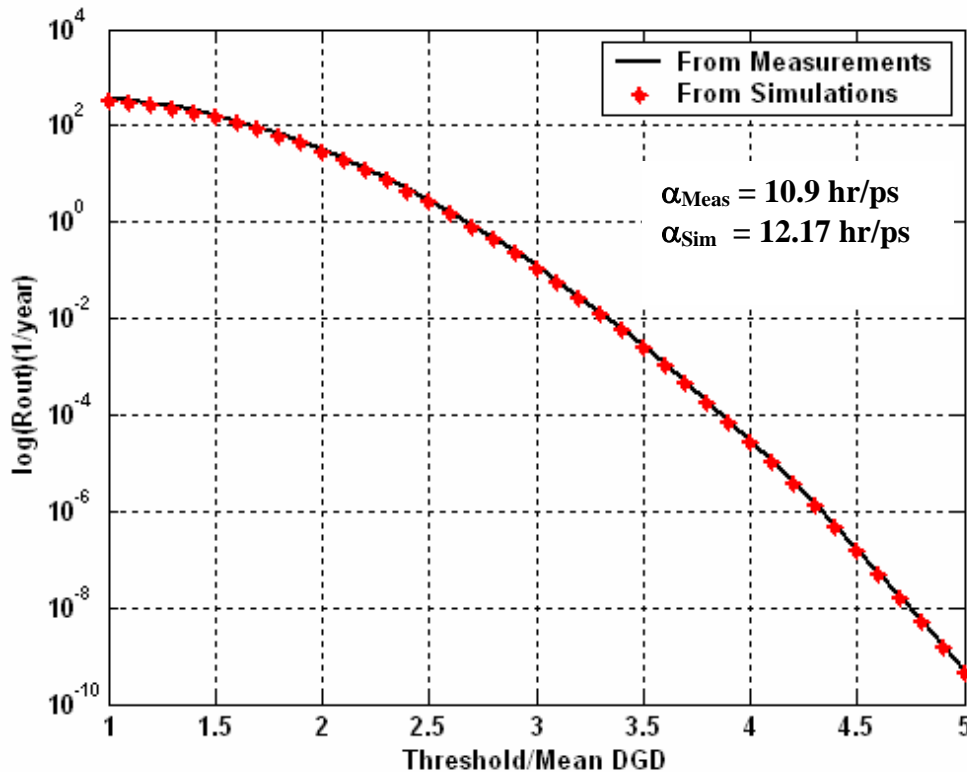
Figure 5.15. Comparison of relative R_{out} values from measured data and simulation data on link 3 calculated using the simplified outage rate expression.

The decorrelation time from the simulated data was around 4.83 days which is very close to the value from the measured data of 5.04 days. The decorrelation bandwidth from the simulated data differed from the value from measured data by about 15 %.

5.4 Concatenated (multi-span) Links

In this section the simulation results for the three two-span links and the only three-span link are discussed. Each span is 95 km long and so each of the two-span links is 190 km long and the three-span link is 285 km long. A 30-nm EDFA band (1535 nm to 1565 nm) is used in all of the simulations.

5.4.1. Two-span link 1-2

Table 5.4. Values of free parameters for link 1-2.

Proportionality constant k (radians/°F)	Number of time-varying sections	Relative filter bandwidth parameter	Gaussian std. deviation (radians)
0.11	8	0.08	$\pi/135$

Table 5.4 above shows the values of the free parameters used in the simulation of two-span link 1-2. The filter used here is comparatively wider than the filter used in the single-span cases. Simulations were repeated every 20 minutes and so a smaller value of Gaussian standard deviation compared to the single-span links was needed.
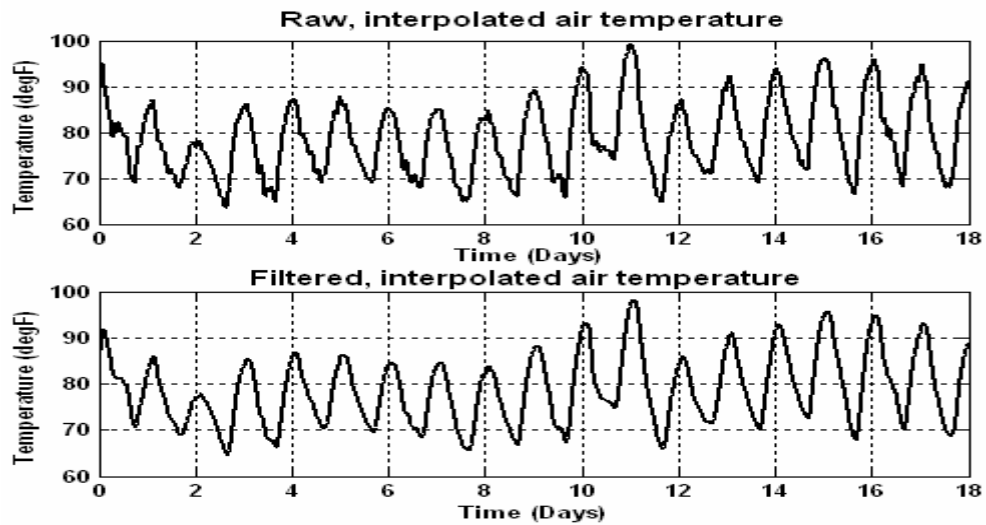

Figure 5.16. (a). Interpolated air temperature; (b) Corresponding filtered temperature.
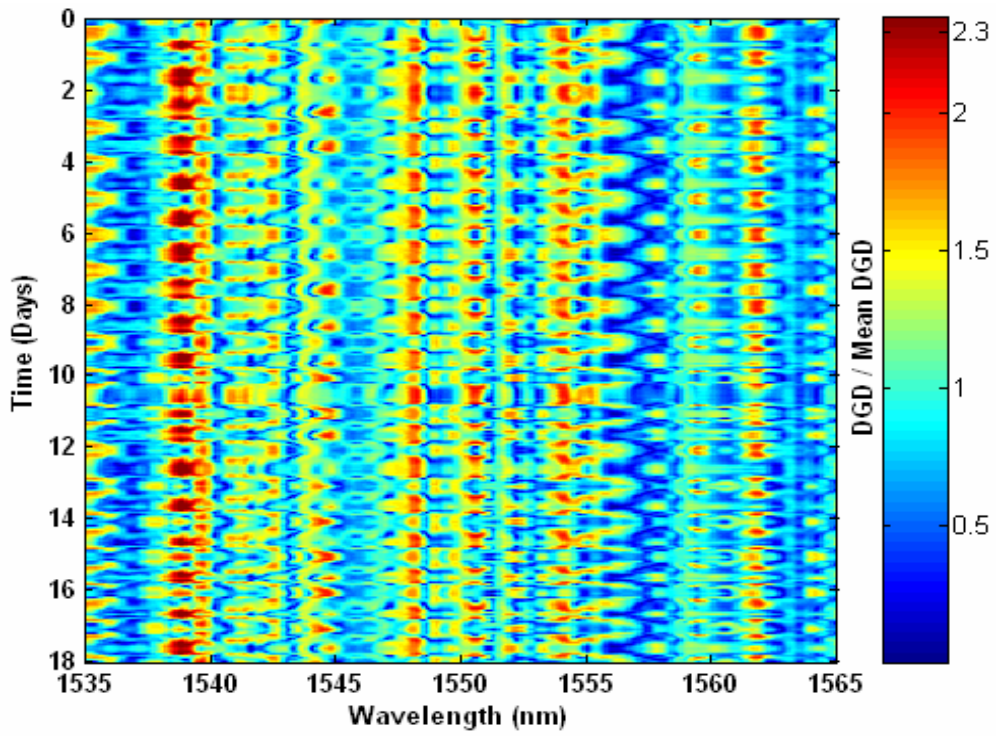
Figure 5.17. (a) Normalized DGD colormap obtained from link 1-2 simulation.
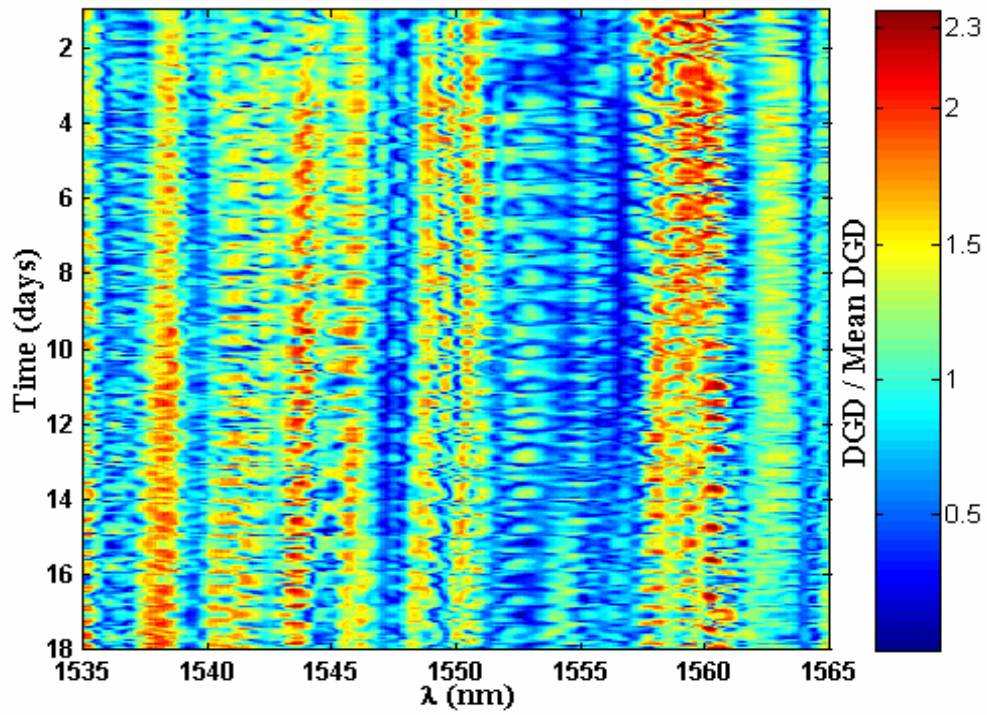

Figure 5.17. (b) Normalized DGD colormap obtained from link 1-2 measurements shown in chapter 2, reproduced here for comparison.

Figure 5.16 shows the measured, interpolated air temperature (top plot) at one location over the 18-day measurement period for link 1-2 discussed in chapter 2 and the corresponding filtered temperature (bottom plot) used in the simulation. Measurements on this link were repeated every 23 minutes and to be consistent simulations were repeated every 20 minutes. The hourly temperature data were interpolated linearly to obtain temperature samples every 20 minutes.

The normalized DGD colormap obtained from link 1-2 simulations is shown in figure 5.17 (a) and the corresponding colormap obtained from measurements, shown in chapter 2, is reproduced here as figure 5.17 (b) for comparison. As mentioned earlier, the sampling interval for simulations was 20 minutes whereas it was 23 minutes for measurements. Looking at figures 5.17 (a) and 5.17 (b), it can be observed that both the colormaps are very similar. They both show fast temporal and spectral variation compared to single-span links and also they both show temporal periodicity. The actual mean DGD obtained from simulation (not mentioned here), was within 2 % of the value from the measurements.

Figures 5.18 (a) and 5.18 (b) show the histogram of simulated normalized DGD and its Maxwellian fit for link 1-2 in linear and log scales respectively. It can be observed from the figures that the agreement between the histogram and the Maxwellian distribution is good. Results from the modified chi-square test on the simulated DGD data are included in table 5.9.
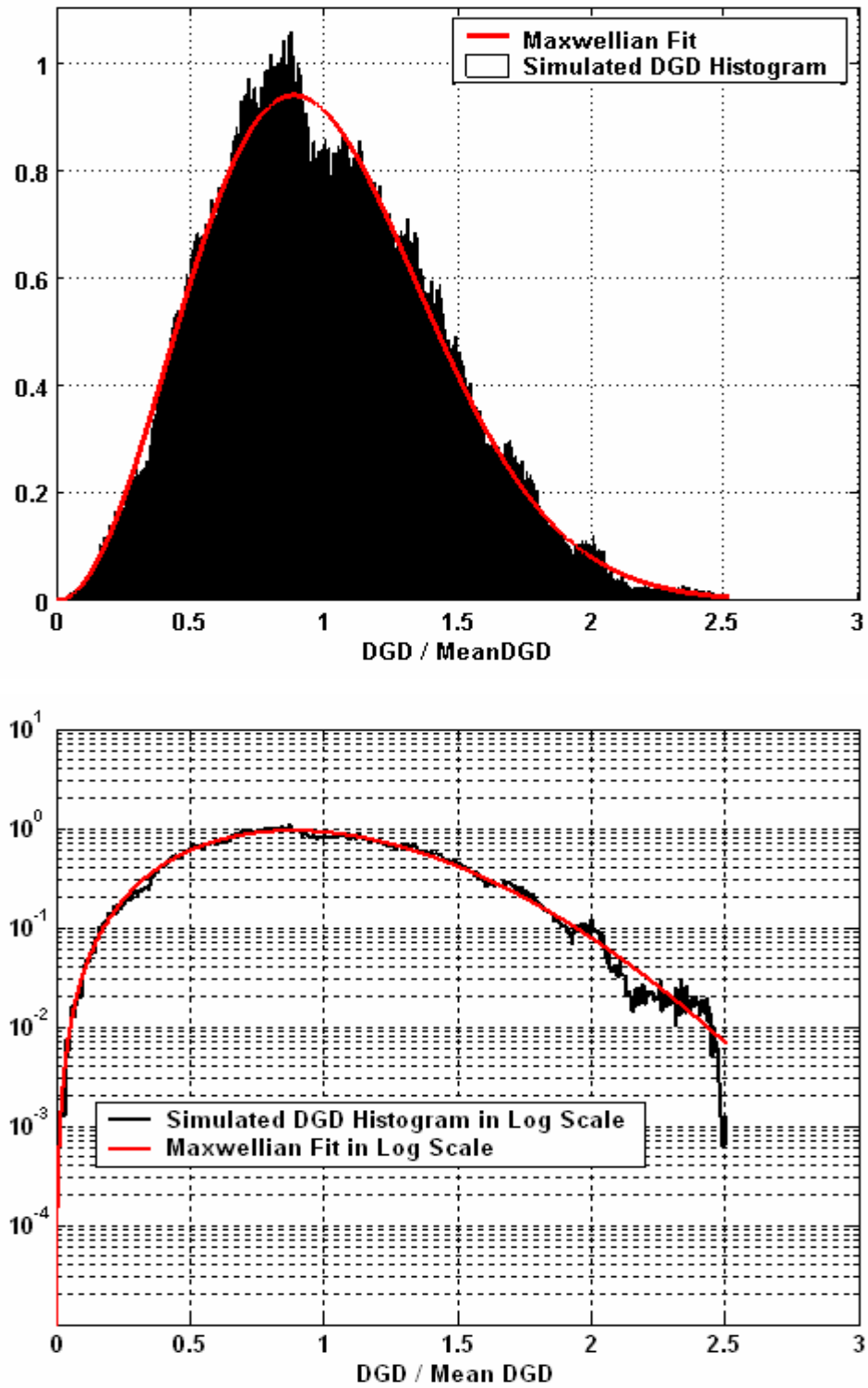
Figure 5.18. Histogram of simulated normalized DGD and its Maxwellian fit for
link 1-2 in (a) linear scale (top) and (b) log scale (bottom).
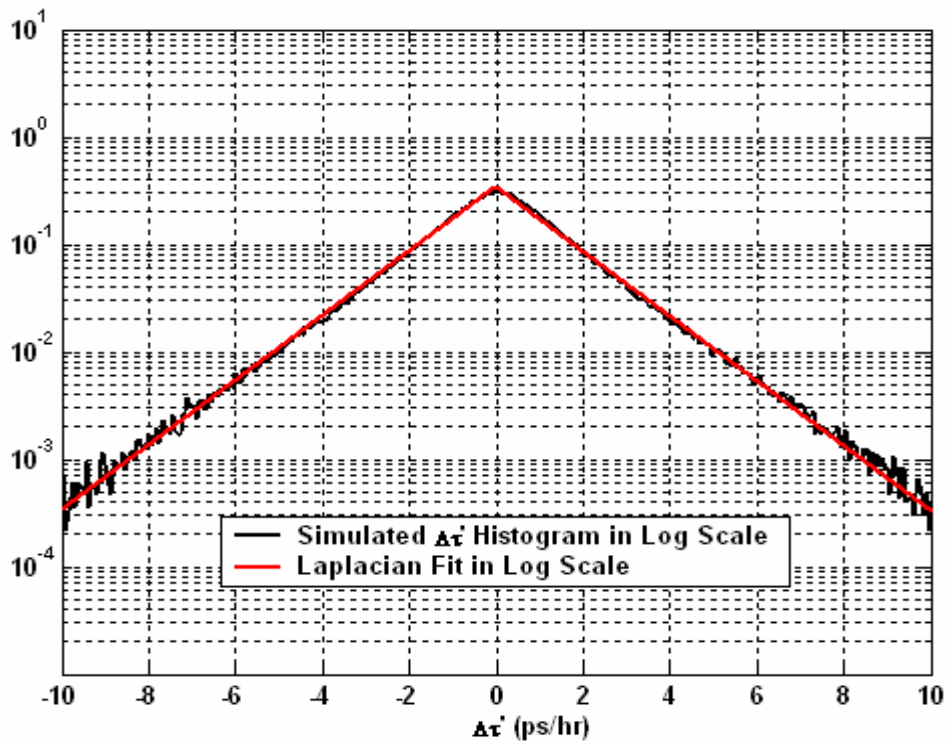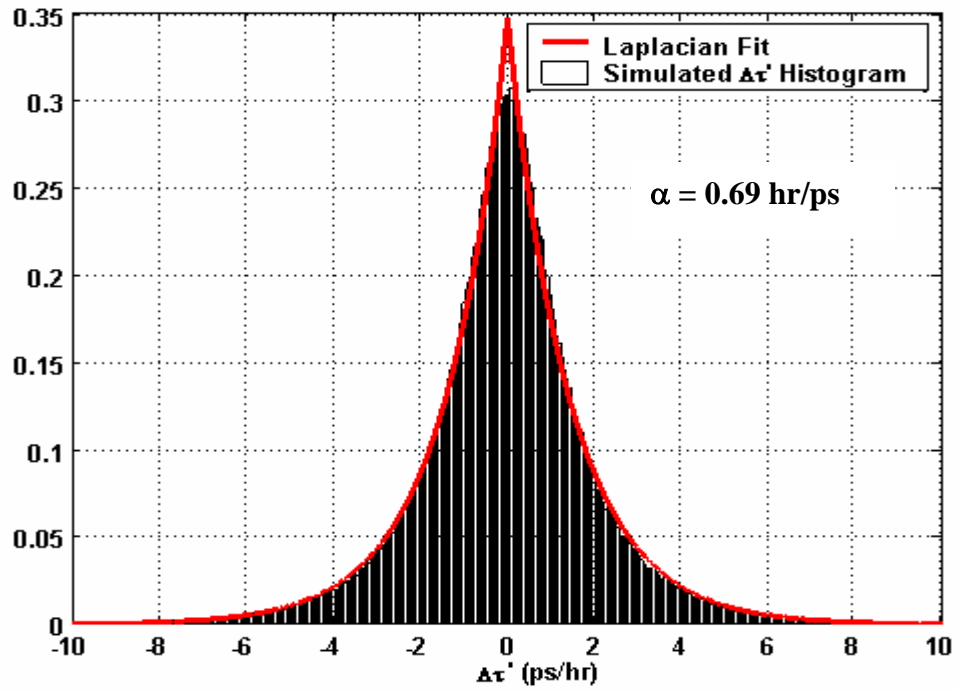
Figure 5.19. Histogram of simulated $\Delta\tau'$ and it Laplacian fit for link 1-2 in (a) linear scale (top) and (b) log scale (bottom).

The histogram of simulated $\Delta\tau'$ and its Laplacian fit for link 1-2 in linear and log scales are shown in figures 5.19 (a) and 5.19 (b) respectively. A good agreement between the simulated $\Delta\tau'$ histogram and the Laplacian distribution is evident from the figures. Results from the modified chi-square test on the simulated $\Delta\tau'$ data are included in table 5.10.

The Laplacian parameter (α) value corresponding to the Laplacian fit shown in figure 5.19, calculated from simulated data is 0.69 hr/ps which is close to the value of 0.6 hr/ps obtained from measured data. Figure 5.20 shows a comparison of the relative first-order mean outage rates using these α values and the simplified outage rate expression (3.2). A good agreement between the values calculated from simulated and measured data is evident from the figure.
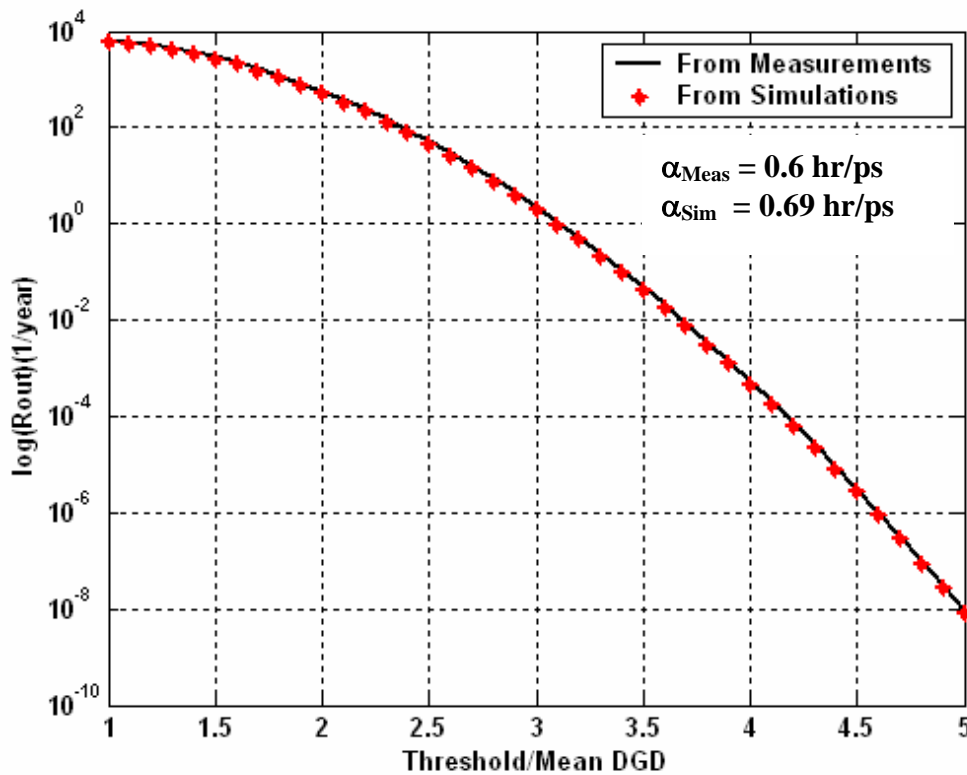
Figure 5.20. Comparison of relative R_{out} values from measured data and simulation data on link 1-2 calculated using the simplified outage rate expression.

The decorrelation time from the simulated data was around 1.66 hours which is very close to the value from the measured data of 1.53 hours. The decorrelation bandwidth from the simulated data differed from the value from measured data by about 10 %.

5.4.2. Two-span link 2-3

Table 5.5. Values of free parameters for link 2-3.

Proportionality constant k (radians/°F)	Number of time-varying sections	Relative filter bandwidth parameter	Gaussian std. deviation (radians)
0.1	8	0.08	$\pi/120$

Table 5.5 above shows the values of the free parameters used in the simulation of two-span link 2-3. The filter used here is same as that of link 1-2.
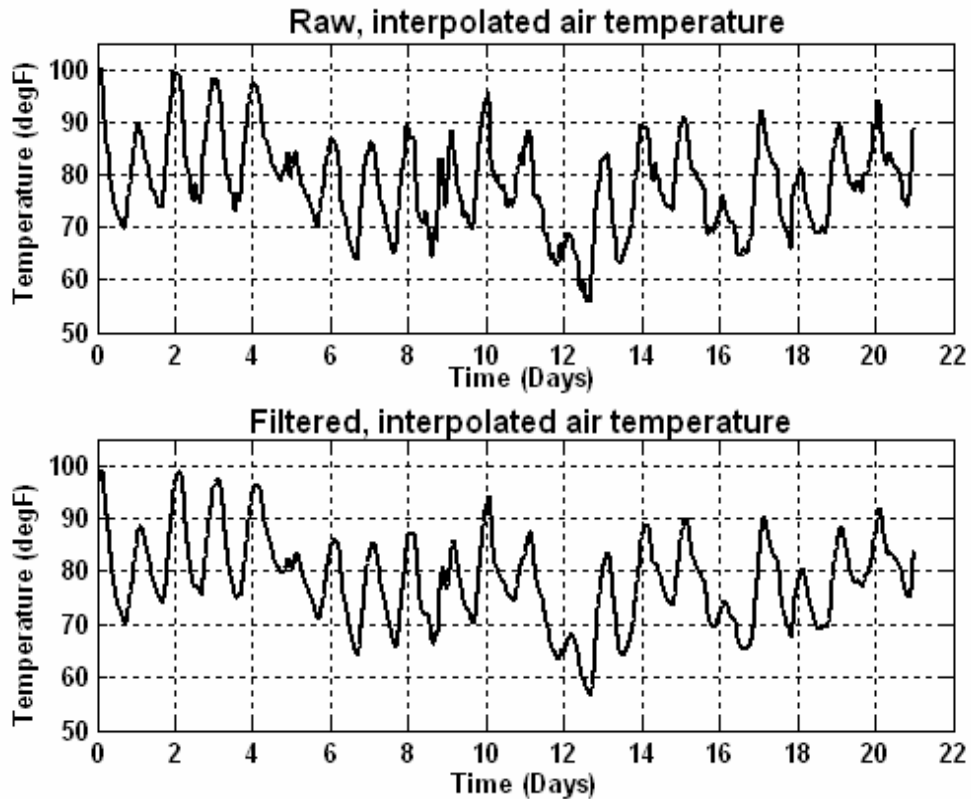
Figure 5.21. (a). Interpolated air temperature; (b) Corresponding filtered temperature.
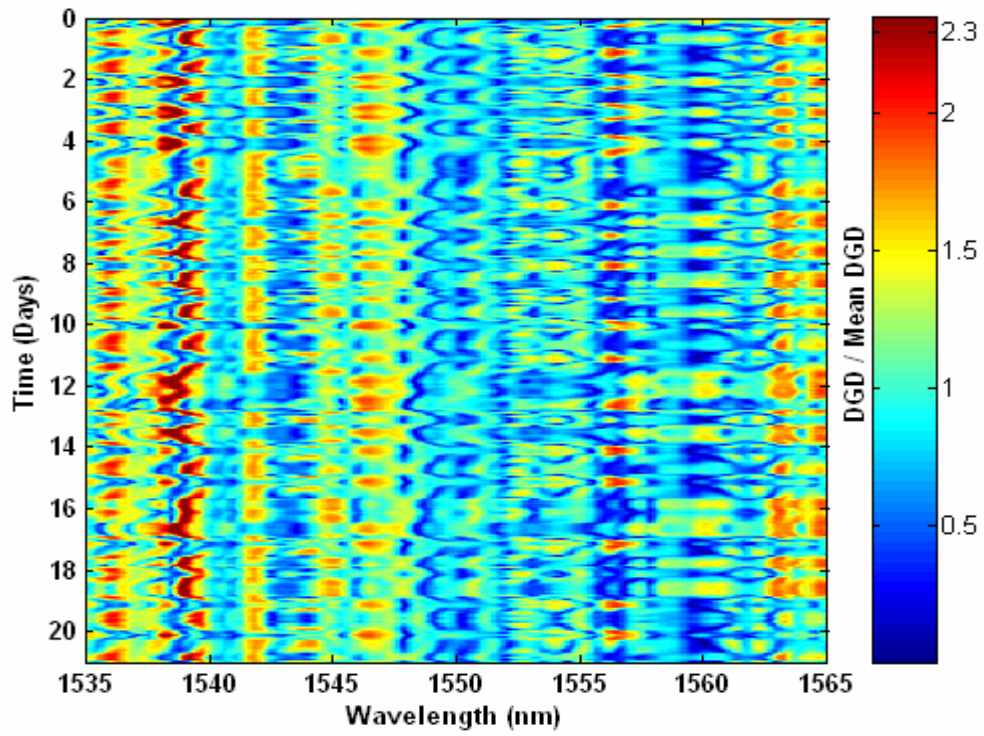
Figure 5.22. (a) Normalized DGD colormap obtained from link 2-3 simulation.
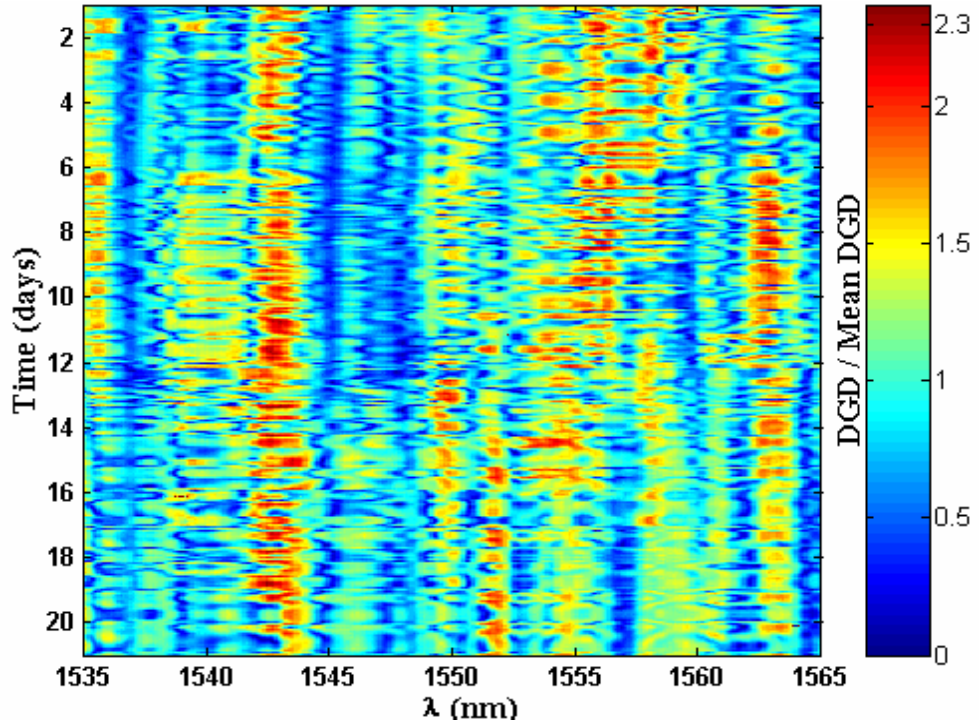
Figure 5.22. (b) Normalized DGD colormap obtained from link 2-3 measurements shown in chapter 2, reproduced here for comparison.

Figure 5.21 shows the measured, interpolated air temperature (top plot) at one location over the 21-day measurement period for link 2-3 discussed in chapter 2 and the corresponding filtered temperature (bottom plot) used in the simulation. Measurements on this link were repeated every 23 minutes and to be consistent simulations were repeated every 20 minutes. The hourly temperature data were interpolated linearly to obtain temperature samples every 20 minutes.

Figure 5.22 (a) shows the normalized DGD colormap obtained from link 2-3 simulation and the corresponding colormap obtained from measurements, shown in chapter 2, is reproduced here as figure 5.22 (b) for comparison. Comparing figures 5.22 (a) and 5.22 (b), it can be observed that both the colormaps look very similar. Both of them show fast temporal and spectral variation and also temporal periodicity. But the locations of the high DGD events are different in both cases. The actual mean DGD obtained from simulation (not mentioned here), was within 3 % of the value from the measurements.

The histogram of simulated normalized DGD and its Maxwellian fit for link 2-3 in linear and log scales are shown in figures 5.23 (a) and 5.23 (b) respectively. It can be observed from the figures that the agreement between the histogram and the Maxwellian distribution is good. Results from the modified chi-square test on the simulated DGD data are included in table 5.9.
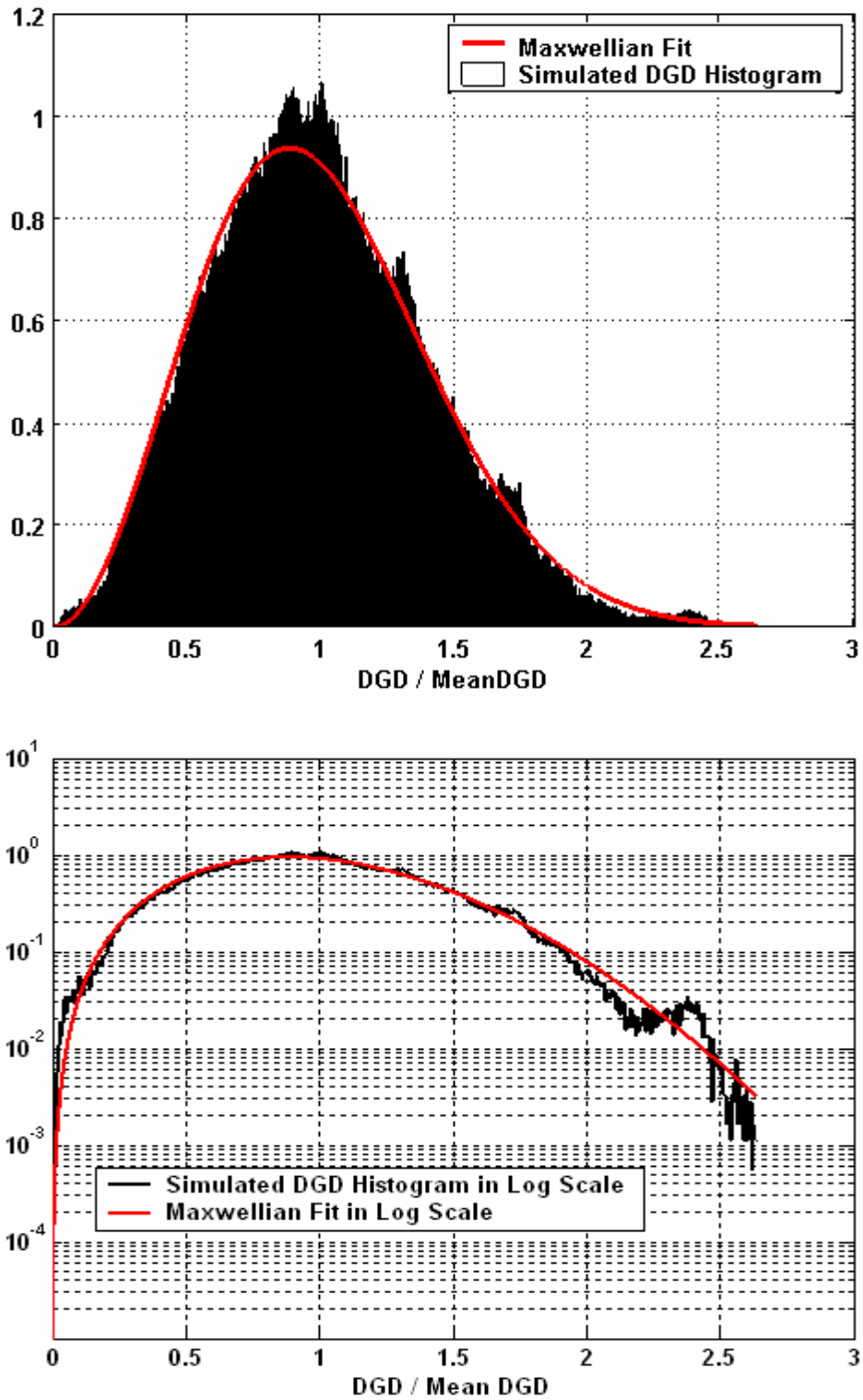
Figure 5.23. Histogram of simulated normalized DGD and its Maxwellian fit
for link 2-3 in (a) linear scale (top) and (b) log scale (bottom).
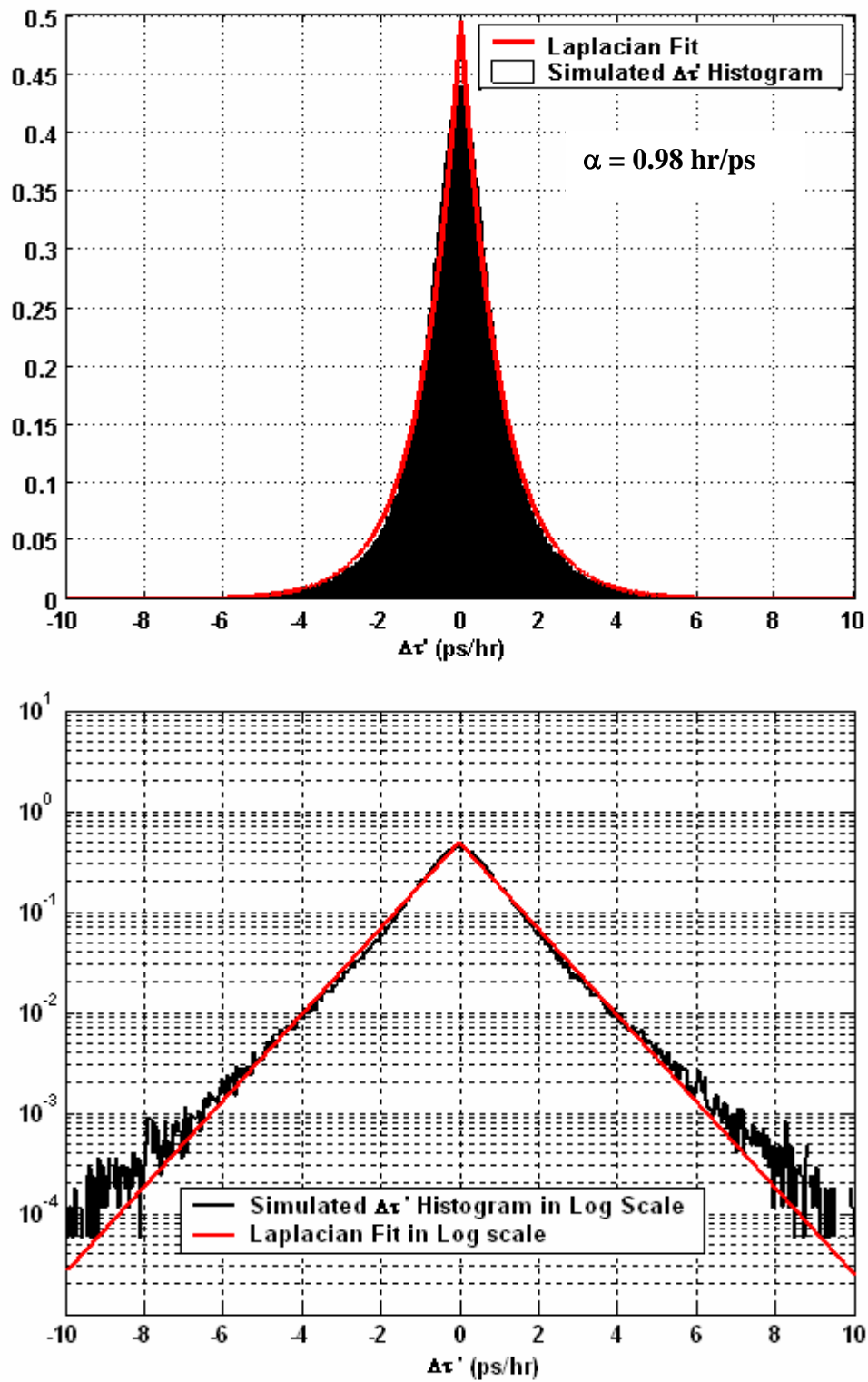
Figure 5.24. Histogram of simulated $\Delta\tau'$ and it Laplacian fit for link 2-3 in (a) linear scale (top) and (b) log scale (bottom).

Figures 5.24 (a) and 5.24 (b) show the histogram of simulated $\Delta\tau'$ and its Laplacian fit for link 2-3 in linear and log scales respectively. It is clear from the figures that the simulated $\Delta\tau'$ histogram and the Laplacian distribution agree well, although the agreement at the tails is not very good. Results from the modified chi-square test on the simulated $\Delta\tau'$ data are included in table 5.10.

The Laplacian parameter (α) value corresponding to the Laplacian fit shown in figure 5.24, calculated from simulated data is 0.98 hr/ps which is close to the value of 0.95 hr/ps obtained from measured data. Figure 5.25 shows a comparison of the relative first-order mean outage rates using these α values and the simplified outage rate expression (3.2). A good agreement between the values calculated from simulated and measured data is evident from the figure.
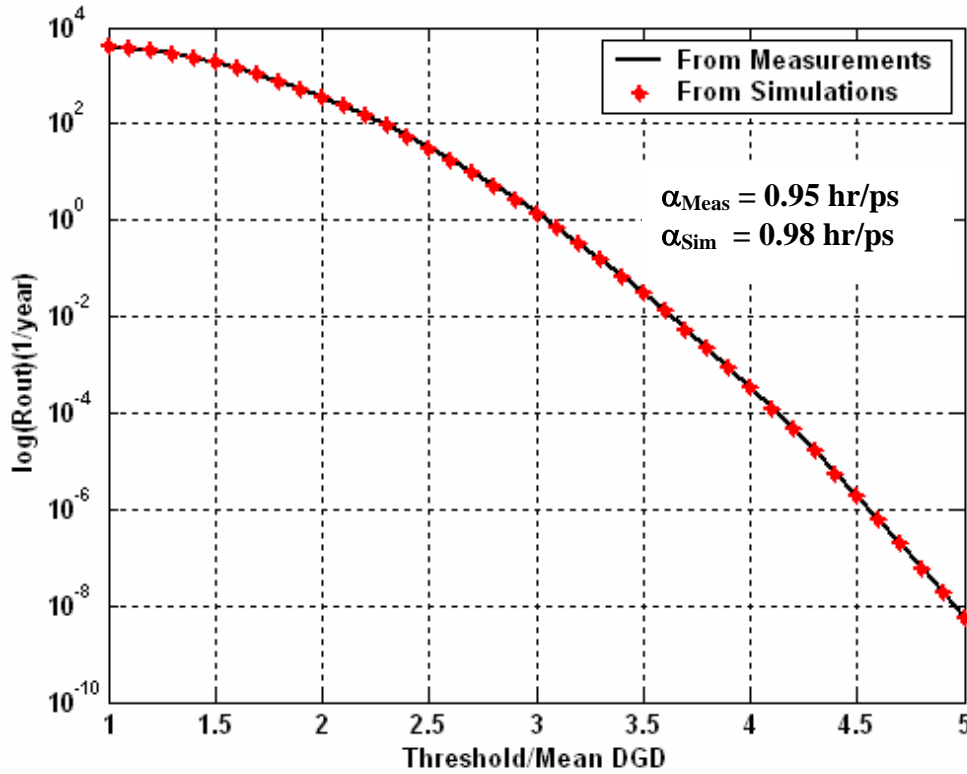
Figure 5.25. Comparison of relative R_{out} values from measured data and simulation data on link 2-3 calculated using the simplified outage rate expression.

The decorrelation time from the simulated data was around 3 hours which is very close to the value from the measured data of 2.3 hours. The decorrelation bandwidth from the simulated data matched exactly with the value from measured data.

5.4.3. Two span link 1-3

Table 5.6 below shows the values of the free parameters used in the simulation of link 1-3. The filter used here is same as that of the other two-span links discussed earlier.

Table 5.6. Values of free parameters for link 1-3.

Proportionality constant k (radians/°F)	Number of time-varying sections	Relative filter bandwidth parameter	Gaussian std. deviation (radians)
0.08	8	0.08	$\pi/120$
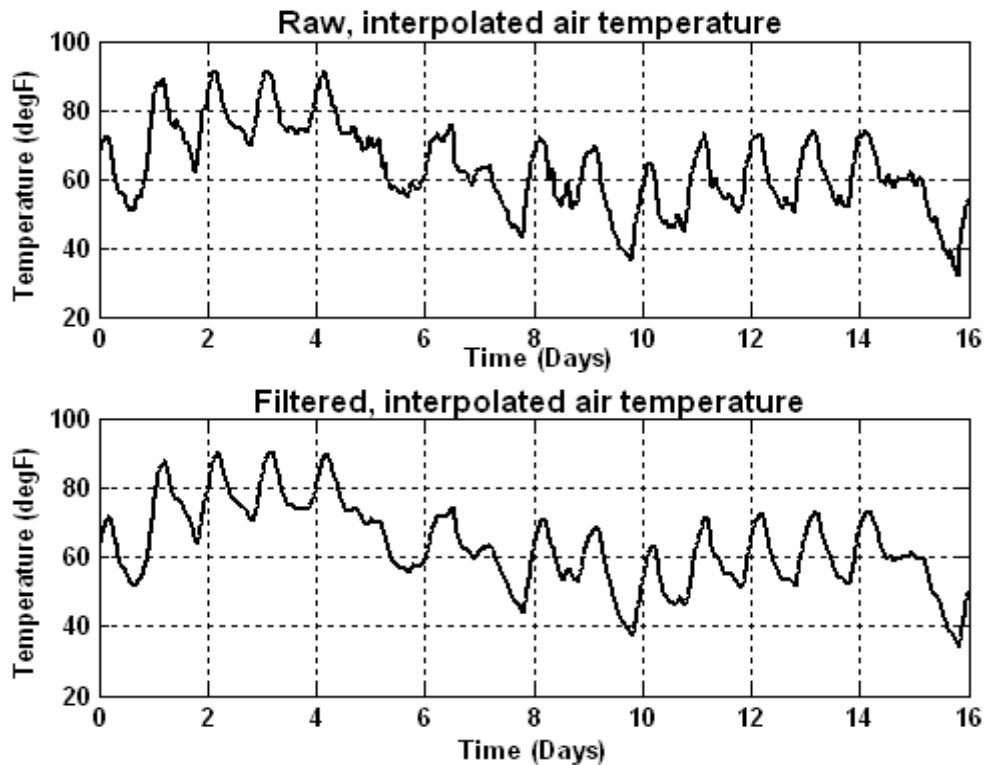
Figure 5.26. (a). Interpolated air temperature; (b) Corresponding filtered temperature.
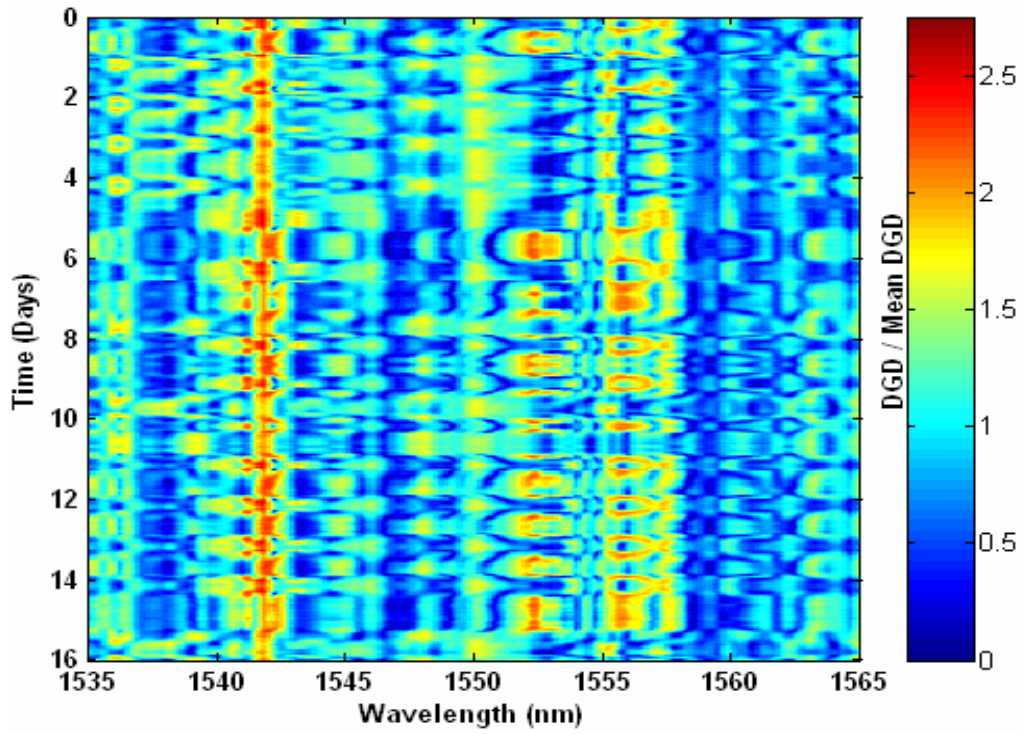
Figure 5.27. (a) Normalized DGD colormap obtained from link 1-3 simulation.
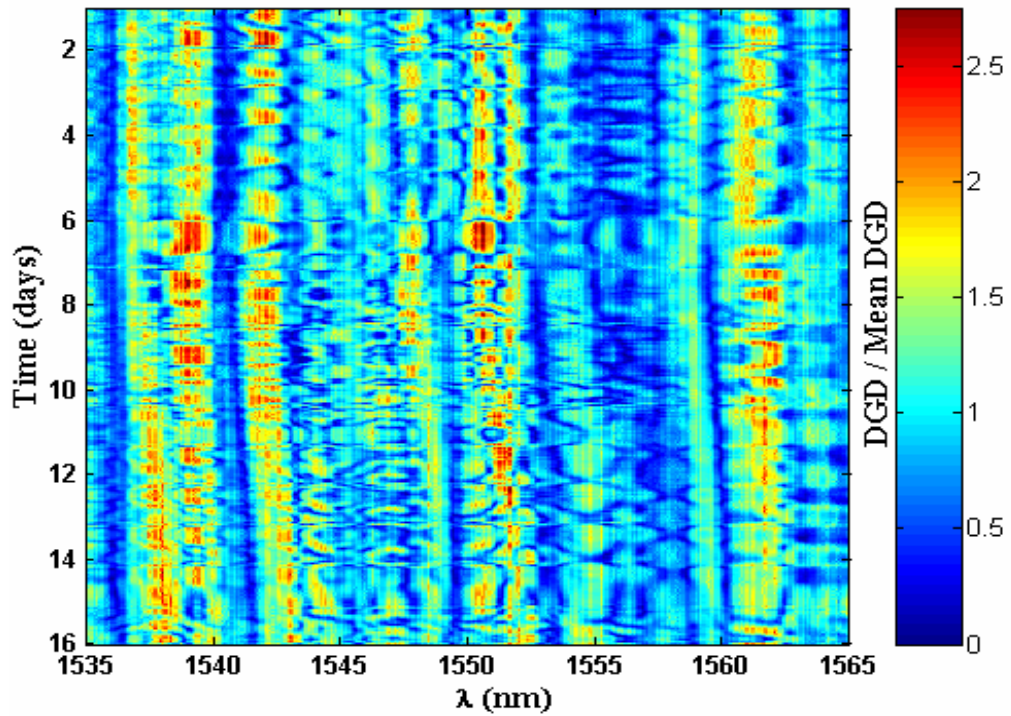
Figure 5.27. (b) Normalized DGD colormap obtained from link 1-3 measurements shown in chapter 2, reproduced here for comparison.

Figure 5.26 shows the measured, interpolated air temperature (top plot) at one location over the 16-day measurement period for link 1-3 discussed in chapter 2 and the corresponding filtered temperature (bottom plot) used in the simulation. Measurements on this link were repeated every 23 minutes and to be consistent simulations were repeated every 20 minutes. The hourly temperature data were interpolated linearly to obtain temperature samples every 20 minutes.

Figure 5.27 (a) shows the normalized DGD colormap obtained from link 1-3 simulation and the corresponding colormap obtained from measurements shown in chapter 2 is reproduced here as figure 5.27 (b) for comparison. Looking at figures 5.27 (a) and 5.27 (b), it can be observed that both the colormaps are very similar in the sense that they show fast temporal and spectral variation and also temporal periodicity. But the locations of the high DGD events are different in both cases. The actual mean DGD obtained from simulation (not mentioned here), was within 1 % of the value from the measurements.

The histogram of simulated normalized DGD and its Maxwellian fit for link 1-3 in linear and log scales are shown in figures 5.28 (a) and 5.28 (b) respectively. It can be observed from the figures that the agreement between the histogram and the Maxwellian distribution is good. Results from the modified chi-square test on the simulated DGD data are included in table 5.9.
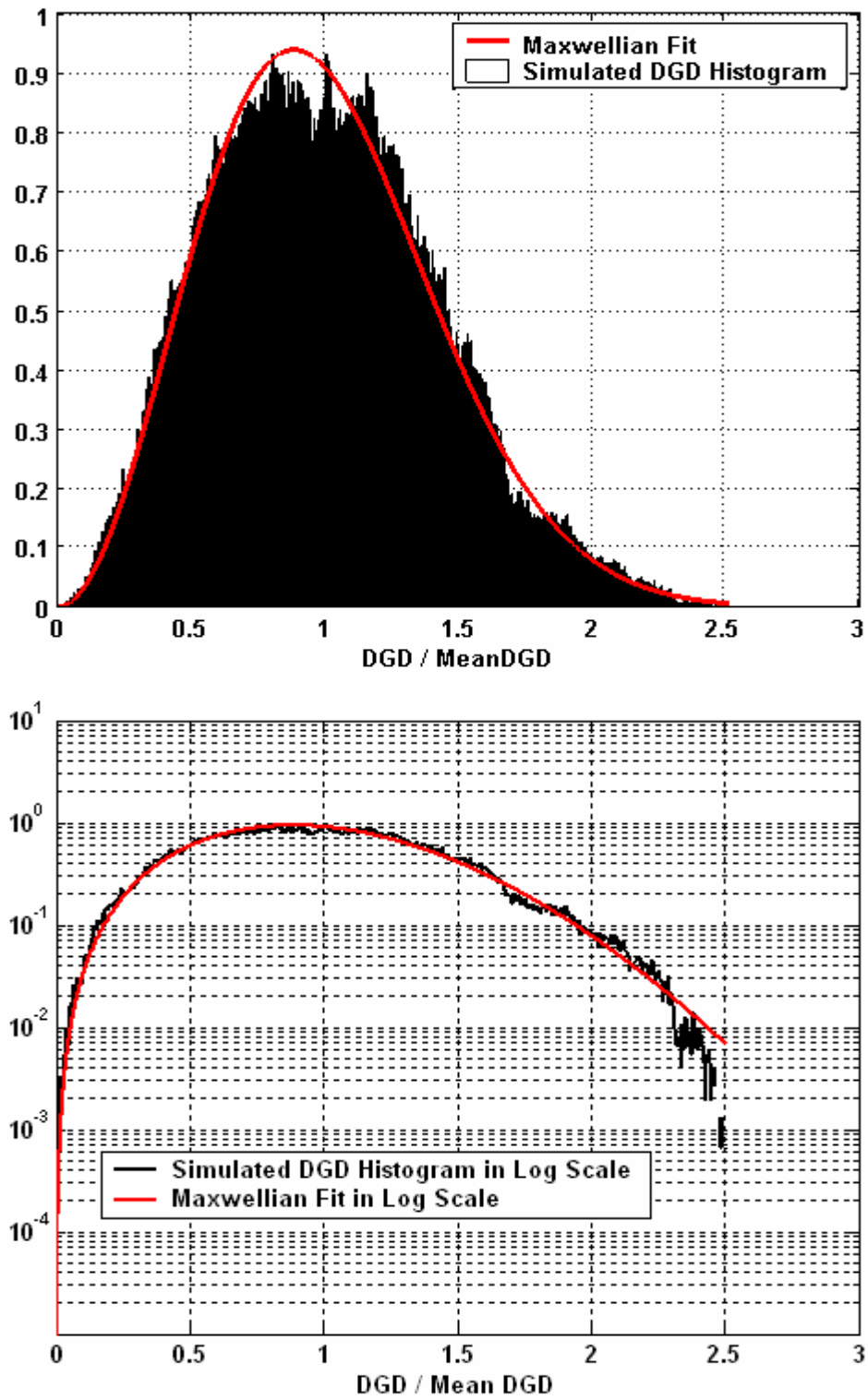
Figure 5.28. Histogram of simulated normalized DGD and its Maxwellian fit for link 1-3 in (a) linear scale (top) and (b) log scale (bottom).
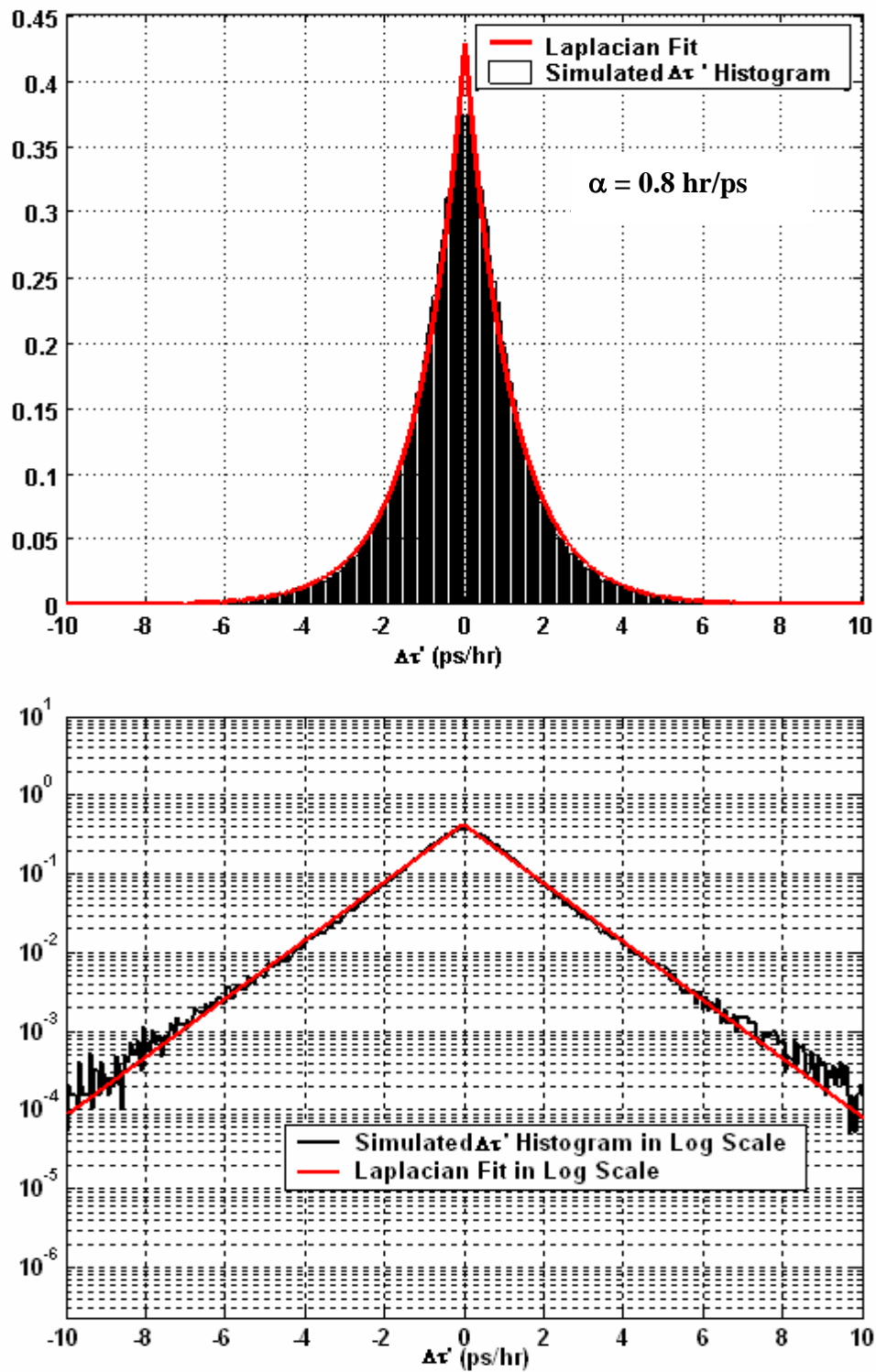
Figure 5.29. Histogram of simulated $\Delta\tau'$ and it Laplacian fit for link 1-3 in (a) linear scale (top) and (b) log scale (bottom).

The histogram of simulated $\Delta\tau'$ and its Laplacian fit for link 2-3 in linear and log scales are shown in figures 5.29 (a) and 5.29 (b) respectively. It is clear from the figures that the simulated $\Delta\tau'$ histogram and the Laplacian distribution agree well. Results from the modified chi-square test on the simulated $\Delta\tau'$ data are included in table 5.10.

The Laplacian parameter (α) value corresponding to the Laplacian fit shown in figure 5.29, calculated from simulated data is 0.8 hr/ps which is close to the value of 0.7 hr/ps obtained from measured data. Figure 5.30 shows a comparison of the relative first-order mean outage rates using these α values and the simplified outage rate expression (3.2). A good agreement between the values calculated from simulated and measured data is evident from the figure.
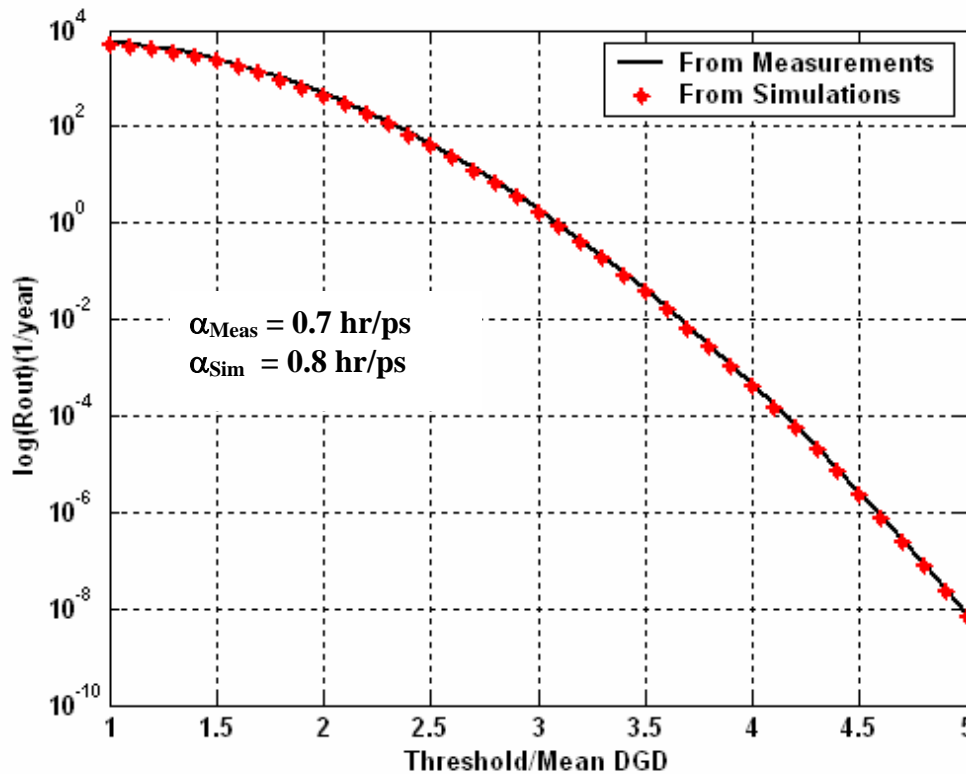
Figure 5.30. Comparison of relative R_{out} values from measured data and simulation data on link 1-3 calculated using the simplified outage rate expression.

The decorrelation time from the simulated data was around 2 hours which is very close to the value from the measured data of 2.3 hours. The decorrelation bandwidth from the simulated data matched exactly with the value from measured data.

5.4.4. Three-span link 1-2-3

Table 5.7 below shows the values of the free parameters used in the simulation of the three-span link 1-2-3. The filter used here is same as that of the two-span links discussed earlier.

Table 5.7. Values of free parameters for link 1-2-3.

Proportionality constant k (radians/°F)	Number of time-varying sections	Relative filter bandwidth parameter	Gaussian std. deviation (radians)
0.15	12	0.08	$\pi/90$
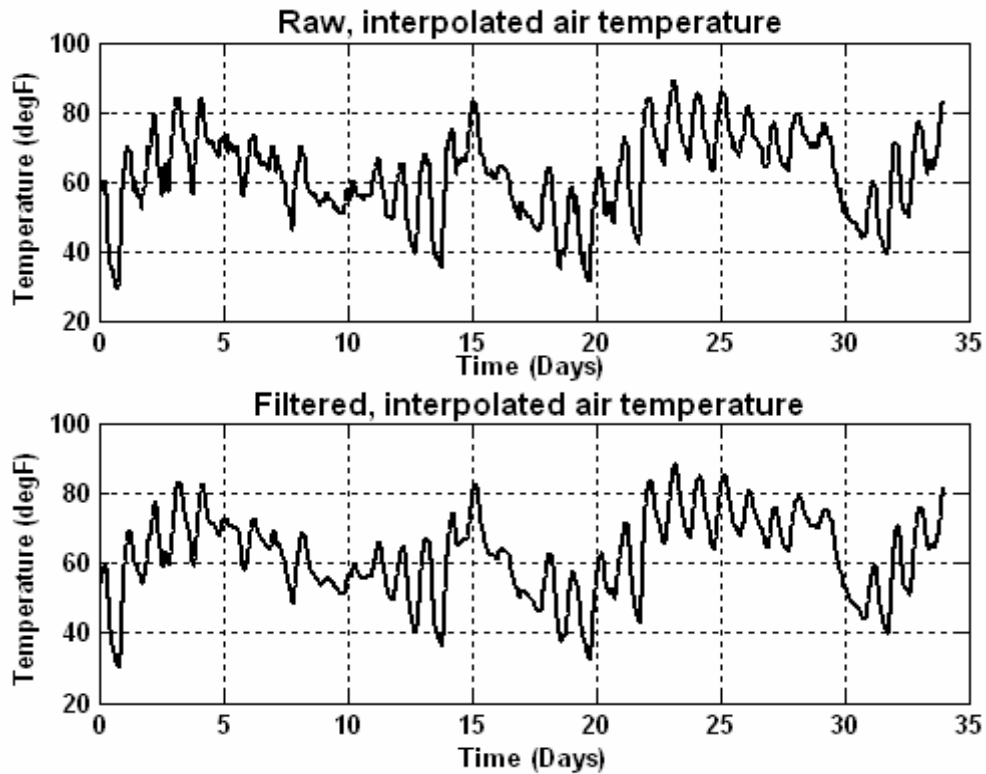
Figure 5.31. (a). Interpolated air temperature; (b) Corresponding filtered temperature.
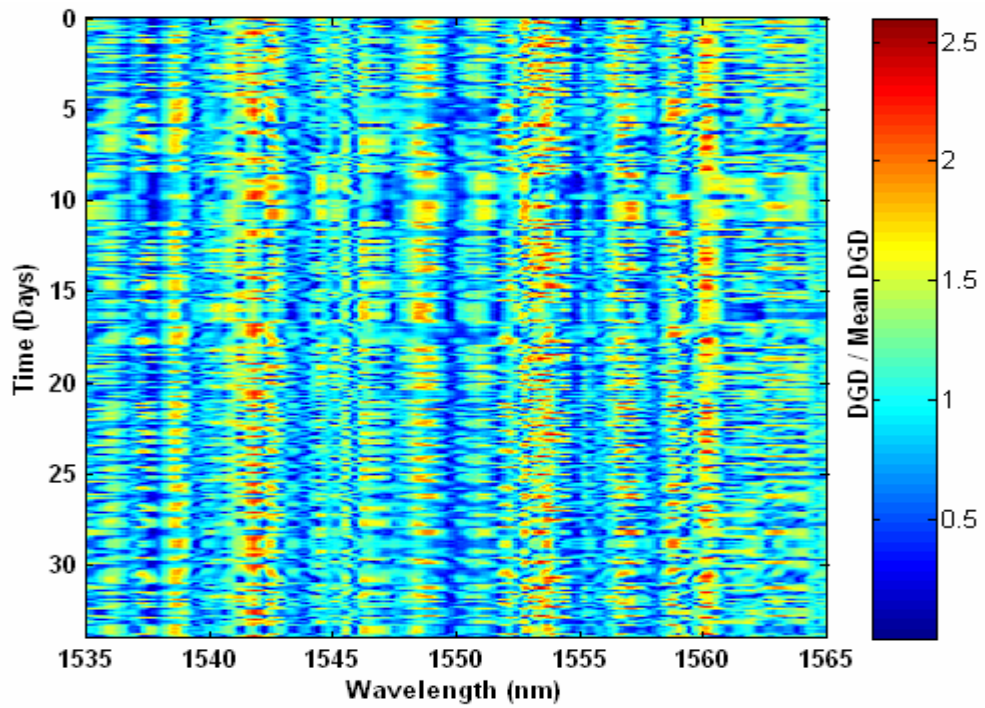
Figure 5.32. (a) Normalized DGD colormap obtained from link 1-2-3 simulation.
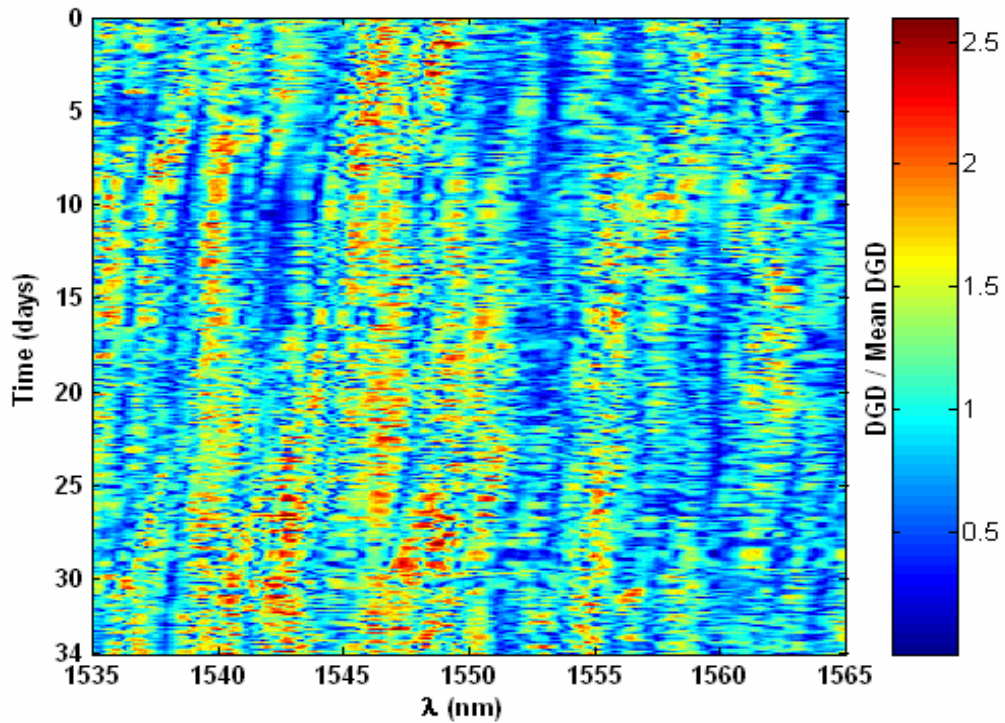
Figure 5.32. (b) Normalized DGD colormap obtained from link 1-2-3 measurements shown in chapter 2, reproduced here for comparison.

Figure 5.31 shows the measured, interpolated air temperature (top plot) at one location over the 34-day measurement period for link 1-2-3 discussed in chapter 2 and the corresponding filtered temperature (bottom plot) used in the simulation. Measurements on this link were repeated every 23 minutes and to be consistent simulations were repeated every 20 minutes. The hourly temperature data were interpolated linearly to obtain temperature samples every 20 minutes.

Figure 5.32 (a) shows the normalized DGD colormap obtained from link 1-2-3 simulation and the corresponding colormap obtained from measurements, shown in chapter 2, is reproduced here as figure 5.32 (b) for comparison. Comparing figures 5.32 (a) and 5.32 (b), it can be observed that both the colormaps are very similar in the sense that they show fast temporal and spectral variation and also temporal periodicity. However, the spectral drift observed in the measured colormap is absent in the simulated colormap and this could be because a time-invariant fixed value of PMD coefficient 'b' is used for each span. The actual mean DGD obtained from simulation (not mentioned here), was within 3 % of the value from the measurements.

The histogram of simulated normalized DGD and its Maxwellian fit for link 1-2-3 in linear and log scales are shown in figures 5.33 (a) and 5.33 (b) respectively. It can be observed from the figures that the agreement between the histogram and the Maxwellian distribution is very good. Results from the modified chi-square test on the simulated DGD data are included in table 5.9.
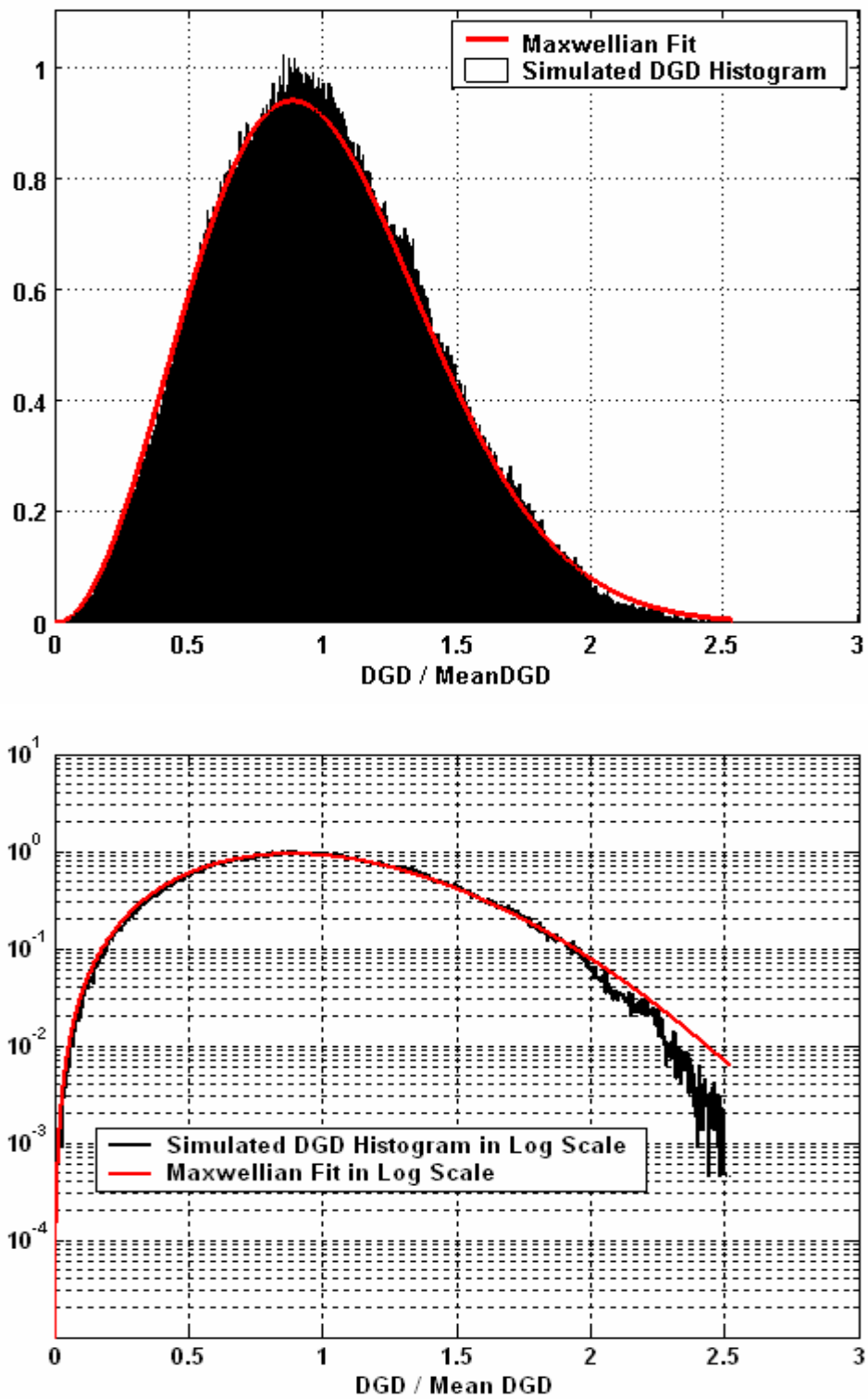
Figure 5.33. Histogram of simulated normalized DGD and its Maxwellian fit for link 1-2-3 in (a) linear scale (top) and (b) log scale (bottom).
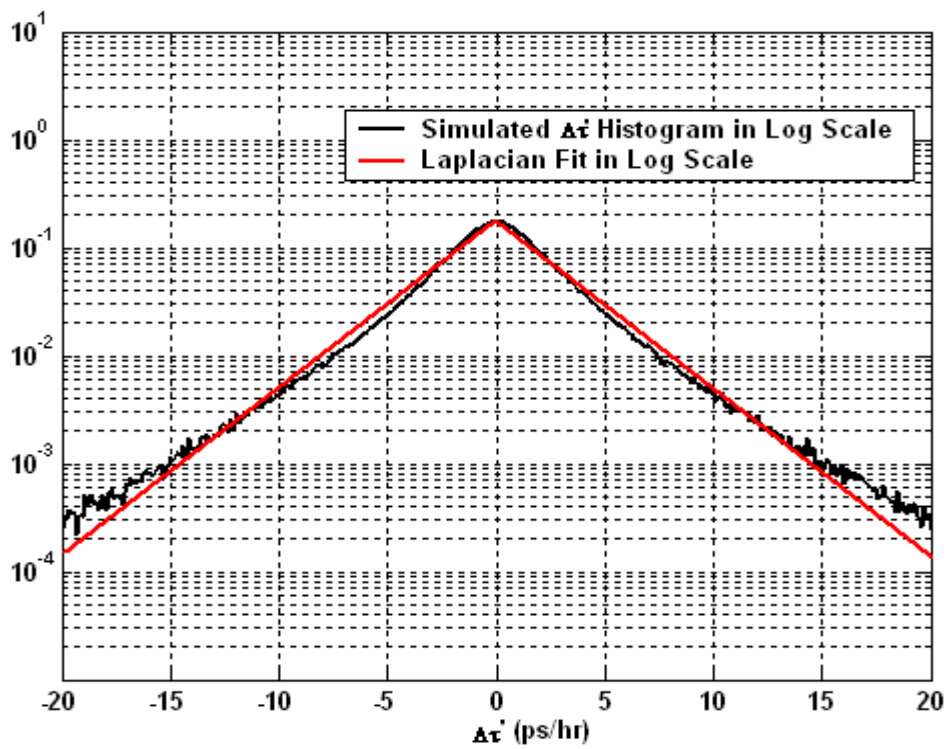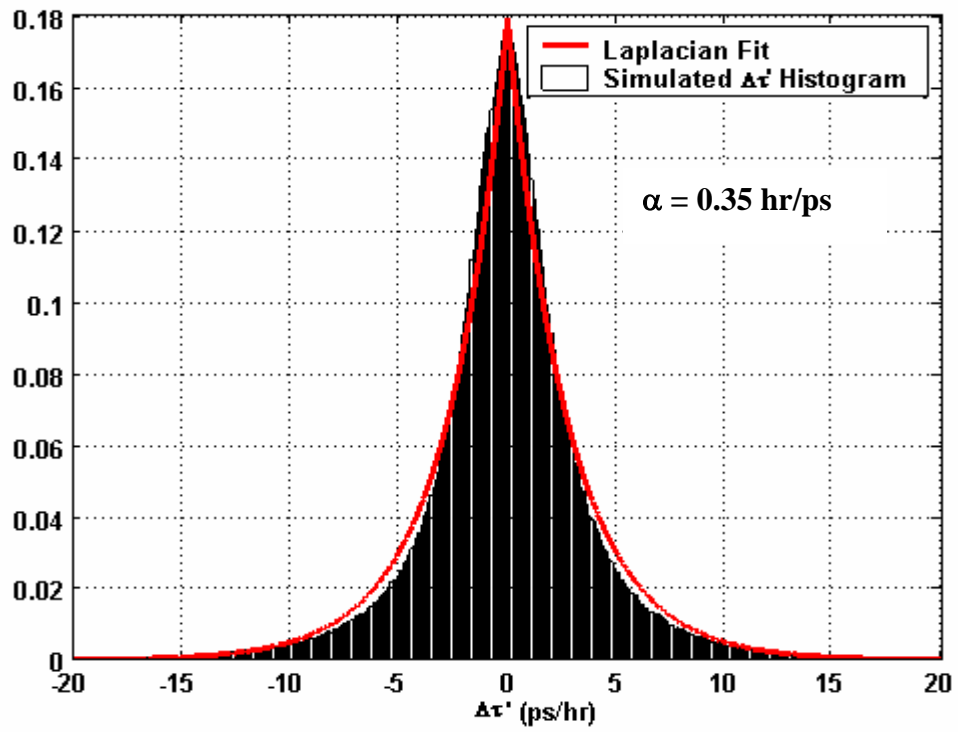
Figure 5.34. Histogram of simulated $\Delta\tau'$ and it Laplacian fit for link 1-2-3 in (a) linear scale (top) and (b) log scale (bottom).

The histogram of simulated $\Delta\tau'$ and its Laplacian fit for link 1-2-3 in linear and log scales are shown in figures 5.34 (a) and 5.34 (b) respectively. It can be observed that the simulated $\Delta\tau'$ histogram and the Laplacian distribution agree well. Results from the modified chi-square test on the simulated $\Delta\tau'$ data are in table 5.10.

The Laplacian parameter (α) value corresponding to the Laplacian fit shown in figure 5.34, calculated from simulated data is 0.35 hr/ps which is close to the value of 0.38 hr/ps obtained from measured data. Figure 5.35 shows a comparison of the relative first-order mean outage rates using these α values and the simplified outage rate expression (3.2). A good agreement between the values calculated from simulated and measured data is evident from the figure.
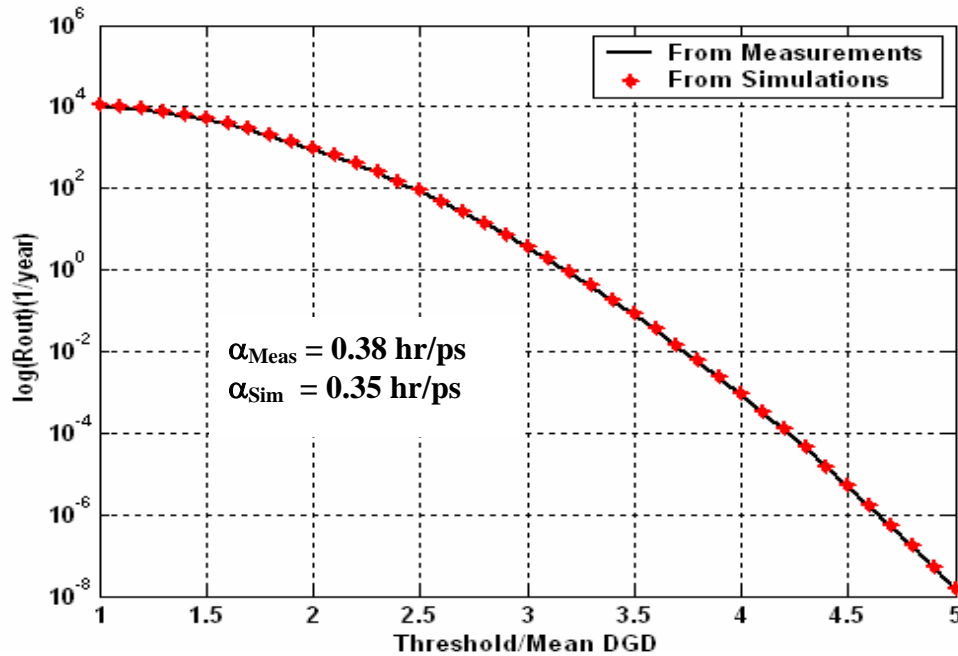
Figure 5.35. Comparison of relative R_{out} values from measured data and simulation data on link 1-2-3 calculated using the simplified outage rate expression.

The decorrelation time from the simulated data was around 1.33 hours which is slightly different than the value from the measured data of 1.83 hours. The decorrelation bandwidth from the simulated data matched exactly with the value from measured data.

Simulation results discussed in sections 5.3 and 5.4 are summarized in table 5.8.

Table 5.8. Summary of simulation results discussed in sections 5.3 and 5.4.

Link configuration	Free parameters of the model				Percent difference between measurements and simulations			
	Constant k	# of time-varying sections	Relative filter BW parameter	Gaussian standard deviation	Mean DGD	Laplacian parameter α	Decorrelation time	Decorrelation bandwidth
Link 1	0.2	4	0.001	$\pi/22$	1 %	14 %	13 %	30 %
Link 2	0.2	4	0.001	$\pi/48$	5 %	7 %	4.5 %	10 %
Link 3	0.2	4	0.002	$\pi/120$	5 %	10.5 %	11 %	15 %
Link 1-2	0.11	8	0.08	$\pi/135$	2 %	13 %	8 %	10 %
Link 2-3	0.1	8	0.08	$\pi/120$	3 %	3 %	23 %	0 %
Link 1-3	0.08	8	0.08	$\pi/120$	1 %	12.5 %	13 %	0 %
Link 1-2-3	0.15	12	0.08	$\pi/90$	3 %	8 %	27 %	0 %

5.5. Goodness-of-fit test results

Results from the modified chi-square test, discussed in Appendix A, applied to the simulated DGD and $\Delta\tau'$ data on the single-, two- and three-span links discussed in sections 5.3 and 5.4 are shown in tables 5.9 and 5.10 respectively. In all but one case, the hypotheses (that simulated DGD data has Maxwellian PDF and the simulated $\Delta\tau'$ data has Laplacian PDF) are accepted.

Table 5.9. Results from the modified chi-square test applied to simulated DGD data.

Fiber Configuration	Degrees of Freedom	Critical Value At Significance Level $\alpha = 0.9$	chi-square Test Statistic From Data	Hypothesis Accept or Reject?
Link 1	100	82.36	30.08	Accept
Link 2	100	82.36	114.75	Reject
Link 3	100	82.36	39.82	Accept
Link 1-2	100	82.36	82.35	Accept
Link 2-3	100	82.36	79.46	Accept
Link 1-3	100	82.36	79.83	Accept
Link 1-2-3	100	82.36	40.58	Accept

Table 5.10. Results from the modified chi-square test applied to simulated $\Delta\tau'$ data.

Fiber Configuration	Degrees of Freedom	Critical Value At Significance Level $\alpha = 0.9$	chi-square Test Statistic From Data	Hypothesis Accept or Reject?
Link 1	82	66.08	6.24	Accept
Link 2	83	66.98	3.23	Accept
Link 3	80	64.28	3.31	Accept
Link 1-2	84	67.88	42.55	Accept
Link 2-3	87	70.58	65.16	Accept
Link 1-3	76	60.69	49.12	Accept
Link 1-2-3	100	82.36	80.21	Accept

5.6. Conclusions

From the simulation results discussed in this chapter, it can be concluded that the enhanced numerical model described in chapter 4 reproduced very well the DGD temporal and spectral behavior observed from measurements, particularly on multi-span links. The histograms of DGD and $\Delta\tau'$ from multi-span link simulations showed good agreement with the expected Maxwellian and Laplacian distributions respectively. The mean DGD and Laplacian parameter (α) values from simulations were very close to those obtained from the measurements. The simulated DGD colormaps looked very similar to the measured colormaps except for the spectral drift. However, it is clear from the simulation results that this spectral drift does not have any noticeable effect on first-order PMD outage analysis, which is the focus of this report. The decorrelation time and decorrelation bandwidth values from simulations were also close to that of the values from the measurements.

In the case of single-span links, the agreement between the simulated DGD histograms and the expected Maxwellian distribution is only marginal in some cases, but the simulated $\Delta\tau'$ histograms showed good agreement with the Laplacian distribution. The simulated DGD colormaps showed all of the major features observed in measured colormaps. The values of mean DGD, Laplacian parameter (α), decorrelation time and decorrelation bandwidth obtained from simulations showed good agreement with those from measurements. However, it is not clear why a very narrowband filter is required for single-span links to filter the temperature data compared to multi-span links. This issue needs to be investigated further.

Hence the numerical model presented in chapter 4 can be used to study the variation of Laplacian parameter, and thereby the first-order PMD outage rates, with link length. Chapter 6 shows the results from such a simulation study on multi-span links of different lengths.

6. SIMULATION STUDY OF FIRST-ORDER PMD OUTAGE RATE VARIATION WITH LINK LENGTH

In this chapter simulation results on multi-span links of different lengths are discussed. The objective here is to study the variation of Laplacian parameter, which is a crucial parameter in determining the first-order PMD outage rates as per the simplified PMD outage rate expression (3.2), with link length. For this study, a set of reference temperature profiles at different locations along the link and a set of values for the free parameters of the numerical model are required. To simplify the study, only a single reference temperature profile is used for the simulations discussed in this chapter, but it is fairly straightforward to modify the model to include a set of temperature profiles representing the temperature dynamics across the entire link.

For all of the simulations discussed in this chapter, the temperature profile from the 34-day measurement period of the three-span link 1-2-3 presented in chapters 2 and 5 is used as the reference profile and it is linearly interpolated as needed depending on the sampling interval. Also, the values of the free parameters from the three-span case are used in the simulations and are listed again in table 6.1. Different values in the range of $\pi/90$ to $\pi/120$ are used for Gaussian standard deviation depending on the sampling interval. A span length of 95 km is assumed for all the simulations. Each span is modeled as a concatenation of 500 shorter fiber segments of which 4 of them have a time varying, temperature-dependent ϕ_n component. A 30-nm EDFA band (1535 nm to 1565 nm) is used in all of the simulations. The PMD coefficients of the three single-span links b1, b2, and b3 (the actual values not reported in this report) are cycled through for multi-span link spans. For instance, the sequence of PMD coefficients used for the 5 spans in a five-span link simulation is b1-b2-b3-b1-b2. The values of the segment length h_n, the coupling angle α_n, and the phase ϕ_n (static as well as time-variant components) are derived from a single set of values used for the link with highest number of spans. For example, in a five-span simulation the values of h_n, α_n, and ϕ_n for the first four spans

are same as the values used in a four-span link simulation. The idea behind this is to have links with large number of spans to be extensions of links with smaller number of spans so that it is easy to study the variation of Laplacian parameter with link length.

Next, the plots and values of metrics obtained from simulation of 2-span (190 km), 4-span (380 km), 5-span (475 km), 7-span (665 km), 9-span (855 km) and 11-span (1045 km) links are presented. Later, the variation of Laplacian parameter with link length observed from simulations and its significance is discussed.

Table 6.1. Values of free parameters used for simulations.

Proportionality constant k (radians/$^\circ$F)	Number of time-varying sections	Relative filter bandwidth parameter	Gaussian std. deviation (radians)
0.15	4 per span	0.08	$\pi/90$ to $\pi/120$

6.1. Two-span link

This link has a length of 190 km and is modeled as a concatenation of 1000 short fiber segments of which 8 of them have a time varying ϕ_n component. Simulations are performed with 20 minute time increments and a value of $\pi/90$ is used for Gaussian standard deviation.

Figure 6.1 shows the normalized DGD colormap obtained from the two-span link simulation. Figures 6.2 (a) and 6.2 (b) show the normalized DGD histogram and its Maxwellian fit in linear and log scales respectively.
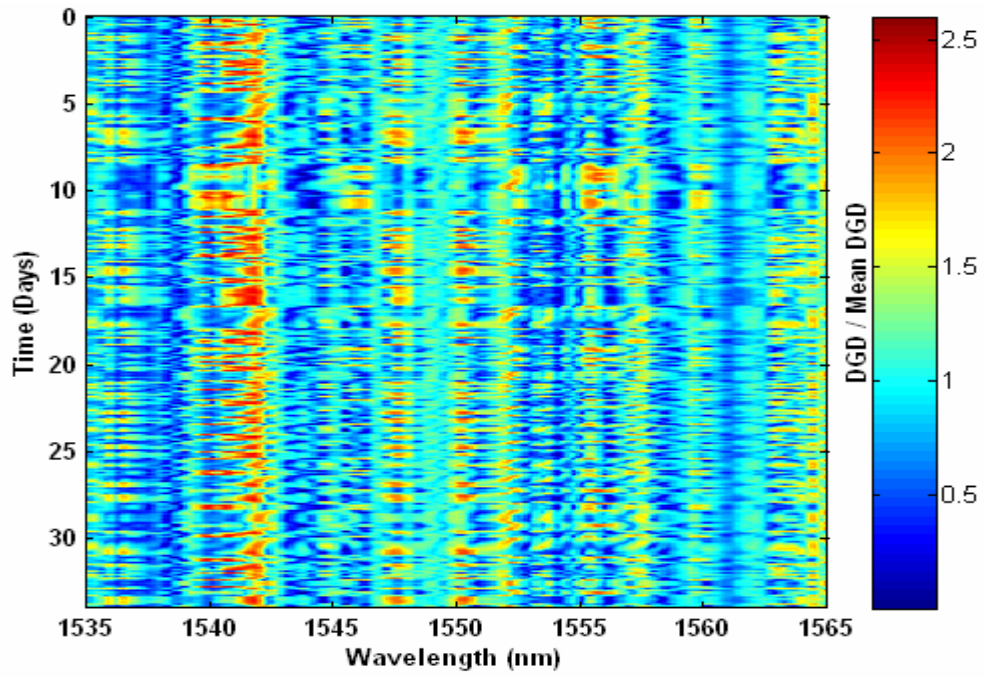
Figure 6.1. Normalized DGD colormap obtained from two-span link simulation.
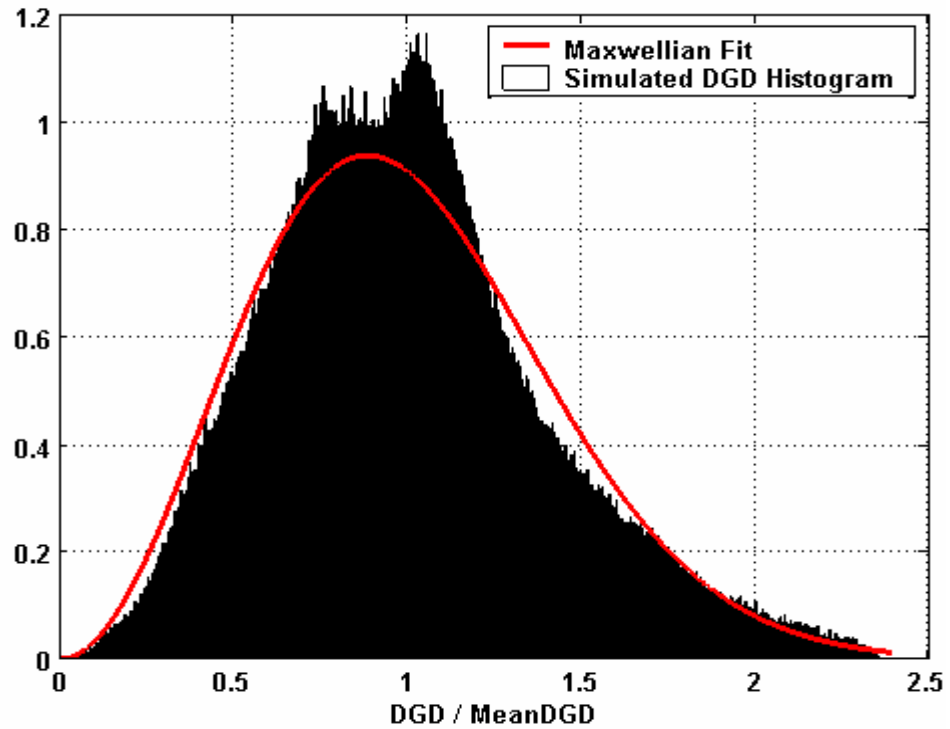
Figure 6.2. (a) Histogram of simulated normalized DGD and its
Maxwellian fit for two-span link in linear scale.
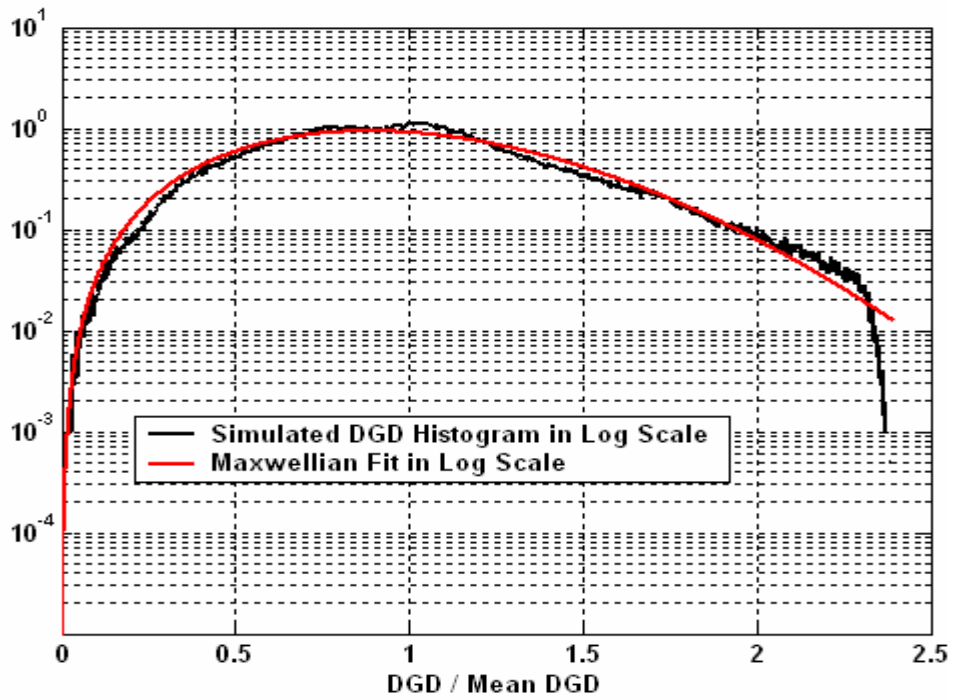
Figure 6.2. (b) Histogram of simulated normalized DGD and its Maxwellian fit for two-span link in log scale.
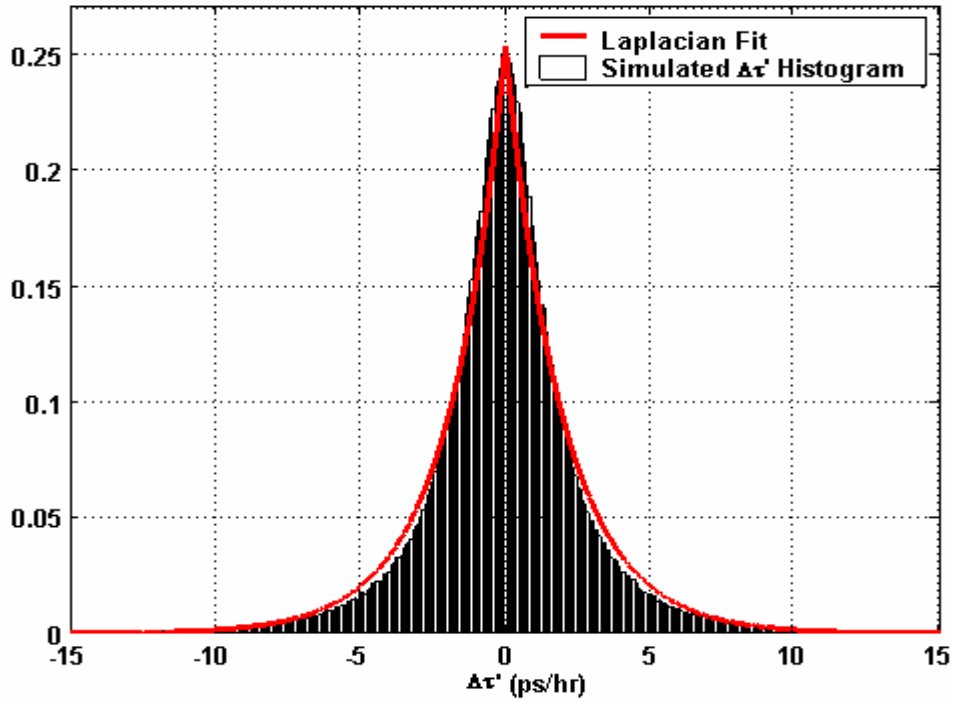
Figure 6.3. (a) Histogram of simulated $\Delta\tau'$ and it Laplacian fit for two-span link in linear scale.
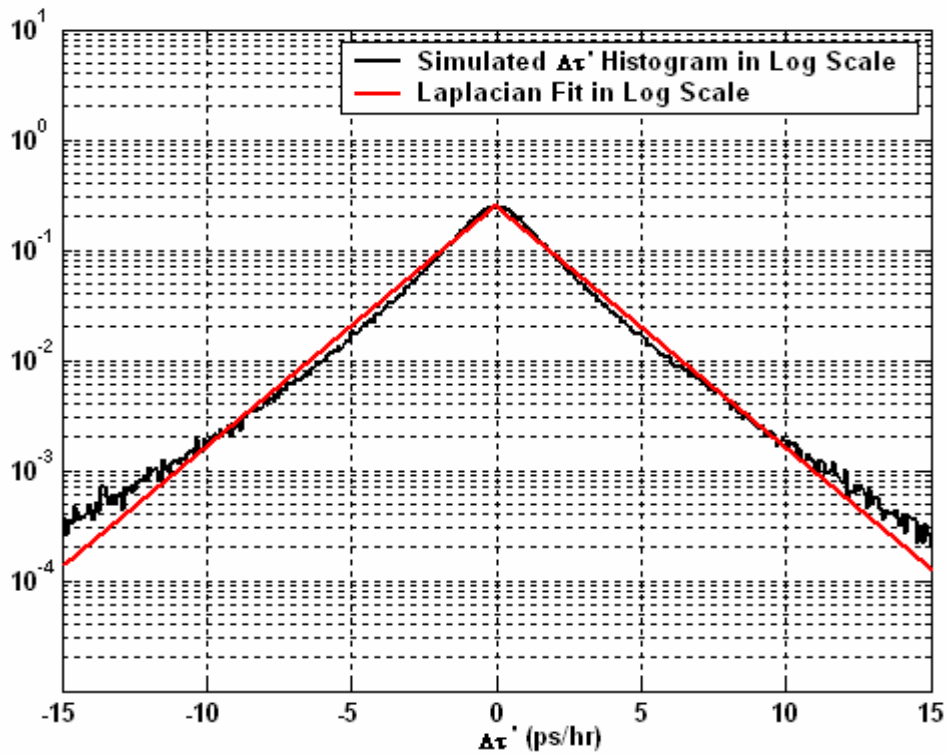
Figure 6.3. (b) Histogram of simulated $\Delta\tau'$ and it Laplacian fit
for two-span link in log scale.

Figures 6.3 (a) and 6.3 (b) show the simulated $\Delta\tau'$ histogram and its Laplacian fit in linear and log scales respectively. These figures show good agreement between the $\Delta\tau'$ histogram and the Laplacian distribution. The Laplacian parameter (α) value corresponding to the Laplacian fits in figures 6.4 and 6.5, calculated from the simulated $\Delta\tau'$ data is 0.504 hr/ps. This value is comparable to the α values of the two-span links presented in chapter 5.

6.2. Four-span link

This link has a length of 380 km and is modeled as a concatenation of 2000 short fiber segments of which 16 of them have a time varying ϕ_n component. Simulations are repeated every 20 minutes and a value of $\pi/90$ is used for Gaussian standard deviation.

Figure 6.4 shows the normalized DGD colormap obtained from the two-span link simulation. Figures 6.5 (a) and 6.5 (b) show the normalized DGD histogram and its Maxwellian fit in linear and log scales respectively.
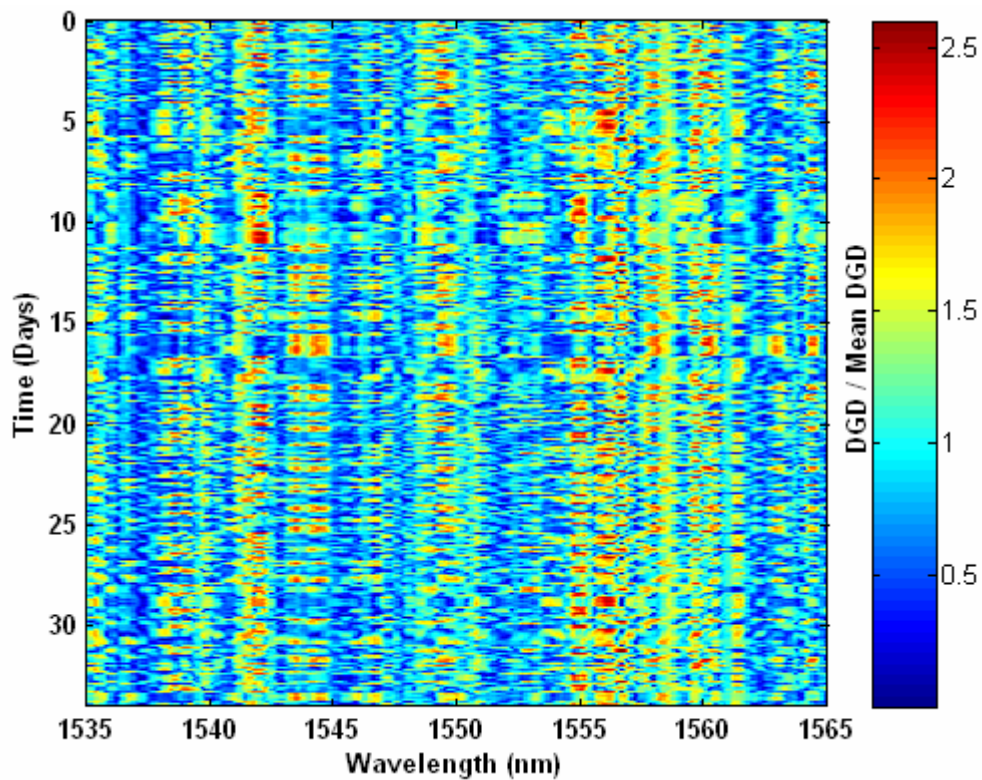
Figure 6.4. Normalized DGD colormap obtained from four-span link simulation.
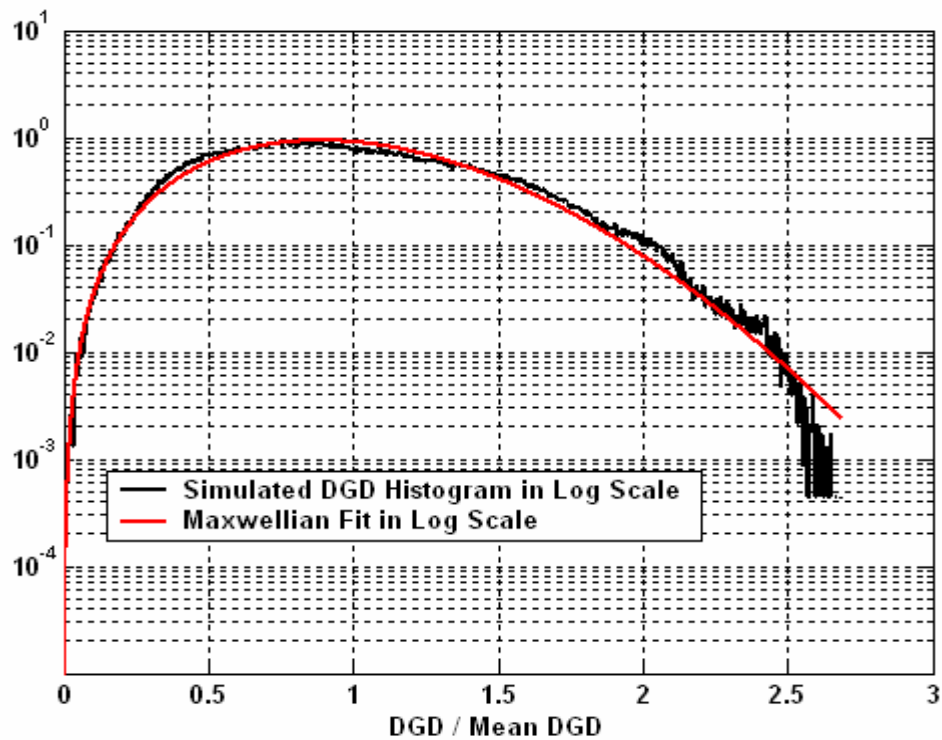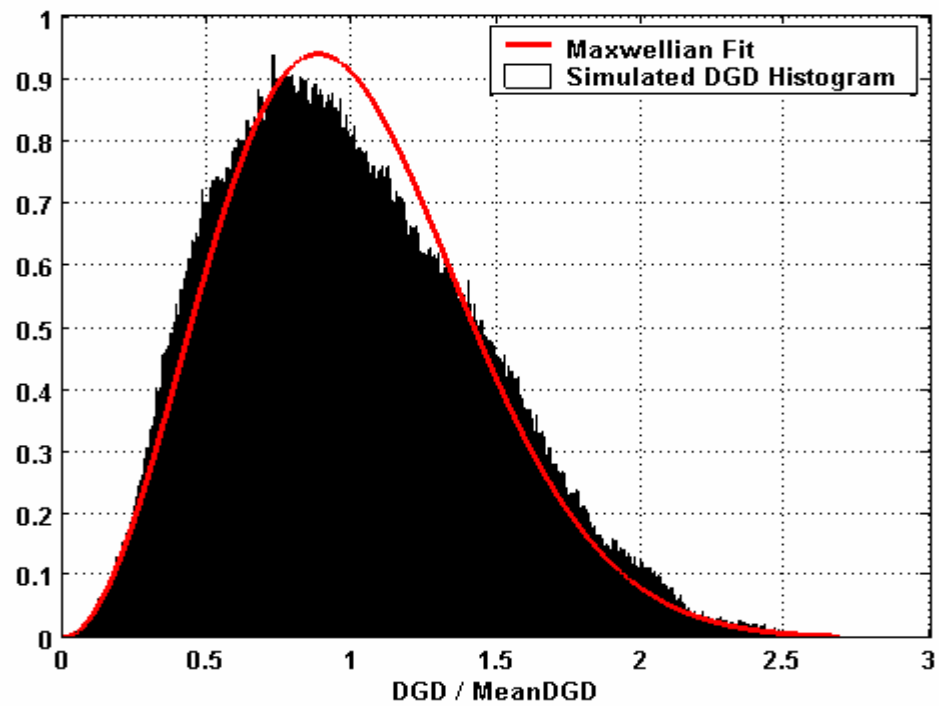
Figure 6.5. Histogram of simulated normalized DGD and its Maxwellian fit
for four-span link in (a) linear scale (top) and (b) log scale (bottom).
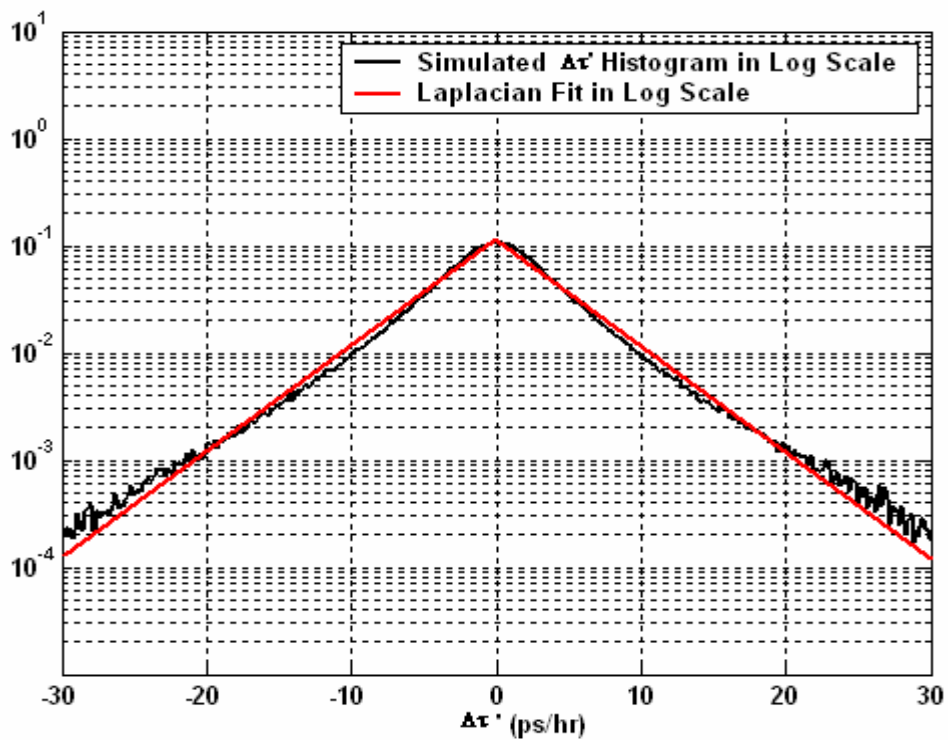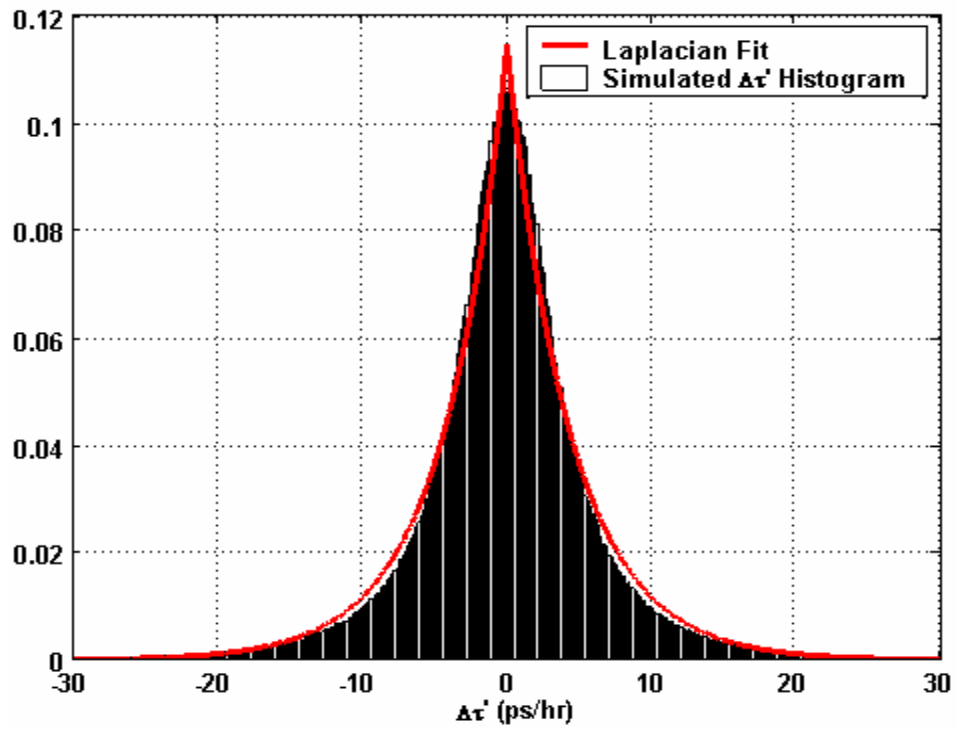
Figure 6.6. Histogram of simulated Δτ' and it Laplacian fit for four-span
link in (a) linear scale (top) and (b) log scale (bottom).

Figures 6.6 (a) and 6.6 (b) show the simulated $\Delta\tau'$ histogram and its Laplacian fit in linear and log scales respectively. These figures show good agreement between the $\Delta\tau'$ histogram and the Laplacian distribution. The Laplacian parameter (α) value corresponding to the Laplacian fits in figure 6.6, calculated from the simulated $\Delta\tau'$ data is 0.23 hr/ps.

6.3. Five-span link

This link has a length of 475 km and is modeled as a concatenation of 2500 short fiber segments of which 20 of them have a time varying ϕ_n component. Simulations are repeated every 10 minutes and a value of $\pi/105$ is used for Gaussian standard deviation.

Figure 6.7 shows the normalized DGD colormap obtained from the two-span link simulation. Figures 6.8 (a) and 6.8 (b) show the normalized DGD histogram and its Maxwellian fit in linear and log scales respectively.
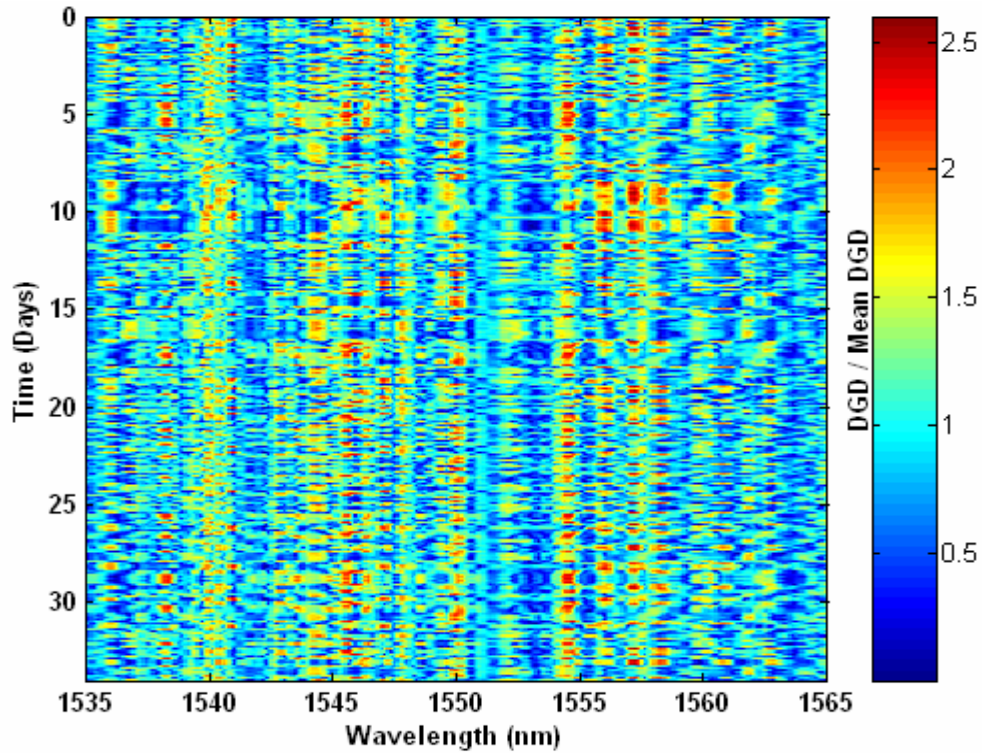
Figure 6.7. Normalized DGD colormap obtained from five-span link simulation.
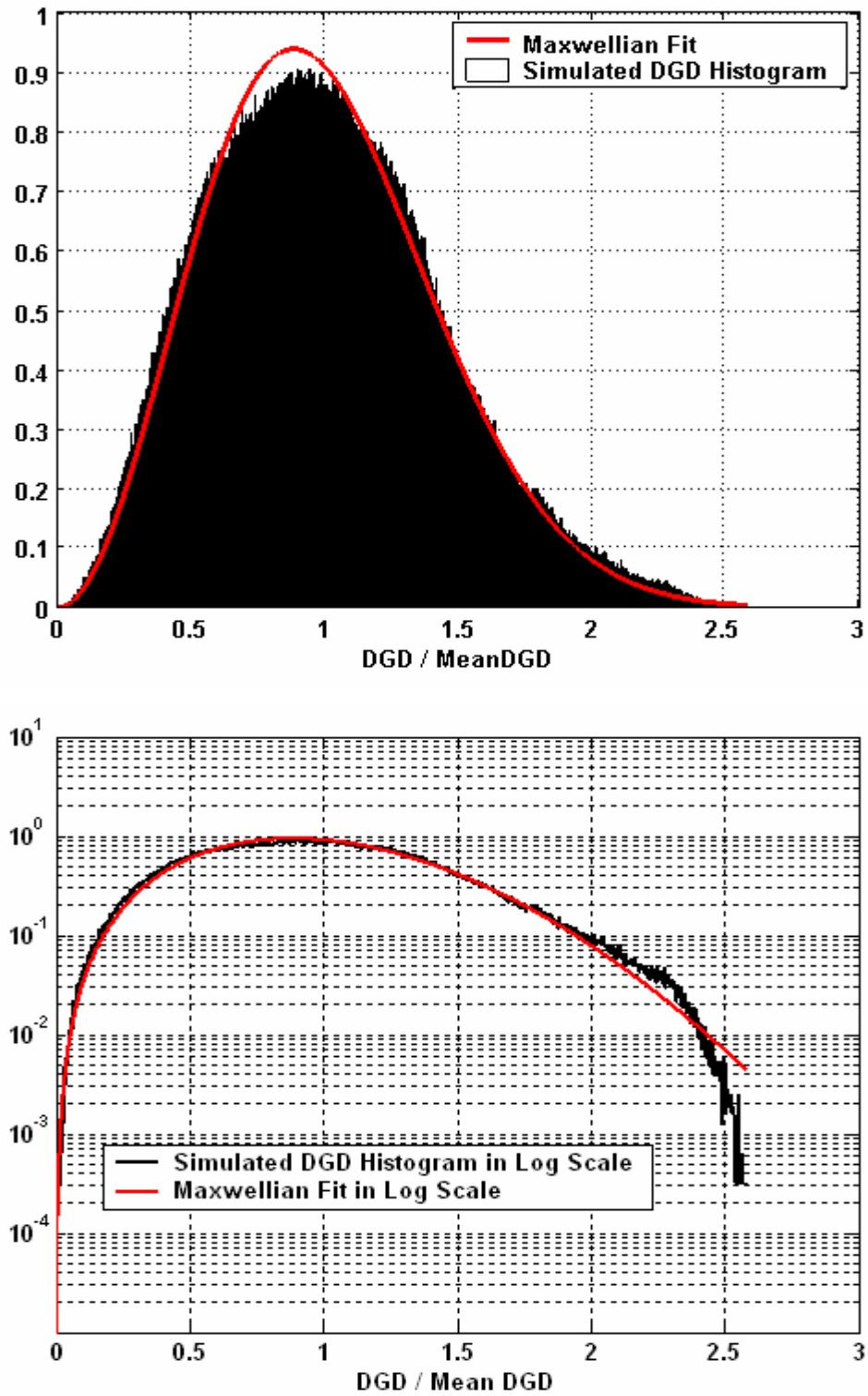
Figure 6.8. Histogram of simulated normalized DGD and its Maxwellian fit
for five-span link in (a) linear scale (top) and (b) log scale (bottom).
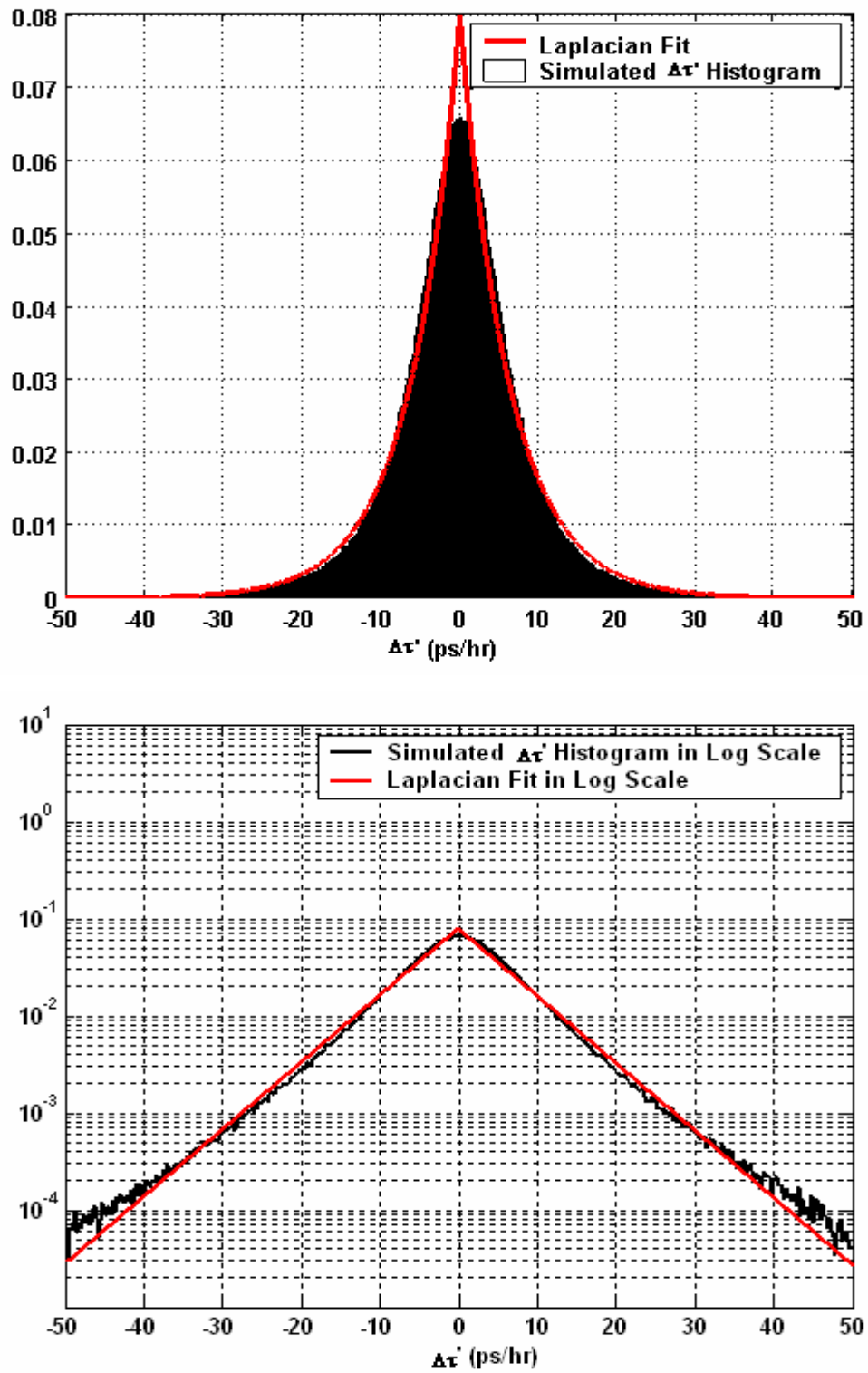
Figure 6.9. Histogram of simulated $\Delta\tau'$ and it Laplacian fit for five-span link in (a) linear scale (top) and (b) log scale (bottom).

Figures 6.9 (a) and 6.9 (b) show the simulated $\Delta\tau'$ histogram and its Laplacian fit in linear and log scales respectively. These figures show good agreement between the $\Delta\tau'$ histogram and the Laplacian distribution except at the center. This discrepancy is discussed in more detail later in this chapter. The Laplacian parameter (α) value corresponding to the Laplacian fits in figure 6.9, calculated from the simulated $\Delta\tau'$ data is 0.159 hr/ps.

6.4. Seven-span link

This link has a length of 665 km and is modeled as a concatenation of 3500 short fiber segments of which 28 of them have a time varying ϕ_n component. Simulations are repeated every 10 minutes and a value of $\pi/105$ is used for Gaussian standard deviation.

Figure 6.10 shows the normalized DGD colormap obtained from the two-span link simulation. Figures 6.11 (a) and 6.11 (b) show the normalized DGD histogram and its Maxwellian fit in linear and log scales respectively.
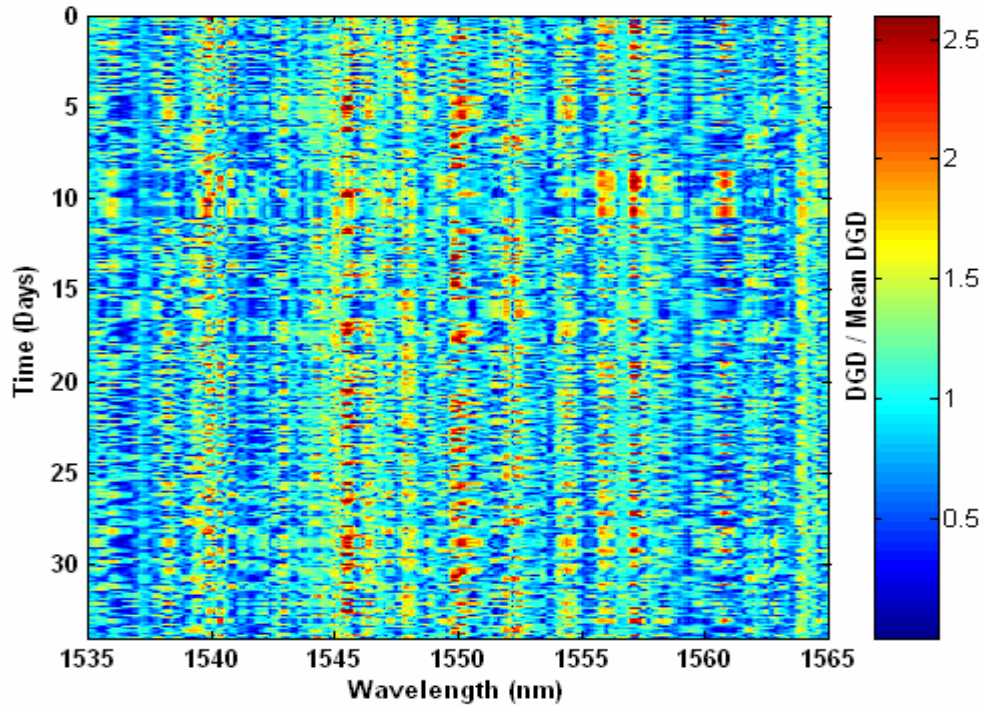
Figure 6.10. Normalized DGD colormap obtained from seven-span link simulation.
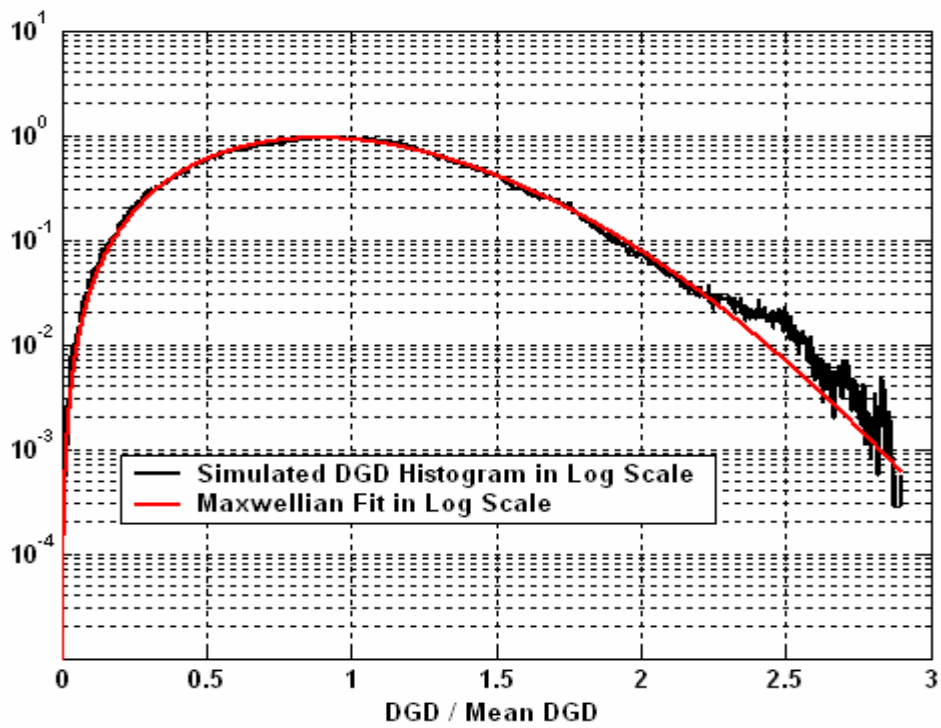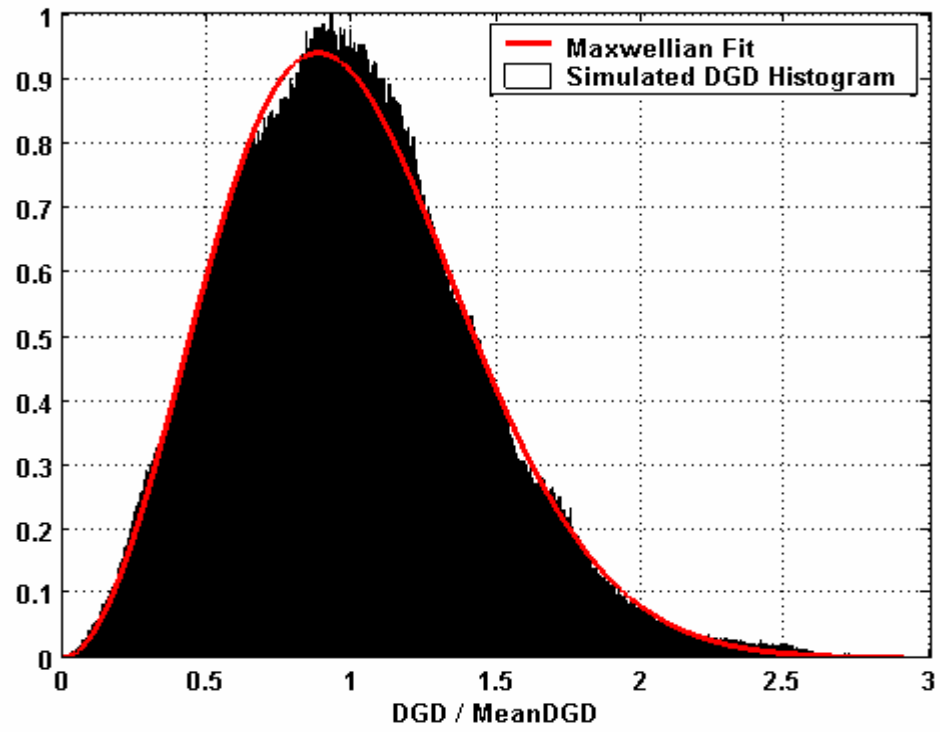
Figure 6.11. Histogram of simulated normalized DGD and its Maxwellian fit for seven-span link in (a) linear scale (top) and (b) log scale (bottom).
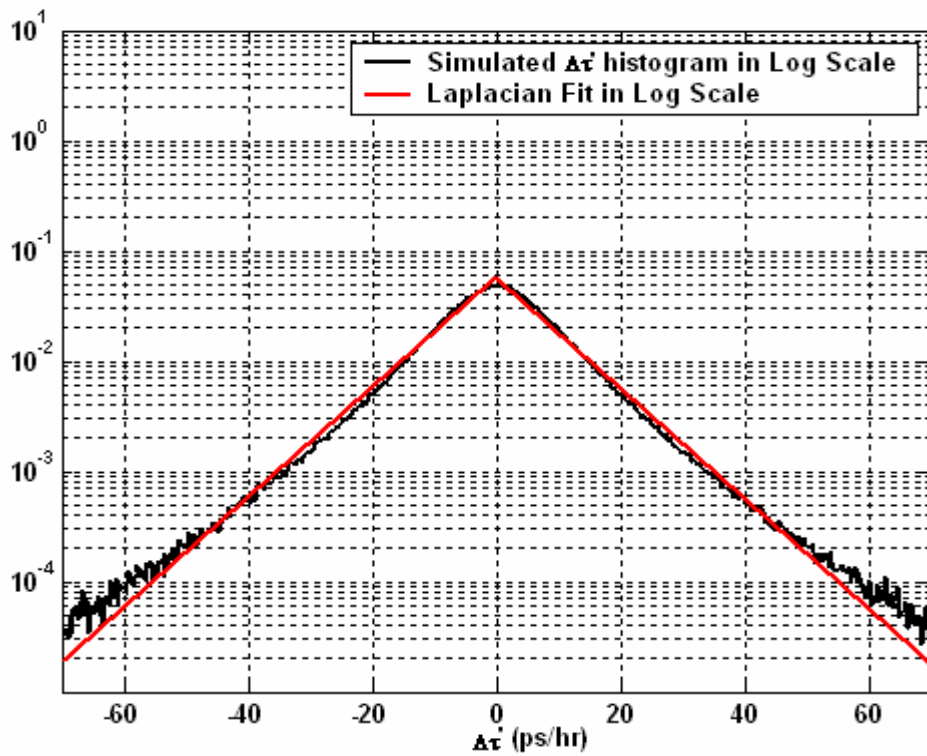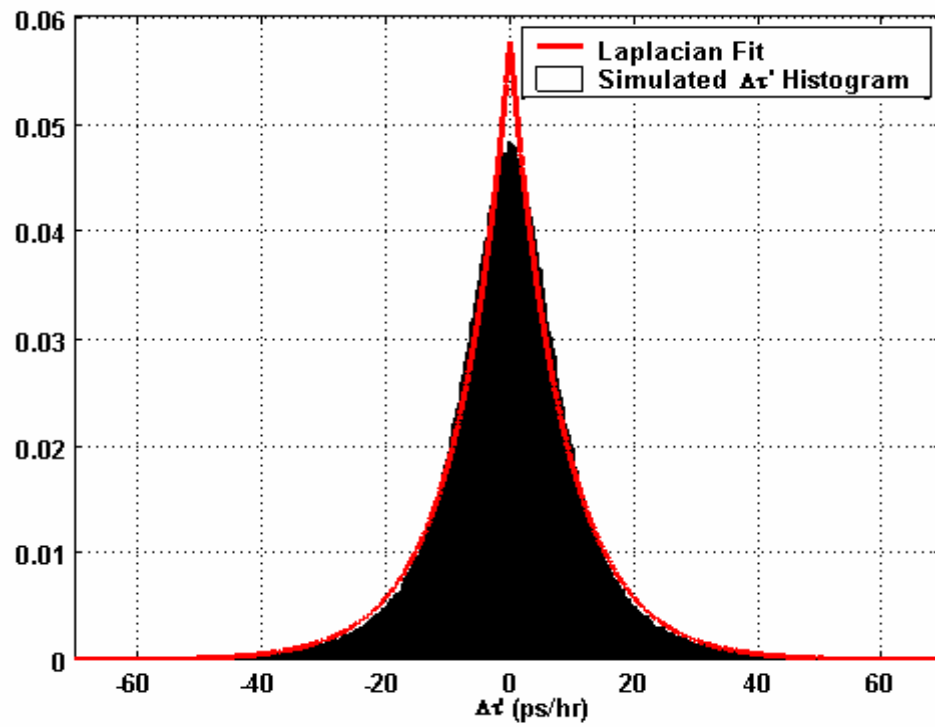
Figure 6.12. Histogram of simulated $\Delta\tau'$ and it Laplacian fit for seven-span link in (a) linear scale (top) and (b) log scale (bottom).

Figures 6.12 (a) and 6.12 (b) show the simulated $\Delta\tau'$ histogram and its Laplacian fit in linear and log scales respectively. These figures show good agreement between the $\Delta\tau'$ histogram and the Laplacian distribution except at the center same as in the five-span case. The Laplacian parameter (α) value corresponding to the Laplacian fits in figure 6.12, calculated from the simulated $\Delta\tau'$ data is 0.115 hr/ps.

6.5. Nine-span link

This link has a length of 855 km and is modeled as a concatenation of 4500 short fiber segments of which 36 of them have a time varying ϕ_n component. Simulations are repeated every 10 minutes and a value of $\pi/105$ is used for Gaussian standard deviation.

Figure 6.13 shows the normalized DGD colormap obtained from the two-span link simulation. Figures 6.14 (a) and 6.14 (b) show the normalized DGD histogram and its Maxwellian fit in linear and log scales respectively.
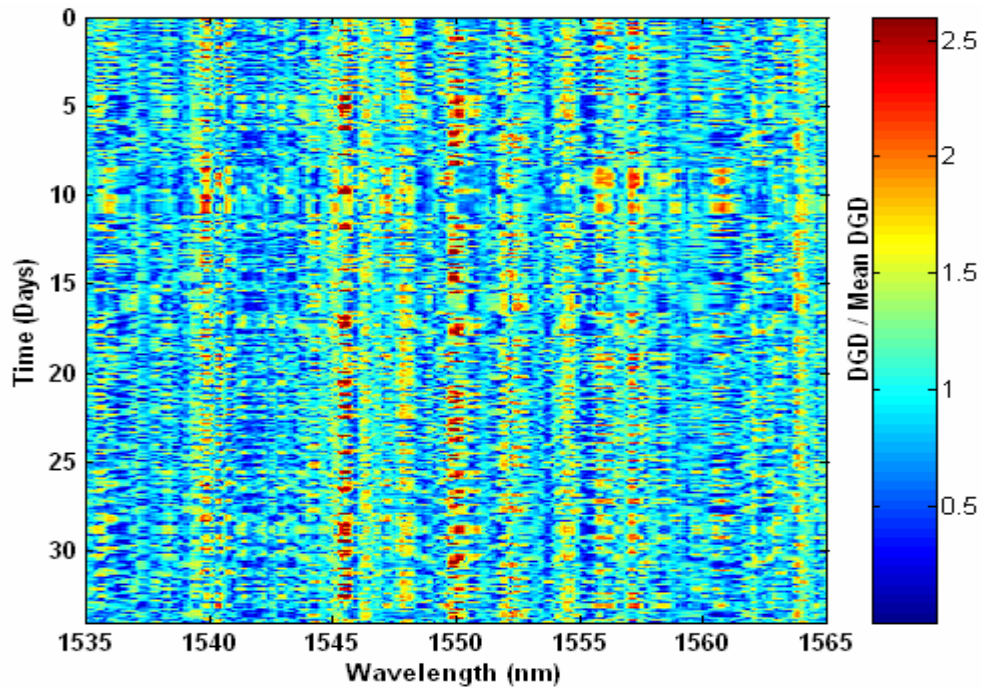
Figure 6.13. Normalized DGD colormap obtained from nine-span link simulation.
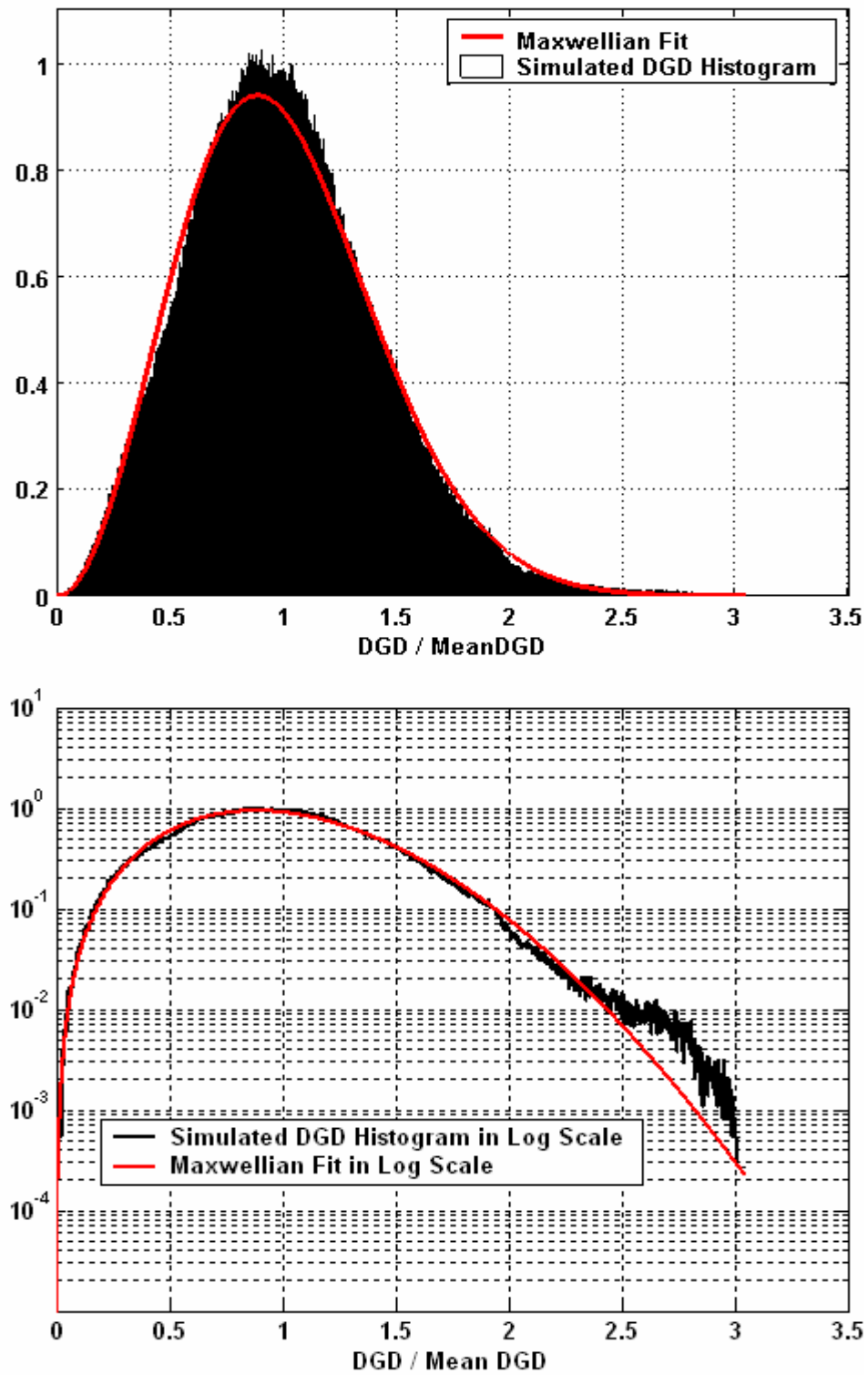
Figure 6.14. Histogram of simulated normalized DGD and its Maxwellian fit for nine-span link in (a) linear scale (top) and (b) log scale (bottom).
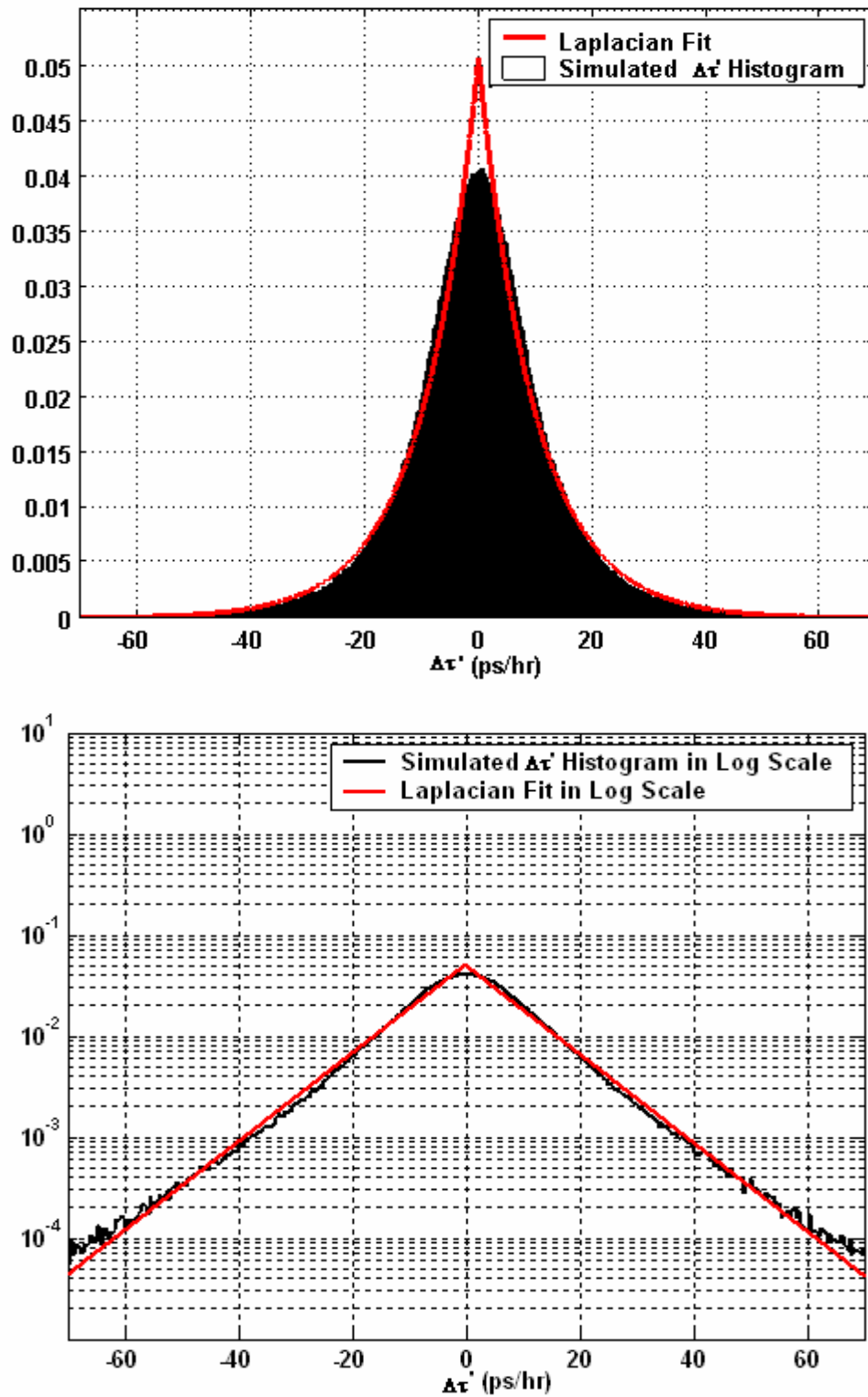
Figure 6.15. Histogram of simulated Δτ' and it Laplacian fit for nine-span link in (a) linear scale (top) and (b) log scale (bottom).

Figures 6.15 (a) and 6.15 (b) show the simulated $\Delta\tau'$ histogram and its Laplacian fit in linear and log scales respectively. These figures show good agreement between the $\Delta\tau'$ histogram and the Laplacian distribution except at the center same as in the five-span and seven-span cases. The Laplacian parameter (α) value corresponding to the Laplacian fits in figure 6.15, calculated from the simulated $\Delta\tau'$ data is 0.101 hr/ps.

6.6. Eleven-span link

This link has a length of 1045 km and is modeled as a concatenation of 4400 short fiber segments of which 44 of them have a time varying ϕ_n component. Simulations are repeated every 10 minutes and a value of $\pi/105$ is used for Gaussian standard deviation.

Figure 6.16 shows the normalized DGD colormap obtained from the two-span link simulation. Figures 6.17 (a) and 6.17 (b) show the normalized DGD histogram and its Maxwellian fit in linear and log scales respectively.
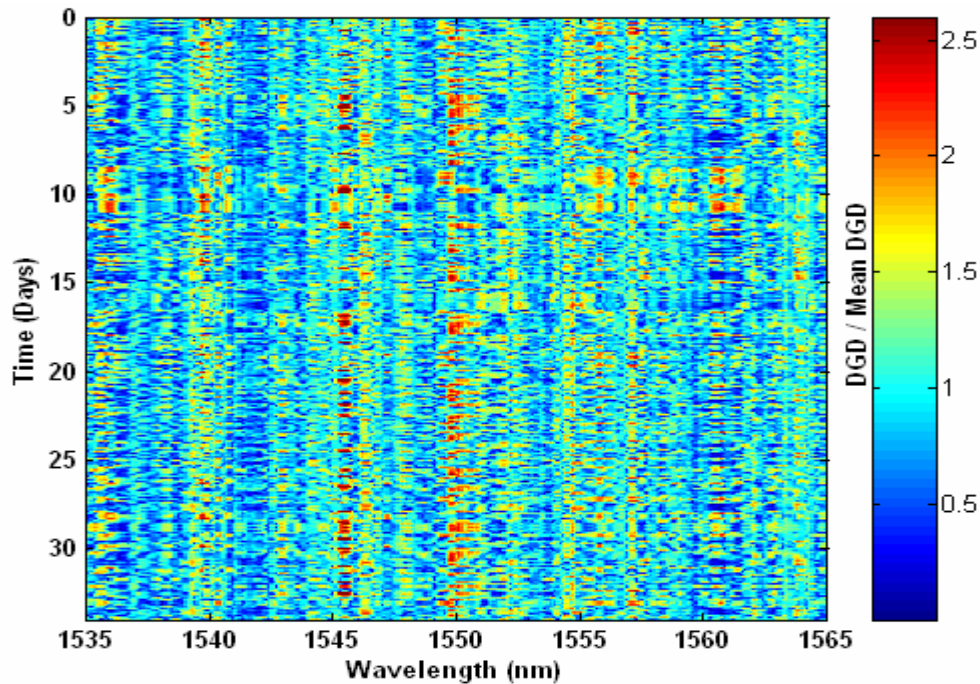

Figure 6.16. Normalized DGD colormap obtained from eleven-span link simulation.
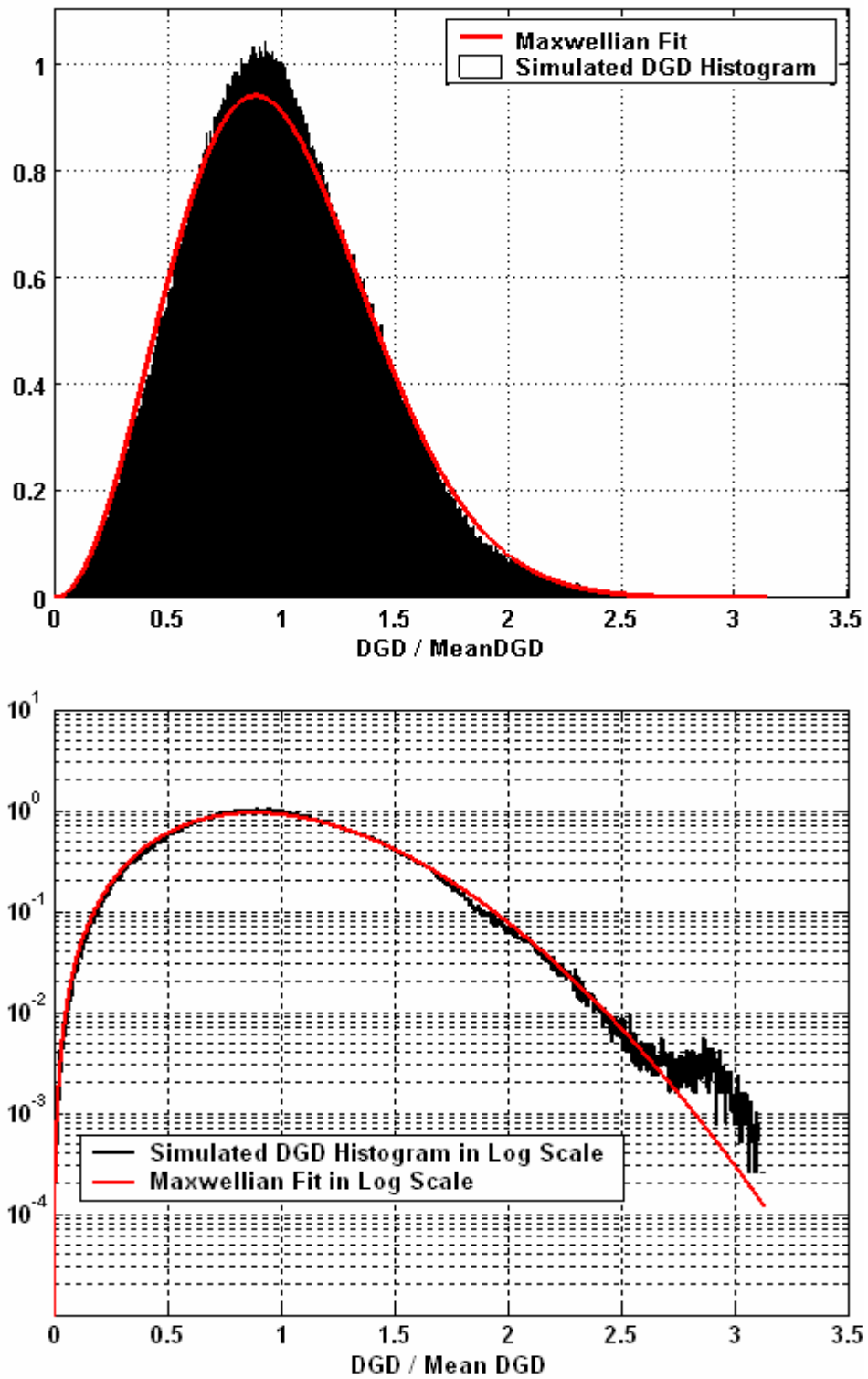
Figure 6.17. Histogram of simulated normalized DGD and its Maxwellian fit for eleven-span link in (a) linear scale (top) and (b) log scale (bottom).
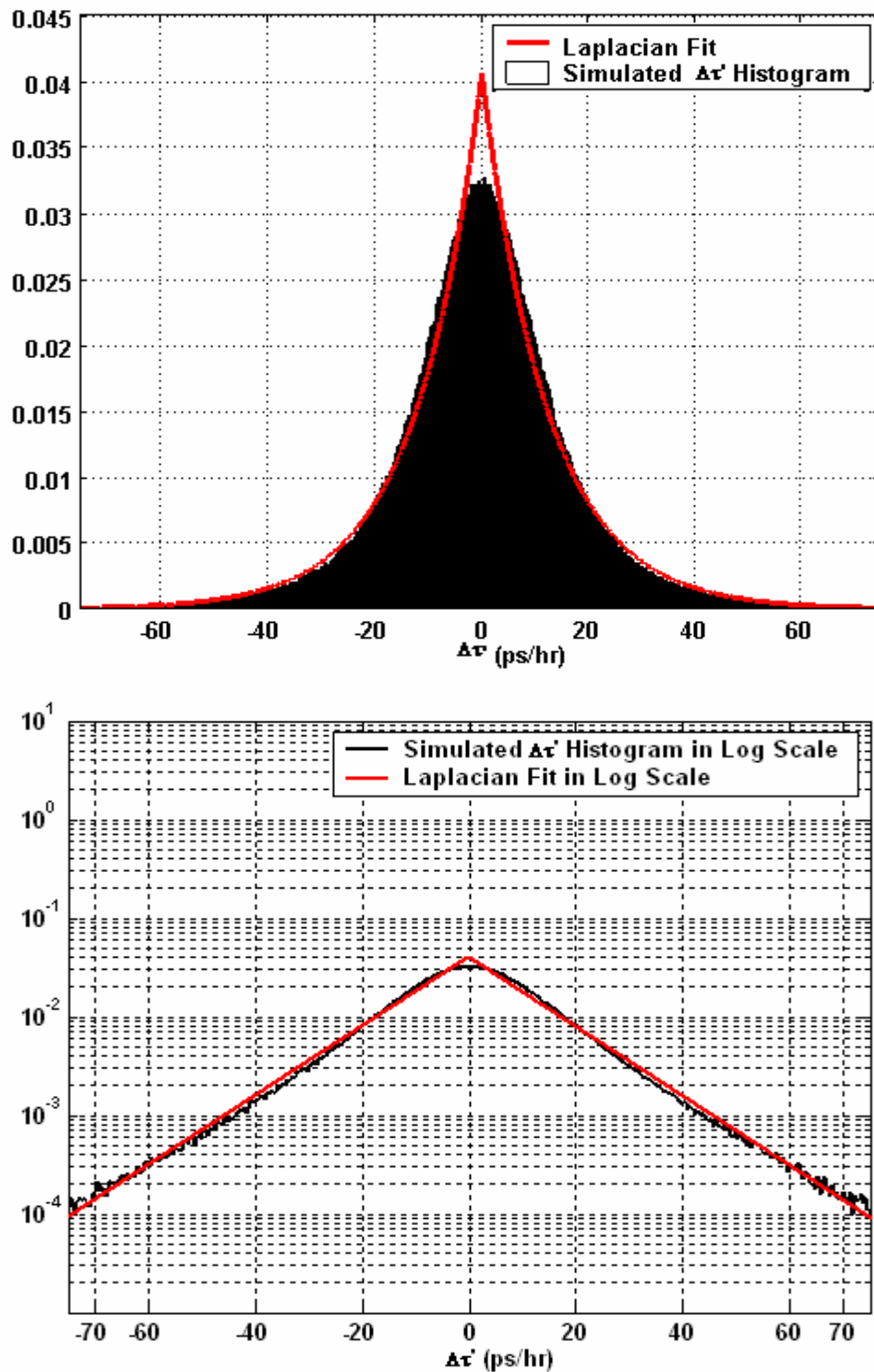
Figure 6.18. Histogram of simulated Δτ' and it Laplacian fit for eleven-span link in (a) linear scale (top) and (b) log scale (bottom).

Figures 6.18 (a) and 6.18 (b) show the simulated $\Delta\tau'$ histogram and its Laplacian fit in linear and log scales respectively. These figures show good agreement between the $\Delta\tau'$ histogram and the Laplacian distribution except at the center same as in the five-span, seven-span and nine-span cases. The Laplacian parameter (α) value corresponding to the Laplacian fits in figure 6.18, calculated from the simulated $\Delta\tau'$ data is 0.081 hr/ps.

6.7. Effect of under-sampling

Looking back at the $\Delta\tau'$ histograms and Laplacian fits in figures 6.9, 6.12, 6.15 and 6.18 corresponding to the five-span, seven-span, nine-span and eleven-span links, we observe that the central peak of each of the histograms doesn't match with its Laplacian fits while the rest of the histogram shows good agreement with the Laplacian fit. This is the effect of under-sampling. This could be rectified by decreasing the time interval between the consecutive simulations. However, with the current version of the Matlab code and the computing resources available, it takes prohibitively long (of the order of weeks) to run the above-mentioned cases with a much smaller sampling interval. Instead to show that the phenomenon observed in the above-mentioned figures is in fact due to under-sampling the four-span link case is repeated with different sampling intervals that are longer than the one corresponding to figure 6.6, which is 20 minutes. Simulation specifications are exactly same as discussed in section 6.2 except for the sampling interval and the Gaussian standard deviation which is varied in accordance with the sampling interval (the longer the sampling interval, the larger the standard deviation). The results obtained are discussed next.

6.7.1. Four-span link with 30-minute sampling interval

The plots and the values of the metrics obtained from four-span link simulation with 30-minute sampling interval are presented in this section. The Gaussian standard deviation used in this case was $\pi/60$. Figure 6.19 shows the normalized colormap from the simulations and it looks very similar to the colormap

corresponding to the case of 20-minute sampling interval. Figures 6.20 (a) and 6.20 (b) show the normalized DGD histogram and it Maxwellian fit in linear and log scales respectively and a good agreement between them is evident from the figures.
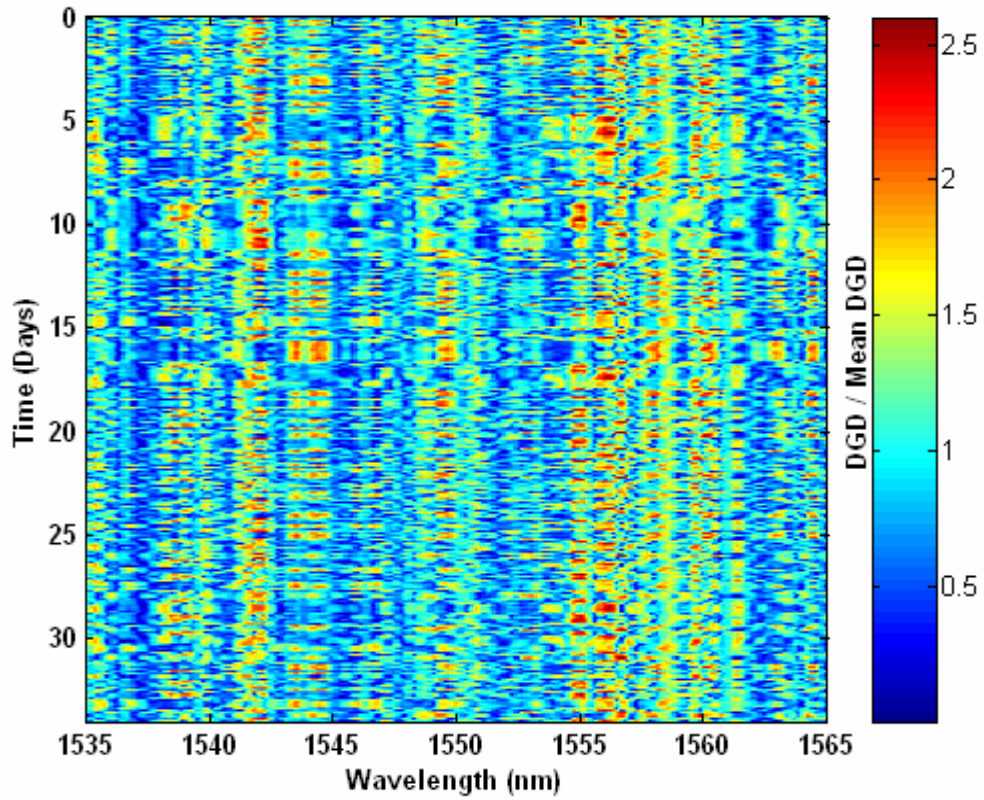
Figure 6.19. Normalized DGD colormap obtained from four-span link simulation with 30-minute sampling interval.
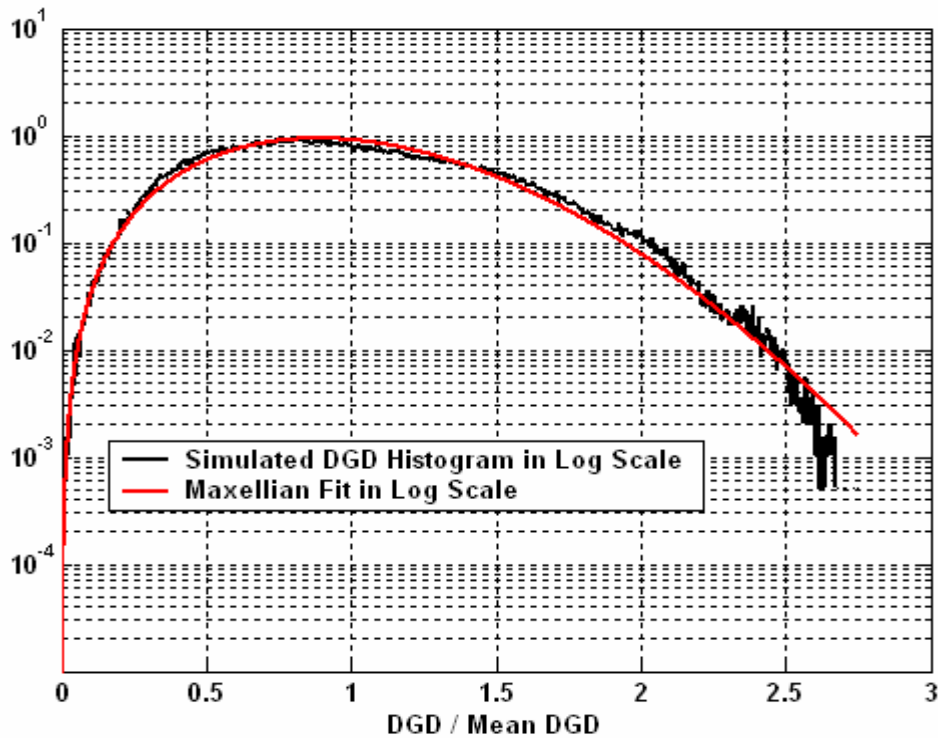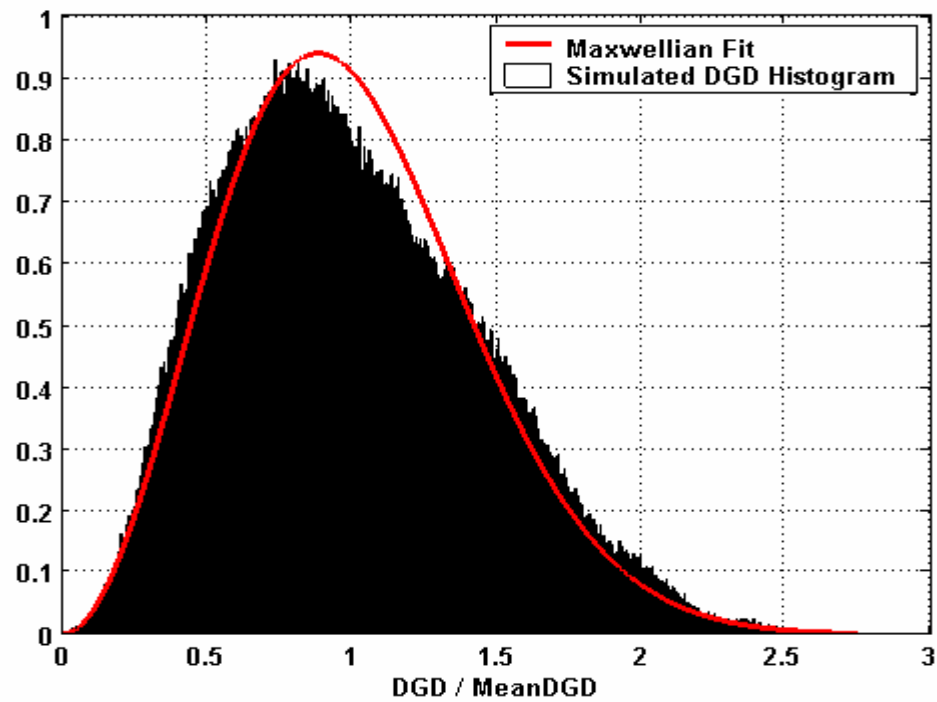
Figure 6.20. Histogram of simulated normalized DGD and its
Maxwellian fit for four-span link with 30-minute sampling
interval in (a) linear scale (top) and (b) log scale (bottom).
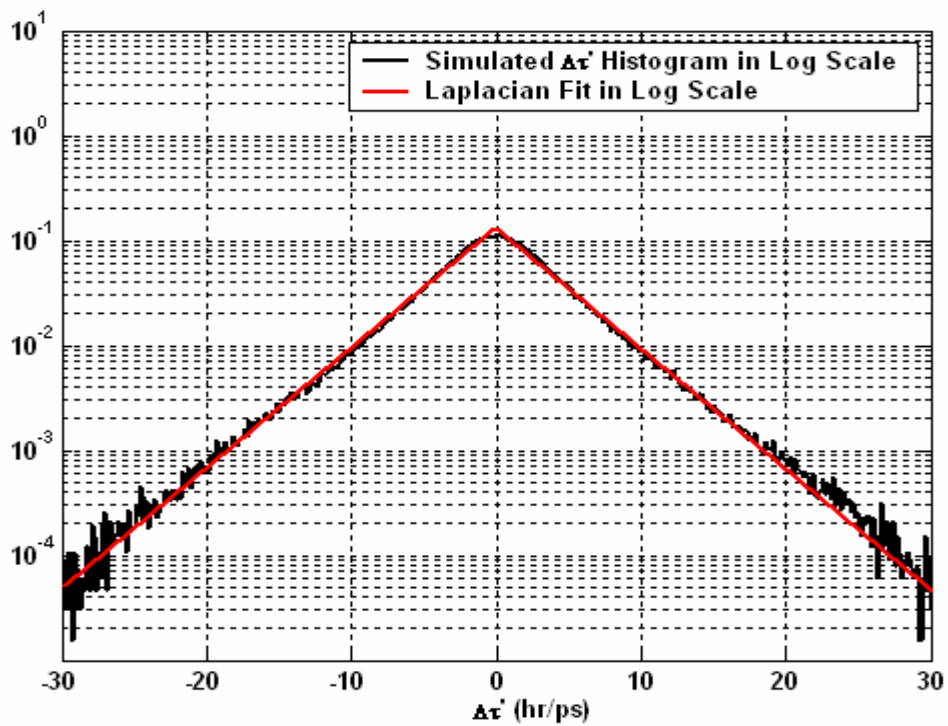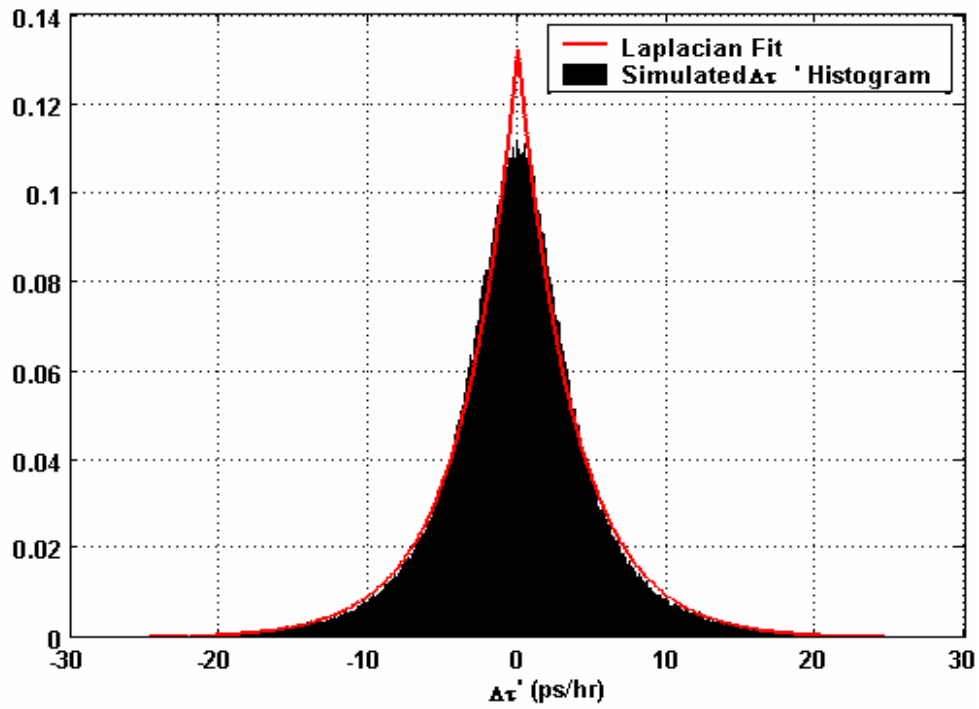
Figure 6.21. Histogram of simulated Δτ' and it Laplacian fit for four-span link with 30-minute sampling interval in (a) linear scale (top) and (b) log scale (bottom).

Figures 6.21 (a) and 6.21 (b) show the simulated $\Delta\tau'$ histogram and its Laplacian fit in linear and log scales respectively. Comparing these figures with the corresponding figures from the 20-minute sampling interval case, figures 6.6 (a) and 6.6 (b), the central peak of the histogram in the 30-minute case does not match with the Laplacian fit whereas it matches well with the fit in the 20-minute case. Since the sampling interval is the main difference between these cases this disagreement can be attributed to under-sampling. The Laplacian parameter (α) value for the 30-minute case is 0.26 hr/ps, which is close to the value from the 20-minute case (0.23 hr/ps) and this is because the above-mentioned disagreement is not that big and the histogram still closely resembles the Laplacian PDF. As can be seen next, the α value will vary significantly from the 20-minute case value (the actual value) as the above-mentioned disagreement increases.

6.7.2. Four-span link with 40-minute sampling interval

The plots and the values of the metrics obtained from four-span link simulation with 40-minute sampling interval are presented in this section. The Gaussian standard deviation used in this case was $\pi/45$. Figure 6.22 shows the normalized colormap from the simulations and it looks very similar to the colormaps corresponding to 20- and 30-minute cases. Figures 6.23 (a) and 6.23 (b) show the normalized DGD histogram and it Maxwellian fit in linear and log scales respectively and a good agreement between them is evident from the figures.

Figures 6.24 (a) and 6.24 (b) show the simulated $\Delta\tau'$ histogram and its Laplacian fit in linear and log scales respectively. Comparing these figures with the corresponding figures from the 20-minute sampling interval case, figures 6.6 (a) and 6.6 (b), the disagreement between the central peak of the histogram and its Laplacian fit in the 40-minute case is much greater than it was between 20- and 30-minute cases. The Laplacian parameter (α) value for the 40-minute case is 0.30 hr/ps, which is different from the 20-minute case (0.23 hr/ps).
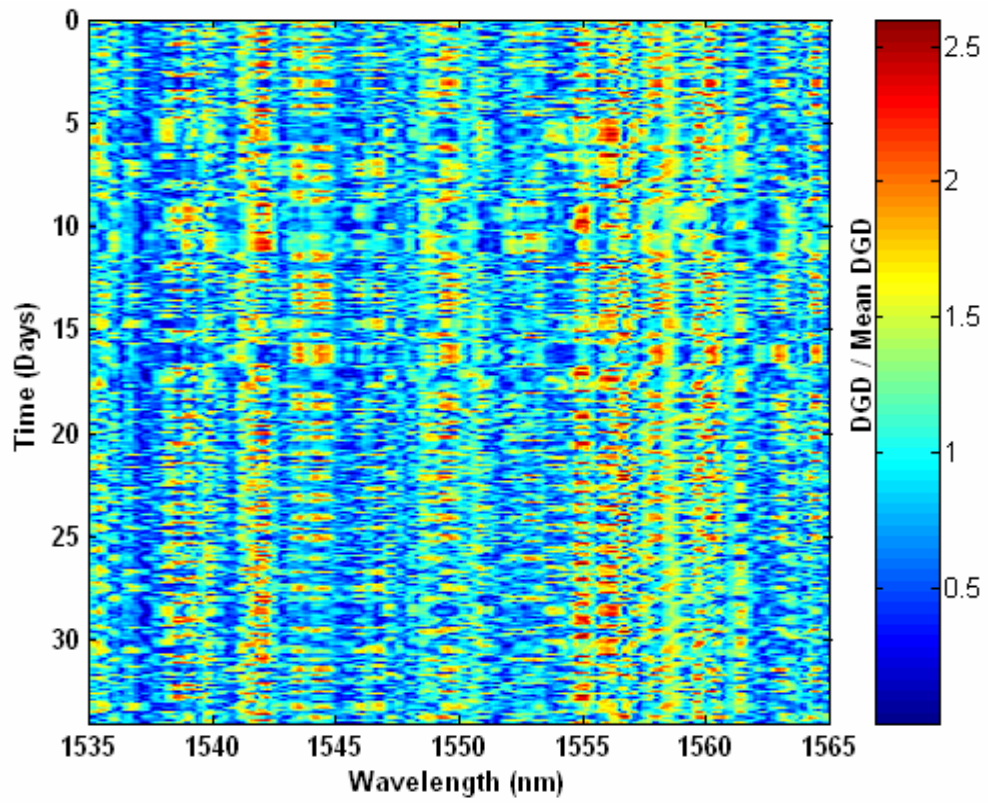
Figure 6.22. Normalized DGD colormap obtained from four-span link
simulation with 40-minute sampling interval.
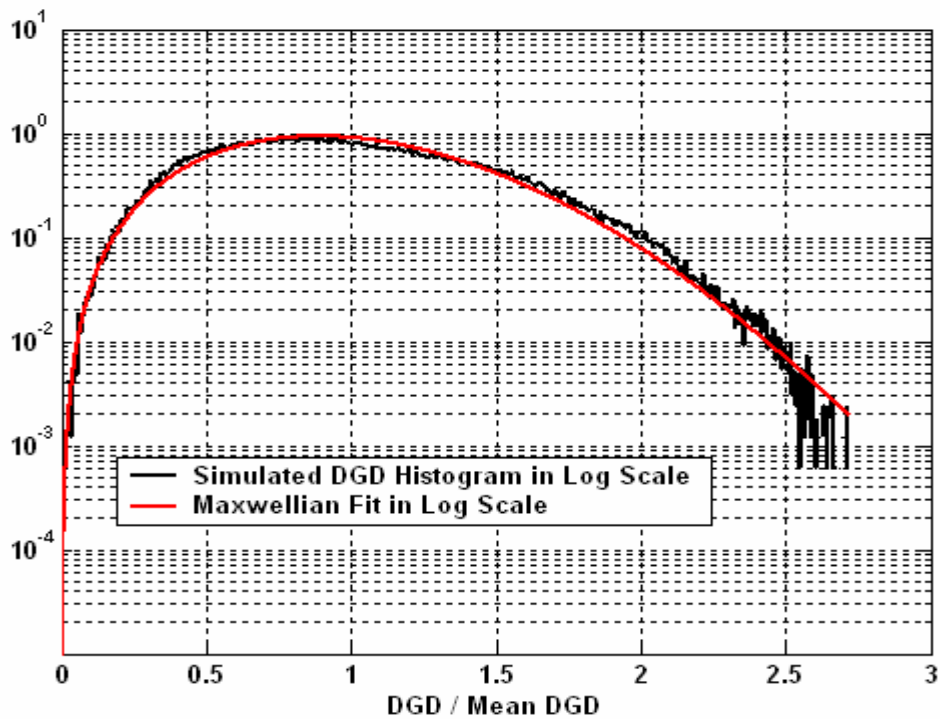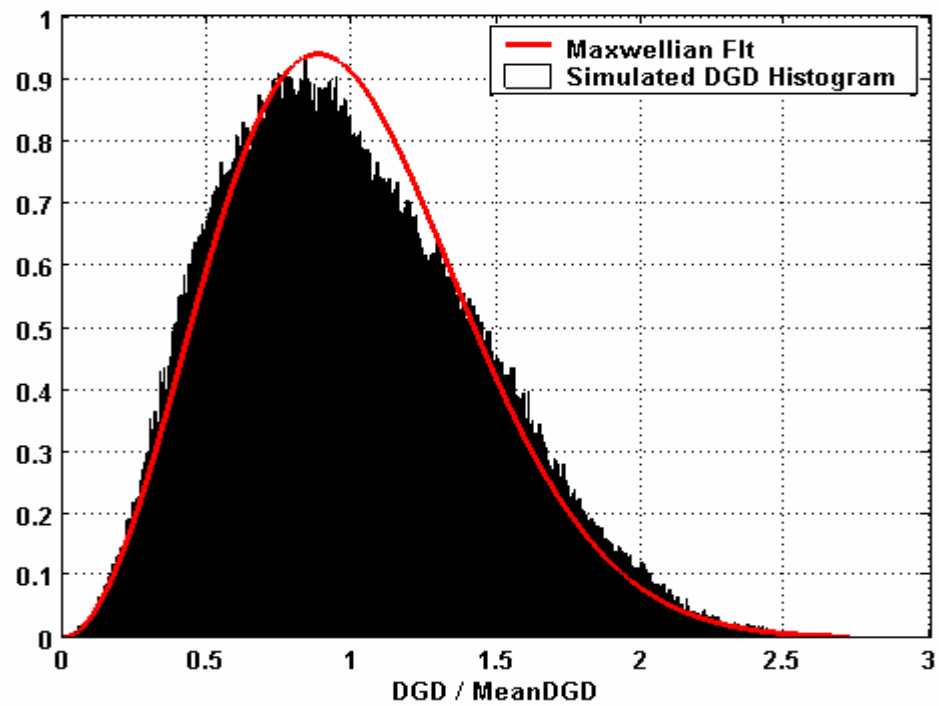
Figure 6.23. Histogram of simulated normalized DGD and its
Maxwellian fit for four-span link with 40-minute sampling
interval in (a) linear scale (top) and (b) log scale (bottom).
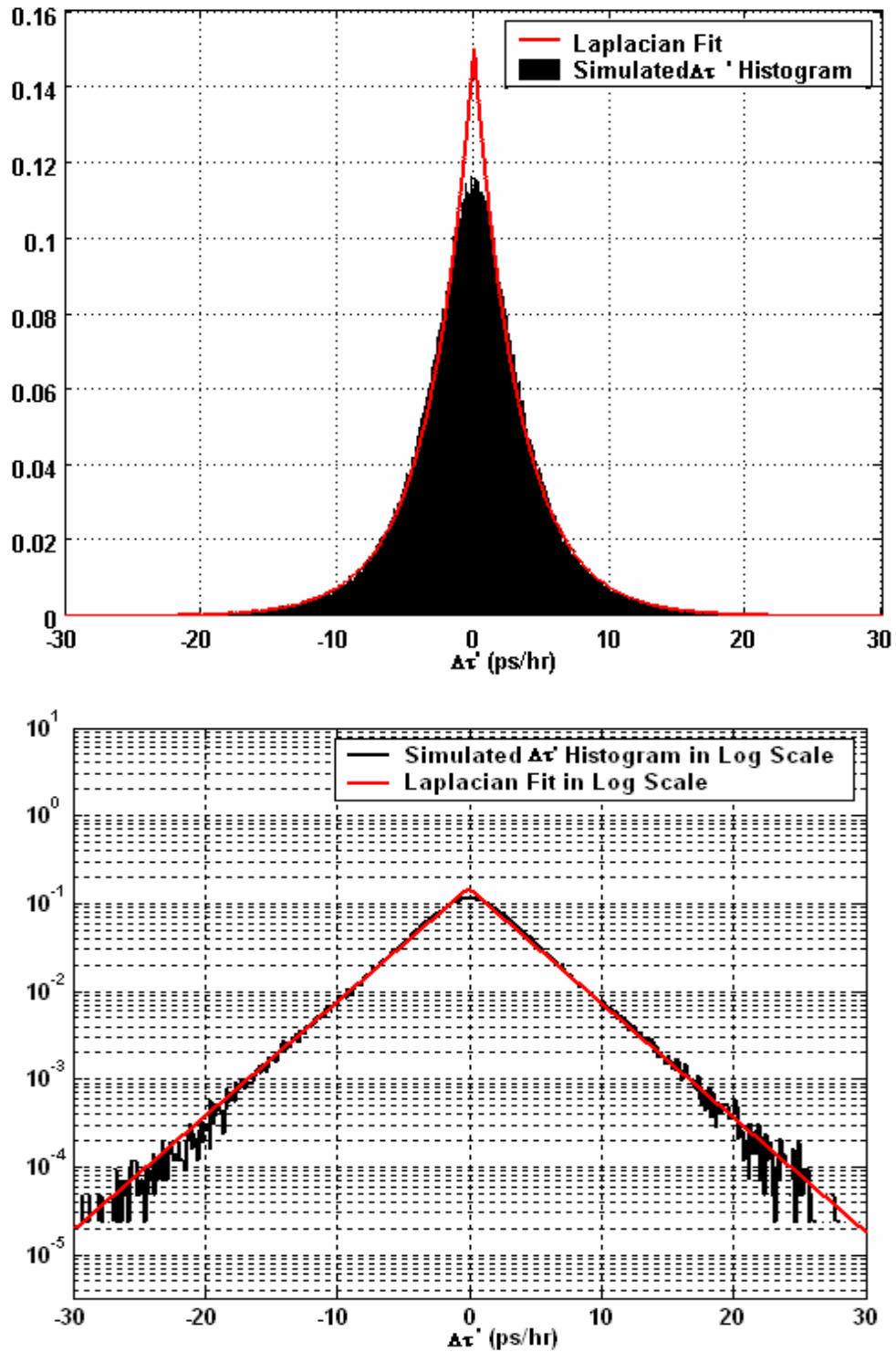
Figure 6.24. Histogram of simulated Δτ' and it Laplacian fit for four-span link with 40-minute sampling interval in (a) linear scale (top) and (b) log scale (bottom).

6.7.3. Four-span link with 60-minute sampling interval

The plots and the values of the metrics obtained from four-span link simulation with 60-minute sampling interval are presented in this section. The Gaussian standard deviation used in this case was $\pi/30$. Figure 6.25 shows the normalized colormap from the simulations and it looks very similar to the colormaps corresponding to 20-, 30- and 40-minute cases. Figures 6.26 (a) and 6.26 (b) show the normalized DGD histogram and it Maxwellian fit in linear and log scales respectively and a good agreement between them is evident from the figures.

Figures 6.27 (a) and 6.27 (b) show the simulated $\Delta\tau'$ histogram and its Laplacian fit in linear and log scales respectively. Comparing these figures with the corresponding figures from the 20-minute sampling interval case, figures 6.6 (a) and 6.6 (b), the disagreement between the central peak of the histogram and its Laplacian fit in the 60-minute case is much greater than it was in the other two cases discussed above. Also, the shape of the histogram has changed and it looks more like a Gaussian distribution. The Laplacian parameter (α) value for the 60-minute case is 0.37 hr/ps, which is quite different from the 20-minute case (0.23 hr/ps).
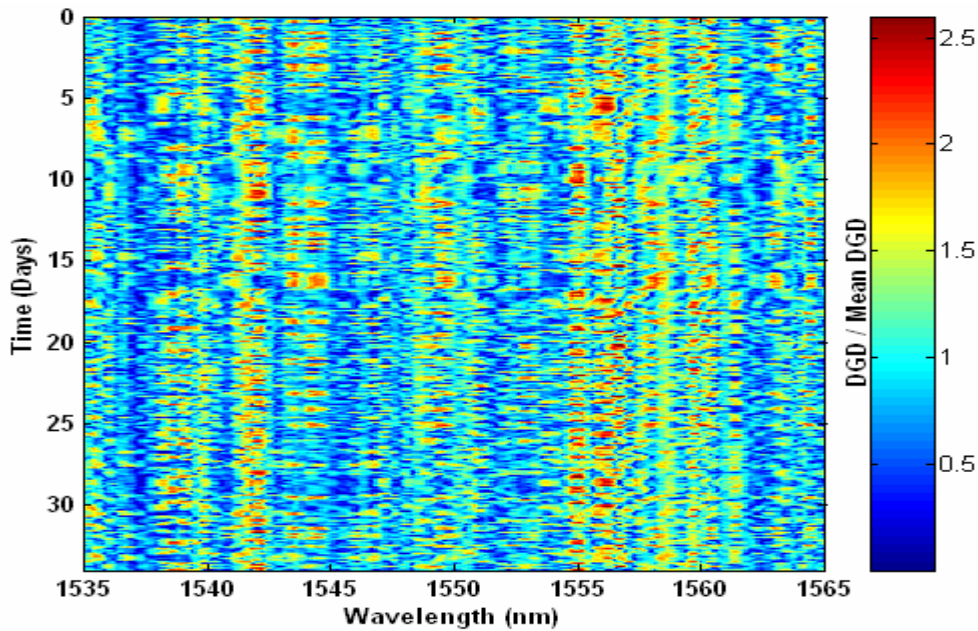
Figure 6.25. Normalized DGD colormap obtained from four-span link simulation with 60-minute sampling interval.
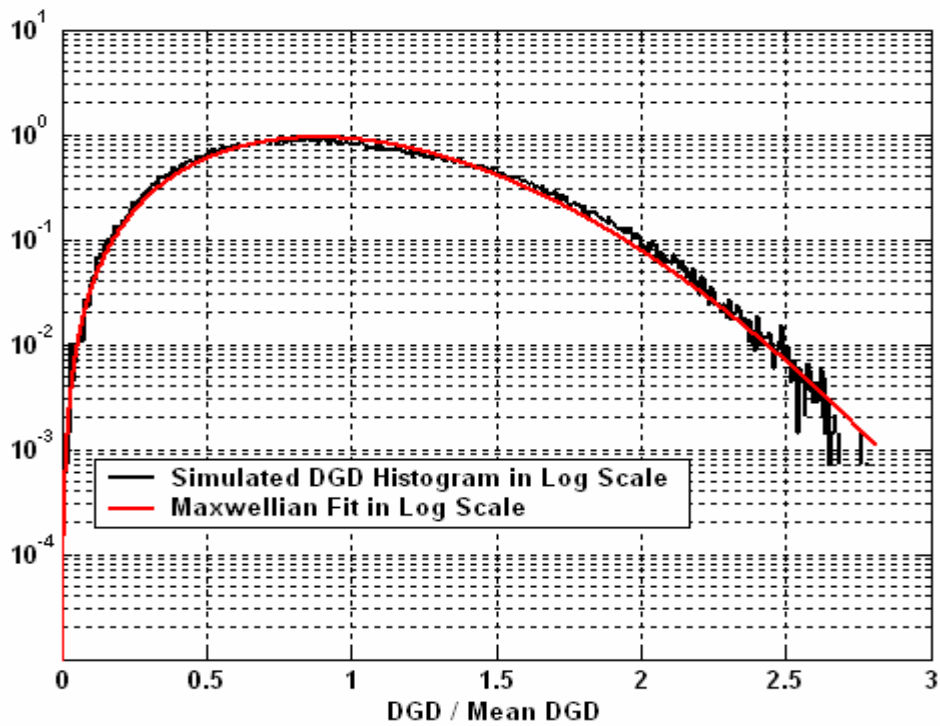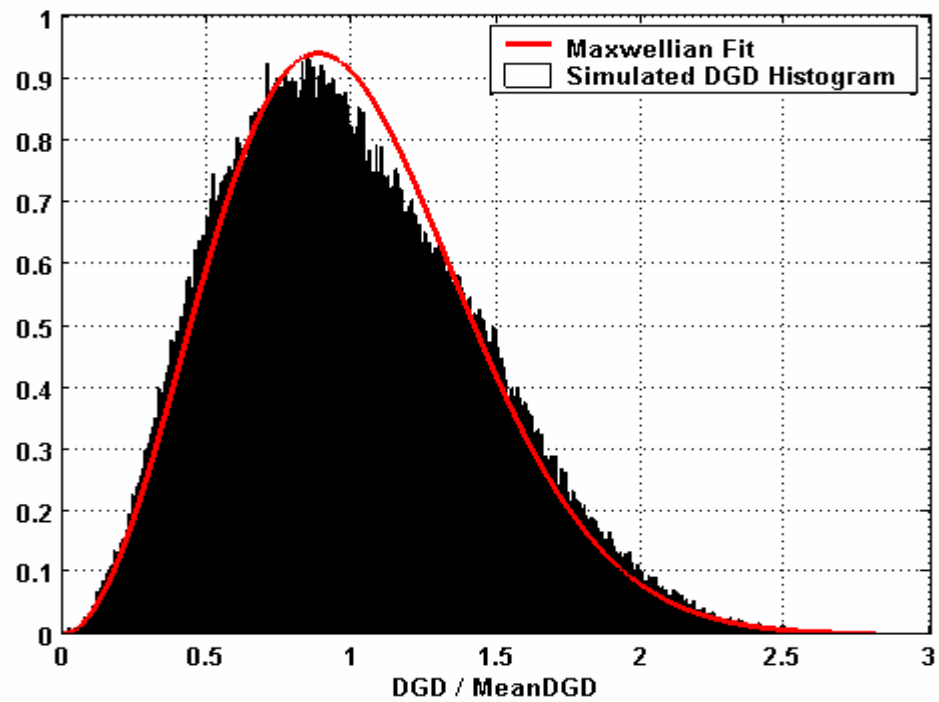
Figure 6.26. Histogram of simulated normalized DGD and its Maxwellian fit for four-span link with 60-minute sampling interval in (a) linear scale (top) and (b) log scale (bottom).
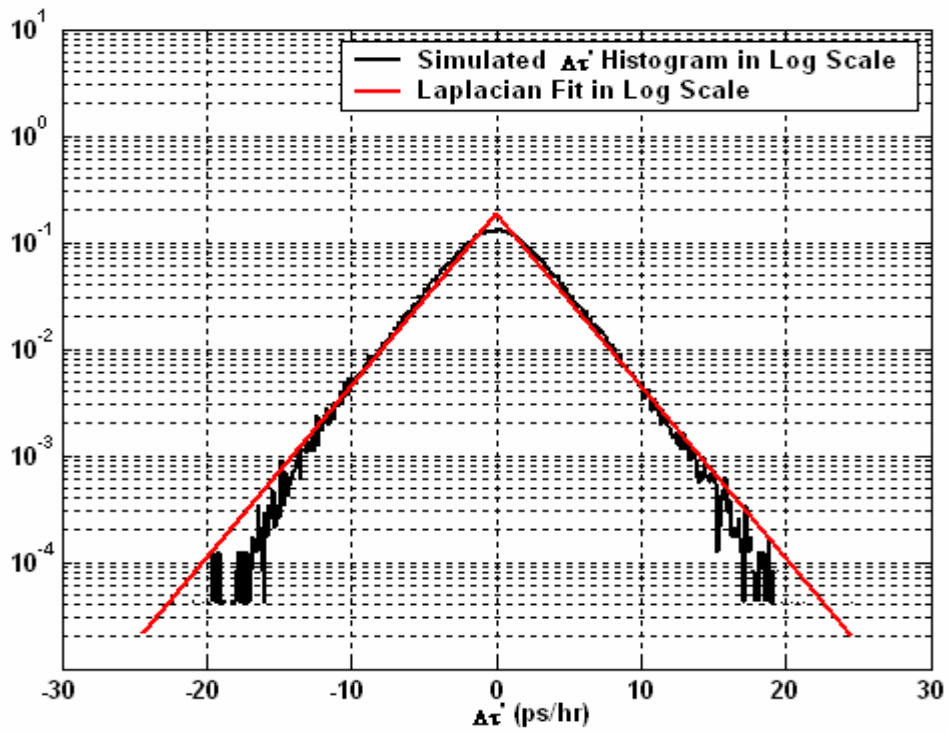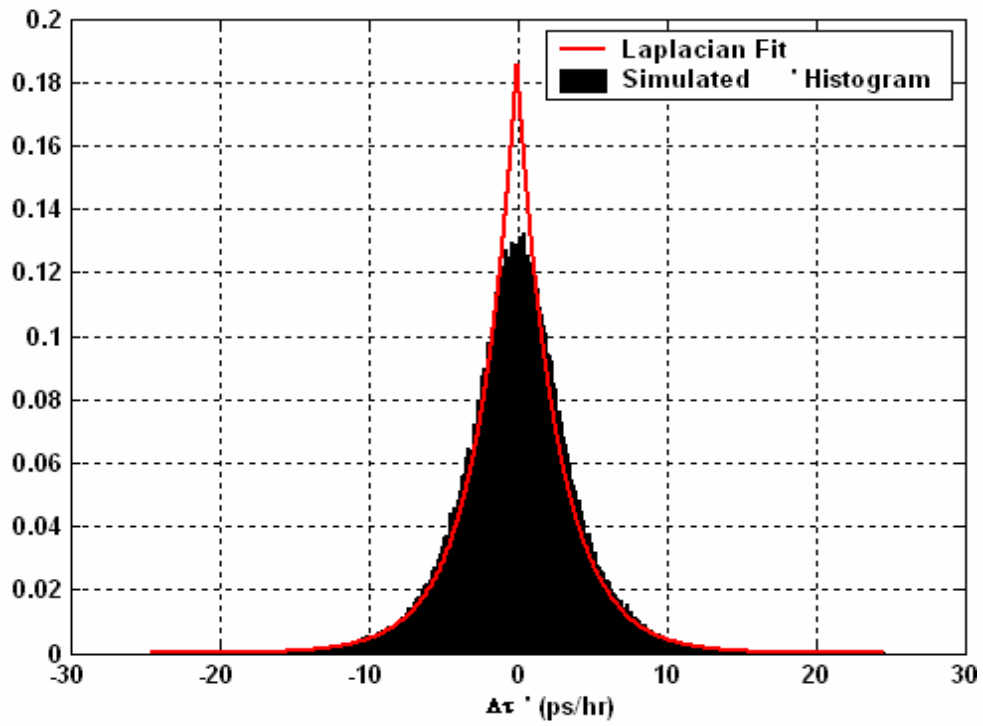
Figure 6.27. Histogram of simulated Δτ' and it Laplacian fit for four-span link with 60-minute sampling interval in (a) linear scale (top) and (b) log scale (bottom).

If we increase the sampling interval further the same trend will continue i.e., the $\Delta\tau'$ histogram will take a true Gaussian shape and the α value will be quite different from the actual value. The appearance of the Gaussian distribution makes more sense by taking a look at the generalized exponential PDF. Both Laplacian and Gaussian distributions are special cases of the generalized exponential PDF. The generalized exponential PDF is given by

$$f_\nu(x) = \frac{\nu}{\sqrt{8}\sigma\Gamma(\frac{1}{\nu})} \; exp\left(-\left| \frac{x-m}{\sqrt{2}\sigma} \right|^\nu \right) \tag{6.1}$$

where v is the mode, $\Gamma(.)$ is Gamma function, m is the mean and σ is the standard deviation. For Laplacian PDF $v = 1$ and for Gaussian PDF $v = 2$. As v approaches infinity, the distribution becomes uniform. This is illustrated in figure 6.28.
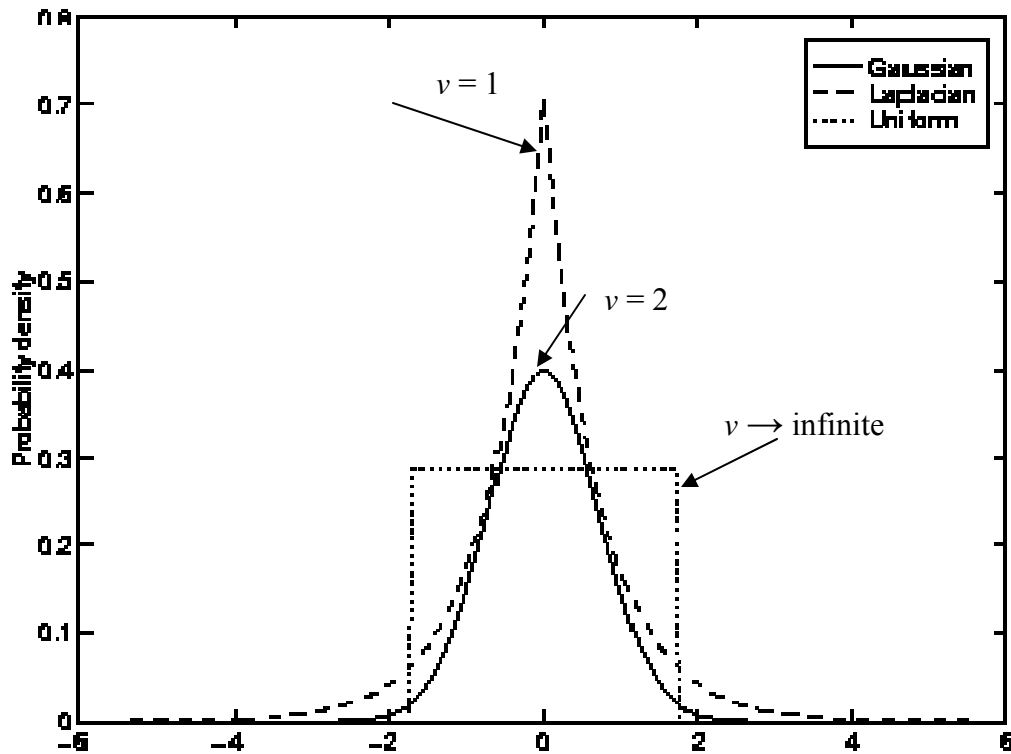
Figure 6.28. Laplacian, Gaussian and uniform distributions (zero mean, unit variance) as special cases of generalized exponential PDF [44].

Hence due to under-sampling, the $\Delta\tau'$ histogram deviates from the Laplacian PDF and approaches a Gaussian PDF first and for long enough sampling interval it will approach a uniform distribution.

The $\Delta\tau'$ histograms for the five-span, seven-span, nine-span and eleven-span links discussed earlier in this chapter look similar to the $\Delta\tau'$ histogram from four-span case with 30-minute sampling interval in the sense that the disagreement between the histogram central peak and it fit is little. Hence the actual values of the Laplacian parameter (α) value for those cases will be very close yet lower than the values mentioned earlier in the chapter at their respective locations. And so these values can be used in the study of variation of α parameter with link length.

6.8. Variation of Laplacian parameter with link length

Table 6.2 lists the values of the Laplacian parameter (α) for all the cases discussed in this chapter and the three-span link discussed in chapter 5. The length and the number of spans of each link are also listed in the table.

Table 6.2. α values for different link lengths.

Number of spans	Link length (km)	Laplacian Parameter (α) (hr/ps)
2	190	0.504
3	285	0.35
4	380	0.23
5	475	0.159
7	665	0.115
9	855	0.101
11	1045	0.081

Figure 6.29 shows the α values in table 6.1 plotted as a function of link length. A curve representing (A/Link length), where A is a constant with units (km-

hr)/ps and link length in km, is also shown in figure 6.29 for comparison. From the figure it is clear that the (A/Link length) curve approximates the variation of α with link length. Hence the Laplacian parameter is inversely proportional of the link length. For the special case considered in this report where all the spans are of equal length 95 km and each span has exactly the same number of fiber segments with a time varying ϕ_n component, the constant 'A' turns out to be equal to the span length and so the fitted curve reduces to $\alpha = (1/\text{Numberofspans})$, the Laplacian parameter is inversely proportional to the number of spans in the link.
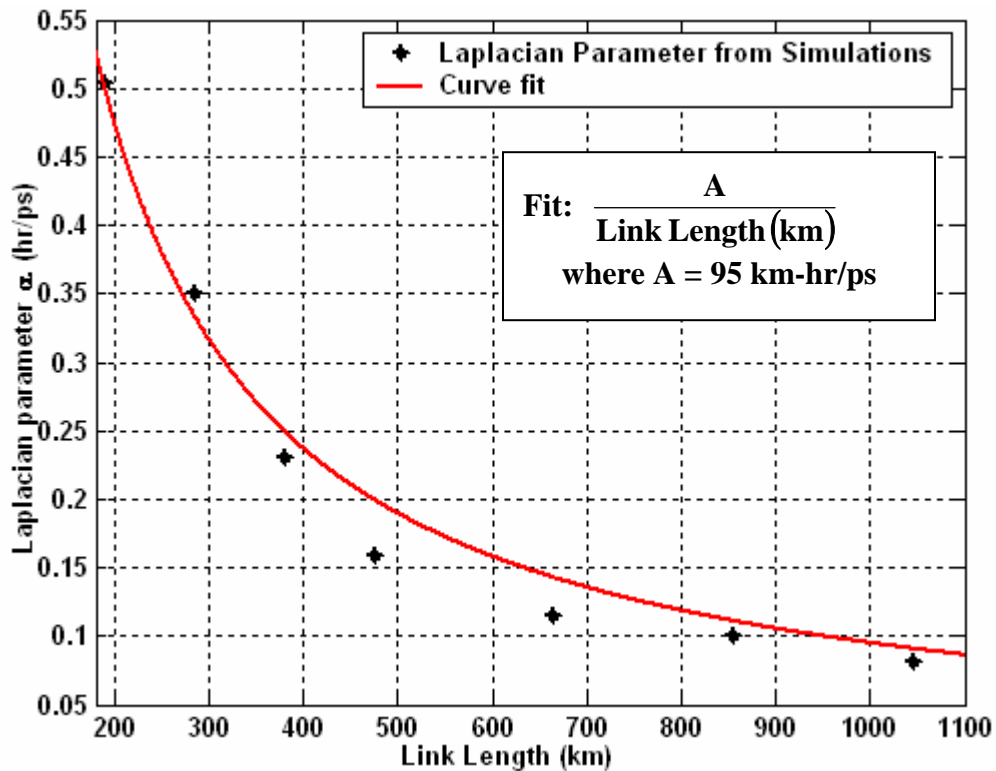
Figure 6.29. Laplacian parameter as a function of link length and (A / Link length) fit.

6.9. Variation of first-order PMD outage rates with link length

The simplified first-order PMD outage rate expression as given by (3.2) is

$$R_{out} = \frac{1}{2\alpha} f_{\Delta\tau}(\Delta\tau_{th})$$
(6.2)

Substituting $\alpha = \dfrac{A}{Link\,Length\,(km)}$, (6.2) reduces to

$$R_{out} = \frac{Link\,Length\,(km)}{2A} f_{\Delta\tau}(\Delta\tau_{th})$$
(6.3)

From the expression of Maxwellian PDF, $f_{\Delta\tau}(\Delta\tau_{th})$ is given by

$$f_{\Delta\tau}(\Delta\tau_{th}) = \frac{32}{\pi^2} \frac{\Delta\tau_{th}^2}{<\Delta\tau>^3} e^{-\left(\frac{4}{\pi}\frac{\Delta\tau_{th}^2}{<\Delta\tau>^2}\right)}$$
(6.4)

where $<\Delta\tau>$ is the mean DGD of the link.

For the special case of equal span lengths and same number of time varying segments for each span the expression simplifies to

$$R_{out} = \frac{Number\,of\,spans}{2} f_\tau(\Delta\tau_{th})$$
(6.5)

The simplified expression for first-order PMD outage rate in (6.3) is very significant in the sense that using this the outage rates can be calculated on any optical fiber link given the length and mean DGD (or the PMD coefficient) of the link. This is best illustrated in the following example.

6.9.1. Example scenario

Consider a scenario with the following specifications:

Bit rate = 40 Gbps

⇨ bit period = 25 ps

Link PMD coefficient 'b' = 0.1 ps/√km

Span length = 80 km; assume equal length spans

Assume all spans have equal number of time varying segments

⇨ Constant A in (6.3) = 80 km-hr/ps

Assume two different 40 Gbps receivers, Rx1 and Rx2, with Rx1 having a DGD threshold of 6.25 ps ($1/4^{th}$ of bit period) and Rx2 having a DGD threshold of 8.33 ps ($1/3^{rd}$ of bit period). Also, assume that the optical fiber is the major contributor of the link DGD and all the optical components along the link have insignificant DGD. Figure 6.30 shows the evolution of the Laplacian parameter (α) with link length and figure 6.31 shows the evolution of mean DGD with link length for the example scenario. The outage rates (R_{out}) as a function of link length, calculated using (6.3), for both the receivers are shown in figures 6.32 and 6.33 in linear and log scales respectively. Figure 6.34 shows the same R_{out} values as a function of normalized receiver DGD threshold (receiver DGD threshold divided by the mean DGD determined at different points along the link).
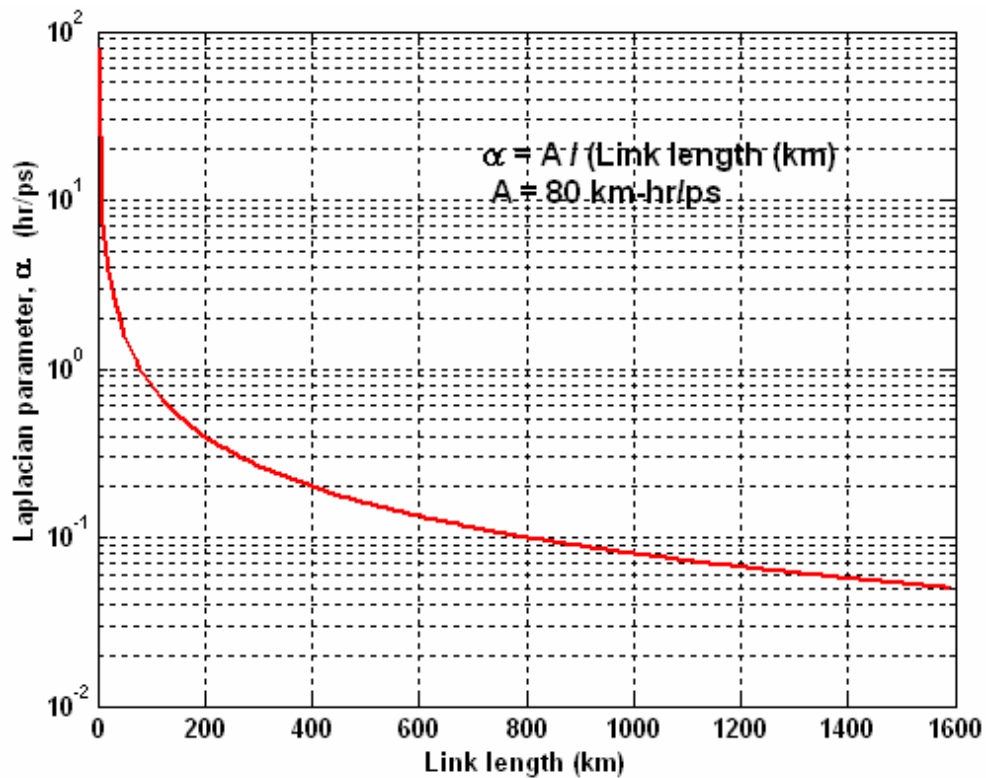
Figure 6.30. α evolution with link length for the example in section 6.9.1.
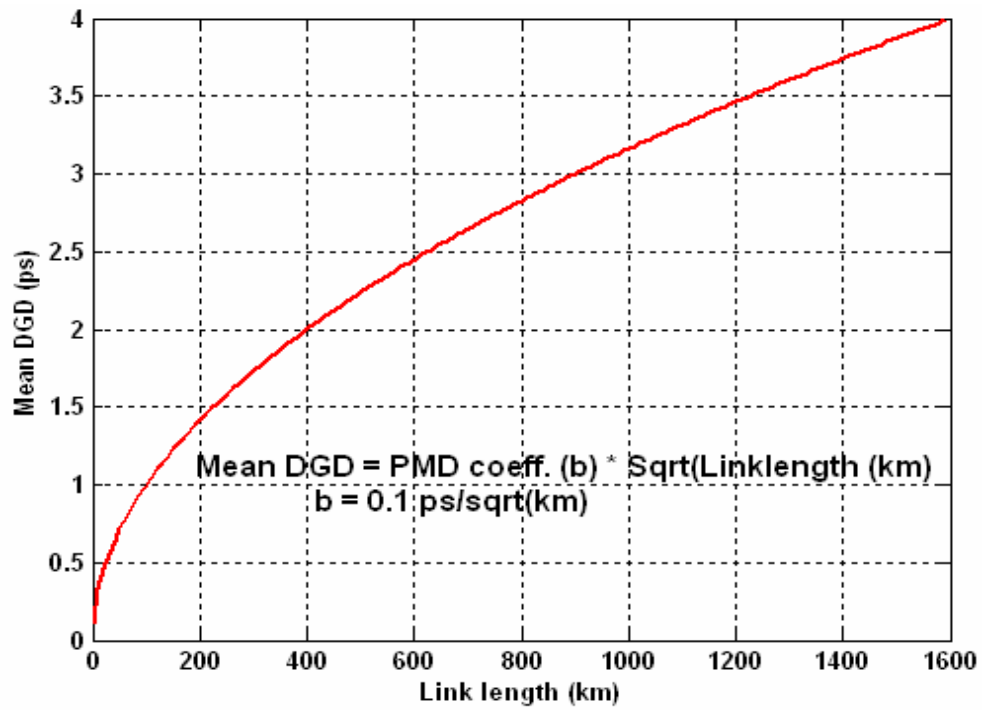
Figure 6.31. Mean DGD evolution with link length for the example in section 6.9.1.
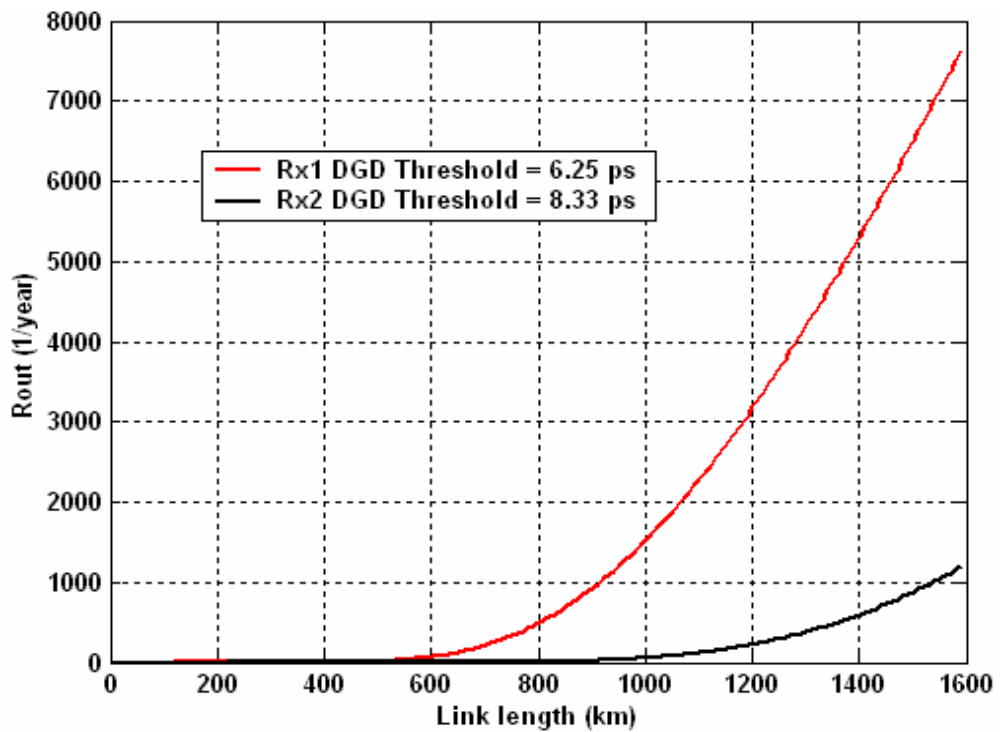
Figure 6.32. R_{out} vs. link length for Rx1 and Rx2 in linear scale
for the example in section 6.9.1.
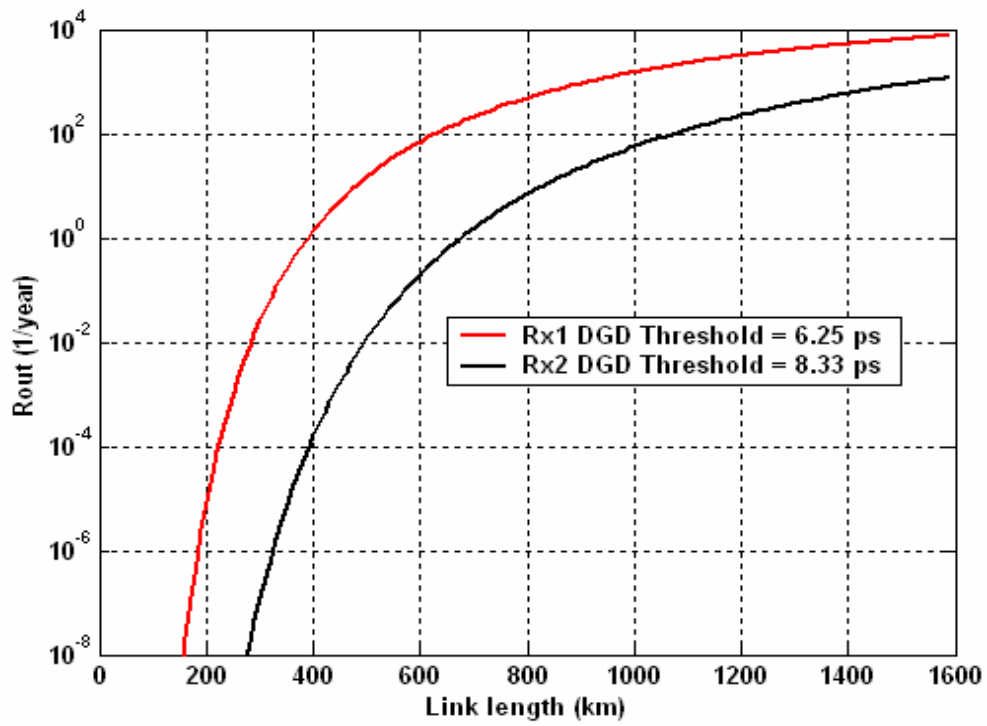
Figure 6.33. R_{out} vs. link length for Rx1 and Rx2 in log scale for the example in section 6.9.1.
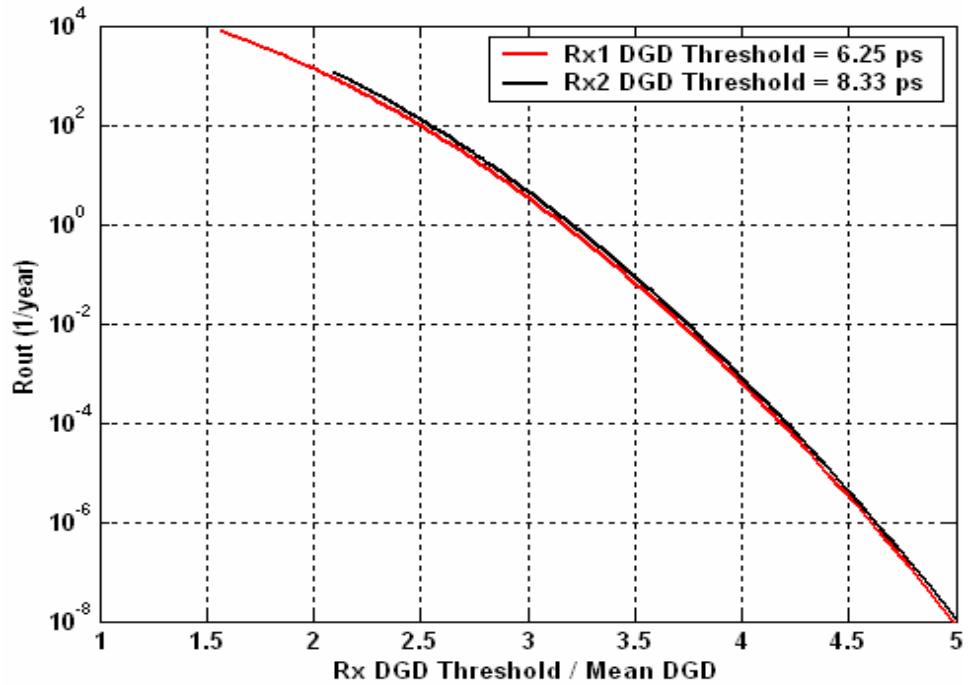
Figure 6.34. R_{out} vs. Rx DGD threshold / Mean DGD for Rx1 and Rx2 in log scale for the example in section 6.9.1.

Table 6.3. Predicted outage rates for the 40 Gbps receiver Rx1 with a DGD threshold of 6.25 ps discussed in the example in section 6.9.1.

Link length (km)	Mean DGD (ps)	α (hr/ps)	Rx1 DGD threshold / Mean DGD	R_{out} for Rx1 (Outages per year)	Mean Time Between Outages (MTBO) Roughly one outage in ...	Outage duration T_{out} (minutes)
200	1.41	0.4	4.42	7.77×10^{-6}	Few millenniums	5.91
400	2	0.2	3.13	1.38	9 months	6.15
600	2.45	0.13	2.55	71.1	5 days	6.30
800	2.83	0.1	2.21	489.15	18 hours	6.43
1000	3.16	0.08	1.98	1517	6 hours	6.54
1200	3.46	0.07	1.80	3172	3 hours	6.65
1400	3.74	0.06	1.67	5310	1 and ½ hours	6.76
1600	4	0.05	1.56	7743	1 hour	6.86

Table 6.4. Predicted outage rates for the 40 Gbps receiver Rx2 with a DGD threshold of 8.33 ps discussed in the example in section 6.9.1.

Link length (km)	Mean DGD (ps)	α (hr/ps)	Rx2 DGD threshold / Mean DGD	R_{out} for Rx2 (Outages per year)	Mean Time Between Outages (MTBO) Roughly one outage in ...	Outage duration T_{out} (minutes)
200	1.41	0.4	5.89	5.7×10^{-14}	Never	7 days
400	2	0.2	4.17	1.6×10^{-4}	Few centuries	4.4
600	2.45	0.13	3.4	0.20	5 years	4.65
800	2.83	0.1	2.95	6.96	1 and ½ months	4.66
1000	3.16	0.08	2.63	56.7	6 days	4.72
1200	3.46	0.07	2.40	225.7	1 and ½ days	4.78
1400	3.74	0.06	2.23	598	15 hours	4.83
1600	4	0.05	2.08	1231	7 hours	4.88

Tables 6.3 and 6.4 show the α, mean DGD, normalized Rx DGD threshold and the outage rate values in figures 6.30 - 6.34 for specific link lengths for Rx1 and Rx2 respectively. These tables also show the mean time between outages (MTBO) and the outage duration Tout values calculated using (2.6) and (2.8). Looking at the outage rate curves in figures 6.32 – 6.34, it is clear that the outage rates increase monotonically with link length. However, we have observed that this monotonic nature is valid only when the receiver DGD threshold is greater than the mean DGD of the link, which is typically the case in reality. This result will have great impact on the network design of major carriers like Sprint who are pushing for high-speed, ultra long-haul, all optical fiber links that could span 1500 to 2000 km. The above results indicate that for such longer link lengths it is extremely important to do PMD outage analysis and develop sophisticated PMD mitigation strategies that can ensure network reliability before higher bit rates (40 Gbps and above) can be transported on them.

6.9.2. A special case

Consider a special case where the ratio between the receiver DGD threshold and the link mean DGD is maintained a constant even as link length is increased, for example, a DGD threshold of 4 ps for a 400-km link with 2 ps mean DGD (ratio of 2) and a DGD threshold of 8 ps for a 1600-km link with 4 ps mean DGD (ratio of 2). For this special case, which is not very realistic, a simple relation exits between outage rate R_{out} and the link length. From (6.4) it is clear that if a constant ratio is maintained between receiver DGD threshold and the mean DGD, $f_{\Delta\tau}(\Delta\tau_{th})$ is inversely proportional to the mean DGD. Also, the mean DGD of a link is directly proportional to the square root of the link length and hence from (6.2) to (6.4) it is evident that R_{out} is directly proportional to the square root of the link length

$$R_{out} \propto \sqrt{\text{Link Length (km)}} \qquad (6.6)$$

It should be noted that this special case also agrees with the monotonic increase of outage rates with link length mention in section 6.91.

7. Conclusions and Future work

7.1. Conclusions

The work mentioned in section 2.3 has been completed successfully, which led to some very useful results. These results were achieved in three steps. First, by analyzing the measured DGD data on different single-, two- and three-span links it was determined empirically that DGD time derivative ($\Delta\tau'$) has a Laplacian PDF and using this, the expression for first-order PMD mean outage rates given by Caponi et al. [1] was reduced to a simple analytical expression that depends on only two parameters that are link-dependent, namely mean DGD and Laplacian parameter. Second, the basic PMD numerical model given by Dal Forno et al. [34] was enhanced to include the temporal component to it which would accurately simulate the PMD characteristics on buried standard single-mode fibers. The temporal component is composed of a linear function of air temperature, the dominant factor, and a Gaussian random variable that accounts for other factors. This enhanced model was validated by comparing the simulation results from the 7 different link configurations used for measurements with the corresponding measured results and verifying the accuracy of the simulated results. Third, the validated, enhanced PMD model was used to model the PMD characteristics on long-haul fiber-optic links of different lengths. The results from these simulations were used to study the variation of the Laplacian parameter, and hence the first-order PMD outage rates, with link length.

From the study it was determined that the Laplacian parameter is inversely related to the link length and the analysis using the simplified outage rate expression in (3.2) showed that the first-order PMD outage rates increase monotonically with the link length provided the receiver DGD threshold is greater than the link mean DGD. This is a very important finding which will have a great impact on the network design of all the major carriers that are pushing for high-speed, all-optical, ultra long-haul optical fiber links. The above finding implies that realizing such links requires sophisticated PMD mitigation strategies to ensure network reliability.

Also, the effects of under-sampling on the shape of $\Delta\tau'$ histogram/PDF were also discussed. Under-sampling leads to a non-Laplacian PDF for $\Delta\tau'$ like the Gaussian PDF first and eventually, for a low enough sampling rate, the uniform PDF. This is due to the fact that Laplacian, Gaussian and uniform PDFs are all special cases of the generalized exponential PDF.

7.2. Future work

This report addressed the basic issue of modeling the temporal PMD behavior on long-haul optical fiber links to predict the first-order PMD outage rates. However, there is ample scope to build on this research work and include much finer details to the model. A list of possible future work ideas are given below:

- All of the simulation cases discussed in this report used only one temperature profile corresponding to one location along the fiber link. However, while modeling PMD on long-haul links it is more realistic to use multiple temperature profiles in the simulation, since temperature profiles could be different for different locations along the fiber link. Adding this detail to the model is straight forward.

- Although the actual mean DGD values of the fiber links discussed in this report were not reported, moderately high values of PMD coefficient were used in the simulations. It would be interesting to see if the results would be any different on fiber links with very low PMD coefficients.

- If long-haul optical links are accessible for making measurements over long periods of time, the monotonic increase in the outage rates with link length, determined through simulations in this report, could be verified through measurements.

- Single-span link simulations required a much narrower filter compared to multi-span links to filter the raw temperature data so as to accurately model PMD characteristics on them. This issue has not been addressed in this report, but needs to be investigated further.

- Although this work focused only on first-order PMD outage analysis, higher-order outage analysis is also very important. The PMD model discussed in this report could be used to extract higher-order PMD data that is needed for higher-order PMD outage analysis.

- In all of the simulation cases discussed in this report, a fixed number of fiber segments per span were modeled as having a time varying ϕ_n component. To be more realistic this parameter could be modeled as a Gaussian or a uniform random variable. It would be interesting to see if the results would be any different because of this change.

- Also, a fixed value of the PMD coefficient 'b' was used in all of the simulation cases discussed in this report. However, this could be made temperature-dependent to replicate the spectral drift observed from the measurements. This detail could be critical for higher-order outage analysis.

REFERENCES

1. R. Caponi, B. Riposati, A. Rossaro, and M. Schiano, "WDM system impairments due to highly correlated PMD spectra of buried optical cables," *Electronics Letters,* 38(14), pp. 737-738, 2002.

2. L.E. Nelson, M. Karlsson, and D.Q. Chowdhury, "Guest editorial, Special issue on polarization-mode dispersion," *Journal of Lightwave Technology*, 22(4), pp. 951-952, 2004.

3. C. Allen, P.K. Kondamuri, D.L. Richards, and D.C. Hague, "Analysis and comparison of measured DGD data on buried single-mode fibers", *Symposium on Optical Fiber Measurements, NIST conference*, USA, pp. 195-198, Sept. 2002.

4. H. Kogelnik, R.M. Jopson, and L.E. Nelson, "Polarization-mode dispersion", *Optical fiber telecommunications: Systems and impairments,* Eds. I.P. Kaminov, and T. Li, San Diego: Academic press, vol. IV B, 2002.

5. P. Hernday, "Dispersion measurements", *Fiber optic test and measurement*, Eds. D. Derickson, New Jersey: Prentice Hall PTR, 1998.

6. C.T. Allen, P.K. Kondamuri, D.L. Richards, and D.C. Hague, "Measured temporal and spectral PMD characteristics and their implications for network-level mitigation approaches," *Journal of Lightwave Technology*, 21(1), pp. 79-86, 2003.

7. M. Karlsson, J. Brentel, and P.A. Andrekson, "Long-term measurement of PMD and polarization drift in installed fibers," *Journal of Lightwave Technology*, 18(7), pp. 941-951, 2000.

8. J.A. Nagel, M. W. Chbat, L. D. Garrett, J. P. Soigné, N. A. Weaver, B. M. Desthieux, H. Bülow, A. R. McCormick, and R. M. Derosier, "Long-term PMD mitigation at 10 Gb/s and time dynamics over high-PMD installed fiber," *Proc. ECOC 2000*, Munich, Germany Vol. II (4.2.1), pp. 31-32, 2000.

9. J. Cameron, L. Chen, X. Bao, and J. Stears, "Time evolution of polarization mode dispersion in optical fibers," *Photonics Technology Letters*, 10(9), pp. 1265-1267, 1998.

10. C. De Angelis, A. Galtarossa, G. Gianello, F. Matera, and M. Schiano, "Time evolution of polarization dispersion in long terrestrial links," *Journal of Lightwave Technology*, 10(5), pp. 552-555, 1992.

11. H. Bulow, and G. Veith, "Temporal dynamics of error-rate degradation induced by polarization mode dispersion fluctuation of a field fiber link," *Proc. ECOC'97*, Vol. I, pp. 115-118, 1997.

12. T. Takahashi, T. Imai, and M. Aiki, "Time evolution of polarization mode dispersion in 120 km installed optical submarine cable, *Electronics Letters*, 29(18), pp. 1605-1606, 1993.

13. T. Kawazawa, and Y. Namihira, "Long-term polarization-mode-dispersion measurement of installed optical submarine cable," *OFC '94*, ThK4, pp. 228-229, 1994.

14. S. Bahsoun, J. Nagel, and C. Poole, "Measurements of temporal variations in fiber transfer characteristics to 20 GHz due to polarization-mode dispersion," *Proc. ECOC'90*, pp. 1003-1006, 1990. Post deadline paper.

15. C.D. Poole, R.W. Tkach, A.R. Chraplivy, and D.A. Fishman, "Fading in lightwave systems due to polarization-mode dispersion," *Photonics Technology Letters*, 3(1), pp. 68-70, 1991.

16. M. Karlsson and J. Brentel, "Autocorrelation function of the polarization-mode dispersion vector," *Optics Letters*, 24(14), pp. 939-941, 1999.

17. M. Shtaif, "Study of the frequency autocorrelation of the differential group delay in fibers with polarization mode dispersion", Optics Letters, 25(10), pp. 707-709, 2000.

18. A. Mecozzi, M. Shtaif, and J.A. Nagel, "Frequency autocorrelation of the differential group delay in optical fibers," *Proc. ECOC 2000*, Vol. II, pp. 91-92, 2000.

19. C.D. Poole, and J. Nagel, "Polarization effects in lightwave systems," in *Optical Fiber Telecommunications*, Eds. I.P. Kaminov, and T.L. Koch, San Diego: Academic Press, vol. III A, 1997.

20. W. Shieh, "Accelerated outage probability testing for PMD induced impairment," *Photonics Technology Letters*, 12(10), pp. 1364-1366, 2000.

21. A. Djupsjobacka, "Calculation of signal outage due to polarization mode dispersion," *Photonics Technology Letters*, 13(7), pp. 660-662, 2001.

22. F. Bruyere, and O. Audouin, "Assessment of system penalties induced by polarization mode dispersion in a 5 Gb/s optically amplified transoceanic link," *Photonics Technology Letters*, 6(3), pp. 443-445, 1994.

23. H. Bulow, "System outage probability due to first- and second-order PMD", *Photonics Technology Letters*, 10(5), pp. 696-698, 1998.

24. J.N. Damask, G. Gray, P. Leo, G. Simer, K. Rochford, and D. Veasay, "Method to measure and estimate total outage probability for PMD-impaired systems," *Photonics Technology Letters*, 15(1), pp. 48-50, 2003.

25. P.J. Winzer, H. Kogelnik, and K. Ramanan, "Precise outage specifications for first-order PMD," *Photonics Technology Letters*, 16(2), pp. 449-451, 2004.

26. G. Biondini, W.L. Kath, and C.R. Menyuk, "Importance sampling for polarization-mode dispersion: techniques and applications", *Journal of Lightwave Technology*, 22(4), pp. 1201-1215, 2004. Invited paper.

27. G. Biondini, W.L. Kath, C.R. Menyuk, "Importance sampling for polarization-mode dispersion," *Photonics Technology Letters*, 14(2), pp. 310-312, 2002.

28. S.L. Fogal, G. Biondini, and W.L. Kath, "Multiple importance sampling for first- and second-order polarization-mode dispersion," *Photonics Technology Letters*, 14(9), pp. 1273-1275, 2002.

29. I.T. Lima, O. Lima, J.Zweck, and C.R. Menyuk, "Efficient computation of outage probabilities due to polarization effects in a WDM system using a reduced Stokes model and importance sampling," *Photonics Technology Letters*, 15(1), pp. 45-47, 2003.

30. C. Geiser, B. Huttner, N. Gisin, R. Caponi, M. Potenza, M. Schiano, M. Artiglia, and I. Joindot, "Measurement of polarisation mode dispersion in fiber amplifiers," *SOFM Boulder 1998*, NIST Special Publication 930, pp. 19-22, 1998.

31. Caponi, M. Potenza, M. Schiano, M. Artiglia, I. Joindot, C. Geiser, B. Huttner, N. Gisin, "Deterministic nature of polarization mode dispersion in fiber amplifiers," *Proc. ECOC'98*, pp. 543-544, 1998.

32. I. Riant, J. Gourhant, and P. Sansonetti, "Polarization-mode dispersion analysis in fiber chromatic dispersion compensators," *Proc. OFC'99*, San Diego, CA, TuS2, pp. 269-271, 1999.

33. J. Vobain, G. Hershenroder, and K. Morl, "Dispersion-compensating fibers with high birefringence," *SOFM Boulder 1996*, NIST Special Publication 905, pp. 93-96, 1996.

34. A.O. Dal Forno, A. Paradisi, R. Passy, and J.P.von der Weid, "Experimental and theoretical modeling of polarization-mode dispersion in single-mode fibers," *IEEE Photonics Technology Letters*, 12(3), pp. 296-298, 2000.

35. "PMD specifications, JME method", *User's guide*, Agilent 8509C, pp. 9-4, 9-5, Agilent Technologies, 2001.

36. National Climatic Data Center website,
    URL: http://www.ncdc.noaa.gov/oa/ncdc.html

37. M. Shtaif, and M. Boroditsky, "The effect of frequency dependence of PMD on the performance of optical communications systems," *Photonics Technology Letters*, 15(10), pp. 1369-1371, 2003.

38. P.K. Kondamuri, C. Allen, D.L. Richards "Laplacian PDF of DGD time derivative and application to predicting PMD-induced outage rates," *Electronics Letters*, 40(8), pp. 503-504, 2004.

39. National Resources Conservation Services website,
    URL: http://www.wcc.nrcs.usda.gov/scan/

40. M. Fontaine, B. Wu, V.P. Tzlov, W.J. Bock and W. Urbanczyk, "Theoretical and experimental analysis of thermal stress effects on modal polarization properties of highly birefringent optical fibers", *Journal of Lightwave Technology*, 14(4), pp. 585-591, 1996.

41. Z.B. Ren, P. Robert, and P.A. Paratte, "Temperature dependence of bend- and twist-induced birefringence in a low-birefringence fiber", *Optics Letters*, 13(1), pp. 62-64, 1988.

42. D. Harris, P.K. Kondamuri, J.J. Pan, C.T. Allen, "Temperature dependence of wavelength-averaged DGD on different buried fibers," *Annual meeting of IEEE Laser and Electro-Optics Society,* Puerto Rico, MJ2, pp. 84-85, Nov. 2004.

43. M.Brodsky, P.Magill, N.J.Frigo, "Polarization Mode Dispersion of Installed Recent Vintage Fiber as a Parametric Function of Temperature" *IEEE Photonic Technology Letters*, 16(1), pp. 201-211, 2004.

44. T. Veldhuizen , "Noise models", http://osl.iu.edu/~tveldhui/papers/MAScThesis/node11.html , Jan 16, 1998.

45. "Chi-square goodness-of-fit test", http://www.itl.nist.gov/div898/handbook/eda/section3/eda35f.htm

APPENDIX A

Modified chi-square goodness-of-fit test

Several goodness-of-fit tests, like the chi-square test, Anderson-Darling test, Kolmogorov-Smirnov test, etc. are available to test if a sample of data belongs to a specific distribution. While some tests are applicable to only continuous distributions or to only certain specific distributions, chi-square test can be applied to any uni-variate distribution for which the cumulative distribution function can be calculated and also it is the most popular goodness-of-fit test. The chi-square test is applied to binned data, like a histogram, but the test requires a sufficient sample size in order for the chi-square approximation to be valid [45].

Chi-square test:

Hypothesis H_0: The sample data belongs to a specified distribution

Test statistic:

$$\chi^2 = \sum_{i=1}^{k} \frac{(N_i - Np_i)^2}{Np_i} \tag{A.1}$$

where k is the number of non-empty bins, N_i is the observed frequency for bin i, N is the total number of sample points, p_i is the probability corresponding to bin i, and Np_i is the estimated frequency for bin i.

The test statistic in (A.1) follows the chi-square distribution with (k-c) degrees of freedom where c is the number of estimated parameters + 1. For Maxwellian and Laplacian distributions c = 1+1 = 2. The hypothesis H_0 above is accepted only if the test statistic $\chi^2 \leq \chi^2_{(\alpha, k-c)}$, where α is the significance level. The values of $\chi^2_{(\alpha, k-c)}$ for different values of α and (k-c) are obtained from chi-square tables and are distribution-independent.

The chi-square test described above is applicable only for independent data sample. The measured and simulated DGD data presented in this report were highly correlated and so are not independent. Hence the chi-square test as it is cannot be applied to that data and so the test had to be modified slightly to make it suitable for

correlated data. The idea here is to estimate the number of independent data points in the sample data set and use that number in the test instead of the total number of the sample data points. With this modification the test statistic would now be

$$\chi^2 = N_{indep} \sum_{i=1}^{k} \frac{\left(\frac{N_i}{N} - p_i\right)^2}{p_i} \qquad (A.2)$$

where N_{indep} is the number of independent samples.

This modified chi-square test was used in the work to test the goodness-of-fit of the measured and simulated DGD and $\Delta\tau'$ data with that of the Maxwellian and Laplacian PDFs respectively. However, the reader is cautioned that the validity of this modified chi-square test could not be verified from the literature.

APPENDIX B

Matlab code used to implement the PMD model

```
%-------------------------------------------------------------------------------
% Matlab code to implement the PMD numerical model
% This file is specific to the 3-span case; Other cases are similar to this
% except that the parameter values are different
% Note: The values of PMD coefficient (b) mentioned here are not the
% actual values used in the simulations
%-------------------------------------------------------------------------------

clear all       % Clears the workspace
clc             % Clears the display screen
tic             % Start timer
datestr(now)    % Current time


%---------------------------------------
% Constants and some parameters
%---------------------------------------
c=3*1.0e8;                          % Speed of light in m/s
lamda=[1535e-9:0.1e-9:1565e-9];     % Wavelength (in m) vector
N=500*3;                            % Number of fiber segments
Len=95*3;                           % Length of fiber in km
meanlen=Len/N;                      % Mean of Gau. distribution for h (in km)
stdlen=0.2*meanlen;                 % Std dev of   "       "
w=(2*pi*c)./lamda;                  % Optical frequency vector (in Hz)


dlam=0.01e-9;                       % Wavelength step (in m)
lam1=lamda+dlam/2;
lam2=lamda-dlam/2;
w1=(2*pi*c)./lam1;
w2=(2*pi*c)./lam2;
dw=(2*pi*c*dlam)./lamda.^2;         % Frequency step (in Hz)


%------------------------------------------
% Raw and filtered temperature data
%------------------------------------------
load tempdata temp1_2_3_interp;   % Load raw data from tempdata file (Units: ºF)
temp2=[ones(1,2000)*mean(temp1_2_3_interp) temp1_2_3_interp];
[btemp atemp]=butter(1,0.08); % Butterworth filter; relative BW parameter of 0.08
temp2_filt=filter(btemp,atemp,temp2);
temp=temp2_filt(1,2001:length(temp2_filt)); % Filtered data
M=length(temp);
```

Temp_term=0.15*temp;   % Temperature term of Phi;
                        % Parameter 'k' value of 0.15 radians/°F
%--
% PMD coefficient matrix b (ps/sqrt(km). (These are not the actual values)
%--
b=[1e-12*ones(M,N/3) 1e-12*ones(M,N/3) 1e-12*ones(M,N/3)];

%--
% Random sequences for h (in km), phi (in radians) and alpha (in radians)
%--
load halphaphisets_3links;   % Load from a file
h=meanlen+meanlen*0.2*hset;   % Segment lengths
phi=ones(M,1)*phiset*pi*2;   % Static Phi values
alpha=ones(M+50,1)*alphaset*pi*2; % Coupling angle values

num_sec=4*3;   % Number of sections with time varying phi
load phivalues_Links1_2_3; % Random part of Phi values

% Final Phi matrix
phi(:,1:round((N)/num_sec):N)=phi(:,1:round((N)/num_sec):N)+(Temp_term'*ones(1
,num_sec)+phi_randn_2508by12*pi/90); % Gaussian standard deviation of pi/90

%---
% Numerical model implementation
%---

for pp=1:M,

   for tt=1:length(lamda),

      %---
      % Determining the resultant Jones Matrix
      %---

      T1=[1 0;0 1];T2=T1;
      L=0;
      for i=1:N,
         p1=sqrt(-1)*((sqrt((3*pi)/8)*b(pp,i)*w1(1,tt)*sqrt(h(1,i))/2)+phi(pp,i));
         p2=sqrt(-1)*((sqrt((3*pi)/8)*b(pp,i)*w2(1,tt)*sqrt(h(1,i))/2)+phi(pp,i));
         P1=[exp(p1) 0;0 exp(-p1)];
         P2=[exp(p2) 0;0 exp(-p2)];
         Q=[cos(alpha(pp,i)) sin(alpha(pp,i));-sin(alpha(pp,i)) cos(alpha(pp,i))];
         R1=P1*Q;
         R2=P2*Q;

```matlab
        T1=R1*T1;
        T2=R2*T2;
        L=L+h(1,i);
    end
    %---------------------
    % DGD calculation
    %---------------------
    U=T1*inv(T2);
    r=eig(U);
    dgd_comp(pp,tt)=abs(angle(r(1)/r(2))/(dw(1,tt)*1e-12));
  end
end
dgd=dgd_comp(1:1:M,:);


%----------------------------------
% Normalized DGD colormap
%----------------------------------
figure(1);
clim=[0 2.6];x=[1535 1565];y=[1 34];
imagesc(x,y,dgd/mean(mean(dgd)),clim);colorbar;
xlabel('Wavelength (nm)');ylabel('Time (Days)');


%-------------------
% Maxwellian fit
%-------------------
[s1 s2]=size(dgd);
d=reshape(dgd,1,s1*s2);
d_norm=d./mean(d);
deltatao_norm=[0:0.0001:max(d_norm)];
qq=sqrt(pi/8)*mean(d_norm);
maxwel_norm=(2*deltatao_norm.^2./(sqrt(2*pi)*qq^3).*exp(-
deltatao_norm.^2./(2*qq^2))); % Maxwellian fit


%---------------------------------------------------------------------
% Normalized DGD histogram and its Maxwellian fit in linear scale
%---------------------------------------------------------------------
figure(2);
[nx_norm,pmd_x_norm]=hist(d_norm,round(sqrt(s1*s2))); % Histogram from
measured data
bar(pmd_x_norm,nx_norm,1);
hold on;plot(deltatao_norm,maxwel_norm,'r','linewidth',2);hold off;
xlabel('DGD/MeanDGD (ps)');title('Normalized DGD Histogram and Maxwellian fit
in linear scale');
```

```
%-------------------------------------------------------------------------------
% Normalized DGD histogram and its Maxwellian fit in log scale
%-------------------------------------------------------------------------------
figure(3);
semilogy(pmd_x_norm,nx_norm,'b',deltatao_norm,maxwel_norm,'r');
xlabel('DGD/Mean DGD (ps)');title('Normalized DGD Histogram and Maxwellian fit
in log scale');

timegap=20/60; % Time interval between measurements

%-----------------------------------------------------------
% Numerical evaluation of DGD time derivative
%-----------------------------------------------------------
dgdder=(dgd(1:s1-1,:)-dgd(2:s1,:))/timegap;
[s11 s22]=size(dgdder);
ddgd=(reshape(dgdder,1,s11*s22));

%---------------
% Laplacian fit
%---------------
dgdderval=-max(abs(ddgd)):0.0001:max(abs(ddgd));
alpha_fit=sqrt(2)/std(ddgd)
laplacianfit=(alpha_fit/2)*exp(-alpha_fit.*abs(dgdderval));

%-------------------------------------------------------------------------------
% DGD time derivative histogram and its Laplacian fit in linear scale
%-------------------------------------------------------------------------------
figure(4);
[nx1,pmd_x1]=hist(ddgd,round(sqrt(s11*s22))); % Histogram of DGD time
derivative
bar(pmd_x1,nx1./(length(ddgd)*(pmd_x1(1,2)-pmd_x1(1,1))),1);grid;
hold on; plot(dgdderval,laplacianfit,'r');
xlabel('ps/hr');title('DGD Derivative Histogram and Laplacian fit in linear scale');

%-------------------------------------------------------------------------------
% DGD time derivative histogram and its Laplacian fit in log scale
%-------------------------------------------------------------------------------
figure(5);
semilogy(pmd_x1,nx1./(length(ddgd)*(pmd_x1(1,2)-
pmd_x1(1,1))),'b',dgdderval,laplacianfit,'r');grid;
xlabel('ps/hr');title('DGD Derivative Histogram and Laplacian fit in log scale');
```

```
%------------------------------------------
% Raw and filtered temperature plots
%------------------------------------------
figure(6);
subplot(2,1,1);plot([(1/(3*24)):1/(3*24):34],temp2(1,2031:4478),'k','linewidth',2);
xlabel('Time (Days)');ylabel('Temperature (degF)'); title('Raw, interpolated air
temperature');grid;
subplot(2,1,2);plot([(1/(3*24)):1/(3*24):34],temp(1,31:2478),'k','linewidth',2);
xlabel('Time (Days)');ylabel('Temperature (degF)'); title('Filtered, interpolated air
temperature');grid;

toc            % End timer
datestr(now) % Simulation end time

save Links1_2_3_95km_k015_filt008_gvarpiby90 % Save the workspace
```